Retinal Ganglion Cell Excitability and Adaptations to Ionic Stress in Glaucomatous Optic Neuropathy

By

Andrew Boal

Dissertation

Submitted to the Faculty of the

Graduate School of Vanderbilt University

in partial fulfillment of the requirements

for the degree of

DOCTOR OF PHILOSOPHY

in

Neuroscience

June 30, 2023

Nashville, Tennessee

Approved:

Bruce D. Carter, Ph.D.

David J. Calkins, Ph.D.

Tonia S. Rex, Ph.D.

Martin J. Gallagher, M.D., Ph.D.

ACKNOWLEDGMENTS

This work would not have been possible without the assistance, guidance, and support of many individuals. First and foremost, I would like to thank my advisor and mentor, Dr. David Calkins. These past four years have proved to be some of the most challenging, yet rewarding, of my life. Dr. Calkins's support and trust along the way allowed me to grow as a scientist and a person, and his generosity and mentorship have prepared me for success as I progress to the next stages of my career. I would also like to thank my committee members, Drs. Bruce Carter, Martin Gallagher, and Tonia Rex. Their advice and insightful questions challenged me to think deeply about my science and the significance of my work in the larger context of disease.

I have also been fortunate to be surrounded by numerous talented and supportive lab mates and colleagues during my time in graduate school. Dr. Michael Risner spent countless hours teaching me patch clamp electrophysiology, helping me troubleshoot all varieties of technical problems, and guiding my lines of scientific inquiry as my projects evolved. I'm also grateful for the help of Drs. Nolan McGrady, Lauren Wareham, Wendi Lambert, and Silvia Pasini, all of whom made significant contributions to my training as a scientist and provided invaluable assistance with my experiments. Brian Carlson and Cathy Formichella also spent significant time and effort assisting and facilitating the progress of my experiments. I'm also especially grateful for the comradery and support of my fellow graduate students in the lab and on the 7th floor, especially Joe Holden and Sarah Naguib, without whom graduate school would have been significantly more difficult and a lot less fun.

I also benefitted greatly from the support of the Neuroscience Graduate Program and the Medical Scientist Training Program. Their administrative and personal support were invaluable as I navigated tough transitions and personal challenges, and I'm lucky to have been affiliated with such talented groups of individuals. Furthermore, I am grateful to have received financial support from the NIH in the forms of the MSTP T32 training grant as well as my F30 fellowship awarded by the National Eye Institute, as well as substantial administrative support from the Vanderbilt Eye Institute.

Finally, I owe a great deal of gratitude to my support network of friends and family whose endless support, encouragement, understanding, and patience have been instrumental in helping me overcome the challenges and obstacles that I have faced along the way. To my sister Kaitlyn, for sticking with me through the toughest of times and being one of the strongest people I know. To my MSTPals, for being sources of both mindless laughter and professional inspiration, for keeping me grounded and reminding me of the importance of always being there for each other in times of need. To Brent, Amanda, and Nikki, for getting me through college and then some, and for their enthusiasm and encouragement over all these years. To Amy Stark, for her love, support, and motivation, and for her willingness to enjoy life and explore the world with me. To my family, for their love, their belief in me, and their unconditional support. I am excited for the next chapter in my life, and I am grateful to have you all by my side.

Thank you all for being there for me and for making this journey memorable.

TABLE OF CONTENTS

LIST OF FIGURES

CHAPTER 1

BACKGROUND AND INTRODUCTION*

1.1 Structure and function of the retina

1.1.1 Neurons of the retina

An organism's ability to detect visible light, allowing it to adapt and respond to its physical environment, offers a considerable evolutionary advantage. So strong is this advantage that some form of visual organ has independently evolved at least 40 different times throughout the course of natural history (Schwab, 2018). In humans, light is collected and focused by the eye onto the retina, a complex and multi-layered neural structure responsible for detecting, encoding, and transmitting visual information to the brain. The retina shares its developmental origins with the central nervous system (Heavner and Pevny, 2012) and makes direct connections between the eye and central targets in the brain. Beyond simply detecting light, the complex circuitry of the retina allows it to perform neural computations and start the process of making sense of the visual scene. However, like the rest of the central nervous system the retina is vulnerable to disease. Understanding the intricacy and heterogeneity of the cells and circuits of the retina provides an important foundation for developing new therapies to combat diseases of the visual system.

The retina is comprised of three primary layers of neuron cell bodies with two distinct layers of synapses (Kolb, 2011)(**Fig. 1.1**). Light entering the retina must first traverse all these layers before being absorbed in the outermost neuron layer (outer nuclear layer), containing cells called photoreceptors. Photoreceptors contain light-sensitive pigments that allow for the conversion of light energy into

---

*Portions of this chapter has been published in the following paper:

- **Boal, A. M.**, Risner, M. L., Cooper, M. L., Wareham, L. K., & Calkins, D. J. (2021). Astrocyte Networks as Therapeutic Targets in Glaucomatous Neurodegeneration. *Cells*, *10*(6), 1368. https://doi.org/10.3390/cells10061368

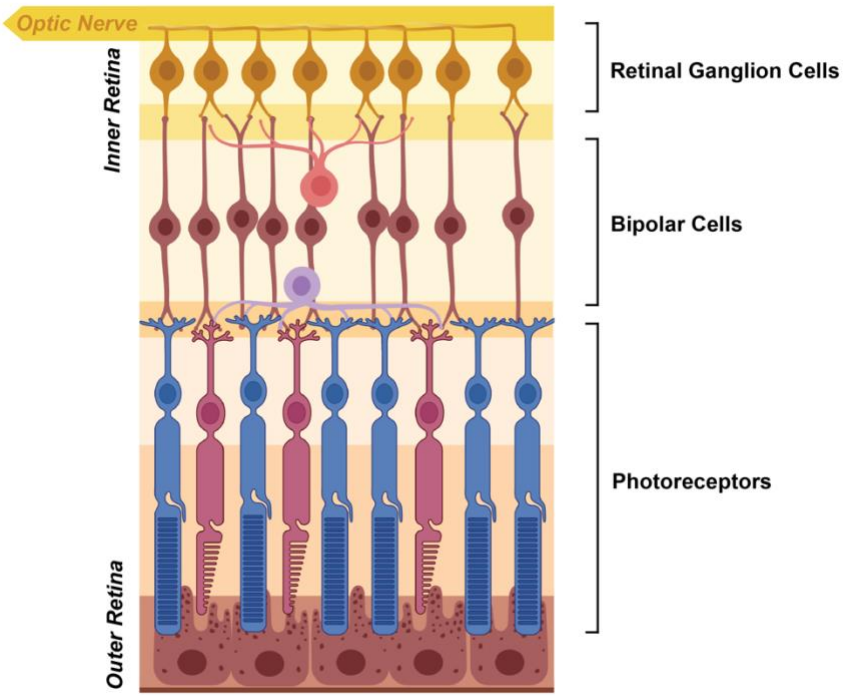

Figure 1.1 The layered neuronal structure of the retina
The retina is a highly organized, layered neural structure. Light passes through from the inner to the outer retina, where it is transduced by photoreceptors. Information is then conveyed through two more primary neuronal processing layers, ultimately getting integrated by retinal ganglion cells (RGCs) in the inner retina. RGCs transmit visual information to the brain via their long axons that comprise the optic nerve. Image created in part with BioRender.com.

bioelectrical signals, which can be conveyed by neurons. These cells can be divided into two primary subtypes, rods and cones, which have distinct biophysical properties that tune them for detecting specific types of light (Kolb, 2013; Fu, 2018). Rods are highly sensitive to low levels of light and facilitate night vision. Cones, on the other hand, function best in brightly lit conditions and provide high acuity and color vision. These differences are due in large part to the type of photosensitive protein, or opsin, contained within each cell (Kolb, 2013). The process of detecting light, called phototransduction, begins when light energy excites the opsin protein and causes a conformational change in retinal, a molecule bound to the opsin, from the 11-*cis* to all-*trans* conformation (Hargrave and McDowell, 1993; Kolb, 2013). This initiates a G protein-mediated signaling cascade, ultimately resulting in the closure of ion channels and hyperpolarization of the photoreceptor plasma membrane (Hargrave and McDowell, 1993; Kolb, 2013). In darkness, photoreceptor membranes are depolarized and release a constant stream of the excitatory neurotransmitter glutamate. Upon absorption of light, the signaling cascade results in the cessation of

glutamate release.

Moving inwards through the retina, the next major layer is a synaptic layer called the outer plexiform layer (Kolb, 2011). Here, the photoreceptors synapse onto neurons called bipolar cells. These connections are key for establishing a set of parallel pathways underlying the ability to detect contrast and which are important contributors to cell type differences highlighted in subsequent chapters. Depending on which type of glutamate receptor a bipolar cell expresses it gives rise to either the ON or OFF pathway, which are sensitive to increases or decreases in light intensity, respectively. Recall that stimulation with light causes a *decrease* in glutamate release from photoreceptors. Thus, ON bipolar cells must invert that signal so that they become excited by light. This is accomplished via metabotropic glutamate receptors, specifically mGluR6 (Nakajima et al., 1993), which respond to decreased glutamate levels by signaling through a G protein cascade and resulting in depolarization of the bipolar cell membrane. OFF bipolar cells, on the other hand, do not require sign inversion and signal through ionotropic glutamate receptors (Slaughter and Miller, 1983). The establishment of these parallel pathways allows for the detection of changes in contrast, and integration of these pathways in subsequent processing layers grants the ability to detect edges between light and dark areas of the visual scene.

Continuing inward, the next neuronal layer (the inner nuclear layer) contains the cell bodies of the bipolar cells as well as two other neuronal cells: amacrine cells and horizontal cells (Kolb, 2011). Horizontal cells interact with photoreceptors in the outer plexiform layer, applying inhibitory feedback that helps enhance contrast and generate color vision via a process called color opponency (Twig et al., 2003; Boije et al., 2016). They can span large distances and are often directly coupled to one another via gap junctions, allowing them to act in both short and long ranges. Amacrine cells send their processes in the opposite direction, reaching up into the inner plexiform layer. Broadly, they are involved in refining the receptive field properties of retinal ganglion cells, the final neuronal level of retinal processing. Amacrine cells are heterogenous, expressing a wide variety of neurotransmitters, taking on variable morphologic configurations, and varying in physiologic properties (Kolb, 1997). Importantly, amacrine cells are vital for establishing diversity in ganglion cells, discussed in depth later.

In the next synaptic layer, the inner plexiform layer, bipolar cells synapse onto retinal ganglion cells. These synapses are glutamatergic, excitatory connections (Kolb, 2012). Retinal ganglion cells (RGCs) are integrators of visual information, responding to activation of numerous photoreceptors across a topographic span of the retina. The way in which this information is integrated, in terms of both topographic space and ON/OFF pathways, establishes the RGC receptive field. RGC receptive fields, the region of visual space that drives their activation, are arranged in a center-surround configuration (Nelson, 2007)(**Fig. 1.2**). ON center RGCs are excited by light stimulation in the center of the receptive field and inhibited by light in the surrounding field (due to the lateral inhibitory action of amacrine cells). The reverse is true for OFF surrounds RGCs. Furthermore, ON/OFF segregation is reflected in the laminar location of bipolar-RGC synapses (Famiglietti and Kolb, 1976). OFF connections are made in the deeper part of the inner plexiform layer whereas ON connections are stratified in the more superficial region. These differences facilitate the morphological identification of the two broad categories of RGCs.

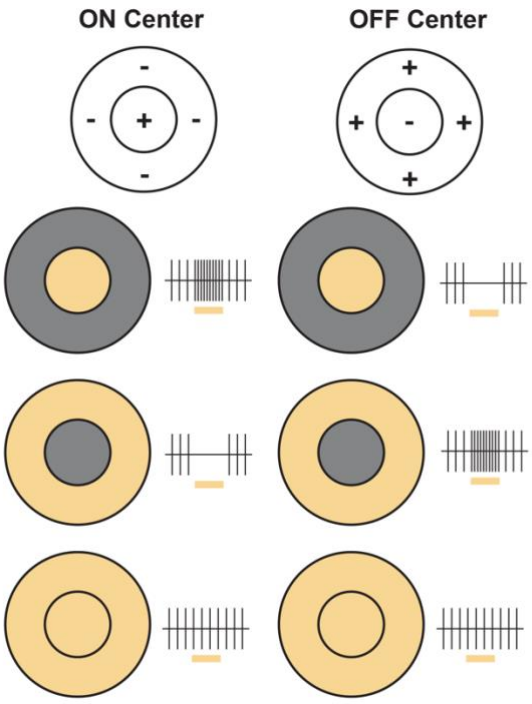

Figure 1.2 The center-surround receptive field
Schematic illustrating the basic principles of ON- and OFF-center receptive fields, showing different configurations of light (yellow) and dark (gray) falling on each representative field. The resultant spiking patterns of the cells are illustrated to the right.

Superficial to the inner plexiform layer lays the ganglion cell layer, where the cell bodies of RGCs (as well as some displaced amacrine cells) reside (Perez De Sevilla Muller et al., 2007; Kolb, 2011). The size and number of ganglion cells scales with eccentricity in the retina. In the central retina, the region of high acuity vision, there are numerous small RGCs. Correspondingly, the receptive fields of these RGCs are smaller and allow for higher frequency sampling of visual space (Dacey, 1993). Further from the central retina, RGCs become larger and less dense, with larger receptive fields. Similar, the amount of

convergence from photoreceptors and bipolar cells to RGCs changes with eccentricity. That is, central RGCs receive input from smaller regions and fewer photoreceptors than peripheral RGCs (Barlow, 1953). Based on this pattern of integration, each RGC is tuned to respond to a certain feature in a certain location of visual space. It translates the variety of excitatory and inhibitory inputs into changes in its membrane potential, generating trains of electrical spikes that are conveyed to the brain and further integrated and interpreted.

Each RGC sends a single axon superficially into the nerve fiber layer, running along the inner surface of the retina. These output fibers group into bundles and all converge on a single point in the centro-nasal retina, where they come together to form the optic nerve (Kolb, 2011). These axons, remaining unmyelinated within the retina, dive outward and pass through the optic nerve head, a structure made up of glial cells and collagenous beams (in the primate). Maintaining retina topography, they then pass out of the eye into the optic nerve proper, which traverses into the brain towards central visual targets, carrying visual information in the form of electrical signals. All information received by the brain is carried by these RGC axons. Thus, the fidelity of the signals carrying visual information to be interpreted in the brain is dependent upon the health of a diverse set of RGCs and their underlying circuitry.

1.1.2 Heterogeneity of retinal ganglion cells

Retinal ganglion ells (RGCs) can be divided into numerous subtypes. Traditionally these divisions were established by differentiating physiologic responses to light stimulation and by characterization of cellular morphology. Recent classification efforts differentiate numerous intrinsic and extrinsic properties, including genetic profile, transcriptomics, morphology, regular topographic spacing, and physiologic response to stimuli (Sanes and Masland, 2015; Shekhar and Sanes, 2021). Based on these variables, approximately 20 – 40 different RGC types of have been identified, depending on species (Sanes and Masland, 2015; Baden et al., 2016; Bae et al., 2018; Tran et al., 2019; Goetz et al., 2022). In the mouse, a common model organism used to investigate ophthalmic disease, this is number likely near 40 (Goetz et

al., 2022). Because the work presented here was performed in the mouse retina, subsequent exploration of RGC heterogeneity will focus on what is known about the mouse.

The broadest classification of mouse RGCs relates to the ON/OFF pathways described in the prior section (Sanes and Masland, 2015). ON center RGCs fire action potentials in response to increases in light intensity occurring in the center of their receptive field. OFF center RGCs, on the other hand, fire in response to decreases in light. There is also a subset of cells that fires in response to both light onset and offset, called ON-OFF RGCs. Additional divisions of RGCs based on light responses can be made by evaluating responses to more complex visual stimuli. Several RGC subtypes are direction selective – that is, they respond more strongly to light moving across the retina in a particular direction (Briggman et al., 2011). This unique property is established by asymmetric connectivity and inhibition between a specific type of amacrine cell, the starburst amacrine cell, and RGCs (Borg-Graham, 2001; Demb, 2007; Briggman et al., 2011). Further yet, direction selective RGCs can be subdivided based upon their preferred direction of motion along the visual axis, as well as by whether they preferentially respond to the onset or offset of moving light across their receptive field. These direction selective cells underly the ability to detect motion in the visual scene (Wei, 2018), an ability that is essential for an organism to interact with its physical environment. Another subset of RGCs is intrinsically photosensitive, in which cells contain their own opsin proteins that allow them to directly respond to light stimulation without activation from photoreceptor-initiated circuits (Schmidt et al., 2011a; Schmidt et al., 2011b). These cells are thought to mediate many of the non-image-forming aspects of the visual system, including modulating circadian rhythms and the pupillary reflex.

Importantly, there is good concordance between the physiologic response properties of RGCs and their morphology. As introduced previously, ON and OFF RGC dendrites are segregated into separate layers of the inner plexiform layer. Concordantly, ON-OFF RGC dendrites are bistratified into both layers. This is also true for direction selective cells and, interestingly, demarcated by the location of starburst amacrine cell dendrites (Famiglietti and Kolb, 1976; Galli-Resta et al., 2000), the cells underlying direction selectivity. The spatial distribution of an RGC's dendrites also frequently reflects its

response properties. For example, RGCs that are direction selective can have asymmetric dendritic arbors that are oriented in the same axis as their preferred direction of motion (Trenholm et al., 2011). RGCs can also be distinguished by their spatial distribution across the retina. Cells of the same type distribute regularly across the retina, avoiding packing too densely into clusters (Rockhill et al., 2000). Conversely, cells of different types distribute randomly in relation to each other.

Additional divisions of RGC subtypes can be made by focusing on molecular expression profiles of RGCs. The intrinsically photosensitive RGCs can be distinguished by their expression of melanopsin, their photopigment (Schmidt et al., 2011b). Directionally selective RGCs can be subdivided by molecular expression profiles, many of which correspond to specific directional preferences (Yonehara et al., 2008; Huberman et al., 2009; Kay et al., 2011; De la Huerta et al., 2012). A subset of RGCs known as alpha-RGCs, among the best understood of the RGC subtypes, are of particular importance for this work. Alpha RGCs are distinguished morphologically by their large cell bodies, large axons, and monostratified dendritic arbors (Krieger et al., 2017). Notably, they can also be identified by robust expression of neurofilament proteins (Peichl et al., 1987; Krieger et al., 2017). In the mouse retina there are four alpha RGC subtypes, each with unique morphology and response to light: ON-sustained, ON-transient, OFF-sustained, and OFF-transient (**Fig. 1.3**). As previously described, ON cells increase their spiking in response to increases in light whereas OFF cells response to light decrements. The sustained and transient

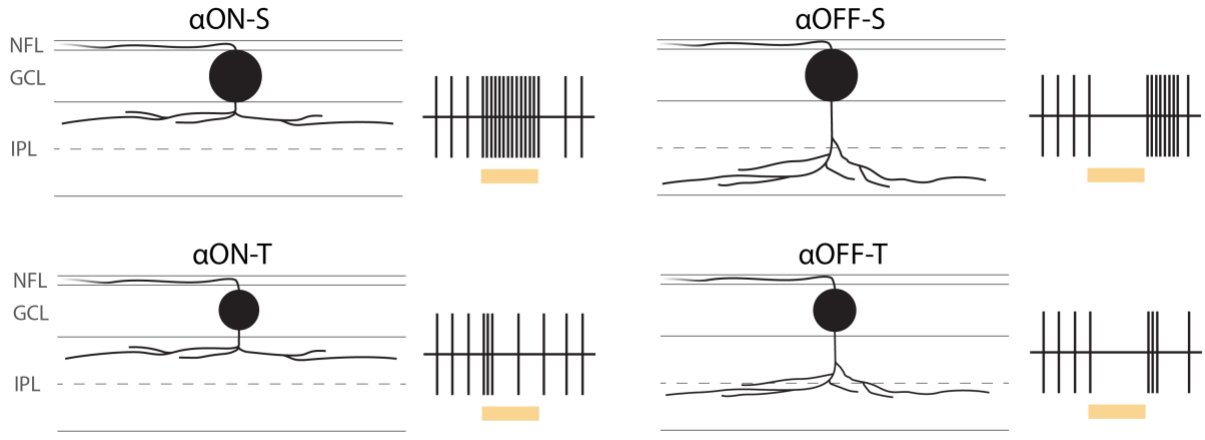

Figure 1.3 Four principal alpha-type retinal ganglion cells
Representative schematics of the morphology (left) and light response (right) of each of the four principal alpha retinal ganglion cells (RGCs): ON-sustained (αON-S), ON-transient (αON-T), OFF-sustained (αOFF-S), and OFF-transient (αOFF-T). NFL: nerve fiber layer, GCL: ganglion cell layer, IPL: inner plexiform layer.

designations refer to the duration of this spiking response. Sustained alpha RGCs have a brisk response that is maintained for a long duration after onset of the preferred stimulus. Transient cells, on the other hand, have a brisk but brief response to the stimulus before returning to their basal level of activity. Combining these molecular, morphologic, and physiologic properties allows for identification of each of these alpha RGC subtypes, as will be described further in subsequent chapters.

1.1.3 Glial cells of the retina

In addition to the layered circuitry of neurons, glial cells reside within the retina and make important physiologic contributions. Glia are neural cells that lack the excitable membranes of neurons but are integral contributors to central nervous system function. There are three types of glial cells in the retina: microglia, astrocytes, and Müller glia (Reichenbach and Bringmann, 2020). Microglia are the resident immune cells of the retina, migrating in from the bloodstream during development (Provis et al., 1996). They protect against pathologic stimuli (Aloisi, 2001), clear toxic byproducts (Li and Barres, 2018; Grubman et al., 2021), and remove cell debris and dying cells (Li and Barres, 2018). Within the retina microglia reside in the ganglion cell layer, in both plexiform layers, and around the blood vessels (Chen et al., 2002).

The other two retinal glia – astrocytes and Müller glia – are grouped into a category called macroglia based on their relatively larger size compared to microglia. The functions of these two cell types will be discussed in depth later in the intro; however, fundamentally they serve as regulators of neural homeostasis. Astrocytes, the most abundant glial cell type in the central nervous system, are distinguished by their star-like morphology and exist in distinct, non-overlapping domains (Bushong et al., 2002; Miller, 2018). In the retina they reside primarily in the nerve fiber layer containing RGC axons and within the ganglion cell layer (Vecino et al., 2016). They also are a vital component of the optic nerve head, the location where RGC axons pass out of the eye and form the optic nerve. In humans, the optic nerve head consists of unmyelinated axons passing through a dense network of transversely oriented astrocytes, within a network of collagenous beams called the lamina cribrosa (Morgan, 2000). The rodent

optic nerve head does not contain a true lamina cribrosa, though it does have a well-structured network of astrocytes that envelop RGC axons (May and Lutjen-Drecoll, 2002). Thus, astrocytes are essential for the maintenance of structure and function of RGC axons.

Müller glia share many similar functions with astrocytes but have a distinct developmental origin (Tworig and Feller, 2021). Müller cell bodies reside in the inner nuclear layer of the retina, near the bipolar cells (Vecino et al., 2016). Uniquely, their radially oriented processes span the full thickness of the retina, extending inwards to the nerve fiber layer and outwards to the photoreceptors. Their complex processes closely interact with the neurons of the retina, ensheathing cell bodies and intertwining with the dendritic connections between cells. This arrangement facilitates their important role in supporting neuronal function.

1.2 Foundations of neuronal electrical activity

1.2.1 Establishing and maintaining the neuronal membrane potential

Neurons encode information as electrical impulses. To achieve this, neurons must carefully regulate the composition of their membranes so that they are electrically excitable. Electrical potentials are established by creating asymmetric gradients of charged ions across the cell membrane. The primary ionic contributors this this gradient are sodium (Na^+) and potassium (K^+), with additional key contributions from calcium (Ca^{2+}) and chloride (Cl^-) (Hodgkin and Huxley, 1952b; a; c; Neher, 1992). Sodium ions are more highly concentrated outside of the neuron than inside, while potassium ions are more highly concentrated inside. Asymmetric gradients of ions across a semi-permeable membrane progress to an equilibrium potential, the point at which the motive forces of diffusion down a concentration gradient and electrical forces due to the charged nature of the ions balances out. This potential is unique for each ion based on its charge and concentrations on either side of the membrane. In multi-ion systems such as across a neuronal membrane, the relative permeability of each ion determines how strongly it contributes to the overall potential of the cell (Goldman, 1943; Hodgkin and Katz, 1949). Importantly, the membrane is selectively permeable to potassium ions, meaning that a small amount is

able to flow across the membrane when the cell is at rest, which is called the leak current (Hodgkin and Huxley, 1947). Because of this, the resting membrane potential of a neuron is strongly determined by the equilibrium potential of potassium, driving it towards a potential of -80 mV relative to the extracellular environment. Thus, alterations to the concentration of potassium can have profound impacts on the electrical state of a neuron, a phenomenon which is leveraged later in this work.

Neurons are not static systems. As such, ionic gradients are constantly in flux and robust systems must be in place to regulate and re-establish resting potentials. Often this task requires ions to be pumped against their concentration gradient by protein complexes that utilize cellular energy in the form of adenosine triphosphate (ATP). The sodium-potassium ATPase (Na^+/K^+-ATPase) is an enzyme found in all cells, but particularly important in neurons, which actively transports sodium and potassium ions to re-establish their proper concentrations on either side of the cell membrane (Skou, 1957). For each molecule of ATP that it utilizes, the Na^+/K^+-ATPase exchanges three sodium ions outwards for two potassium ions inward. These pumps are comprised of three different subunits and can exist in various different isoforms (Clausen et al., 2017). The composition of these subunits can impact the kinetics of the enzyme function, and vary by cell type as well as subcellular location (Clausen et al., 2017). Retinal ganglion cells contain the alpha1, alpha3, beta1, and beta1 subunits (Wetzel et al., 1999). This expression is not uniform across the cell; for example, there is greater expression of the alpha3 isoform in the axon bundles than in the axon (Wetzel et al., 1999). This may reflect the differing demands imposed on the different compartments of the retinal ganglion cell, a concept that will be explored in depth later in the context of disease.

Regulating membrane potentials is massively energetically demanding, and neurons can expend up to three quarters of their total energy on running the Na^+/K^+-ATPase (Ames et al., 1992; Attwell and Laughlin, 2001). Proper ATPase function is vital for the health and function of the neuron and even slight disruptions could lead to dysregulation of the ion concentrations in the extracellular space, like potassium which in homeostatic conditions is maintained at very low extracellular levels. To supplement the action of neuronal Na^+/K^+-ATPase, neurons are positioned in proximity with glial cells which can provide additional clearance capacity for elevated extracellular potassium concentration (Newman et al., 1984;

Odette and Newman, 1988; Karwoski et al., 1989). Such a mechanism helps ensure that the extracellular milieu remains properly regulated under homeostatic conditions. This arrangement is of particular importance in times of increased stress on the neurons, a concept explored in depth later.

1.2.2 Action potential generation and propagation

The fundamental unit of signaling within a neuron is the action potential. The action potential is a rapid depolarizing pulse in the membrane voltage that can be regenerated and propagated along the length of a neuron. An action potential is initiated when the membrane potential of a neuron reaches a threshold of depolarization. To reach this threshold, small excitatory and inhibitory input currents from other neurons are summed together. This integration of inputs can adjust the likelihood and frequency of action potential generation, making the neuron an integrator of inputs (Bean, 2007; Spruston, 2008).

Once the threshold potential is reached, a series of activation and inactivation of ion channels occurs in a stereotyped manner causing the rapid depolarization, called the rising phase, a sharp repolarization, the falling phase, and finally a period of undershoot before the resting membrane potential is reestablished (**Fig. 1.4**). Currents of sodium and potassium ions are the primary drivers of this process, though calcium currents can have an important influence on shaping the action potential (Bean, 2007). At rest, the ion-permeable pore of a voltage-gated sodium channel is blocked by an activation gate (de Lera Ruiz and Kraus, 2015). At action potential initiation, these activation gates rapidly open and allow the influx of sodium ions, raising the membrane voltage (Catterall, 2010). Once the voltage rises to the peak of the action potential a second molecular gate on the sodium channel, the inactivation gate, rapidly closes

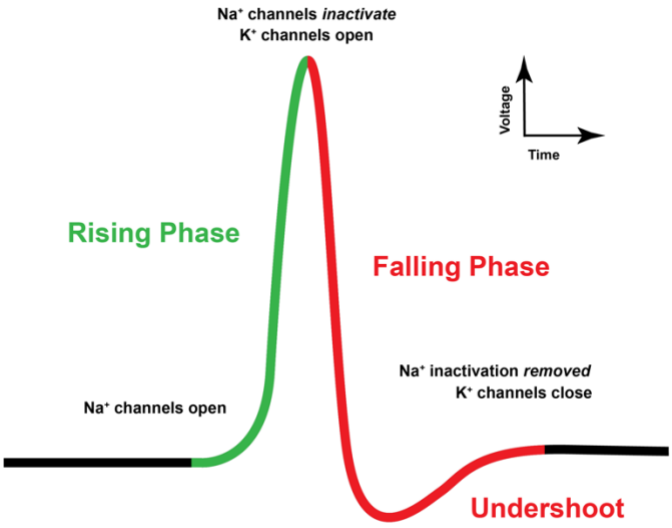

Figure 1.4 Phases of the action potential
Representation of the rising (green) and falling (red) phases of the action potential. Key changes in voltage-gated sodium and potassium channel permeability are noted at the relevant positions on the time-voltage axes.

and halts the flow of sodium across the membrane (de Lera Ruiz and Kraus, 2015). While the inactivation gate is in place no additional action potentials can be initiated. Around this point voltage-gated potassium channels, which have different activation kinetics than the sodium channels, open and allow rapid efflux of potassium (Bean, 2007; Catterall, 2010). This potassium flow rapidly reverses the change in membrane potential, causing it to polarize back towards more negative potentials. As the membrane voltage falls enough, the gates of the voltage-gated sodium channel change conformation, removing the inactivation gate and replacing the activation gate (Bean, 2007; de Lera Ruiz and Kraus, 2015). Due to higher permeability of potassium the membrane potential will undershoot its resting potential, resulting in a period known as the afterhyperpolarization (Sah and Faber, 2002). Typical membrane permeability is then re-established, and the neuron is then capable of firing another action potential.

Action potentials are initiated in the axon of a neuron, proximal to the cell soma. At this site, voltage-gated ion channels are clustered at a high density to facilitate the process described above (Wollner and Catterall, 1986). A specialized complex of proteins, called the axon initial segment, binds these voltage-gated channels and acts as a physical barrier that aids in the compartmentalization of the neuron (Leterrier, 2018). The axon initial segment is anchored to the cell's cytoskeleton, with the protein ankyrin-G as a central scaffold upon which the remainder of the complex can be anchored (Kordeli et al., 1995; Leterrier, 2016). The composition and structure of the axon initial segment plays a central role in both generating and shaping the action potential (Bender and Trussell, 2012), and variations in this structure can underly differences in spiking activity between cells. The axon initial segment is central to this work for two key reasons. First, it is an early step in the establishment and maturation of neuronal polarization (Rasband, 2010). That is, it marks the development of the axon and is central for proper signaling in the central nervous system. Second, the axon initial segment can be a dynamic and plastic structure that changes in response to physiologic and pathologic stressors (Grubb and Burrone, 2010; Yamada and Kuba, 2016b; Jamann et al., 2021). Features such as the length or distance of the axon initial segment from the cell soma influence the cell's spiking output (Grubb and Burrone, 2010; Hamada et al.,

2016; Raghuram et al., 2019; Fekete et al., 2021), and can shift to alter cellular excitability. Both concepts are explored in depth in later chapters.

In addition to being the site of action potential generation, the axon is responsible for conducting the action potential along its length to the terminus of the neuron. It must maintain the fidelity of the signal without loss of amplitude or frequency of action potential spikes. Neurons are relatively poor conductors of electricity on their own, and an action potential will degrade over a short distance if not renewed (Kress and Mennerick, 2009). Thus, action potentials are fired repeatedly along the full length of the axon. Due to the inactivation of sodium channels, there is a refractory period during which a segment of membrane cannot fire another action potential. This allows for unidirectional propagation toward regions of the membrane that are not refractory. The speed of conduction along an axon is affected by the dimensions of the axon itself (Gasser and Erlanger, 1927), with larger diameter neurons having faster conduction. Most important for the speed of conduction, however, is myelination of axon fibers (Suminaite et al., 2019). Myelin is an insulting material that surrounds the axon, formed in the central nervous system by glial cells called oligodendrocytes. This insulation decreases the axon's capacitance and dramatically increases the electrical conduction speed. The myelination is interrupted at regular intervals at points called Nodes of Ranvier, where voltage-gated ion channels are clustered to allow for the regeneration of the action potential (Rasband and Peles, 2015). In addition to increasing conduction speed myelin decreases the metabolic demand of neurons, increasing their efficiency (Neishabouri and Faisal, 2011).

There is considerable cell-cell variability in these factors affecting action potential generation and propagation, leading to a diversity in intrinsic physiologic properties. Voltage-gated sodium and potassium channels are families of channels made up of subtypes, each of which has unique properties that shape neuronal excitability (Catterall et al., 2005; Kim and Nimigean, 2016). In mammals there are ten identified isoforms of voltage-gated sodium channels (Na_V), which are differentially expressed in different tissues (Catterall et al., 2005). Of these, $Na_V1.1$, $Na_V1.2$, $Na_V1.3$, and $Na_V1.6$ have been found in the central nervous system, including the retina (Fjell et al., 1997; Caldwell et al., 2000; Boiko et al.,

2003; Van Wart et al., 2005; Engelmann et al., 2008; Catterall, 2012). Retinal ganglion cells in particular express significant amounts of $Na_V1.1$, $Na_V1.2$, and $Na_V1.6$ (Mojumder et al., 2007). The isoform $Na_V1.6$ is critical for the initiation and propagation of action potentials (Rush et al., 2005; Engelmann et al., 2008) and densely localized to the axon initial segment and at Nodes of Ranvier (Caldwell et al., 2000; Akin et al., 2015). $Na_V1.1$ is found primarily in the cell body, while $Na_V1.2$ is located in unmyelinated or pre-myelinated axons (Catterall et al., 2010). $Na_V1.2$ is activated at higher voltages than $Na_V1.6$ and plays an important role in modulating neuronal excitability (Lena and Mantegazza, 2019).

There are numerous different subtypes of potassium channels that play diverse roles in modulating neuronal electrical activity. In retinal ganglion cells, inwardly rectifying K^+ (K_{ir}), ATP-sensitive K^+ (KATP), tandem-pore domain K^+ (TASK), voltage-gated K^+ (K_v), ether-à-go-go (Eag) and Ca^{2+}-activated K^+ (K_{Ca}) channels have been detected (Zhong et al., 2013). Of note, K_{ir} and TASK channels affect the resting membrane potential and modulate RGC excitability, K_v channels modulate the falling phase, shape, and frequency of action potentials, and K_{Ca} channels are important regulators of a neuron's capacity for repetitive firing (Zhong et al., 2013). Alterations in the expression of voltage-gated sodium and potassium channels can affect the electrical properties of neurons and impact their role in a neural circuit. Furthermore, pathologic insults to these channels could have profound impacts on proper neural function. A subset of these potassium channels responsible for mediating cellular excitability and repetitive firing are of particular interest to this work and discussed in more depth later.

1.2.3 Experimental measurements of neuronal electrical activity

Significant insight into the electrical activity of neurons has been gained through a technique known as patch clamp electrophysiology. By using electrodes placed inside small glass tubes pulled out to a microscopically thin tip, electrical measurements of individual cells can be done. Depending on the configuration of this setup, a variety of different measurements can be done. All the electrophysiologic data presented in this work was done using the whole-cell recording configuration (Van Hook and Thoreson, 2014). To achieve this, a fluid-filled glass pipette with a tip diameter of just a few micrometers

is brought into proximity of a neuron viewed under a microscope. The pipette fluid is carefully matched to approximate the intracellular ionic environment. During the approach, gentle positive pressure is applied to prevent material from being sucked up into the pipette. When the pipette is immediately adjacent to the cell membrane the positive pressure is released and a seal is formed between the membrane and pipette tip. To establish whole-cell configuration a brisk pulse of negative pressure is applied, breaking through the membrane. This brings the intracellular compartment into electrochemical continuity with the inside of the pipette where the electrode resides, with low enough resistance to measure electrical potential differences between the inside of the cell and a reference electrode placed in the extracellular solution (**Fig. 1.5**).

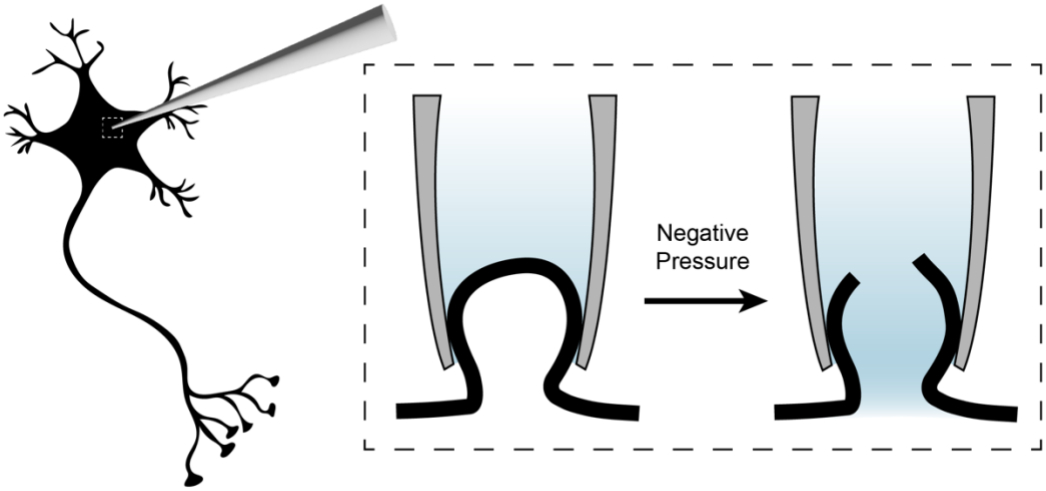

Figure 1.5 Schematic of the whole cell patch clamp configuration
To achieve whole cell patch clamp configuration, a small micropipette is brough into close proximity of the neuron soma (left). A strong seal is formed between the pipette and the cell membrane (inset, left). Then a quick pulse of negative pressure breaks the membrane, creating electrochemical continuity between the pipette and the intracellular space (inset, right).

After establishing whole-cell configuration, two basic types of measurements can be made (Van Hook and Thoreson, 2014). The intracellular compartment becomes part of a larger circuit under the control of the experimenter. To measure the voltage across the neuronal membrane, the experimenter must hold the net current across the membrane constant, in a setup known as current clamp. Likewise, currents in and out of the cell can be determined by holding the voltage steady, known as voltage clamp. During these recordings various stimuli can be applied to the cell as the experimenter measures the

resultant change in voltage or currents. Clamping can also be used to stimulate the cells, by rapidly changing the voltage or current at which a cell is being held and measuring the resultant electrical changes. Furthermore, this configuration allows for manipulation of the makeup of the intracellular and extracellular solutions. In this work, current-clamp recordings of the membrane voltage are done during both light stimulation and during brief pulses of depolarizing current. Additionally, the extracellular ionic composition is altered to challenge the cells with potentially pathologically relevant stimuli. This powerful methodology facilitates careful experimentation on the factors underlying typical neurophysiology and can offer insight into pathophysiological mechanisms altering neuronal excitability.

1.3 Neuron-Glia interactions

1.3.1 Physiologic functions of astrocytes and Müller glia

The two macroglia of the retina, astrocytes and Müller glia, have numerous and diverse functions. Fundamentally, they can be characterized as homeostatic support cells for neurons and neuronal networks. There is much overlap between the roles of astrocytes and Müller glia, though their cell bodies reside in different regions of the retina (Hollander et al., 1991). Shared duties of these cells include establishing the blood-retinal barrier (Tout et al., 1993; Wareham and Calkins, 2020), regulating the extracellular ionic environment (Karwoski et al., 1989; Kofuji and Newman, 2004), and providing metabolic support to neurons (Rouach et al., 2008; Toft-Kehler et al., 2018; Cooper et al., 2020). Despite the importance of astrocytes in regulating synaptic signaling between neurons elsewhere in the central nervous system, Müller glia are more closely located to the synapses of the retina and largely carry this responsibility (Newman, 2004).

Like other regions in the central nervous system, the barrier between the retina and the bloodstream is tightly regulated to selectively control the substances that can cross from the periphery into the neural tissue (Diaz-Coranguez et al., 2017). Both astrocytes and Müller cells tightly wrap around retinal blood vessels, forming a physical barrier and containing proteins that allow for selective transport of materials into the retina (Cabezas et al., 2014; Diaz-Coranguez et al., 2017). Their association with both blood

vessels and neurons allows glia to couple neuronal energetic demand to blood flow and the delivery of nutrients (Pellerin and Magistretti, 1994; Kasischke et al., 2004; Newman, 2015; Mahmoud et al., 2019). In addition to offering metabolic support, retinal glia further support neuronal activity by aiding in the regulation of the contents of the extracellular space. Sustained, repetitive firing of action potentials leads to a buildup of extracellular potassium ions that can exceed the capacity of neuronal Na^+/K^+-ATPase (Larsen et al., 2016). Prolonged potassium elevation can disrupt the normal electrical activity of neurons and even lead to degeneration (Zhao et al., 2021). Retinal glia supplement potassium clearance by expressing channels that allow concentration-dependent uptake of excess ions (Newman et al., 1984; Odette and Newman, 1988; Karwoski et al., 1989; Kofuji and Newman, 2004; Wallraff et al., 2006). Importantly, the homeostatic capacity of retinal macroglia is shared among numerous cells so that no single astrocyte or Müller cell is overwhelmed.

1.3.2 Connectivity of astrocytes in the retina and optic nerve

The physiologic influence of astrocytes on neurons is potentially quite topographically broad because astrocytes are densely interconnected via gap junctions. Gap junction-to-gap junction connections allow astrocytes to function as a far-reaching syncytium, rather than being isolated as single cell units. Through these networks, astrocytes accomplish diverse tasks such as providing metabolic substrates in the form of lactate to neurons and regulating the extracellular ion gradients through spatial buffering.

Gap junctions directly connect neighboring cells, conducting inter-cell communication through electrical currents and the direct passage of small molecules. Gap junctions are formed from a large diversity of connexin (Cx) proteins. These proteins are assembled as complexes of six subunits, which are known as connexons. The connexons are inserted into the cell membrane and can then link adjacent cells via three main types of gap junction connections. First, gap junctions may be formed by two connexons both consisting of the same proteins (homotypic). Second, gap junctions may form between two distinct connexons, where each contains six of the same Cx proteins (heterotypic). Third, the composition of each

individual connexon may be mixed (heteromeric) and form any variety of connection (for review see (Koval et al., 2014)).

Connexins are expressed by a variety of cells across different tissues. Within the central nervous system (CNS), connexins are expressed widely by glial cells and a subset of neurons (Sohl et al., 2005). Macroglia, predominantly astrocytes and oligodendrocytes, have strong connexin expression and form gap junction networks that allow them to function as a "panglial syncytium" (for a detailed review of glial connexins, see (Giaume et al., 2021)). There is a diversity in connexin type and distribution across this glial network. Such diversity necessitates a detailed understanding of the connexin makeup for targeted therapeutic intervention.

Astrocytes in both the human and rodent CNS predominately express Cx30 and Cx43, which are heterogeneously distributed in different brain regions (Koulakoff et al., 2008). For example, the ratio of Cx30 to Cx43 is higher in the thalamus than other regions, such as the cortex (Griemsmann et al., 2015). Conversely, Cx43 dominates white matter tracts, such as in the optic nerve (Nagy et al., 1999). The dense network of astrocytes in the optic nerve head is highly linked by Cx43 gap junctions (**Fig. 1.6**). Connections between two astrocytes are mediated by homotypic gap junctions (either Cx30/Cx30 or Cx43/Cx43), whereas connections between astrocytes and other cell types, primarily oligodendrocytes, are mediated by heterotypic gap junctions (Orthmann-Murphy et al., 2007). Astrocytic Cx43 also form structures known as hemichannels. Hemichannels are formed when a connexon inserts into the membrane of one cell with no binding partner on another cell, acting as a potential conduit between the intracellular and extracellular space. While hemichannels are

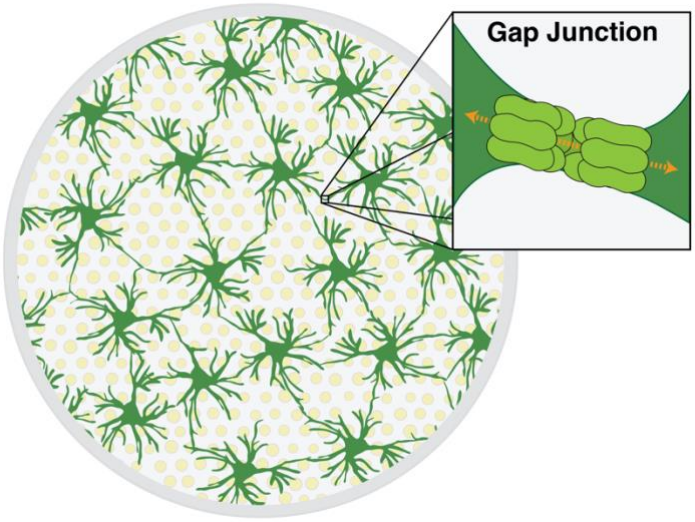

Figure 1.6 Schematic cross section of the rodent optic nerve head demonstrating Cx43 gap junctions
Optic nerve astrocytes (dark green) are arranged in a network that lies perpendicular to the direction of axons (yellow). These cells are interconnected via gap junctions composed of two adjoining hexamers of Cx43 (light green), as shown in the inset. The junctions allow for electrical coupling and the passage of molecules up to ~1.2 kilodaltons in size from cell to cell.

important components of gliotransmission (glial-mediated release of neurotransmitters) in the central nervous system (Abudara et al., 2018), their role in the retina and optic nerve is better understood within the pathophysiologic context and will be discussed later. The remainder of this chapter focuses on astrocyte functions that are in part dependent upon gap junction-mediated networks, including the provision of metabolic substrates to neurons and the buffering of the contents of the extracellular space.

1.3.3 Astrocytic redistribution of metabolic resources

Astrocytes are the only significant source of glycogen in the brain. Increased neuronal metabolic demand prompts astrocytes to break down their glycogen stores, undergo glycolysis, and donate lactate to the neurons for energy (Kasischke et al., 2004; Rouach et al., 2008; Herrero-Mendez et al., 2009; Jakoby et al., 2014; Mongeon et al., 2016; Supplie et al., 2017). Astrocytic glycogen supports the metabolic demands of both physiological synaptic signaling and action potential propagation, and acts as a reservoir of metabolic substrates when neurons are stressed. A large body of evidence supports the theory that astrocytes are a primary supplier of energy to highly active neurons through the astrocyte neuron lactate shuttle (Cali et al., 2019). Astrocytes undergo aerobic glycolysis and produce L-lactate, which is passed to neurons through monocarboxylate transporters. Monocarboxylate transporters are ubiquitously expressed plasma membrane proteins responsible for carrying molecules with one carboxylate group, including the key metabolites lactate and pyruvate, across the cell membrane. The transporters are expressed by both astrocytes and neurons, allowing for the shuttling of lactate from one cell to the other. The release of lactate from astrocytes is positively correlated with neurotransmission, indicating that the release is regulated by neuronal metabolic demand. At excitatory synapses, the uptake of glutamate by astrocytes stimulates glycolysis and lactate production within the astrocytes (Pellerin and Magistretti, 1994), allowing for delivery of metabolites to supplement the increased metabolic needs of neurons during excitation (Machler et al., 2016). Neurons convert this lactate into pyruvate for use in oxidative metabolism, producing abundant adenosine triphosphate (ATP). Astrocytic lactate release appears to be especially important in times of prolonged metabolic demand or transiently decreased metabolic supply

from the bloodstream. With prolonged stimulation of neurons there is early oxidative metabolism, which is subsequently sustained over time by activation of the astrocyte neuron lactate shuttle (Kasischke et al., 2004). In many diseases, including glaucoma, neuronal hyperactivity and metabolic dysregulation are early subclinical features (Risner et al., 2018; Cooper et al., 2020). Thus, the astrocyte neuron lactate shuttle represents a protective force against these early stressors.

Physiologically, astrocytic lactate supply is vital for various neuronal processes, including plasticity and recovery after stress (Suzuki et al., 2011). The stimulation of lactate release is required for the establishment of long-term potentiation (LTP) at glutamatergic synapses in the hippocampus (Gao et al., 2016). The astrocyte neuron lactate shuttle is also important for stressed tissue. If neural white matter tissue is exposed to conditions simulating transient ischemia, astrocytic glycogen stores can sustain axonal function for a period. Depletion of astrocytic glycogen rapidly accelerates the decline in function (Brown et al., 2003), highlighting an important defense against ischemic conditions.

Interestingly, glycogen is not uniformly distributed throughout the brain (Brown, 2004). Such regional variability could lead to a topographic imbalance in the size of metabolic reservoir, increasing the vulnerability of certain regions to metabolic stress. However, the astrocytic glycogen stores are not sequestered to just local availability and can be redistributed according to metabolic needs. Cx43 gap junctions allow the nonselective passage of molecules up to ~1-1.2 kilodaltons in size including a number of metabolically significant molecules, notably glucose (Harris, 2007).

Astrocytic metabolic networks play a key role in supporting neural activity. Glucose trafficking through astrocyte gap junctions plays an important role in maintaining hippocampal synaptic activity (Rouach et al., 2008). Importantly, in the retina and optic nerve glycogen stores can redistribute over a long distance to support neural function in response to acute and chronic stress (Cooper et al., 2020).

The transfer of glucose between astrocytes is driven by a concentration gradient (Rouach et al., 2008), allowing nutrient-rich regions to supply regions with high demand. In a similar manner to the mechanism described in lactate production, neural activity mediated regulation of metabolite transfer is reported. For example, astrocytes are suggested to exhibit greater Cx43 expression in co-culture with

neurons than in monoculture (Koulakoff et al., 2008). Furthermore, excitotoxic treatments triggering neuronal death in vivo lead to a downregulation of connexins in astrocytes located in close proximity to dying neurons (Koulakoff et al., 2008). The activity of neurons directly influences astrocytic regulation of Cx43 gap junctions (Hasel et al., 2017).

The mechanism by which this occurs appears to be related to synaptic signaling. Synaptic activity has been directly linked to upregulation of gap junctional communication (Rouach et al., 2000). Excitatory neuronal transmission increases extracellular glutamate and potassium levels, which in turn enhances gap junctional coupling between astrocytes (Enkvist and McCarthy, 1994). Activity-dependent enhancement of coupling is accomplished by post-translational modification of Cx43 channels, increasing the number of active channels within gap junction plaques (Rouach et al., 2000; De Pina-Benabou et al., 2001). Such regulation has important physiological consequences. Blocking gap junctions (pharmacologically and genetically), as well as flooding the astrocytic network with metabolically inert D-lactate prevents long-term potentiation (LTP) in mouse cortex, thus eliminating an important component of synaptic plasticity (Murphy-Royal et al., 2020). Local delivery of high levels of L-lactate, the metabolically active enantiomer that can be utilized by neurons, rescues the phenotype and allows for the re-establishment of LTP independent of astrocytic networks (Murphy-Royal et al., 2020). The importance of astrocytic Cx43 for sufficient lactate delivery suggests individual astrocytes are unable to meet the energy demands required for synaptic plasticity and other energetically intensive processes; rather, broad metabolic networks are required to meet such demands. Further, it illustrates that this connectivity is dynamically modulated by neuronal metabolite insufficiency.

As a response to insufficient neuronal metabolites, astrocytes can regulate cerebral blood flow and coordinate this regulation broadly though gap junctional networks. Propagation of calcium waves through astrocytic gap junctions controls arteriolar dilation and thus regional blood flow (Munoz et al., 2015; Charvériat et al., 2017). Such coordination is important for maintaining sufficient blood flow, and thus nutrient delivery, in the face of challenges to perfusion. In the eye, targeted miRNA knockdown of glial Cx43 expression compromises the reactivity of both arterioles and venules to challenges to ocular

perfusion (Liu et al., 2021). Regulation of central nervous system blood flow is a key function and an important mechanism for supporting neuronal metabolism during the changing balance between metabolic supply and demand.

1.3.4 Astrocyte networks and extracellular buffering

Astrocytes tightly regulate extracellular concentration of ions and neurotransmitters used for synaptic transmission. Glutamate and potassium are two important examples of such products whose concentrations are tightly regulated by astrocytes. Astrocytic glutamate uptake is the main route of glutamate clearance from the excitatory synapse, and the primary mechanism by which the neurotransmitter is recycled (Bergles and Jahr, 1998; Anderson and Swanson, 2000; Mahmoud et al., 2019). The uptake of glutamate against its concentration gradient is mediated by sodium-dependent transporters, primarily GLT-1 and GLAST (Rothstein et al., 1996). These proteins take in three Na^+ and one H^+ with each molecule of glutamate, while one K^+ ion is transported outwards (Levy et al., 1998).

Astrocytes also dynamically modulate extracellular potassium through both active and passive means. Mechanisms for potassium flux include Na/K–ATPase pumps, Na/K/Cl cotransporters, and inwardly-rectifying potassium channels (mainly $K_{ir}4.1$) (Kofuji and Newman, 2004; Larsen et al., 2014). Astrocytic potassium regulation is essential for regulating synaptic firing and plays a role in modulating neural network firing dynamics (Wang et al., 2012; Pacholko et al., 2020). Deficiencies in this regulation can lead to aberrant neuronal excitability in the setting of elevated local extracellular potassium concentrations (Kocsis et al., 1983).

Astrocytes contribute to the maintenance of the extracellular space through spatial buffering, in which local extracellular increases of a metabolite can be countered by a dispersion to regions of lower concentration (Newman et al., 1984; Odette and Newman, 1988; Karwoski et al., 1989). Gap junctions allow for the expansion of buffering responsibility across a network of cells. Buffering through astrocytic networks increases the capacity for removal of excess K+ and glutamate, limiting the accumulation during periods of increased neuronal firing. In the hippocampus, this helps to tone down neuronal

excitability. Eliminating these networks through genetic deletion of connexin proteins stresses the buffering capacity of individual astrocytes, leading to cell swelling and decreased uptake (Pannasch et al., 2011). The neuronal consequences of this disconnection are increased excitability, higher presynaptic release probability, and alteration of the postsynaptic receptor composition. However, some coupling-deficient astrocytes may have a large capacity for K+ clearance, as measured by the rate of change in extracellular potassium concentrations during stimulation (Wallraff et al., 2006). Still, pathological insults may tip the scale; mice without astrocytic coupling show an increased susceptibility to experimental generation of epileptiform events (Wallraff et al., 2006).

The importance of gap junctional coupling extends beyond local ionic redistribution. Neuronal activity causes a depolarization of the astrocyte cell membrane. The electrical coupling of adjacent cells through gap junctions minimizes the magnitude of depolarization in any individual cell, allowing for the efficient maintenance of the electrochemical driving force responsible for potassium and glutamate uptake (Ma et al., 2016). An intact astrocytic network allows astrocytes to function more efficiently, regulating local increases in extracellular glutamate and potassium and preventing highly active or diseased neurons from inducing aberrant excitability in neighboring cells. Dysregulation of extracellular glutamate and potassium places immense stress on neurons and can be neurotoxic. Astrocytes are essential to the regulation of these molecules, and astrocytic networks provide an additional protective buffer against this stress. Disruption of the network could serve to amplify even small pathologic insults, making these networks potentially quite relevant in neurodegenerative disease.

1.4 Glaucoma and other optic neuropathies

1.4.1 Diseases of the optic nerve

The optic nerve is formed by the axons of the retinal ganglion cells (RGCs) as they bundle together near the posterior pole of the eye and pass out of the globe. Of particular importance is the region at which axons pass out through the scleral connective tissue of the eye, in a structure known as the optic nerve head. Here, axons take a right angle turn and pass through an organized support scaffolding. In

humans this is known as the lamina cribrosa, a combination of perpendicularly oriented astrocytes and collagenous beams (Elkington et al., 1990; Morgan, 2000). Mice lack a true lamina cribrosa with the collagenous beams but do still have a dense network of astrocytes forming the optic nerve head (May and Lutjen-Drecoll, 2002). From there, RGC axons travel together postero-medially beyond the orbit, where they join up with the contralateral optic nerve in a structure called the optic chiasm. At the chiasm, a portion of the axons cross the midline while others remain ipsilateral. The degree and nature of this crossing is dependent upon species (Neveu and Jeffery, 2007). Organisms that have more binocular vision, like humans and other primates, have a higher degree of axons remaining ipsilateral whereas organisms with less binocular overlap, such as mice, have a greater proportion of axons crossing midline. After the chiasm the fibers travel towards central targets where RGC axons synapse onto nuclei in the thalamus, midbrain, and more.

Damage to RGC axons at any point along the optic nerve can lead to vision loss. Optic neuropathy, or the loss of axons in the optic nerve, can result from damage within the eye, at the optic nerve head, or along the full path of RGC axons to the brain (Feldman et al., 2022). The etiologies, or causes, of optic neuropathy are broad and diverse. Damage can result from direct or indirect trauma, inflammation, infection, ischemia, toxins, nutritional deficits, compression of the nerve, radiation, or genetic diseases (Osborne and Balcer, 2021). Two of the most common underlying causes (besides glaucoma) are ischemic optic neuropathy and optic neuritis (Osborne and Balcer, 2021).

Ischemic optic neuropathy, which is more common in older individuals, occurs as a result of inadequate blood flow to the optic nerve (Hayreh, 2009). Cases of ischemic optic neuropathy occur most frequently in the anterior portion of the optic nerve, near the optic nerve head, in regions that receive blood supply from branches of the posterior ciliary artery (Hayreh, 2001; 2009). Disruption of blood flow can occur from periods of hypoperfusion (Hayreh, 2004), thromboembolic events (Lieberman et al., 1978), or from inflammatory conditions that damage the blood vessels directly (Hayreh et al., 1998). Ischemic optic neuropathies result in pallor and swelling of the optic disc on exam, and frequently results in irreversible damage to the optic nerve with consequent vision loss (Osborne and Balcer, 2021).

Optic neuritis, seen most in younger individuals, is an inflammatory condition in which the immune system attacks the tissue of the optic nerve (Hickman et al., 2002; Petzold et al., 2014; Osborne and Balcer, 2021). It is most frequently associated with the condition multiple sclerosis, an autoimmune disease affecting the myelin sheath of axons, but can also be the result of other conditions (Petzold et al., 2014). Optic neuritis most frequently occurs unilaterally, resulting in partial or total vision loss. In most cases the course is self-limiting, with most patients recovering vision within a few weeks (Beck and Gal, 2008). However, the condition often reoccurs if the underlying condition is not appropriately managed (Beck and Gal, 2008).

Glaucomatous optic neuropathy (glaucoma), the focus of this work, is the leading cause of irreversible vision loss worldwide and is projected to affect an estimated 111.8 million by the year 2040 (Tham et al., 2014). Glaucoma is a distinct group of neurodegenerative conditions that involve the progressive dysfunction and loss of retinal ganglion cell axons, often as a result of sensitivity to intraocular pressure (IOP) (Calkins, 2012; Calkins and Horner, 2012; Nickells et al., 2012). The major component of IOP that can vary from person to person comes from a fluid called the aqueous humor, which fills the anterior chamber of the eye between the cornea and the lens. This fluid is in a balanced state between production, in a structure called the ciliary body, and drainage through multiple outflow pathways (Goel et al., 2010; Roy Chowdhury et al., 2015) (**Fig. 1.7**). In many cases of glaucoma patients have elevated IOP, which conveys mechanical stress back through the eye to the axons as they pass through the optic nerve head (Downs, 2015). However, this is not the case for all patients as glaucoma can result from a diverse set of etiologies as discussed in the next section. Regardless of the cause, untreated glaucoma results in the

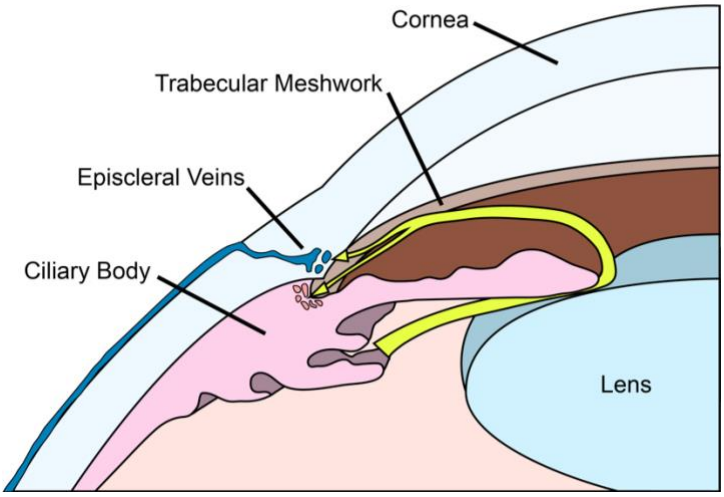

Figure 1.7 Aqueous humor production and drainage
A schematic representation of the flow of aqueous humor (yellow arrows) as it is produced by the ciliary body, flows into the anterior chamber, and is drained via the trabecular meshwork and uveoscleral outflow pathways.

irreversible loss of axons in the optic nerve, which leads to visual field loss and can result in complete vison loss.

1.4.2 Etiologies of glaucoma

The causes of glaucoma can be grouped into two broad categories: open-angle glaucoma and closed-angle glaucoma (Weinreb et al., 2014). This designation refers to the angle between the cornea and the iris in the anterior chamber, the site in which aqueous humor drainage occurs. In closed-angle glaucoma, this drainage pathway becomes acutely obstructed, leading to rapid rise in IOP that can be painful. Factors increasing the risk of developing closed-angle glaucoma are Asian descent, female sex, and older age (Zhang et al., 2020). Open-angle glaucoma, which does not feature this blockage of the iridocorneal angle, is by far the most common variant in the United States (Friedman et al., 2004; Day et al., 2012). Open-angle glaucoma can develop either as a primary disease or as a secondary disease, resulting from some other insult such as corticosteroid use (Kersey and Broadway, 2006), trauma (De Leon-Ortega and Girkin, 2002), inflammation (Merayo-Lloves et al., 1999), or other conditions like pigment dispersion or pseudo-exfoliation (Weinreb et al., 2014; Plateroti et al., 2015; Scuderi et al., 2019). The other types of open-angle glaucoma are primary open angle glaucoma (POAG) and normal tension glaucoma (NTG).

In POAG an imbalance develops between aqueous humor production and drainage, leading to elevated intraocular pressure. Contrary to acute angle closure, pressure elevation is more moderate and painless (Kass et al., 2002). This pressure over time stresses the retinal ganglion cell axons and leads to slow but progressive vision loss. Besides elevated IOP, major risk factors for the development of POAG include a family history of the disease, older age, and being of African descent (Moyer and Force, 2013). NTG, on the other hand, is a form of open-angle glaucoma that is associated with normal IOP (Killer and Pircher, 2018). It shares many clinical features with POAG and has a similar progression of RGC degeneration and painless visual field loss. There are a few hypotheses for the mechanisms of NTG, in the absence of mechanical stress imposed by abnormally high pressure (Killer and Pircher, 2018). The first

theory is that individual variation may make certain people more susceptible to the stress of IOP, even within “normal ranges” (Chen et al., 2015). It is also hypothesized that NTG is linked to dysregulated blood flow at the optic nerve, less severe than ischemic optic neuropathy but enough to lead to a chronic mismatch in supply and demand (Flammer, 1994). Finally, stress may be imposed on the lamina cribrosa by an imbalance between IOP on the ocular side and the pressure of cerebrospinal fluid on the brain side (Price et al., 2020a). It’s likely that more than one, if not all, of these factors contribute to the pathophysiology of NTG (Killer and Pircher, 2018).

There are also several genes linked to the development of glaucoma including myocilin (Stone et al., 1997), optineurin (Rezaie et al., 2002), and WD repeat domain 36 (Monemi et al., 2005). However, these monogenic causes make up a small percentage of the total cases of glaucoma, while the remaining primary glaucoma cases are thought to be polygenic (Kwon et al., 2009). Despite the varied causes of glaucoma many cases have similar resultant pathologies and progression of symptoms, with shared mechanisms of RGC degeneration.

1.4.3 Clinical presentation of glaucoma

The early clinical stages of glaucoma may go unnoticed by patients. It is estimated that only 10-50% of all people with glaucoma know that they have it (Rotchford et al., 2003; Hennis et al., 2007; Sathyamangalam et al., 2009; Leite et al., 2011; Budenz et al., 2013). In severe stages, patients may notice loss of their visual field, particularly in the periphery, though more subtle deficits may also be present (Hu et al., 2014). Importantly, by the time noticeable symptoms develop patients have already irreversibly lost a significant portion of their retinal ganglion cells (Kerrigan-Baumrind et al., 2000). However, most glaucoma detected early is noted on exam by a clinician before a patient notices symptoms.

On fundoscopic exam glaucoma presents with cupping of the optic disc, which is the optic nerve head as viewed from the clinician’s perspective (Weinreb and Khaw, 2004). This cupping occurs due to loss of RGC axons, which come together to form the optic nerve at that point. As they degenerate, the

nerve fiber layer thins and leaves an empty space, the “cup”. Next, during the exam intraocular pressure is typically measured as well. As previously discussed, many but not all forms of glaucoma are associated with elevated IOP so this is an important diagnostic step. Additionally, a clinician will examine the anterior segment of the eye for signs related to and/or causative of elevated IOP (Cohen and Pasquale, 2014). POAG will not present with remarkable findings on anterior segment exam but causes such as closed-angle glaucoma or exfoliation glaucoma will be evident.

Further diagnostic testing can be done to aid in the diagnosis of glaucoma and to track disease progression. Visual field testing done in each eye can be used to detect regions of vision loss and monitor disease progression over time (Broadway, 2012), although its utility in early diagnosis may be limited (Quigley et al., 1992). Structural measurements of the ganglion cell layer and nerve fiber layers can also be made, using an imaging technology called optical coherence tomography (OCT). Glaucoma results in a measurable thinning of these layers, and OCT is a sensitive tool for diagnosis and monitoring glaucoma progression (Bussel et al., 2014). Early detection of glaucoma is key, as intervention before significant tissue loss can help preserve vision and maintain quality of life (Kass et al., 2002; Leske et al., 2007).

1.4.4 Hypotensive therapies and the need for neuroprotection

Intraocular pressure is the only modifiable risk factor for glaucoma, and the only target of currently approved therapies. Lowering of IOP, even in patients with NTG, has been demonstrated to significantly slow or prevent the progression of vision loss (Kass et al., 2002; Anderson and Normal Tension Glaucoma, 2003; Leske et al., 2007). For open angle glaucoma, hypotensive therapy is achieved using pharmacological and surgical approaches.

Pharmacologic treatments are targeted to either decrease the production or increase the drainage of the aqueous humor. These are typically delivered to the eye by topical application of eye drops. The most common first line class of drugs utilized is prostaglandin analogues, such as latanoprost (Stein et al., 2021). Though the mechanism is incompletely understood, these are thought to work by causing changes in the extracellular matrix of the uveoscleral aqueous outflow pathways, increasing drainage (Toris et al.,

2008). Other classes of drugs work by increasing aqueous drainage through the other outflow pathway, the trabecular meshwork (Woodward and Gil, 2004). These include drugs that cause pupil constriction, cholinomimetics such as pilocarpine, as well as alpha2 adrenergic agonist drugs like brimonidine. A newer class of drugs, Rho kinase inhibitors such as ripasudil, also act by increasing the outflow of aqueous (Inoue and Tanihara, 2013). Brimonidine also targets the other end of aqueous humor dynamics by decreasing aqueous humor production (Toris et al., 1995). Other classes of drugs that share this mechanism are topical beta blockers, like timolol (Zimmerman, 1993), and carbonic anhydrase inhibitors, like acetazolamide (Stoner et al., 2022). Combined formulations of these drugs are also often used, with the goal of acting on multiple pathways to reduce IOP.

In more severe or treatment-resistant cases of open-angle glaucoma, various surgical approaches can be used to lower IOP. The least invasive of these methods is laser trabeculoplasty, in which pulses from a laser are targeted at the trabecular meshwork. Laser treatment can lead to significant and sustained decreases of IOP by increasing aqueous outflow (Wong et al., 2015). In other severe cases with persistently high IOP, incisional approaches can be taken to lower pressures. These include trabeculectomy, or the creation of a new outflow path, and the placement of aqueous drainage devices (Investigators, 2000). More recent surgical options are less invasive. Called microinvasive glaucoma surgery (MIGS), these surgical approaches are targeted at lowering IOP while minimally disrupting the ocular tissue. These can be very effective and involve fewer complications (Fellman et al., 2020).

Despite the numerous effective tools available for lowering IOP, there is a persistent need for the development of new therapeutic tools. Even with clinically optimal IOP management many patients will continue to experience disease progression and vision loss (Heijl et al., 2002). As with other neurodegenerative diseases, much emphasis has been placed on the importance of developing neuroprotective treatments (Wareham et al., 2020). In order to modify the irreversible and vision-threating aspect of the disease, the loss of retinal ganglion cells, treatments must be developed that can protect cells from degenerating in response to glaucomatous stress. Development of such therapies

requires an intimate understanding of ganglion cell physiology and mechanisms of degeneration, as well as the protective and maladaptive roles played by all the cells in the retina.

1.5 Early pathophysiologic changes in glaucoma

1.5.1 Modeling glaucoma in rodents

Modeling glaucoma in animals allows for careful investigation of the mechanisms of glaucomatous degeneration. A wide variety of organisms has been used, including primates (Burgoyne, 2015), dogs (Kuchtey et al., 2011), cows (Gerometta et al., 2004), and zebrafish (Skarie and Link, 2008). Rodents, especially mice, are a popular model organism owing to the ease of genetic manipulation and the wide variety of available tools. Mouse models of glaucoma typically involve either genetic mutations, leading to a slow, age-dependent increase in intraocular pressure (IOP), or extrinsic manipulations causing acute IOP elevations.

The most used chronic genetic model of glaucoma is the DBA/2J mouse, which develops a form of pigment dispersion glaucoma. In these mice, mutations in the glycosylated protein nmb (*Gpnmb*) and tyrosinase-related protein 1 (*Tyrp1b*) genes lead to iris stromal atrophy, with intermediates of pigment production to leaking out and obstructing aqueous humor outflow (Anderson et al., 2002). The result is an age-dependent increase in IOP, with pressures reaching significant elevation by about 8 months of age (Libby et al., 2005). Over time these mice develop significant axonal degeneration and RCG loss. However, there is individual variability in the progression of the disease, with a distribution of pressures and pathology (Inman et al., 2006). Further considerations for using this model include the difficulty in additional genetic manipulation and the longer experimental timeline as the mice must be aged for months. Because of these, alternative inducible models of glaucoma have been developed.

Acutely inducible glaucoma models carry the advantage of being able to be done in a variety of different species and genetic backgrounds. These models typical involve manipulation of aqueous humor dynamics to increase IOP to varying degrees and over varying timelines (Pang and Clark, 2020). There are also pressure independent models, such as optic nerve crush or retinal ischemia/reperfusion injury,

which cause damage to RGCs but do not accurately recapitulate many features of human glaucoma (Lafuente et al., 2002; McGrady et al., 2022).

An early strategy for inducible modeling of glaucoma in rodents involves the injection of hypertonic saline into the episcleral veins (Morrison et al., 1997). This causes considerable sclerosis and obstruction of aqueous outflow, leading to significant degrees of IOP elevation that can persist for months in some animals. The model leads to a 10–100% of optic nerve axon loss, but many animals also develop excessive inflammation. Due to pressure elevations that are often much more significant than seen in human disease, individual variability, and the necessary surgical skills, this method is not used frequently in modern studies. Another sclerosis-based model utilized in rodents is laser photocoagulation of the trabecular meshwork (Ueda et al., 1998; Levkovitch-Verbin et al., 2002). Again, this leads to an obstruction of aqueous outflow, acutely elevating IOP. With this model IOP elevations are also quite significant, with a sharp spike in pressure. IOP elevations are more transient than in hypertonic saline models, and repeated treatments can be necessary to sustain pressure elevation (Aihara et al., 2003). This model is also associated with higher degrees of RGC death and evidence of significant RGC dysfunction in a shorter time frame than seen in human disease (Grozdanic et al., 2003), suggesting that it may be a larger and more acute injury model.

Non-sclerotic inducible glaucoma models typically involve the injection of a foreign substance into the anterior chamber to disrupt aqueous humor dynamics. One strategy is injecting a viscous substance, such as hyaluronic acid (Benozzi et al., 2002) or silicone oil (Zhang et al., 2019). These offer the advantages of being easier to perform than some of the sclerotic models as well as the ability to be a reversible insult (Nam et al., 2022). Rapid IOP elevation can be achieved, although early models required repeated injections to sustain elevation (Benozzi et al., 2002).

The model applied in this work is the microbead occlusion model of glaucoma (Sappington et al., 2010). In this model a small volume of polystyrene microbeads is injected into the anterior chamber of the eye. The beads travel with the flow of the aqueous humor and embed into the trabecular meshwork, accumulating and obstructing outflow. This obstruction is not complete and leads to a more moderate

degree of elevation compared to the aforementioned models, with IOP increasing about 20-40% above baseline measurements (Risner et al., 2018; Cooper et al., 2020; Risner et al., 2022). Occasionally a variant of this model, using magnetic microbeads, is applied (Samsel et al., 2011; Ito et al., 2016). This brings the advantage of being able to direct the beads into the iridocorneal angle but may be more traumatic and damage the trabecular meshwork.

With the microbead occlusion model IOP elevation can be achieved fairly rapidly, with elevations evident by two days after injection (Sappington et al., 2010). This elevation is sustained over a period of weeks and can be maintained out to 6+ weeks with repeat injections (Naguib et al., 2021). The pathophysiologic progression of disease laid out in this section is described within the time course of this model in mice. Early RGC dysfunction occurs within 1-2 weeks (Risner et al., 2018; Calkins, 2021), with overt signs of axonal degeneration and RGC death occurring much later, around 4 weeks and after (Calkins, 2021; Naguib et al., 2021; Risner et al., 2022). With this model, a more detailed understanding of the glaucomatous stress responses of RGCs and retinal glia has been developed.

1.5.2 Compartmentalized degeneration

Glaucomatous degeneration occurs as a result of RGC axonal damage at the optic nerve head (Quigley et al., 1981; Burgoyne, 2011). This localized axonopathy causes damage and dysfunction both proximal and distal to the site of injury. Within the axon, the injury leads to disrupted mechanisms of transport along the cytoskeleton. Evidence suggests that transport in the anterograde direction, away from the soma, is preferentially affected (Crish et al., 2010; Dengler-Crish et al., 2014). Deficits in transport can be detected early, after about 2 weeks of IOP elevation in the microbead occlusion model, preceding outright degeneration and cell death. This transport mechanism, involving the “walking” of kinesin proteins along the polarized microtubule structure within the axon, is vital for the movement of newly synthesized proteins and organelles, like mitochondria, down the long cell process and results in a deficit of these distal to the injury (Miller and Sheetz, 2004; Chang et al., 2006; De Vos et al., 2008). Following this transport deficit, axons distal to the injury begin to undergo a degenerative process characterized by

breakdown of the axonal structure and surrounding myelin. Ultimately, the central visual targets of the RGC axons in the thalamus and midbrain begin to degenerate (Crish and Calkins, 2015; Van Hook et al., 2020). Glaucomatous injury has even been linked to pathology in the visual cortex, two synapses downstream of the affected RGC axons (You et al., 2021).

Damage also occurs in the RGC proximal to the site of injury, affecting the dendrites and soma of the cell. Pruning of the dendritic tree also occurs prior to outright degeneration (Calkins, 2012). This process involves the complement-dependent and microglia-mediated loss of RGC dendritic complexity and length (Berry et al., 2015; Williams et al., 2016). Concurrently there is a loss of synapses on the RGC dendrites, reducing the input of visual information onto RGCs from bipolar and amacrine cells (Agostinone and Di Polo, 2015). This synapse loss and dendritic pruning occurs in both the ON and OFF sublaminas of the inner plexiform layer, but there is evidence (discussed in more depth later) that the OFF pathway may be preferentially affected (El-Danaf and Huberman, 2015; Ou et al., 2016). The cell somas of RGCs persist for some time despite degeneration of both axonal and dendritic components, remaining intact for many weeks in the microbead model (Calkins, 2012).

Proximal and distal programs of degeneration likely are separate processes, supported by evidence that dendritic pruning and axonal changes can proceed independently of each other (Risner et al., 2020a). This suggests that there are distinct mechanisms governing RGC degeneration which could be separately targeted. For example, mice lacking Bcl-2-associated X (BAX) protein, which are protected against apoptotic cell death, have reduced dendritic pruning and soma death in experimental glaucoma but still exhibit axonal deficits (Risner et al., 2022). Conversely, mice expressing the mutant *Wld*^{S} (slow *Wallerian degeneration*) allele that delays the Wallerian degeneration phenotype are protected against axonal effects of experimental glaucoma (Risner et al., 2021b). These studies nicely illustrate that multiple independent programs govern RGC degeneration and highlight the compartmentalized nature of these effects (Calkins, 2012).

1.5.3 Glial response

In glaucoma, astrocytes in the retina and optic nerve undergo significant changes throughout the course of disease. Early in disease they undergo morphological changes to become “reactive” astrocytes, a subset of which can be neurotoxic and amplify RGC death (Sun et al., 2013; Liddelow et al., 2017; Cooper et al., 2018; Cooper et al., 2020; Guttenplan et al., 2020). The induction of one neurotoxic subtype is mediated by microglial activation, where inflammatory stimuli cause microglia to release several pro-inflammatory cytokines. These in turn induce a neurotoxic astrocyte phenotype (Liddelow et al., 2017). Reactive astrocytes are key mediators of RGC death in glaucoma (Guttenplan et al., 2020). Interestingly, this same process of microglial activation and cytokine release alters the functional properties of astrocytic Cx43. Activated microglia stimulate an increase in astrocytic Cx43 hemichannel activity while simultaneously decreasing gap junctional coupling between astrocytes (Retamal et al., 2007). The involvement of Cx43 in the glial inflammatory response suggests that changes in Cx43 function may be involved in the early cellular responses to elevated IOP.

Gap junctions and hemichannels have seemingly opposing pathophysiologic roles. There are many neuroprotective functions of astrocytic gap junctional coupling. In contrast, hemichannels appear to have a pro-degenerative role during pathologic insult. Classically thought to be closed or inactive in a physiologic state, recent evidence supports a role for astrocyte Cx43 hemichannels in mediating processes such as the tuning of glutamatergic signaling through glial neurotransmitter release (Chever et al., 2014; Meunier et al., 2017). Nevertheless, prolonged stressors such as ischemia and oxidative stress can cause pathologic hemichannel opening (Danesh-Meyer et al., 2016). Their opening in this context is typically deleterious, associated with inflammation, changes in cell membrane potential, and difficulty with osmoregulation (Quist et al., 2000). Hemichannels have been implicated as a major cause of tissue swelling post-injury (Quist et al., 2000).

Inflammation is a prominent feature of numerous diseases, and astrocytes are a key cellular component of the neuroinflammatory response (Sofroniew, 2015). In general, inflammatory cytokines decrease gap junctional coupling between astrocytes, although there is some evidence that different

inflammatory conditions can affect Cx43 differentially, either increasing or decreasing coupling (Kielian, 2008; Liao et al., 2010). Hemichannels are also a key factor in inflammatory conditions. Proinflammatory cytokines, such as interleukin-1β and tumor necrosis factor-α, decrease the localization of Cx43 to the cell membrane (Retamal et al., 2007). The administration of lipopolysaccharide, an endotoxin found on gram-negative bacteria that is frequently used to experimentally induce inflammation, accelerates the degradation of Cx43 proteins in addition to decreasing expression (Liao et al., 2010). Alongside this structural change, there is a decrease in intercellular gap junctional communication with a concomitant increase in hemichannel activity (Retamal et al., 2007). In this context, hemichannels act as a key pro-inflammatory mediator. A major consequence of hemichannel opening is the extracellular release of ATP, which can bind to purinergic receptors and activate the NLRP-3 inflammasome (Price et al., 2020b), a protein complex that initiates inflammatory cell death. Specifically blocking Cx43 hemichannels decreases overall inflammation and protects against tissue damage (Chen et al., 2018). This effect appears to be in part due to decreased inflammasome activation (Louie et al., 2021). In fact, specific blockade of Cx43 hemichannels is actively being investigated as a potential therapeutic for many neurologic and non-neurologic diseases (Galinsky et al., 2017; Mao et al., 2017; Chen et al., 2018; Tonkin et al., 2018; Kuo et al., 2020; Price et al., 2020b).

It is less clear whether Cx43 gap junctional coupling is exclusively protective or maladaptive in pathological conditions. From a metabolic perspective, the redistribution of resources through the gap junctional network seems to be neuroprotective. From a buffering perspective, the network allows astrocytes to regulate the extracellular environment more effectively. However, because of the nonselective nature of these gap junctions there is also the potential that they mediate the spread of damaging cues. In one study, overexpression of Cx43 in injury-resistant glioma cells left the cells more vulnerable to damage, as they were increasingly coupled to more vulnerable cells (Lin et al., 1998). There was an associated increase in the spread of calcium waves through the cells. Calcium waves are the primary means of astrocytic signaling, in the absence of an excitable membrane, and coordinate important physiologic processes such as glial neurotransmitter release (Bazargani and Attwell, 2016). However,

excessive and dysregulated intracellular calcium signaling can activate pro-apoptotic pathways (Pinton et al., 2008). Gap junctional networks could mediate excessive calcium spread from astrocyte to astrocyte, acting as a conduit for the propagation of disease. The Cx43 overexpression leading to death of neighboring glioma cells may have been a cell-type specific effect, however. In studies involving a variety of animal models of neurologic diseases, increasing gap junctional coupling is associated with decreased neuronal death and improved histologic measures (Kim et al., 2018; Freitas-Andrade et al., 2020).

The initial site of stress conveyed to axons by elevated intraocular pressure is at the optic nerve head (ONH) (Morrison et al., 2011), the portion of the optic nerve where the unmyelinated RGC axons pass through the sclera. This region of the nerve is densely populated with astrocytes, which offer structural and physiologic support to the axons and are involved in early responses to the stress of elevated IOP. Astrocytes are also present in significant quantities throughout the inner retina. In both humans and rodents there are astrocytic networks localized to the ganglion cell layer and the nerve fiber layer, which see significant degenerative changes in severe glaucoma. Immunolabeling shows that these are continuous with the optic nerve astrocytes (Zahs et al., 2003; Kerr et al., 2011).

Astrocytes in the retina express both Cx43 and Cx30. Cx30 is localized primarily to astrocytic endfeet near blood vessels whereas Cx43 is more diffusely distributed along the astrocyte (Zahs et al., 2003; Kerr et al., 2011). There is also some expression of Cx43 in retinal Müller glia, though this varies by animal model and occurs in significantly lower levels than in astrocytes (Kerr et al., 2010). Within the optic nerves of humans and rodents, particularly in the ONH, there is dense immunolabeling of Cx43 localized to astrocytes (Morgan, 2000; May and Lutjen-Drecoll, 2002; Kerr et al., 2010). A densely connected astrocytic network may be of particular physiologic importance for the ONH portion of the nerve. The axons in this region are unmyelinated. Without myelination, axons have decreased signaling efficiency and much higher metabolic demand (Neishabouri and Faisal, 2011). Astrocytic Cx43-mediated networks may be important for supporting the demand of this region and serve as a defense against

pathologic stress. Alterations in the function of this network could increase the susceptibility of this key visual pathway to stress and injury.

Glial activation in the retina and optic nerve is an early and persistent feature of glaucoma (Wang et al., 2002). Real time PCR comparing primary cultures of astrocytes from normal and glaucomatous human eyes indicate that expression of *GJA1* is higher in glaucomatous astrocytes compared to normal age matched controls (Hernandez et al., 2008). Structurally, changes in immunolabeling of Cx43 on the optic nerve head have been demonstrated in a study of post-mortem eyes of glaucoma patients (Kerr et al., 2011). There was a significant increase in Cx43 on astrocytes within in the lamina cribrosa, at the site of mechanical stress to the ONH. In the retina there was an increase in both the intensity and amount of Cx43 labeling in the ganglion cell layer. These patterns parallel those seen in animal models of optic nerve injury, although they reflect changes over a longer time scale.

The mechanism of injury in glaucomatous neurodegeneration involves an increased genetic and/or environmental susceptibility to elevated IOP at the optic nerve head. Exposing primary human ONH astrocytes to elevated hydrostatic pressure causes a decrease in intercellular communication and a redistribution of Cx43 away from the cell membrane (Malone et al., 2007). The remaining gap junctions on the membrane are also more highly phosphorylated. Phosphorylation on several serine and tyrosine residues in the C-terminal region of the Cx43 protein can dramatically decrease the permeability of the gap junction (Lampe and Lau, 2004; Ek-Vitorin et al., 2018). Thus, even when there is increased Cx43 expression, as seen in glaucomatous tissue, there is a decrease in the permeability of gap junctions. As seen in other models of neurologic disease, astrocytes in glaucomatous optic nerves have increased expression of Cx43, which leads to increased hemichannel activity, but paradoxically there is a decrease in gap junctional communication. The structural changes in Cx43 distribution have important functional implications for the progression of glaucoma. Though astrocytic Cx43 networks are protective against metabolic stress to an extent, astrocytes lose their gap-junctional coupling when deprived of glucose for longer periods of time (Lee et al., 2016). Chronic metabolic deprivation also increases hemichannel permeability (Contreras et al., 2002). Axons in the glaucomatous optic nerve are energy depleted and

exhibit signs of chronic metabolic stress, marked by decreased available glucose and lower expression of the monocarboxylate transporters involved in the astrocyte neuron lactate shuttle (Harun-Or-Rashid et al., 2018).

In the microbead occlusion mouse model of glaucoma, elevated IOP in one eye causes the mobilization of glycogen stores from the unaffected eye to the damaged eye (Cooper et al., 2020). This redistribution improves axon function and visual function in the acceptor eye but leaves the donor eye vulnerable to subsequent damage. Genetically knocking out Cx43 in these mice eliminates this transfer of resources. This evidence emphasizes both the neuroprotective and maladaptive potential of astrocytic networks in the context of degenerative disease.

Alongside metabolic changes, oxidative stress is a key factor in the pathophysiology of glaucoma (Chrysostomou et al., 2013). It is also a regulator of gap junctional coupling. In other cells, like osteocytes, high levels of oxidative stress tend to decrease coupling and increase hemichannel activity (Kar et al., 2013). Increasing Cx43-mediated coupling in cultured cells is protective against hydrogen peroxide-induced cytotoxicity, suggesting that it helps mitigate the damage caused by oxidative stress (Kar et al., 2013; Zhao et al., 2017). The changes to astrocytic coupling caused by glaucoma may be part of a vicious cycle that causes further metabolic stress, as the injured regions are cut off from distant glycogen supply. It also likely decreases the ability of astrocytes to defend against cytotoxic damage. However, this may serve to isolate an injured region, preventing the further spread of damage to other sites.

Studies of unilateral optic nerve damage offer an insight into the role of gap junctional networks into the spread of pathology. Animal studies demonstrate that unilateral trauma results in changes to the eye contralateral to the injury, with marked alterations to retinal astrocytes, microglia, and ganglion cell populations (Bodeutsch et al., 1999; Kanamori et al., 2005; Panagis et al., 2005; Sobrado-Calvo et al., 2007; Macharadze et al., 2009). The response in the contralateral eye is weaker than in the eye ipsilateral to the injury, but still significantly greater than control tissue from uninjured animals. Astrocytes in the contralateral retinal ganglion cell and nerve fiber layers take on a reactive phenotype, characterized by

cellular hypertrophy and increased labeling of glial fibrillary acidic protein (GFAP) (Kerr et al., 2012). They also express greater levels of Cx43, raising the possibility that this spread of damage could be mediated by astrocytic networks.

1.5.4 Altered RGC excitability

Early pathophysiologic changes in glaucoma, particularly those that appear to precede cell death, represent promising targets for neuroprotective therapies. A key change in RGC physiology in response to glaucomatous stress is an alteration in electrical excitability. Many neurodegenerative diseases involve challenges to processes, such as intrinsic neuronal properties and astrocytic spatial buffering, that maintain axon function and neuronal excitability (Zeron et al., 2002; van Zundert et al., 2008; Sompol et al., 2017). In the microbead glaucoma, an enhancement of neuronal excitability occurs fairly early in the course of disease, around two weeks of IOP elevation (Risner et al., 2018). Excitability enhancement is reflected experimentally by abnormally brisk responses to light stimulation and direct application of depolarizing current (two methods used extensively in this work and described in more depth later). This change is caused by altered expression of voltage-gated sodium channels responsible for action potential generation (Risner et al., 2018). It is possible that this change underlies an adaptive mechanism whereby increasing firing rate helps maintain the encoding of light stimuli, preventing the selective degeneration of poorly functioning cells. However, this mechanism may also be maladaptive. As previously mentioned, RGCs are metabolically stressed by IOP elevation. Hyperexcitable cells require higher energy supplies to maintain ionic balance across their membrane and generate action potentials. Thus, in a pathological context hyperexcitability may push the metabolic demand of these cells beyond the available supply, worsening the degree of stress. Indeed, hyperexcitability and degeneration appear closely linked in neurodegenerative disease (Siskova et al., 2014).

The period of early hyperexcitability is followed by a decrease in RGC excitability, to levels below normal functioning (Risner et al., 2020b; Risner et al., 2021b; Risner et al., 2022). This timepoint coincides with the early stages of pathological evidence of degeneration in the optic nerve, and likely

reflects highly dysfunctional RGCs no longer effectively communicating light information to the brain. While hyperexcitability is driven largely by axogenic changes, later decreases in excitability may be the result of changes to both synaptic input (Agostinone and Di Polo, 2015) and axonal properties (Risner et al., 2020b). This work investigates axonal mechanisms that could potentially underlie this change and may link excitability changes to susceptibly to degeneration.

1.5.5 Dysregulation of the extracellular milieu

A shared hallmark of many neurodegenerative diseases is pathologic alteration to the composition of the extracellular space in neural tissue. These alterations can be both a result and cause of neuronal dysfunction, involved in a vicious cycle that ultimately leads to cell death. One of the most notable of such alterations involves the accumulation of abnormal proteins in the extracellular space, which is often a key diagnostic criterion for neurodegenerative disease. In Alzheimer's disease, a neurodegenerative disorder that leads to memory and cognitive impairments, abnormal deposits of the amyloid beta protein form in the extracellular space, forming plaques (Rahman and Lendel, 2021). In Parkinson's disease, a neurodegenerative disease affecting the brain's motor system, extracellular buildup of abnormal alpha synuclein protein can significantly contribute to the pathology (Yamada and Iwatsubo, 2018). Often these protein accumulations place further stress on neurons by disrupting normal physiologic processes, such as impeding synaptic transmission (Diogenes et al., 2012) or impeding regulation of the ion gradients that govern membrane potential (Shrivastava et al., 2015). Compounding these abnormal protein aggregates are disruptions to the extracellular matrix, a scaffold of proteins and other molecules that provide structural support to cells in tissue (Downs et al., 2022; Johnson et al., 2022). Disruptions of this structure contribute to the spread of pathology from cell to cell, speeding up disease progression (Moretto et al., 2022). Consequently, targeting the extracellular matrix is being investigated in a neuroprotective capacity (McGrady et al., 2021).

Central to the themes of this work are disrupted homeostasis of extracellular ion and neurotransmitter levels in neurodegeneration. These processes are tightly linked to the interactions

between neurons and glia which, as introduced above, become altered in neurodegeneration. Most directly linked to cell death are dysregulations in the homeostasis of the excitatory neurotransmitter glutamate and the cation calcium. During excitatory neurotransmission glutamate is released into the extracellular space. Under typical conditions this transmitter is quickly taken back up by neuronal and glial transporters. In periods of excess firing or pathologic disruptions, extracellular levels of glutamate can build up as these reuptake mechanisms are overwhelmed. Excess glutamate levels can in turn lead to neuronal death via a process known as excitotoxicity (Dong et al., 2009). This further disrupts important cellular functions and places additional extrinsic stress on neurons via increased oxidative stress (Nicholls, 2004), increased metabolic and mitochondrial pressure (Duchen, 2004), and impaired calcium ion regulation (Friedman, 2006; Mattson, 2007; Dong et al., 2009). Disruption of glutamate reuptake is seen across a variety of different neurodegenerative diseases, including Parkinson's disease (Wang et al., 2020), Huntington's disease (Lievens et al., 2001), and Alzheimer's disease (Brymer et al., 2023).

Another important homeostatic process disrupted in neurodegenerative disease is the regulation of extracellular potassium. Like glutamate and calcium, potassium levels are linked to neuronal firing and excitability. Elevations in potassium concentration contribute to abnormal neuronal membrane potentials and excitability and can further contribute to excitotoxic cell death. Like glutamate, potassium is regulated by a combination of neuronal and glial proteins, as described in more depth above. Alterations in these regulatory mechanisms, particularly with respect to glial uptake of potassium, can be seen in amyotrophic lateral sclerosis (Bataveljic et al., 2012) and Alzheimer's disease (Nwaobi et al., 2016). Elevated extracellular potassium, along with altered expression and function of neuronal potassium channels can in turn lead to neuronal hyperexcitability, increased oxidative stress, and further metabolic pressures, thereby further stressing neurons to the point of excitotoxic cell death (Frazzini et al., 2016).

Many of these alterations are seen specifically in glaucoma as well, highlighting shared processes of neurodegeneration and emphasizing the importance of understanding these processes in order to protect neuronal function. In addition to intrinsic changes to excitability challenging the metabolic support network, there are extrinsic factors imposing additional stress on RGCs. As previously

introduced, retinal glia perform myriad homeostatic roles to maintain RGC function in periods of stress. A glial function tightly linked to neuronal excitability is the regulation of the ionic contents of the extracellular space. Extracellular ionic conditions are tightly regulated to maintain normal excitability and minimize cellular stress. Changes to the balance of ions across a neuronal membrane places additional demand on Na/K-ATPases, which are highly metabolically demanding. Acute alterations to ionic balance, such as an elevation of extracellular potassium, can also cause neuronal depolarization and further alter excitability.

Potassium ions are of particular importance in the context of glaucomatous degeneration. Potassium concentration is tightly regulated by astrocytes and Müller glia under physiologic conditions, rarely fluctuating more than a few millimolar (Heinemann and Lux, 1977). However, glial mechanisms regulating extracellular potassium can become disrupted in glaucoma via alterations to the function of both Müller glia and astrocytes (Fischer et al., 2019a; Fischer et al., 2019b; Cooper et al., 2020). Dysregulated potassium can contribute to RGC degeneration via interaction with apoptotic cell death pathways (Diem et al., 2001b; Koeberle et al., 2010).

The consequences of altered extracellular milieu, particularly elevated potassium concentrations, is a central focus of this work. A vicious cycle of hyperexcitability, ionic imbalance, and metabolic stress represents a potential target for early intervention to prevent cell death. This work seeks to understand how different types of RGCs respond to this stress and regulate their excitability in health and disease.

1.5.6 Evidence for differential susceptibility of RGCs in glaucoma

Certain RGC types appear to be more sensitive to IOP-related stress than others. In various models of experimental glaucoma, properties such as RGC light response, dendritic branching, and synapse loss appear to proceed at different rates for different RGC cell types (Della Santina et al., 2013; El-Danaf and Huberman, 2015; Ou et al., 2016; Kong et al., 2021; Risner et al., 2021b). Across these modalities, there is building evidence that OFF RGCs may be more sensitive to glaucomatous stress than their ON counterparts. These cells show greater degrees of reduced synaptic input in the OFF sublamina of the

inner plexiform layer (El-Danaf and Huberman, 2015; Ou et al., 2016) and are less protected by the *Wld*^{S} mutation (Risner et al., 2021b). Certain subtypes, such as alpha OFF-transient cells, may be even more susceptible to stress based on their intrinsic properties (Della Santina et al., 2013; Risner et al., 2021b).

Discerning which properties of RGCs may make them more sensitive to IOP-related stress may elucidate specific targetable mechanisms for neuroprotection. There is growing evidence that intrinsic electrical properties of RGCs, such as those governing their excitability, are key distinguishers of their physiologic function (Werginz et al., 2020; Wienbar and Schwartz, 2022). Recent studies have also used optic nerve injury models to try to determine molecular properties of RGCs that make them either more or less susceptible to degeneration (Tran et al., 2019). This work seeks to merge these two concepts, evaluating factors that distinguish the excitability properties of two RGCs and determining how those may impact their resilience to stress in experimental glaucoma.

1.6 Hypothesis and specific aims

1.6.1 Central hypothesis

We propose that differential sensitivity to ionic stress is a key factor regulating RGC excitability, and that there are adaptive mechanisms employed in response to glaucomatous damage to regulate neuronal excitability.

1.6.2 Aims

Aim 1: Determine the interaction between retinal ganglion cell (RGC) type-intrinsic excitability differences and sensitivity to ionic stress.

Across the central nervous system there is considerable heterogeneity in neuronal physiology, even within a small region, with variably tuned electrical properties allowing for complex patterns of information encoding. In the innermost layer of the retina, there are at least 20-40 different types of RGCs, which are responsible for transmitting visual information from the retina to the brain. RGC heterogeneity is functionally significant, as it facilitates the encoding of complex visual stimuli. Recently there has been growing interest in how intrinsic electrical properties, such as mechanisms driving action

potential generation, further distinguish different RGC types beyond well-defined differences in presynaptic circuitry. Here, we tested intrinsic excitability differences between two major types of RGCs, alpha ON-Sustained and alpha OFF-Sustained cells, in the context of an acute ionic stressor. We evaluated neuronal responses to depolarizing current and measured properties of action potential generation to test the working hypothesis that *intrinsic physiologic differences between RGCs are driven in part by the sensitivity of the cells to the extracellular potassium concentration.*

Aim 2: Determine how RGCs adapt to prolonged ionic stress in glaucoma.

To develop treatments that can protect against neurodegenerative disease it's important to understand how neurons respond to stress, delineating adaptive and maladaptive changes. In glaucoma retinal ganglion cells, the neurons in the retina that convey visual information to the brain, degenerate due to stress related to sensitivity to intraocular pressure. Though there are treatments that can effectively control pressure, some patients with glaucoma still lose vision. Studies of experimental glaucoma show that early in the disease, retinal ganglion cells are stressed with dysregulated potassium homeostasis and exhibit altered intrinsic electrical properties. Here, we utilized an inducible glaucoma model in mice to measure changes in RGC excitability in the setting of acutely elevated extracellular potassium. We determined the differential effects of acute ionic stress after prolonged intraocular pressure elevation to test the working hypothesis that *retinal ganglion cells undergo adaptive changes in response to glaucomatous stress to lessen the impact of dysregulation of the extracellular milieu.*

Aim 3: Evaluate the contribution of the axon initial segment (AIS) dimensions to RGC excitability, in development and disease.

The excitability of a neuron is regulated by structural components of the axon. The axon initial segment (AIS) is a protein scaffold enriched for voltage-gated ion channels and is the site of axon potential generation. The dimensions of the AIS, such as its distance from the soma and the length of the scaffold, significantly influence a neuron’s excitability. Establishment of AIS structure is well regulated, with its dimensions distinguishing the light encoding properties between similar RGC subtypes.

Interestingly, the AIS is a plastic structure which can adapt in response to physiologic and pathologic stimuli to maintain appropriate action potential generation. Here, we utilize *in vivo* and *in vitro* approaches to evaluate properties governing AIS development and adaptation to degenerative stress in order to test the working hypotheses that *1. Axon development and degeneration can be modeled in vitro* and *2. Alterations to AIS structure explain physiologic differences in neuronal excitability and underlie degenerative changes in axonopathy*.

CHAPTER 2

SENSITIVITY TO EXTRACELLULAR POTASSIUM UNDERLIES TYPE-INTRINSIC DIFFERENCES IN RETINAL GANGLION CELL EXCITABILITY*

2.1 Introduction

The central nervous system is composed of many neuronal classes and types defined by genetic, neurochemical, morphologic, and physiologic properties that determine function. This biologic complexity is apparent across neural tissues and exemplified in the retina, which is a projection of the diencephalon. Different retinal neuronal classes and types interact through synaptic and electrical signals, forming local receptive fields. Receptive field elements converge, diverge, and converge again to optimize the signal-to-noise ratio of graded potentials received by postsynaptic retinal ganglion cells (RGCs) (Cohen and Sterling, 1990; Copenhagen et al., 1990; Asari and Meister, 2012). RGCs integrate postsynaptic potentials, generate spike trains that encode sensory information, and relay action potentials with high fidelity to central targets (Uzzell and Chichilnisky, 2004; Pillow et al., 2005). The presence of a large diversity in RGC response properties underlies the ability to encode complex visual scenes (Baden et al., 2016).

Currently, RGC types are distinguished by both intrinsic and extrinsic properties, including genetic profile, transcriptomics, morphology, regular topographic spacing, and physiologic response to stimuli (Sanes and Masland, 2015; Shekhar and Sanes, 2021). Based on these variables, 20 – 40 different RGC types of have been identified, depending on species (Sanes and Masland, 2015; Baden et al., 2016; Bae et al., 2018; Tran et al., 2019; Goetz et al., 2022). Measuring RGC response bias to light increments and decrements has been a mainstay in RGC taxonomy, but this method tests both extrinsic influences,

---

*Content in this chapter has been published in the following paper:

- **Boal, A. M.**, McGrady, N. R., Risner, M. L., & Calkins, D. J. (2022). Sensitivity to extracellular potassium underlies type-intrinsic differences in retinal ganglion cell excitability. *Frontiers in cellular neuroscience*, *16*, 966425. https://doi.org/10.3389/fncel.2022.966425

such as presynaptic inputs, and intrinsic mechanisms, such as threshold for action potential generation. Alternatively, evidence suggests RGC types may be physiologically defined by measuring their responses to application of hyperpolarizing or depolarizing currents (Margolis and Detwiler, 2007; Mitra and Miller, 2007b; a; Cai et al., 2011). Testing these intrinsic properties is important because inherent differences can significantly influence spiking output in RGCs, establishing different light responses in cells with similar synaptic inputs (Emanuel et al., 2017; Werginz et al., 2020; Wienbar and Schwartz, 2022).

Here, we tested physiologic differences between two RCG types with distinct synaptic inputs, alpha ON-Sustained (αON-S) cells, which generate sustained firing of action potentials to light increments, and alpha OFF-Sustained (αOFF-S) cells, which are inhibited by light and produce sustained firing upon light decrement. We found that these two types also demonstrate different intrinsic responses to application of depolarizing currents and correspondingly distinct action potential (AP) waveforms. We also demonstrated that sensitivity to extracellular K^+ concentrations may mechanistically underlie these differences in excitability profiles and establish thresholds for depolarization block, which is a mechanism that limits neuronal firing rate during excess depolarization due to inactivation of voltage-gated sodium channels. These results support the growing body of evidence that RGC responses are not only determined by presynaptic circuitry but also are significantly impacted by variability in intrinsic neuronal mechanisms.

2.2 Materials and methods

2.2.1 Animals

We obtained C57Bl/6J mice (6 male, 2 female, 14-17 weeks old) from Jackson Laboratories (Bar Harbor, ME, RRID: IMSR_JAX:000664). Mice were housed at the Vanderbilt University Division of Animal Care and maintained on 12-hr light/dark cycle. Animals were allowed water and standard rodent chow *ad libitum*. All animal experiments were approved by the Vanderbilt University Medical Center Institutional Animal Care and Use Committee.

2.2.2 Electrophysiological recordings

Animals were euthanized via cervical dislocation, eyes were enucleated, and the retinas were dissected out under long-wavelength illumination (630 nm, 800 μW/cm^2, FND/FG, Ushio, Cypress, CA). Retinas were placed in carbogen-saturated Ames' medium (US Biologic, Memphis, TN) supplemented with 20 mM D-glucose and 22.6 mM $NaHCO_3$ (pH 7.4, 290 Osm). Each retina was mounted flat onto a physiological chamber, inner retina facing upwards, and perfused at a rate of 2 ml/min with Ames' medium maintained at 35°C (Model TC-344C, Warner Instruments, Hamden, CT).

Retinal ganglion cells (RGCs) were viewed under DIC using an Andor CCD camera attached to an Olympus BX50 upright microscope at 40×. RGCs were targeted for intracellular recording with pipettes pulled from borosilicate glass (I.D. 0.86mm, O.D. 1.5mm; Sutter Instruments, Novato, CA) and filled with (in mM): 125 K-gluconate, 10 KCl, 10 HEPES, 10 EGTA, 4 Mg-ATP, 1 Na-GTP, and 0.1 ALEXA 555 (Invitrogen, Carlsbad, CA). The intracellular solution pH was 7.35 and osmolarity was 285 Osm. Pipettes containing intracellular solution had a resistance between 4–8 MΩ. Whole-cell signals were amplified (Multiclamp 700B, Molecular Devices, San Jose, CA) and digitized at a sampling rate of 10 kHz (Digidata 1550A, Molecular Devices, San Jose, CA). Access resistance was monitored and maintained ≤30 MΩ. All recordings were performed in current-clamp whole-cell patch-clamp configurations.

During baseline recordings we measured resting membrane potential (RMP), spontaneous spiking, light-evoked spike activity (full-field 365+460nm, 300 μW/cm2, 3-s duration, CoolLED, pE-4000, Andover, UK), and current-evoked spiking while clamping the cell at 0 pA. Current-evoked spiking was measured during stepwise application of 1 s current pulses, ranging from 0 to +300 pA in 10 pA increments, with a 2 s inter-stimulus interval. Very few αOFF-S cells exhibited sustained spiking at stimuli greater than 300 pA so we set that as the upper limit for recordings. Current was clamped at 0 pA between test pulses.

2.2.3 High extracellular potassium recordings

A second batch of Ames' medium was prepared as described above, but with an additional 5 mM of KCl (i.e., high K^+). After baseline recordings were completed for each cell, the high K^+ medium was washed into the recording chamber while the RGC spontaneous membrane voltage was continuously recorded. Before performing experiments, we allowed a wash on period of 5-6 min, allowing RGC membrane potential to stabilize. High K^+ experimental recordings (RMP, spontaneous activity, light-evoked spiking, current-evoked spiking) were then performed as described above. After high K^+ experiments, the extracellular medium was switched back to the baseline solution, and RGC membrane voltage was continuously measured during a wash off period of 10-20 min, allowing RGCs to recover. Full recovery typically took 10-15 min, although it occasionally required up to 20 min. We limited the number of experimental protocols to reduce the time of high K^+ exposure. Furthermore, to limit potential cumulative effects of high K^+ wash on/off, we limited the total number of cells that were recorded from each retina to no more than four.

2.2.4 RGC Physiology Analysis

Raw electrophysiology data files were analyzed in Python 3.9 (RRID: SCR_008394) using the pyABF 2.3.5 module (Harden, 2022) and SciPy 1.7.1 modules (RRID: SCR_008058)(Virtanen et al., 2020). The SciPy.Signal "find_peaks" function was used for action potential (AP) detection with specified parameters of 20 mV minimum prominence and a distance threshold of 1.5 ms between spikes. Spike rates for current-evoked spiking protocols were reported as the average rate for 2 adjacent 10 pA increments of stimulation (20 pA bins). For AP shape analysis, a cubic spline function was fit to each AP waveform to increase resolution. The AP half-width was measured as the duration of the AP, in ms, where the membrane potential was above the midway point between each AP peak and minimum after-hyperpolarization.

2.2.5 Immunohistochemistry and Imaging

After physiology, retinas were placed in 4% paraformaldehyde (PFA) at 4°C for 24 hr. After fixation, retinas were immunolabeled for choline acetyltransferase (ChAT, 1:100; Millipore, Burlington, MA, Cat. #AB144P, RRID: AB_2079751) and ankyrin-G (AnkG, 1:200; NeuroMab N106/36; Antibodies, Inc Cat. # 75-146, RRID:AB_10673030). Retinas were first blocked in 5% normal donkey serum for 2 hr, then incubated in primary antibodies for 3 d at 4°C, and finally incubated for 2 hr at room temperature with donkey anti-goat Alexa 647 and donkey anti-mouse Alexa 488 secondary antibodies (Jackson ImmunoResearch, West Grove, PA; RRID: AB_2340437, RRID:AB_2341099). We used an Olympus FV1000 inverted microscope to obtain micrographs of RGC profiles. Image analysis, including creating orthogonal projections used for visualization of dendritic stratification depth, was performed using ImageJ (NIH, Bethesda, MD). Soma size was determined in ImageJ by outlining the area encompassed by the soma in the maximum Z-stack projection from the confocal image of each dye-filled cell.

2.2.6 Axon Initial Segment Measurements

8 αON-S and 6 αOFF-S cells had identifiable AIS labeling. Fluorescence of AnkG was measured from the edge of the soma along the axon of each RGC in ImageJ. Background fluorescence was subtracted from AnkG intensity profiles using a rolling ball filter with a radius of 50. Smoothed AnkG profiles were generated using a Savitzky-Golay filter with a first order polynomial fit. Axon initial segment (AIS) bounds were systematically defined as the extent where smoothed ankG values were greater than 50% of the difference between baseline and maximum intensity. 1 αON-S AIS was excluded from analysis as its length was identified as a significant outlier by Grubbs' Test (alpha = 0.05).

2.2.7 Data Analysis and Statistical Tests

All data are reported as mean ± standard error of the mean (SEM) unless otherwise indicated. All statistical tests were performed in GraphPad Prism 9 (Graphpad Software, San Diego, CA). All data sets were checked for normality. Where appropriate, parametric statistical tests (unpaired t-test, paired t-test,

2-way ANOVA, simple linear regression) were performed. Additional statistical analysis was done performed using mixed-effects analysis where indicated. We defined statistical significance as a p-value of 0.05 or less. Exact p-values are indicated in figure legends, alongside the specific statistical test used for each analysis.

2.3 Results

2.3.1 Intrinsic cell type-specific differences in spike rate and waveform

We targeted α-type RGCs from intact retinas for whole-cell current-clamp recording and dye filling by identifying large cell bodies. Following physiology, we recovered morphology of dye-filled cells by confocal microscopy. As before (Risner et al., 2018; Risner et al., 2020a; Risner et al., 2021b), we separated RGC types based on soma size, dendritic stratification within the inner plexiform layer (IPL), and light-evoked responses. Here, we focused our analysis on two well-characterized αRGCs: αON-S (n = 11 cells from 6 mice) and αOFF-S RGCs (n = 6 cells from 5 mice) (Krieger et al., 2017).

αON-S RGCs possessed large cell bodies (307.7 ± 22.9 μm^2) with dendritic arbors projecting within the proximal plexus formed by starburst amacrine cell dendrites, which we identified by choline acetyltransferase (ChAT) labeling (Famiglietti and Kolb, 1976; Galli-Resta et al., 2000)(**Fig. 2.1A**). αOFF-S RGCs also possessed large somas (209.2 ± 16.2 μm^2) although smaller than αON-S RGC bodies (p=0.0089). αOFF-S RGC dendritic arbors extended just beyond the distal ChAT band formed by starburst amacrine cell dendrites (**Fig. 2.1B**). Similar to previous reports (Risner et al., 2020a), we found αOFF-S RGC resting membrane potential (RMP) significantly more depolarized versus αON-S RGCs (-55.2 ± 1.0 mV vs. -59.7 ± 0.8 mV, p=0.004, **Fig. 2.1C**). RMP variability was consistent with previously published results (Pang et al., 2003; Risner et al., 2018). In addition to RMP, αON- and αOFF-S RGCs produced distinct voltage-gated responses to light stimulation. In the absence of light, αON-S RGC produced few action potentials (2.56 ± 0.69 Hz), but these cells generated robust and sustained spiking during light onset (**Fig. 2.1D**). αOFF-S RGCs spontaneously fired action potentials in the dark (12.61 ± 3.85 Hz), and light stimulation hyperpolarized membrane potential, reducing spiking. At light offset,

αOFF-S RGCs membrane potential increased, and these cells produced a brisk sustained volley of spikes, returning to baseline firing after about 3 s (**Fig. 2.1E**).

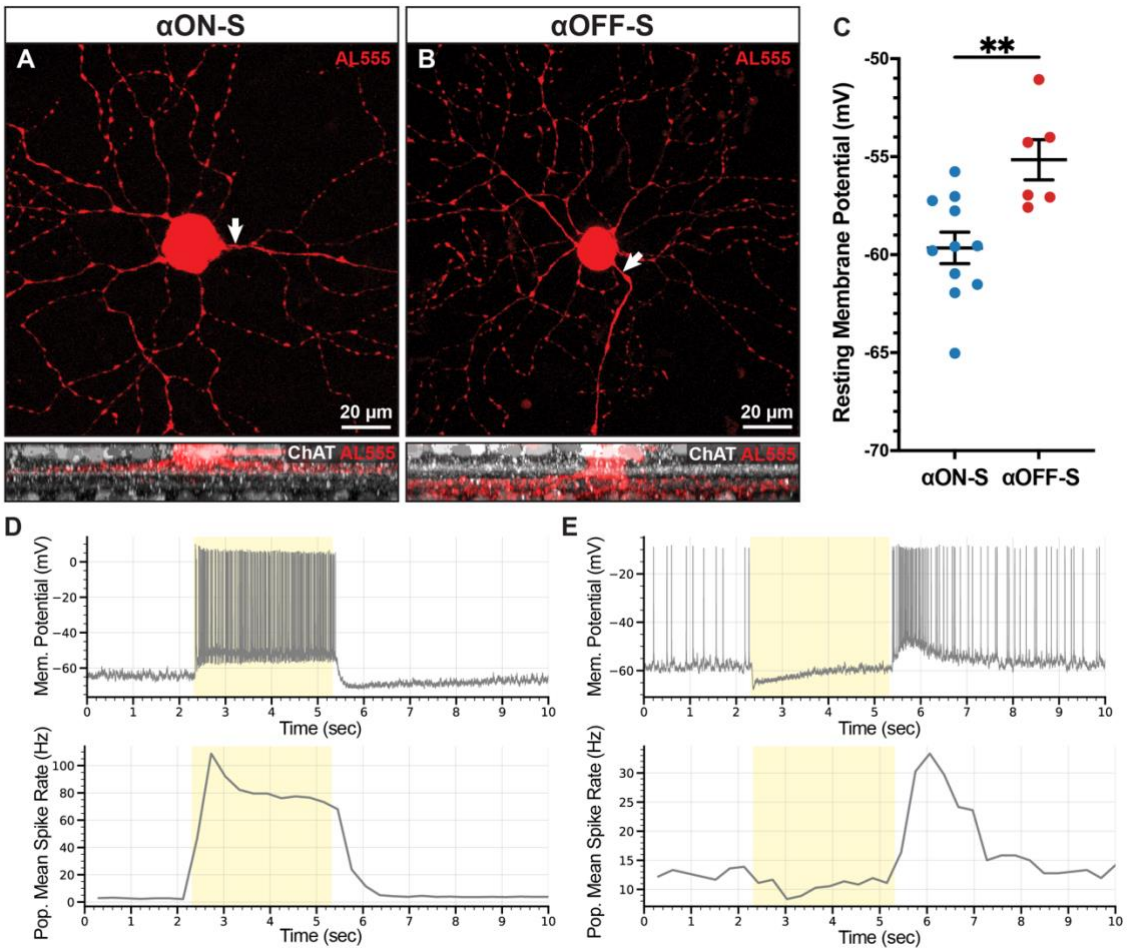

Figure 2.1 Morphologic and physiologic characterization of retinal ganglion cells (RGCs)
Patched cells were filled with Alexa-fluor 555 dye (AL555, red) and morphologically reconstructed with confocal microscopy. **(A-B)** Representative maximum intensity projections of alpha ON-sustained (αON-S) and alpha OFF-sustained (αOFF-S) RGCs demonstrate characteristic soma size and dendritic branching patterns (upper). White arrows indicate the axonal projection. Orthogonal projections of representative AL555-filled cells co-labeled for choline acetyltransferase (ChAT, white) demonstrate the branching of αON-S and αOFF-S dendrites in the ON- and OFF-sublaminas of the inner plexiform layer, respectively (lower). **(C)** αOFF-S RGCs have a more depolarized resting membrane potential (mean = -55.2 mV, n = 6) than αON-S (mean = -59.7 mV, n = 11) (p = 0.004, unpaired t test). Error bars +/- standard error of the mean. **(D-E)** Representative current-clamp traces of the responses of αON-S (D, upper) and αOFF-S (E, upper) RGCs to full-field light stimulation (yellow span) show the characteristic light responses of the two cell types. Mean firing rates of all αON-S (D, lower; n = 11) and αOFF-S (E, lower; n = 6) binned into 200ms intervals during light stimulation (yellow). ******: $p < 0.005$.

Similar to their light responses, RGCs also produce distinct responses to hyperpolarizing current injections (Mitra and Miller, 2007a; Margolis et al., 2010; Sladek and Nawy, 2020). Here, we investigated distinguishing properties of αON- and αOFF-S RGCs in response to depolarizing currents (Twyford et al., 2014; Kameneva et al., 2016). We performed current-clamp (0 pA) recordings and measured responses of

αRGCs to 1 s pulses of depolarizing current, ranging from 0 to 300 pA. We noticed αON-S RGCs typically required strong depolarizing currents to induce robust spiking (**Fig. 2.2A**, left). To the counter, αOFF-S RGCs often produced a sustained train of action potentials in response to relatively small depolarizing current injections, but larger depolarizing currents often reduced spiking (**Fig. 2.2A**, right). In addition to stimulus strength increasing variability in spike rate, we noted strong depolarizing currents

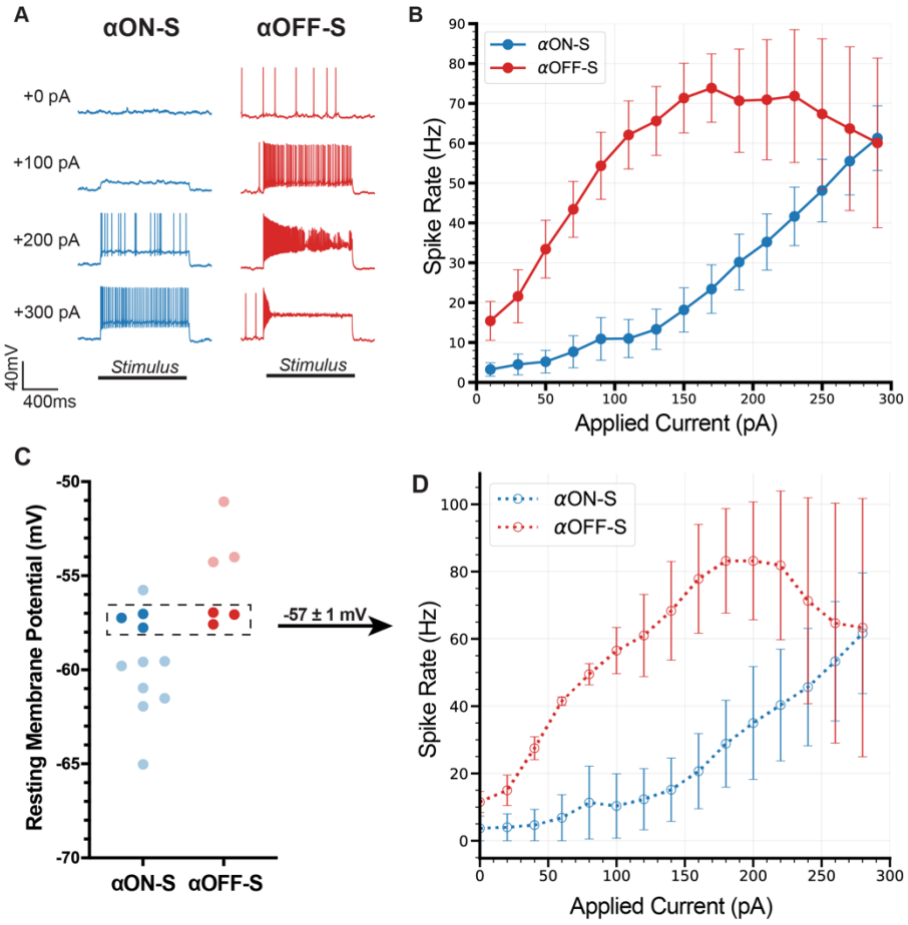

Figure 2.2 Current-evoked spike dynamics demonstrate cell type–intrinsic differences
The voltage responses of RGCs were recorded during 1 sec pulses of depolarizing current (0-300 pA, 2 sec inter-stimulus interval). **(A)** Representative current-clamp responses of αON-S (left) and αOFF-S (right) cells to 0, 100, 200, and 300 pA pulses. As magnitude of test current increases αOFF-S spike trains become more irregular and repetitive spiking is reduced. **(B)** αON-S and αOFF-S cells respond differently to the same magnitude of stimulation. αOFF-S cells fire more rapidly but ultimately plateau and decrease in rate. A two-way ANOVA analyzing the effects of cell type and depolarizing current on spike rate demonstrates a significant interaction between cell type and current ($p < 0.0001$). **(C)** To control for the influence of resting membrane potential (RMP) on current-evoked spiking we selected a subset of cells from both αON-S (n=3) and αOFF-S (n=3) cells with overlapping RMPs (-57 +/- 1 mV) for analysis. **(D)** This subset of αON-S and αOFF-S cells still respond differently to the same magnitude of stimulation, closely resembling the pattern of the full sample (Fig 2B). Two-way ANOVAs indicate that there is no significant difference between the current-spiking relationship for the subset vs. full sample for either αON-S ($p=0.9317$) or αOFF-S ($p=0.9618$). Error bars: +/- standard error of the mean.

increased variability in spike shape (**Fig. 2.2A**, right). We quantified the relationship between test current and spike rate of αON- and αOFF-S RGCs. We found a significant interaction between cell type and test current ($p < 0.0001$), indicative of cell type-intrinsic differences in excitability (**Fig. 2.2B**). To control for the potential influence of differing RMPs on these results (see **Fig. 2.1C**), we selected a subset of cells from each type with similar RMPs (-57 ± 1 mV, **Fig. 2.2C**) for comparison. We found that the current-

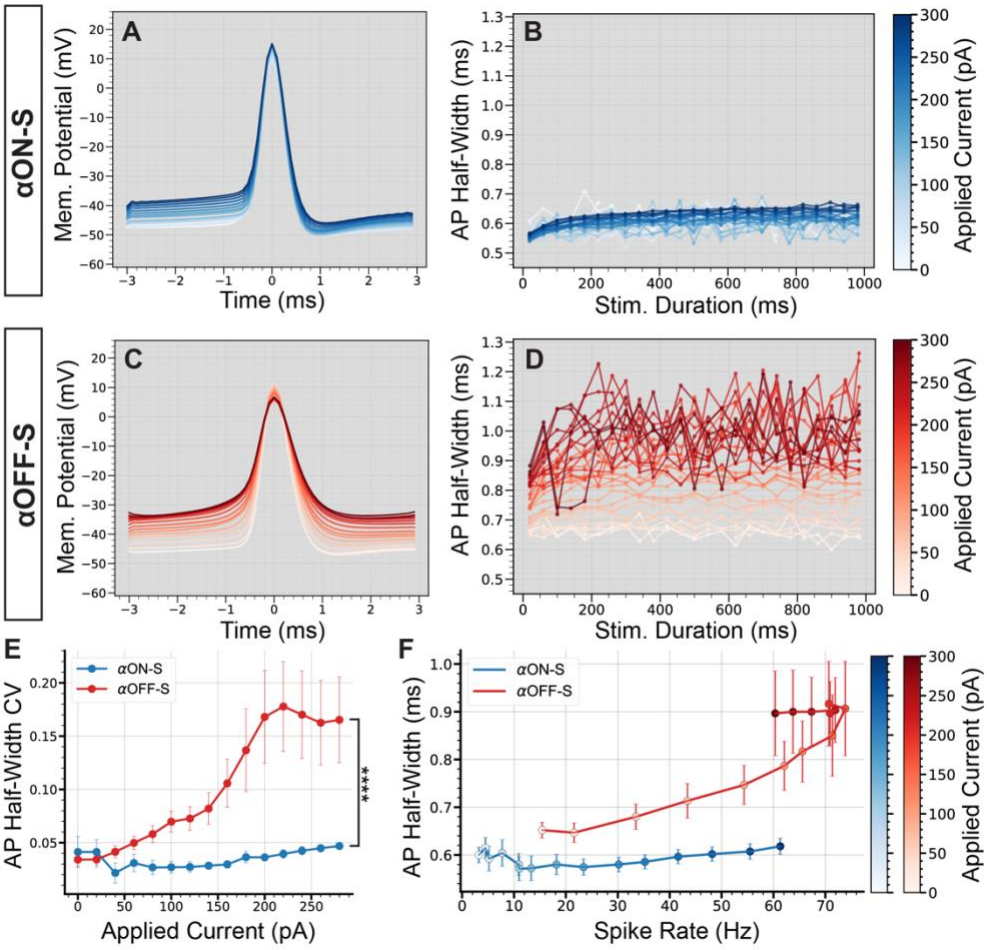

Figure 2.3 Cell type-specific differences in firing dynamics are reflected in the action potential shape

(A) Mean action potential (AP) shapes for αON-S cells at each current step. **(B)** Mean AP half-width vs. stimulus duration for each current level of αON-S cells. **(C)** Mean action potential (AP) shapes for αOFF-S cells at each current step. **(D)** Mean AP half-width vs. stimulus duration for each current level of αOFF-S cells. **(E)** AP half-width coefficient of variation (CV) vs. applied current for αON-S and αOFF-S cells. As depolarization increases, the variability of AP width increases significantly more for αOFF-S cells than αON-S (Mixed effects analysis interaction between current and cell type, $p < 0.0001$). **(F)** The mean spike rate at each current injection vs. the AP half-widths. αOFF-S RGCs demonstrate significant rate-dependent spike widening (simple linear regression, nonzero slope $p < 0.0001$) while αON-S RGCs do not ($p = 0.0668$). Error bars = mean +/- standard error of the mean.

spiking relationships of this subset closely resembled the pattern of the full sample of cells (**Fig. 2.2D**), and we did not detect a significant difference in current-evoked spike rates for the subset versus full sample for either αON-S (p=0.9317) or αOFF-S RGCs (p=0.9618).

As mentioned above, we noticed relatively small test currents appeared to impact αOFF-S RGC AP shape more than αON-S RGC APs. We determined if depolarizing currents distinctly affect αON-S versus αOFF-S RGCs by averaging AP waveforms at each test current. αON-S RGC AP waveforms remained relatively similar across test currents (**Fig. 2.3A**). During the duration of larger test currents, αON-S RGC AP half-width modestly increased, though remained consistent (**Fig. 2.3B**). The AP width of αOFF-S RGCs, however, grew larger with increasing depolarization (**Fig. 2.3C**). Interestingly, at larger currents, αOFF-S AP half-width variability appeared greater compared to αON-S RGCs (**Fig 2.3D**). To quantify this variability, we determined the coefficient of variation (CV) of AP half-widths for each stimulus. We found as depolarization increased, the variability of αOFF-S RGC AP half-width significantly increased compared to αON-S RGCs ($p < 0.0001$, **Fig. 2.3E**).

Others have found spike rate influences AP shape (de Polavieja et al., 2005). Because we found current-evoked spike rate is dependent on cell type (**Fig. 2.2**), we measured the influence of spike rate on AP half-width for both αON- and αOFF-S RGCs to determine if differences in AP width could be explained solely by firing rate (**Fig. 2.3F**). We found αOFF-S RGC AP half-widths significantly increased as spike rate increased ($p < 0.0001$). To the counter, αON-S RGC AP half-widths remained relatively stable as spike rate increased ($p = 0.0668$). These data suggest αON- and αOFF-S RGCs can be distinguished, in regard to AP width, by their dependence on spike rate.

2.3.2 Sensitivity to K^+ determines RGC type-specific differences in spike rate and waveform

Rate-dependent spike widening is largely mediated by K^+ currents during action potential repolarization (Ma and Koester, 1996). Based on this premise, we determined if modulating the K^+ concentration gradient could explain cell type-specific differences in RMP, spike rate, and spike width. We employed a within-subjects approach where recordings were performed before and after bath

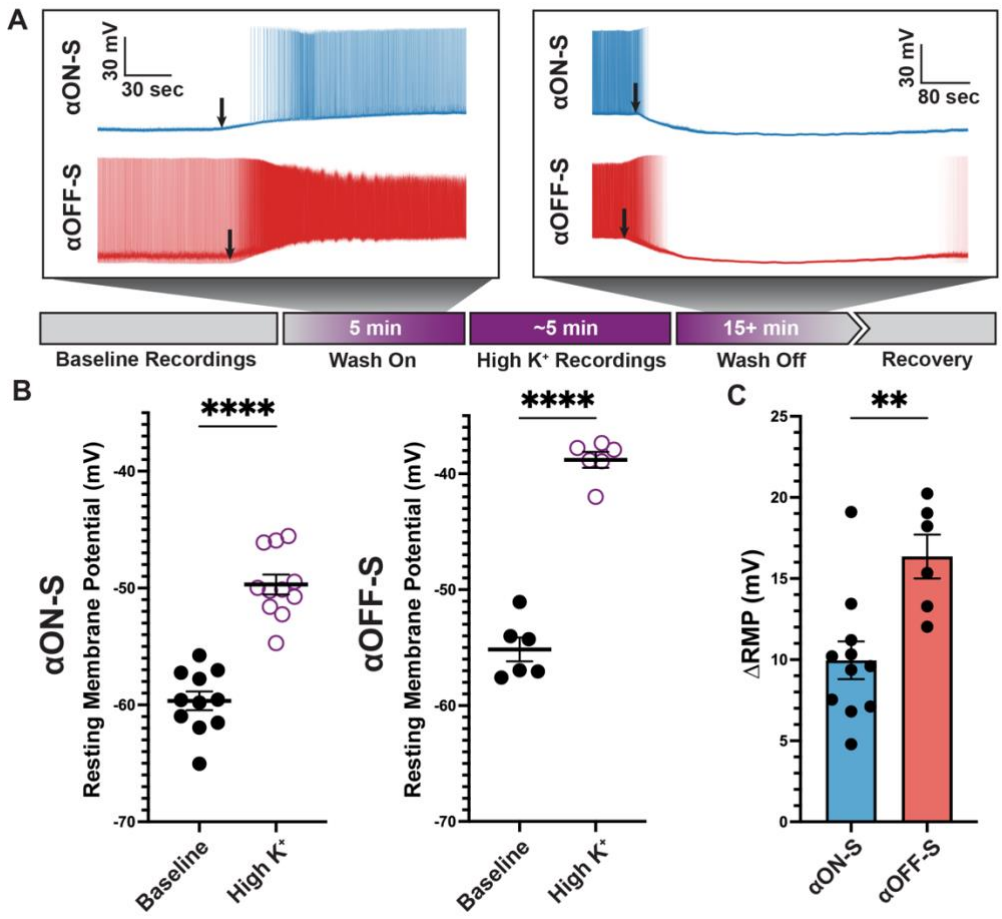

Figure 2.4 αOFF-S cells are more depolarized by elevated extracellular potassium
(A) Schematic timeline of experiment, and representative spontaneous voltage responses of αON-S and αOFF-S cells during high K^+ medium (additional 5mM KCl) wash on and off. Black arrows indicate onset of significant depolarization (left) or repolarization (right). **(B)** Resting membrane potentials (RMP) measured for each cell before and after addition of 5mM KCl. High K^+ significantly depolarized both αON-S and αOFF-S cells (paired t tests, $p < 0.0001$ for both). **(C)** Change in RMP (ΔRMP) after high K^+ addition. ΔRMP was significantly greater for αOFF-S cells (unpaired t test, $p = 0.0038$). Error bars: +/- standard error of the mean.

application of extracellular medium containing additional KCl (extra 5 mM, high K^+, **Fig 2.4A**). The additional 5 mM K^+ in this experimental approach brought the total extracellular K^+ concentration to 8 mM, making this treatment a physiologic depolarizing stimulus (Heinemann and Lux, 1977). High K^+ significantly depolarized RMP of both cell types ($p < 0.0001$ for both, **Fig. 2.4B**). Notably, RMP of αON-S and αOFF-S cells did not appear equally affected by high K^+ treatment. We analyzed this apparent difference by computing the difference in baseline and high K^+ RMP (ΔRMP). We found ΔRMP of αOFF-S cells significantly greater than αON-S RGCs ($p = 0.0038$, **Fig. 2.4C**).

We next sought to determine how differences in sensitivity to high K^+ on RMP may influence current-evoked spiking of αRGC types. We measured spiking using the same depolarizing current stimulation protocol described earlier (**Fig. 2.2**). High K^+ treatment not only increased spontaneous spiking of αON-S RGCs, but also increased spiking at smaller test currents and appeared to cause depolarization block at test currents where it previously did not occur (**Fig. 2.5A**). Overall, we found high K^+ significantly altered the test current-spike rate relationship of αON-S RGCs ($p = 0.0397$, **Fig. 2.5B**).

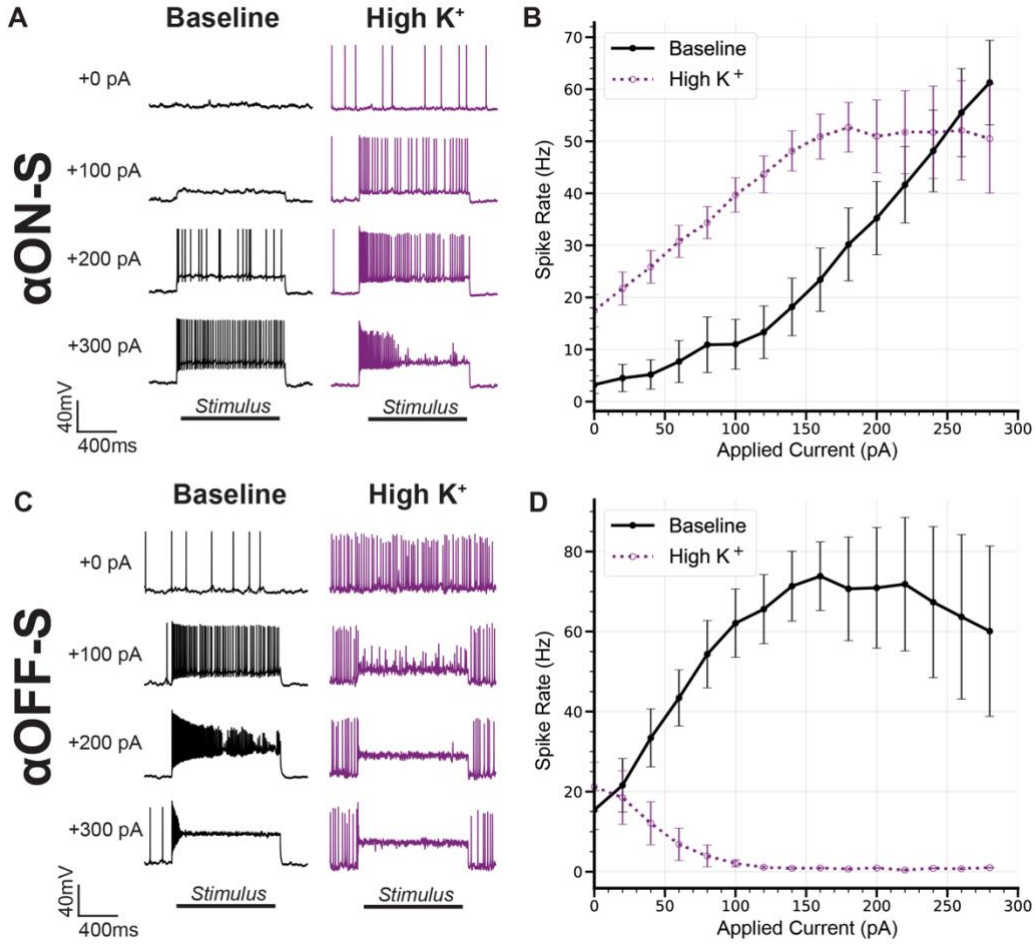

Figure 2.5 αOFF-S firing dynamics are more sensitive to elevated extracellular potassium
(A) Representative current-clamp responses of αON-S cells to 0, 100, 200, and 300 pA pulses, before and after washing on high K^+. **(B)** The current-spiking relationship for αON-S before and after high K^+. High extracellular K^+ significantly alters the current-spiking relationship (2-way ANOVA, Potassium-Stimulation interaction effect $p = 0.0397$). Elevated potassium increases the firing rate of αON-S RGCs at most current steps but induces a plateau and decrease in rate with variably widened and failed action potentials with stronger depolarizations. **(C)** Representative current-clamp responses of αOFF-S cells to 0, 100, 200, and 300 pA pulses, before and after washing on high K^+. **(D)** The current-spiking relationship for αOFF-S before and after high K^+. High extracellular K^+ significantly alters the current-spiking relationship (2-way ANOVA, Potassium effect $p = 0.0005$). In the presence of elevated K^+, the rates of αOFF-S cells are significantly decreased and quickly drop to zero with increased stimulation, with many failed action potentials. Error bars: +/- standard error of the mean.

High K^+ treatment also dramatically altered αOFF-S cell current-induced spiking. Increasing test current strength in αOFF-S cells caused depolarization block, reducing spike rate and increasing the number of failed APs (**Fig. 2.5C**). Overall, we found high K^+ significantly changed the test current-spike rate relationship of αOFF-S RGCs ($p = 0.0005$, **Fig. 2.5D**).

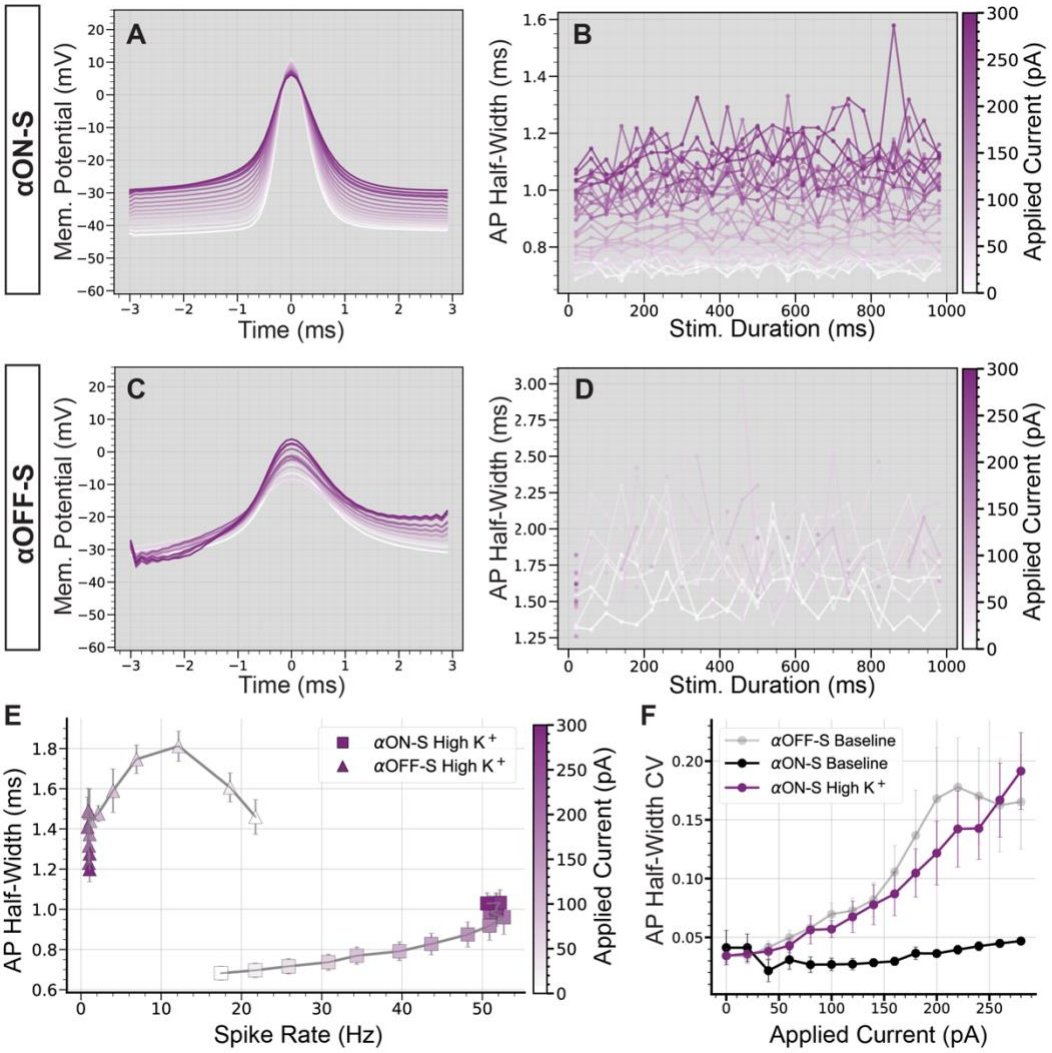

Figure 2.6 Elevated extracellular potassium significantly alters action potential shape
(A) Mean action potential (AP) shapes for αON-S cells in high K^+ conditions at each current step. **(B)** Mean AP half-width vs. stimulus duration for each current level of high K^+ αON-S cells. **(C)** Mean action potential (AP) shapes for high K^+ αOFF-S cells at each current step. **(D)** Mean AP half-width vs. stimulus duration for each current level of high K^+ αOFF-S cells. **(E)** The mean spike rate at each current injection vs. the AP half-widths for cells in high K^+ conditions. High K^+ αON-S RGCs demonstrate significant rate-dependent spike widening (simple linear regression, nonzero slope $p < 0.0001$) **(F)** The coefficient of variation (CV) of AP half-widths vs. magnitude of current pulse for αON-S before and after elevated K^+, and comparison to αOFF-S baseline relationship. Mixed effects analysis of potassium and current on half width for αON-S cells shows a significant interaction between current and potassium ($p = 0.0253$). Mixed effects analysis of half-width CVs for αON-S + high K^+ and αOFF-S at baseline demonstrates no significant difference between the groups ($p = 0.7190$). Error bars: +/- standard error of the mean.

Finally, we investigated the impact of high K^+ on spike rate and AP shape. In addition to increasing spike rate and facilitating depolarization block (**Fig. 2.5**), high K^+ augmented AP width in αON-S cells (**Fig. 2.6A**). Similar to αOFF-S RGC APs produced under baseline conditions (**Fig. 2.3D**), we observed high K^+ treatment not only increased αON-S cell AP half-width but also increased variability, especially at larger test currents (**Fig. 2.6B**). High K^+ also increased αOFF-S cell AP width (**Fig. 2.6C**) and considerably decreased αOFF-S spiking, essentially eliminating sustained spiking at stronger depolarizations (**Fig. 2.6D**). Interestingly, under high K+ conditions αON-S cells demonstrated a significantly linear correlation between spike rate and AP width (**Fig. 2.6E**) – similar to αOFF-S cells under baseline conditions (**Fig 2.3F**). Furthermore, the relationship between current and AP half-width CV of αOFF-S cells under baseline conditions and αON-S cells treated with high K^+ was not statistically different ($p = 0.719$, **Fig 2.6F**).

Evidence suggest intrinsic excitability of RGCs is in part due to axon initial segment (AIS) morphology (Werginz et al., 2020; Wienbar and Schwartz, 2022). In particular, the scaling of the AIS in α-Sustained cells is important for fine tuning spiking thresholds and varies systematically by retinal topography (Raghuram et al., 2019). To evaluate the potential influence of AIS scaling on our results we labeled recorded cells for ankyrin-G (AnkG), a scaffolding protein that defines the AIS (**Fig. 2.7A,B**; n=7 αON-S, n=6 αOFF-S). We measured AIS distance from soma and length based on AnkG immunofluorescence. We did not detect a significant difference between AIS distance from the soma (**Fig. 2.7C,** p=0.3897) or AIS length (**Fig. 2.7D,** p=0.1145) between αON- and αOFF-S RGCs. Because the length of the AIS is linked to threshold for AP generation (Jamann et al., 2021) as well as a higher threshold for depolarization block (Werginz et al., 2020; Wienbar and Schwartz, 2022) we investigated the relationship between AIS length and current-evoked spiking in our cells. We used linear regression to determine the slope of this relationship at each test current (**Fig. 2.7E**). At smaller test currents (0-140pA) αOFF-S cells had a positive correlation between AIS length and spike rate, whereas there was a moderately negative correlation for αON-S cells (**Fig. 2.7F**). However, at larger test currents (180-300pA) the relationship for αOFF-S cells flipped, with cells with longer AISs exhibiting lower spike rates. R^2

values for regressions (**Fig. 2.7G**) were moderately high (0.35-0.61) for αOFF-S except at test currents correlating with the onset of depolarization block (160-180 pA, R^2=0.05-0.20), while they were fairly low at all currents for αON-S cells (0.06-0.20).

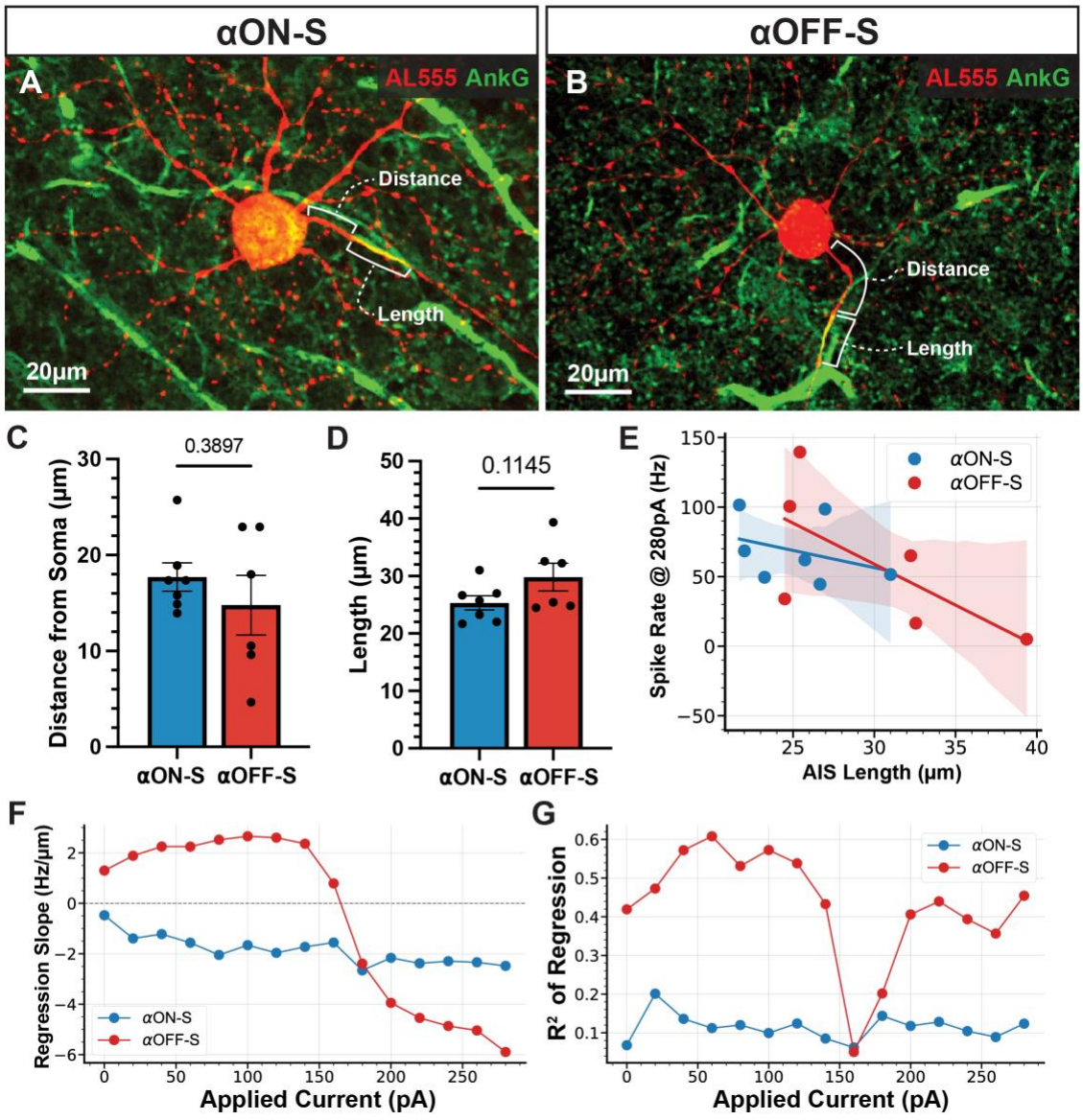

Figure 2.7 The relationship between AIS length and evoked spike rate varies by cell type and strength of stimulation

(A-B) Representative images of Alexa 555 (AL555, red) dye-filled αON-S (A) and αOFF-S (B) retinal ganglion cells labeled for the axon initial segment (AIS) protein ankyrin-G (AnkG, green). Annotations demonstrate the dimensions of AIS distance from soma and length which are quantified below. **(C-D)** AIS distance from soma (C) and length (D) do not differ significantly between the two RGC types (p = 0.38397, unpaired t-test; p = 0.1145, unpaired t-test). Error bars: +/- standard error of the mean. **(E)** Example scatter plot and linear regression best fit lines of the relationship between AIS length and current-evoked spiking rate, for 280 pA current injection. Shaded regions are 95% confidence intervals for best fit lines. **(F)** The slope of the regression best fit lines at each test current for αON-S and αOFF-S RGCs. **(G)** R^2 values of the linear fits at each test current for αON-S and αOFF-S RGCs.

2.4 Discussion

2.4.1 αON-S and αOFF-S RGCs exhibit distinct excitability profiles and spike waveforms

Our findings indicate αON-S and αOFF-S RGCs maintain distinct resting membrane potentials (RMPs) and voltage-gated responses to depolarizing currents, in addition to differences in light-evoked activity (**Figs. 2.1, 2.2**). We found αOFF-S RGCs produced more robust responses to small depolarizing currents compared to αON-S RGCs (**Fig. 2.2**). This difference is driven by more than simply the higher spontaneous activity of αOFF-S in these recording conditions since the slope of the increase in rate is greater for αOFF-S than αON-S cells (**Fig. 2.2B**). In response to larger current injections, αOFF-S RGCs often produced few full spikes, followed by aborted action potentials, and sustained membrane potential, indicating depolarization block. To the counter, αON-S RGC responses remained robust to large current injections (**Fig. 2.2**). These differences persisted even when controlling for RMP (Fig. 2C,D) lending support to RGC-intrinsic mechanisms driving differences in spike rate and depolarization block. While our interpretations are limited by our sample size, these findings confirm and extend the evidence that ON and OFF RGC responses are differentially dependent on stimulus amplitude (Twyford et al., 2014; Kameneva et al., 2016).

In addition to spike rate, we found αON-S and αOFF-S RGC AP width to be differentially dependent on stimulus strength. αOFF-S RGC AP half-width dramatically increased as depolarizing current increased, whereas αON-S RGC AP half-width modestly increased in response to increasing depolarizing currents (**Fig. 2.3A-D**). This AP widening phenotype closely resembles previously reported results in RGCs (Goethals et al., 2021). Stronger depolarizing currents also increased AP half-width variability in αOFF-S RGCs while αON-S RGC half-width variability remained constant across test currents (**Fig. 2.3E**). αOFF-S RGC AP width variability increased prior to the onset of depolarization block (60-160 pA, **Fig. 2.2B**), suggesting for an interaction between mechanisms generating depolarization block and maintaining AP half-width. We tested this notion by comparing AP half-width to spike rate for each test current (**Fig. 2.3F**). We found αOFF-S RGC AP half-width significantly

correlated with spike rate, but the same did not hold true for αON-S RGCs. Our findings suggest that mechanisms generating depolarization block and regulating AP half-width are related, representing a fundamental physiologic difference between αON-S and αOFF-S RGCs.

An overall limitation to this study is measurements of current-evoked responses under physiologic conditions may not completely isolate cell-intrinsic activity. Indeed, current injected at the soma will spread to both axonal and dendritic compartments. Depolarizing dendritic membranes will not only produce postsynaptic plasticity that influences voltage-gated activity, but also may induce presynaptic plasticity that can impact voltage-gated activity of the postsynaptic cell (Markram et al., 1997; Feldman, 2012). Notwithstanding, other methods for measuring intrinsic responses such as genetic models, culture systems, or pharmacology may also affect intrinsic responses.

2.4.2 Sensitivity to extracellular K^+ underlies differences in RGC spiking and AP width

Rate-dependent spike widening is driven by K^+ currents (Ma and Koester, 1996; Kasten et al., 2007). Moreover, computational modeling also links differences in K^+ permeability to the distinct stimulation thresholds for AP failure and depolarization block in ON versus OFF RGCs (Kameneva et al., 2016). Based on this premise, we sought to probe sensitivity to K^+ gradients as a potential physiologic underpinning for the distinct excitability profiles and AP widths we observed in αON-S and αOFF-S cells.

Application of high K^+ medium expectedly depolarized RMP of both αRGC types but had a significantly more pronounced effect on αOFF-S RGCs (**Fig. 2.4B,C**). Similarly, the current-spiking relationship for both cell types was altered (**Fig. 2.5**). αON-S cells maintained spiking activity, but additional depolarizing current input to αOFF-S cells overwhelmed spike generation capacity (**Fig. 2.5**). These experiments support our key finding that αON-S and αOFF-S RGCs have different sensitivities to the K^+ concentration gradient across their membranes. Intriguingly, the current-spiking and AP shapes of αON-S cells under high K^+ conditions closely resembled those of αOFF-S cells under baseline conditions (**Fig. 2.6**). Under these conditions, αON-S cell AP failure increased and firing rate decreased with

stronger depolarizing stimulation. Furthermore, the high K^+-induced changes in αON-S AP shape at large depolarizations mirrored those seen in αOFF-S cells.

Evidence suggest AIS scaling mediates intrinsic excitability (Raghuram et al., 2019; Werginz et al., 2020; Wienbar and Schwartz, 2022). Thus, we investigated the scaling of the AIS as a potential contributor to differences in spike rate and depolarization block (**Fig. 2.7**). For our sample, we did not detect significant differences in αON- and αOFF-S RGC AIS dimensions (**Fig. 2.7C,D**). A limitation of this study is that we did not recover the topographic location of cells in our sample, which is important because AIS dimensions can vary with retinal topography (Raghuram et al., 2019), though we have previously reported our RGC samples are biased to the mid-to-peripheral retina (Risner et al., 2018) but without bias in respect to topography (Boal et al., 2020). Intriguingly, we found that the relationship between AIS length and spike rate varied not only by cell type, but also by the strength of stimulation (**Fig. 2.7F**). At low currents, αOFF-S cells with longer AISs had higher evoked spike rates. This corroborates previous evidence that AIS length is a driver of AP generation threshold (Jamann et al., 2021). However, with stronger stimulation this relationship flipped. Beyond the point where depolarization block began to occur in the majority of αOFF-S RGCs, the cells with longer AISs had lower spike rates. Furthermore, AIS length accounted but for a small amount of the variance in αON-S cell spike rates (**Fig. 2.7G**). These results support the notion that the contributions of the AIS to spiking output vary by cell type but also suggest that AIS structure cannot completely explain RGC excitability and threshold for depolarization block.

The ability of increased extracellular K^+ to shift the response properties of αON-S toward those of αOFF-S suggests that sensitivity to extracellular K^+ is an important component shaping the different responses of the two RGC types. There are numerous potential targets for identifying the mechanistic underpinning of this difference in K^+ sensitivity, due to the diversity of K^+ channels expressed in RGCs (Zhong et al., 2013). Channels associated with rate-dependent spike widening (as seen in **Fig. 2.3F** and **2.6E**) and modulating neuronal excitability, such as those mediating A-type voltage-gated K^+ currents (Ma and Koester, 1996; Holmqvist et al., 2002), or the Ca^{2+}-activated BK channels (Wang et al., 1998;

Gu et al., 2007) may be promising for future investigation. RGC type-specific expression data (Tran et al., 2019; Goetz et al., 2022) present an opportunity to gain a detailed understanding of which channels may contribute to these physiological differences.

2.4.3 Linking intrinsic neuronal properties to cell-type specific vulnerabilities to degeneration

In addition to contributing to voltage-gated responses of αON-S and αOFF-S RGCs under physiologic conditions, the difference in K^+ sensitivity between these two cells may have important implications in a pathological context, which is an ongoing topic of investigation in our laboratory. Extracellular K^+ concentration is tightly regulated under physiologic conditions, rarely fluctuating more than a few millimolar and not exceeding 12 mM in local concentration (Heinemann and Lux, 1977). However, mechanisms regulating extracellular K^+ concentration can become disrupted in glaucoma (Fischer et al., 2019a; Fischer et al., 2019b), a neurodegenerative disease affecting RGCs and their axonal projection to the brain. Furthermore, select K^+ channels can contribute to RGC degeneration via interaction with apoptotic pathways (Diem et al., 2001b; Koeberle et al., 2010). RGCs are a highly heterogeneous population, with different types defined by morphology, physiology, and molecular markers (Sanes and Masland, 2015; Baden et al., 2016; Bae et al., 2018; Tran et al., 2019). Importantly, certain cell types may be more vulnerable to glaucomatous degeneration than others, especially OFF RGCs, measured in terms of dendritic field size, arbor complexity, and excitability (Della Santina et al., 2013; El-Danaf and Huberman, 2015; Ou et al., 2016). Stressed RGCs exhibit enhanced excitability early in glaucoma, preceding frank degeneration (Risner et al., 2018; McGrady et al., 2020; Risner et al., 2020a), and are metabolically restricted (Inman and Harun-Or-Rashid, 2017; Casson et al., 2021). Given type-specific differences in K^+ sensitivity, dysfunctional K^+ homeostasis in glaucoma could impose different degrees of stress on αON-S and αOFF-S cells, influencing changes to excitability, AP generation, and sustained firing, contributing to type-specific vulnerability to disease.

Broadly, understanding intrinsic neuronal properties could offer insight into the progression of many neurodegenerative diseases, which are heterogenous and affect a wide variety of central nervous

system regions and cell types. Despite their disparate etiologies and pathophysiologic processes, many of these diseases share common hallmark features of progression. Notably, many diseases including Alzheimer's Disease (Palop and Mucke, 2016), Parkinson's Disease (Subramaniam et al., 2014), and Amyotrophic Lateral Sclerosis (Vucic et al., 2008) also exhibit neuronal hyperexcitability early in their progression. This pathophysiologic change stresses neurons, affecting metabolic demand and calcium load, pushing neurons beyond their threshold for cellular damage towards death. Further, cell type-specific vulnerability is not unique to glaucoma (Saxena and Caroni, 2011; Fu et al., 2018). Intrinsic morphologic, physiologic, and biochemical properties might underpin increased sensitivity to degeneration during stress (Fu et al., 2018). Understanding which intrinsic properties underly selective vulnerability in disease offers insight into early degenerative mechanisms and potential therapeutic targets.

CHAPTER 3

RETINAL GANGLION CELLS ADAPT TO IONIC STRESS IN EXPERIMENTAL GLAUCOMA

3.1 Introduction

Glaucoma is the leading cause of irreversible vison loss worldwide (Tham et al., 2014). The disease involves progressive degeneration of retinal ganglion cells (RGCs) and their axons, which carry visual information from the eye to central targets in the brain. Aging is the leading risk factor, though sensitivity to intraocular pressure (IOP) is the only modifiable risk factor. In glaucoma, stress evolving from sensitivity to IOP challenges RGC axons as they pass unmyelinated through the optic nerve head of the retina. Many patients continue to lose vision despite efforts to manage IOP with topical and surgical hypotensive therapies (Heijl et al., 2002), underscoring the need to identify new therapeutics based on mechanistic understanding of how RGCs and their axons respond to glaucomatous stress.

Development of neuronal-based therapies for the treatment of glaucoma requires identification of targets involved in pathophysiology, target-specific therapeutics, and biomarkers to assay outcomes (Calkins, 2021). Early progression in experimental glaucoma involves enhanced RGC excitability with a concurrent reduction in axon function (Risner et al., 2018). Prolonged stress ultimately overcomes the adaptive mechanisms and leads to RGC degeneration (Sappington et al., 2010; Naguib et al., 2021; Risner et al., 2021b; Risner et al., 2022). The RGC population is heterogeneous (Sanes and Masland, 2015; Baden et al., 2016; Bae et al., 2018; Tran et al., 2019), with RGC-intrinsic factors shaping their individual response properties (Emanuel et al., 2017; Werginz et al., 2020; Wienbar and Schwartz, 2022). Importantly, such intrinsic differences may predispose certain RGC types to be particularly sensitive to IOP-related stress (Della Santina et al., 2013; El-Danaf and Huberman, 2015; Ou et al., 2016; Risner et al., 2021b). Previously, we established that different RGC subtypes exhibit varied sensitivities to elevated extracellular potassium (Boal et al., 2022). Dysregulation of potassium ion (K^+) homeostasis and channel

expression contribute to altered excitability in neurodegenerative diseases, including glaucoma, and represent potential targets for early diagnosis and treatment (Hall et al., 2015; Frazzini et al., 2016; Cacace et al., 2019; Fischer et al., 2019a; Fischer et al., 2019b; Kim et al., 2021).

Here, we utilized our inducible mouse model of glaucoma (Sappington et al., 2010; Calkins et al., 2018) to investigate how prolonged exposure to elevated IOP changes RGC sensitivity to acutely elevated extracellular K^+. Following four weeks of IOP elevation, alpha ON-sustained (αON-S) and alpha OFF-sustained (αOFF-S) RGCs had reduced responses to light and depolarizing current stimulation, consistent with previous results (Risner et al., 2021b; Risner et al., 2022). In controls with normal IOP, challenging RGCs with high extracellular K^+ led to membrane depolarization, blunted spike rate, and action potential (AP) widening in both αON-S and αOFF-S cells. IOP elevation reduced the effects of elevated K^+ in both RGC types. Compared to controls, RGCs exposed to elevated IOP were less depolarized and maintained greater current-evoked spiking during acute K^+ elevation. Furthermore, K^+-dependent AP widening was decreased, though the impact of IOP on AP widths differed for αON-S and αOFF-S cells. Immunolabeling of the axon initial segment (AIS), the site of AP initiation in neurons, revealed that IOP elevation did not structurally alter AIS scaffolding for either RGC type.

These results suggest that, after four weeks of IOP elevation, RGCs undergo an adaptive process that reduces sensitivity to acutely elevated K^+ while diminishing their excitability. Differences between αON-S and αOFF-S in how AP widths vary with IOP exposure and K^+ conditions support evidence for cell-type specific responses to stress. This adaptation involves altered AP generation, indicating an axongenic process, but it is not solely reflective of axonal structural plasticity.

3.2 Materials and methods

3.2.1 Animals

We obtained 15 C57Bl6/J mice (8 males, 7 females, 12-20 weeks old) from Jackson Laboratories (Bar Harbor, ME). These numbers were determined, based upon our previous experience with this model and recording strategy (Risner et al., 2018; Risner et al., 2021b; Boal et al., 2022), to provide a sufficient

number of each cell type for statistical comparisons. Mice were housed at the Vanderbilt University Division of Animal Care and maintained on 12-hr light/dark cycle. Animals were allowed water and standard rodent chow *ad libitum*. All animal experiments were reviewed and approved by the Vanderbilt University Medical Center Institutional Animal Care and Use Committee.

3.2.2 Intraocular pressure elevation and measurement

Mice were anesthetized with isoflurane (2.5%) and administered tropicamide (1%), proparacaine (0.5%), and lubricating drops in both eyes. For the four week intraocular pressure (IOP) elevation group (4wk IOP) we bilaterally injected 1.5 µL of 15 µm polystyrene microbeads (Invitrogen, Carlsbad, CA) into the anterior chamber of the eye (Sappington et al., 2010) using borosilicate glass pipette attached to a micromanipulator (M3301R, WPI, Sarasota, FL), driven by a microsyringe pump (DMP, WPI, Sarasota, FL). For the 4wk saline control group (4wk Ctrl) we bilaterally injected an equal volume of sterile phosphate-buffered saline (PBS) into the anterior chamber using the same system. Mice were injected in cohorts of five at a time. For 4wk Ctrl, a second cohort of five was done because an insufficient number of cells of interest were recorded from the first. Animals of both sexes were evenly split between experimental groups ($p=0.5581$, chi-squared test).

For IOP measurements, mice were lightly anesthetized with isoflurane (2%) and pressures were measured using rebound tonometry (iCare Tonolab; Vantaa, Finland). IOP for each eye was determined as the mean of 15 consecutive measurements. For the two days preceding anterior chamber injections we measured IOP for each group and averaged these values to determine baseline IOP. Beginning two days post-injection, IOP was measured three times per week for the duration of the 4wk experimental period.

3.2.3 Electrophysiology

Approximately 4 weeks (±2 days) following anterior chamber injection mice were euthanized via cervical dislocation and decapitation, eyes were enucleated, and the retinas were dissected out under long-wavelength illumination (630 nm, 800 µW/cm^2, FND/FG, Ushio, Cypress, CA). Retinas were placed in carbogen-saturated Ames' medium (US Biologic, Memphis, TN) supplemented with 20 mM D-glucose

and 22.6 mM $NaHCO_3$ (pH 7.4, 290 Osm). Each retina was mounted flat onto a physiological chamber, inner retina facing upwards, and perfused at a rate of 2 mL/min with Ames' medium maintained at 35°C (Model TC-344C, Warner Instruments, Hamden, CT).

Retinal ganglion cells (RGCs) were viewed under differential interference contrast (DIC) using an Andor CCD camera attached to an Olympus BX50 upright microscope at 40x magnification. RGCs with large somas were targeted for intracellular recording with pipettes pulled from borosilicate glass (I.D. 0.86mm, O.D. 1.5mm; Sutter Instruments, Novato, CA) and filled with (in mM): 125 K-gluconate, 10 KCl, 10 HEPES, 10 EGTA, 4 Mg-ATP, 1 Na-GTP, and 0.1 ALEXA 555 dye (Invitrogen, Carlsbad, CA). The intracellular solution pH was 7.35 and osmolarity was 285 Osm. Recording pipettes filled with intracellular solution had a resistance between 4–8 MΩ. Whole-cell current-clamp signals were amplified (Multiclamp 700B, Molecular Devices, San Jose, CA) and digitized at 10 kHz (Digidata 1550A, Molecular Devices, San Jose, CA). Access resistance was monitored periodically during recordings and maintained ≤30 MΩ.

We measured resting membrane potential (RMP), spontaneous spiking, light-evoked spike activity (full-field 365+460nm, 3.4 mW/cm^2, 3-s duration, CoolLED, pE-4000, Andover, UK), and current-evoked spiking while clamping the cell at 0 pA. Current-evoked spiking was measured during stepwise application of 1 s depolarizing current pulses, ranging from 0 to +300 pA in 10 pA increments, with a 2 s inter-stimulus interval. Current was clamped at 0 pA between pulses.

3.2.4 High extracellular potassium recordings

A second batch of Ames' medium was prepared as described above, but with an additional 5 mM of KCl (i.e., high K^+), bringing the total K^+ concentration to 8mM. Following completion of baseline recordings, high K^+ medium was washed into the recording chamber while RGC membrane voltage was continuously recorded. Prior to high K^+ experimental recordings, we allowed a wash on period of 5-6 min, allowing RGC membrane potential to stabilize. Recordings (RMP, spontaneous activity, light-evoked spiking, current-evoked spiking) were then performed as described above. After high K^+

experiments the extracellular medium was switched back to the baseline solution and RGC membrane voltage was continuously measured during a wash off period of 10-20 min, allowing RGCs to recover baseline RMP and spontaneous activity. Full recovery typically took 10-15 min, although it occasionally required up to 20 min. We limited the number of experimental protocols to reduce the time of high K^+ exposure. Furthermore, to limit potential cumulative effects of K^+ wash on/off, we limited the total number of cells that were recorded under high K^+ to no more than 3 from each retina.

3.2.5 RGC physiology analysis

Raw data files from electrophysiologic recordings were analyzed in Python 3.9 using the pyABF 2.3.5 (Harden, 2022) and SciPy 1.7.1 modules (Virtanen et al., 2020). Action potentials (APs) were detected from membrane voltage data using the SciPy "find_peaks" function with parameters of 20 mV minimum prominence and a distance threshold of 1.5 ms. Spike rates for current-evoked spiking protocols were reported as the average rate for 2 adjacent 10 pA increments of stimulation (20 pA bins). For AP width measurements, a cubic spline function was fit to each AP waveform and half-width was measured as the duration, in ms, where the membrane potential was above the midway point between AP peak and minimum after-hyperpolarization.

3.2.6 Immunohistochemistry and imaging

Immediately following recordings, retinas were fixed in 4% paraformaldehyde and incubated at 4°C for 24 hr. After fixation, retinas were immunolabeled for choline acetyltransferase (ChAT, 1:100; Millipore, Burlington, MA, Cat. #AB144P) and ankyrin-G (AnkG, 1:200; NeuroMab N106/36; Antibodies, Inc Cat. # 75-146). Tissue was blocked in 5% normal donkey serum for 2 hr, then incubated in primary antibodies for 3 d at 4°C, and finally incubated for 2 hr at room temperature with donkey anti-goat Alexa 405 and donkey anti-mouse Alexa 488 secondary antibodies (Jackson ImmunoResearch, West Grove, PA). Z-stack images of dye-filled RGCs were obtained using an Olympus FV1000 inverted microscope at 40x magnification. Image analysis, including creating orthogonal projections used for visualization of dendritic stratification depth, was performed using ImageJ (NIH, Bethesda, MD).

3.2.7 Axon initial segment analysis

We evaluated 11 4wk IOP cells (5 αON-S and 6 αOFF-S) and 18 4wk Ctrl cells (9 αON-S and 9 αOFF-S) with identifiable axon initial segments (AISs) as defined by a segment of ankyrin-G (AnkG) labeling that colocalized to a filled RGC axon. AnkG fluorescence was measured in ImageJ starting from the edge of the soma along the axon in a max-intensity Z projection limited to the extent of the axonal process. Background fluorescence was subtracted from AnkG intensity profiles using a rolling ball filter with a radius equal to approximately 15% of the data length. Smoothed AnkG profiles were generated using a Savitzky-Golay filter with a first order polynomial fit. Axon initial segment (AIS) bounds were algorithmically defined as the extent where smoothed AnkG values were greater than 50% of the difference between baseline and maximum intensity.

3.2.8 Data analysis and statistical tests

All data are reported as mean ± standard error of the mean (SEM) unless otherwise indicated. All statistical tests were performed in GraphPad Prism 9 (Graphpad Software, San Diego, CA). All data sets were checked for normality. Where appropriate, parametric statistical tests (unpaired t-test, paired t-test, 2-way ANOVA, simple linear regression) were performed. When data were not normally distributed, appropriate nonparametric tests (e.g. Mann-Whitney test) were performed. For ANOVA tests, p-values were corrected for multiple comparisons. Where noted, determination of the influence of sex on high K+-induced change in RMP was determined by multiple linear regression modeling (ΔRMP ~ Intercept + Cell Type + Experimental Group + Sex). We defined statistical significance as a p-value of 0.05 or less. Exact p-values and the specific statistical test used for each analysis are listed in the figure legends or results text.

3.3 Results

3.3.1 Elevated IOP alters RGC electrophysiology

We performed bilateral injections of either polystyrene microbeads to occlude the anterior chamber (n=5 animals, 10 eyes) or sterile phosphate-buffered saline (n=10 animals, 20 eyes) and

measured intraocular pressure (IOP) for four weeks (**Fig. 3.1**). Following injections, IOP in saline-injected eyes remained unchanged from baseline (**Fig. 3.1A**). Following microbead occlusion, IOP increased 46% above their baseline (**Fig. 3.1A**), exceeding IOP in saline control eyes by 44% (**Fig. 3.1B**, $p<0.0001$). IOP elevation in microbead eyes was sustained for the duration of the experiment (**Fig. 3.1A**).

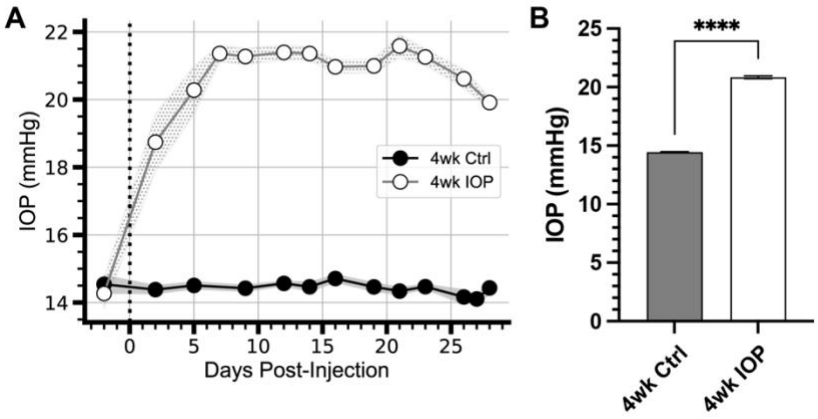

Figure 3.1 IOP elevation due to microbead occlusion of the anterior chamber
(A) Intraocular pressure (IOP) of microbead-injected eyes (4wk IOP) increases rapidly following injection (vertical dotted line) and remain elevated for the duration of the 4 wks. The IOP of saline-injected eyes (4wk Ctrl) remains unchanged from baseline. Shaded region: ± standard error of the mean. (B) Mean IOP for each eye across all days following microbead injection significantly elevates compared to Ctrl ($p = 0.000046$, unpaired t test). Error bars: ± standard error of the mean. ****$p < 0.0001$

After four weeks mice were sacrificed and retinas prepared for electrophysiologic recordings. As previously described (Risner et al., 2018; Risner et al., 2020a; Risner et al., 2021b; Boal et al., 2022), we targeted αRGCs for recording by identifying large cell bodies and confirmed cell types by characterizing soma size, dendritic stratification within the inner plexiform layer (Famiglietti and Kolb, 1976; Galli-Resta et al., 2000), and light-evoked responses (**Fig. 3.2**). We focused analysis on two well-characterized and readily identifiable αRGC types: αON-Sustained (αON-S) and αOFF-Sustained (αOFF-S) (Krieger et al., 2017). In the saline (4wk Ctrl) group we recorded 10 αON-S RGCs (7 eyes, 4 mice; 8 cells from males, 2 from females) and 10 αOFF-S RGCs (8 eyes, 7 mice; 5 male, 5 female). In the microbead group (4wk IOP) we recorded 10 αON-S RGCs (9 eyes, 5 mice; 4 male, 6 female) and 7 αOFF-S RGCs (7 eyes, 5 mice; 3 male, 4 female). Cells from mice of both sexes were evenly represented among αON-S and αOFF-S for 4wk Ctrl ($p=0.1596$, chi-squared test) and 4wk IOP ($p=0.9062$, chi-squared test).

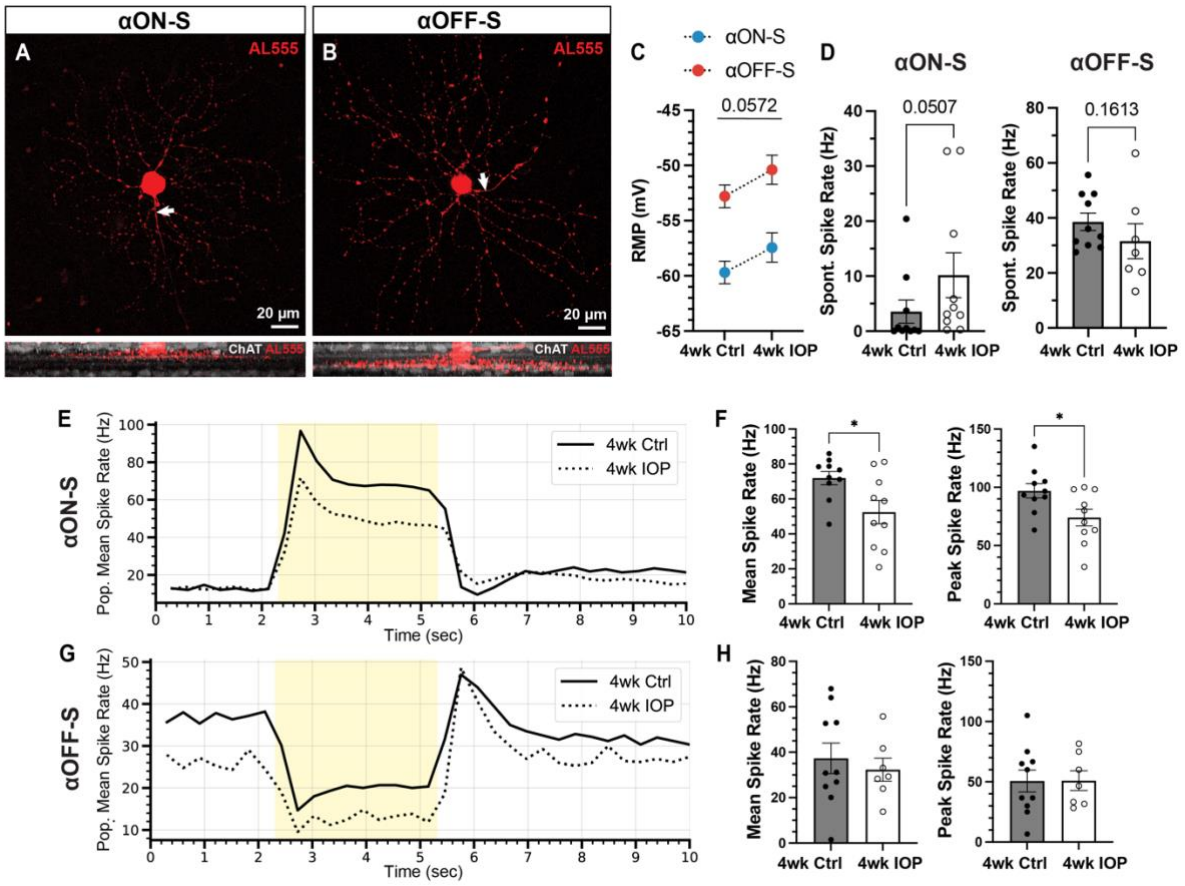

Figure 3.2 Elevated IOP alters membrane and light-evoked spiking characteristics in αON-S and αOFF-S RGCs

(A,B) Morphologic and physiologic characterization of retinal ganglion cells (RGCs). Patched cells were filled with Alexa-fluor 555 dye (AL555, red) and morphologically reconstructed with confocal microscopy. Representative maximum intensity projections of alpha ON-sustained (αON-S, A) and alpha OFF-sustained (αOFF-S, B) RGCs demonstrate characteristic soma size and dendritic branching patterns (upper). White arrows indicate the axonal projection. Orthogonal projections of representative AL555-filled cells co-labeled for choline acetyltransferase (ChAT, white) demonstrate the branching of αON-S and αOFF-S dendrites in the ON- and OFF-sublaminas of the inner plexiform layer, respectively (lower). (C) Resting membrane potentials (RMP) for both cell types from 4wk Ctrl and IOP groups. RGC RMPs in the 4wk IOP group are more depolarized than controls ($p = 0.0572$, 2-way ANOVA). (D) Spontaneous spiking rates for αON-S and αOFF-S RGCs. αON-S cells in the 4wk IOP group trend towards greater spontaneous spiking ($p = 0.0507$, Mann-Whitney test), whereas 4wk IOP αOFF-S cells trend towards less spontaneous spiking ($p = 0.1613$, Mann-Whitney test). (E) Mean firing rates of αON-S cells in the 4wk Ctrl and 4wk IOP groups binned into 200 ms intervals during light stimulation (yellow). (F) Mean (left) and peak (right) light-evoked spike rates for αON-S cells. 4wk IOP decreases both measures (mean: $p = 0.0202$, unpaired t-test; peak: $p = 0.0251$, unpaired t-test). (G) Mean firing rates of αOFF-S cells in the 4wk Ctrl and 4wk IOP groups binned into 200 ms intervals during light stimulation (yellow). (H) Mean (left) and peak (right) light-evoked spike rates for αOFF-S cells. Error bars: ± standard error of the mean. *$p < 0.05$.

Four weeks of IOP elevation altered the resting membrane and light-evoked spiking characteristics of both RGC types. RGCs from the 4wk IOP group had a depolarized resting membrane potential (RMP) relative to controls (**Fig. 3.2C**, p=0.0572; αON-S +2.25 mV, αOFF-S +2.41 mV). Spontaneous spiking in the absence of light also appeared altered (**Fig. 3.2D**), with αON-S cells trending

towards greater spiking (p=0.0507) and αOFF-S cells trending toward less spiking (p=0.1613). The membrane voltage response to light stimulation for αON-S was significantly blunted after IOP elevation (**Fig. 3.2E,F**), with cells from the 4wk IOP group exhibiting diminished mean (p=0.0202) and peak (p=0.0251) spike rates in response to light onset. Light-evoked spiking also appeared altered in αOFF-S cells (**Fig. 3.2G,H**), although not quite as overtly as αON-S cells. Mean and peak spike rates were not significantly different between experimental groups (**Fig. 3.2H**), though the histogram of mean spike rates (**Fig. 3.2G**) appeared qualitatively altered by 4wk IOP, with spiking at light offset tending to be less sustained.

3.3.2 4wk IOP RGCs are less sensitive to elevated extracellular potassium

Since potassium homeostasis may be altered in glaucoma (Fischer et al., 2019a; Fischer et al., 2019b), we next sought to investigate how 4 weeks of IOP elevation alters the sensitivity of RGCs to acutely elevated extracellular potassium. As previously described (Boal et al., 2022), we performed a within-subjects experimental design with recordings before and after application of extracellular medium

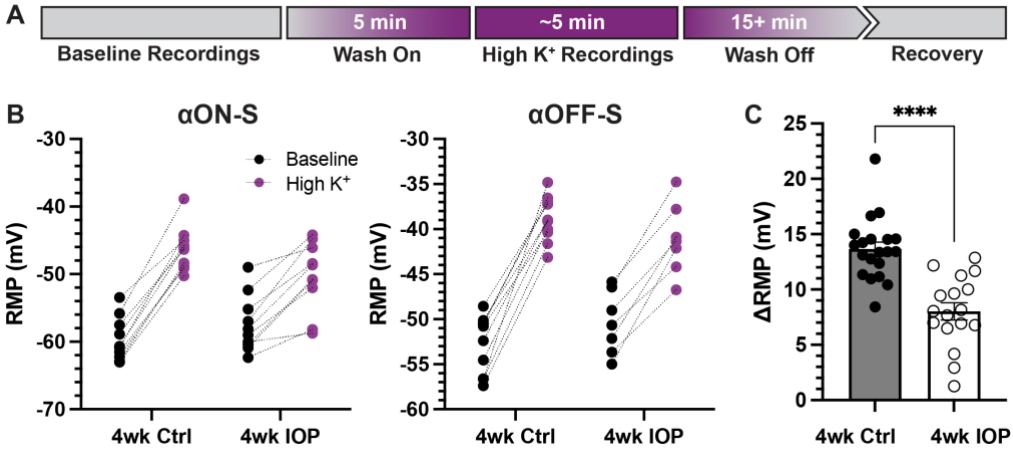

Figure 3.3 Elevated IOP reduces the influence of extracellular potassium on RGC depolarization
(A) Timeline illustrating the design of acutely elevated extracellular potassium (High K^+) experiments. Following baseline recordings, extracellular medium with an extra 5 mM KCl is washed on for 5 min until membrane potentials stabilized. High K^+ recordings are done, and then high K^+ is washed off with regular extracellular medium until full recovery of membrane potential and spontaneous spiking, at least 15 min. (B) Resting membrane potentials (RMPs) for αON-S and αOFF-S cells in both experimental groups before and after high K^+ wash on. There is a significant interaction effect between K^+ and IOP for both αON-S (p = 0.0002; 2-way repeated measures ANOVA) and αOFF-S (0.0063) cells. (C) The change in RMP following high K^+ wash on for each cell, separated by experimental group. Cells exposed to 4wk IOP elevation are significantly less depolarized by high K^+ (p = 0.00000091, Mann-Whitney test). Error bars: ± standard error of the mean. ****p < 0.0001

containing additional KCl (extra 5 mM, high K^+, **Fig 3.3A**). For both αON-S and αOFF-S high K^+ depolarized the RMP, regardless of experimental group (**Fig. 3.3B**, $p<0.0001$ for both cell types). However, there was a statistically significant interaction between IOP group and potassium effect on RMP for both cell types ($p=0.0002$, αON-S; $p=0.0063$, αOFF-S). Comparison of the high K^+-evoked depolarization of RMP (ΔRMP) between experimental groups demonstrated that 4wk IOP RGCs were significantly less depolarized by the acutely elevated potassium (**Fig. 3.3C**, $p<0.0001$). The sex of the mouse from which an RGC came was not significantly associated with ΔRMP ($p=0.1572$, multiple linear regression model).

αON-S and αOFF-S RGCs have distinct responses to depolarizing current (Twyford et al., 2014; Kameneva et al., 2016), which are in part related to their different sensitivities to extracellular potassium (Boal et al., 2022). We measured the spiking response of αRGCs to 1 s depolarizing current injections ranging from 0 to +300 pA, before and after washing on high K^+ medium (**Fig. 3.4**), to determine how

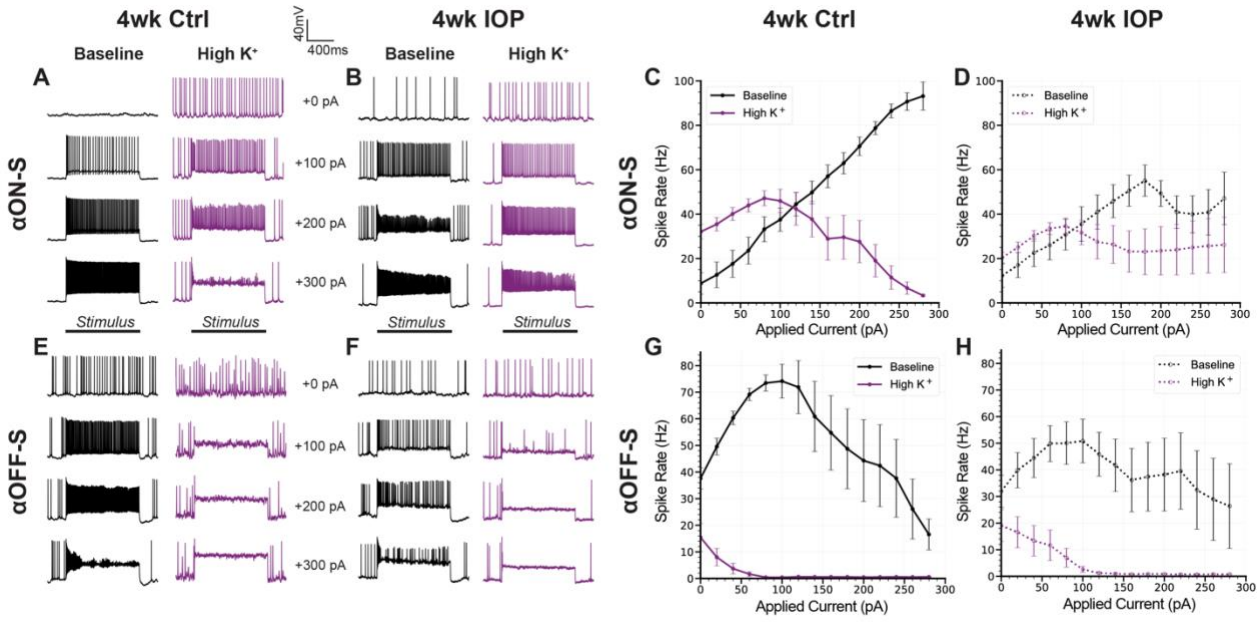

Figure 3.4 Current-evoked spiking is less depressed by high K^+ after IOP elevation
(A-B) Representative current-clamp responses of αON-S cells from both experimental groups to 0, 100, 200, and 300 pA pulses, before and after washing on high K^+. (C-D) The spiking responses of αON-S cells to depolarizing current pulses ranging from 0 to 300 pA, before and after high K^+. (E-F) Representative current-clamp responses of αOFF-S cells from both experimental before and after washing on high K^+. (G-H) The spiking responses of αON-S cells to depolarizing current pulses, before and after high K^+. The difference in spike rates between baseline and high K^+ groups for all cells is lower in the 4wk IOP group than in the 4wk Ctrl ($p = 0.0317$, unpaired t-test). Error bars: ± standard error of the mean.

4wk IOP exposure alters these properties. In saline controls, high K^+ appreciably altered the current-spiking relationship of both αON-S and αOFF-S cells. In baseline extracellular media control αON-S RGCs (**Fig. 3.4A,C**) exhibited little spiking at low depolarizations but spike rates increased as the strength of depolarization increased. After high K^+ wash on, spike rates were higher at small depolarizations but began to plateau and then slow as the strength of depolarization was increased. Control αOFF-S RGCs (**Fig. 3.4E,G**) exhibited a different pattern of current-evoked spiking than αON-S, but were also appreciably impacted by high K^+. In baseline media control αOFF-S cells had relatively high spike rates that initially increased with increasing stimulation, but reached a peak and began to subsequently decrease beyond about 100 pA of depolarization. High K^+ considerably decreased spike rates, which quickly fell to 0 Hz with increasing magnitudes of depolarization. In 4wk IOP αRGCs, high K^+ appeared to have a lesser effect on current-evoked spiking than in controls. For αON-S cells (**Fig. 3.4B,D**), 4wk IOP excitability was diminished at baseline relative to controls, exhibiting less of an increase in spike rate with increasing stimulation ($p<0.001$, simple linear regression). High K^+ again blunted spike rates ($p=0.0002$), though not to the same degree as in controls. 4wk IOP exposure likewise diminished αOFF-S excitability at baseline (**Fig. 3.4F,H**), with peak firing rates trending lower ($p=0.0639$, unpaired t test), and lessened the impact of high K^+ on spiking, with cells appearing to maintain the ability to fire at greater magnitudes of depolarization than in controls. Across both cell types, the absolute difference in firing rates between high K^+ and baseline conditions was less in the 4wk IOP group than in the 4wk control group ($p=0.0317$).

We previously found differences in excitability between αON-S and αOFF-S were reflected in the shape of their action potentials (APs), and that high K^+ promoted rate-dependent AP widening (Boal et al., 2022). We measured AP half-widths in both experimental groups to determine if decreased potassium sensitivity in 4wk IOP RGCs was reflected at the level of AP generation (**Fig. 3.5**). Control αON-S cells (**Fig. 3.5A,C**) exhibited minimal AP widening with increased stimulation at baseline. High K^+ media widened αON-S APs and increased rate-dependent widening. Control αOFF-S cells (**Fig. 3.5E,G**) had a moderate degree of rate-dependent AP widening at baseline, and high K^+ caused further widening. After

4wk IOP elevation, αON-S APs (**Fig. 3.5B,D**) had slightly wider APs at baseline than controls (p=0.0133, unpaired t test). However, 4wk IOP αON-S APs appeared less widened in high K^+ medium relative to baseline. 4wk IOP αOFF-S cells (**Fig. 3.5F,H**) did not have appreciably different AP shapes at baseline compared to controls (p=0.6867). Further, they too had less K^+ induced AP widening than control αOFF-S cells. In total, the mean change in AP half-width after high K^+ application for all cells was significantly less for 4wk IOP RGCs than for controls (p=0.0061).

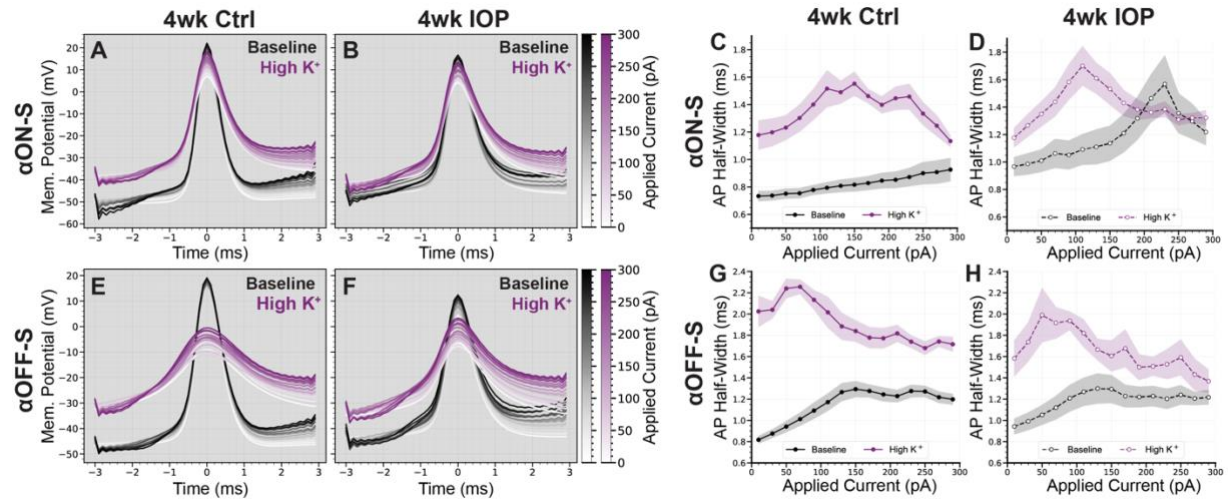

Figure 3.5 IOP elevation reduces the influence of high K^+ on action potential shape
(A-B) Mean action potential (AP) shapes of αON-S cells in baseline and high K+ conditions at each current step, for 4wk Ctrl (A) and 4wk IOP (B) groups. (C-D) Action potential half-widths of αON-S cells in baseline and high K+ conditions at each current step, for 4wk Ctrl (C) and 4wk IOP (D) groups. (E-F) Mean action potential (AP) shapes of αOFF-S cells in baseline and high K+ conditions at each current step, for 4wk Ctrl (E) and 4wk IOP (F) groups. (G-H) Action potential half-widths of αOFF-S cells in baseline and high K+ conditions at each current step, for 4wk Ctrl (C) and 4wk IOP (D) groups. The potassium-induced widening of action potentials is lessened after 4wks IOP elevation (p = 0.0061, unpaired t-test). Shaded regions: ± standard error of the mean.

Finally, we explored a potential mechanism for the observed differences in RGC excitability and potassium sensitivity. Scaling of the axon initial segment (AIS) is implicated in mediating intrinsic excitability of RGCs (Raghuram et al., 2019; Werginz et al., 2020; Wienbar and Schwartz, 2022). The AIS, marked by labeling for scaffolding protein ankyrin-G (AnkG), is a complex that clusters voltage-gated ion channels in the proximal portion of the axon and serves as the site of AP generation (Zhou et al., 1998; Gasser et al., 2012; Huang and Rasband, 2018; Leterrier, 2018). The dimensions of the AIS are plastic and can change in response to stimuli, such as chronically elevated extracellular potassium (Grubb and Burrone, 2010) and sustained sensory input (Jamann et al., 2021), in order to modulate neuronal

excitability. Because changes to the AIS have been implicated in neurodegenerative disease (Sun et al., 2014b; Marin et al., 2016; Hatch et al., 2017), we investigated whether altered AIS dimensions were associated with the decreased RGC potassium sensitivity in our microbead model. We labeled filled RGCs for AnkG and measured the AIS distance from the soma and length (**Fig. 3.6A**) for each RGC axon. There were 11 4wk IOP cells (5 αON-S and 6 αOFF-S) and 18 4wk Ctrl cells (9 αON-S and 9 αOFF-S) with identifiable axon initial segments. The AIS distance (**Fig. 3.6B**) and length (**Fig. 3.6C**) from 4wk IOP RGCs was not statistically different than those of control RGCs.

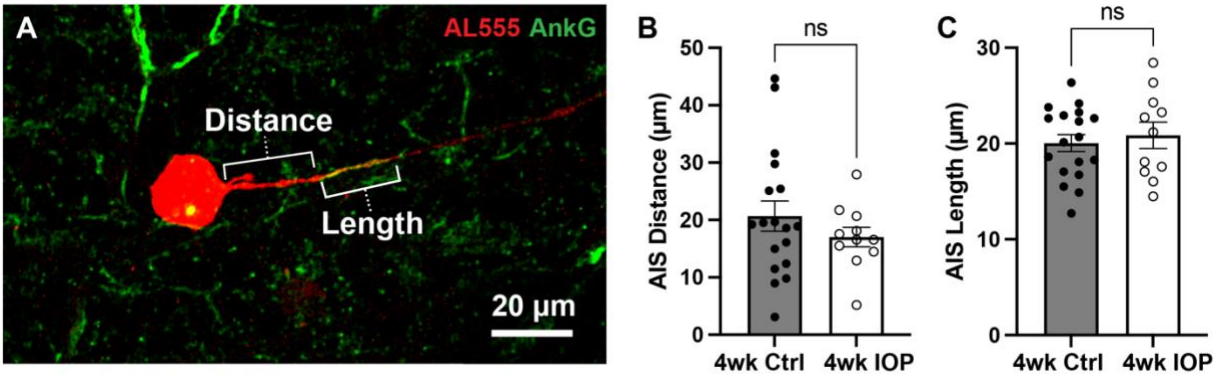

Figure 3.6 Axon initial segment dimensions are unchanged by IOP elevation
(A) Representative image of Alexa 555 (AL555, red) dye-filled RGC labeled for the axon initial segment (AIS) scaffolding protein ankyrin-G (AnkG, green). Annotations demonstrate the dimensions of AIS distance from soma and length which are quantified. (B-C) The AIS distance from the soma (B) and length (C) for all RGCs with AnkG-labeled axons. 4wk IOP does not significantly alter either of these dimensions (Distance: $p = 0.3194$, unpaired t-test; Length: $p = 0.6007$, unpaired t-test). Error bars: ± standard error of the mean.

3.4 Discussion

3.4.1 Blunted RGC excitability occurs alongside a reduced sensitivity to high K^+ conditions

The data presented here support evidence of RGC excitability changes with prolonged exposure to elevated IOP and offer insight into how RGCs respond to the acute stress of elevated extracellular potassium. We hypothesized intrinsic differences in K^+ sensitivity between αON-S and αOFF-S RGCs may drive a preferential susceptibility to elevated IOP-induced degeneration. In the present study we did not evaluate the degree of RGC death by counting somas in the retina or axons in the optic nerve. Previous work in the same model has established at the four-week timepoint there is some degeneration of axons but minimal loss of RGC somas in the retina (Ward et al., 2014; Bond et al., 2016; Risner et al.,

2021b; Risner et al., 2022). As in previous experiments at the four-week time point (Risner et al., 2021b; Risner et al., 2022) we observed reduced light- and current-evoked RGC spiking (**Figs. 3.2, 3.4**). Though the excitabilities of both αRGC types appear altered in the 4wk IOP group relative to controls, there appears to be a marginally larger effect size on the αON-S cells. These findings could represent a preferential susceptibility to IOP-related stress; however, excitability changes may also be an adaptive response.

We challenged RCGs with acutely elevated extracellular K^+ to determine how sensitivity to ionic stress changes with prolonged IOP elevation and how this impacts excitability. As expected, high K^+ media depolarized RGC membranes for both cell types and both experimental groups (**Fig. 3.3**). Remarkably, 4wk IOP elevation significantly diminished this effect, suggesting that there is decreased RGC sensitivity to acute ionic stress. We examined the impact of potassium on RGC excitability to determine if this difference was related to intrinsic changes, such as altered axonal K^+ ion channel expression or function (**Fig. 3.4**). Stepwise application of depolarizing currents reflected previously determined cell type (Twyford et al., 2014; Kameneva et al., 2016; Yang et al., 2018; Boal et al., 2022) and IOP dependent (Risner et al., 2022) differences in RGC excitability, and high K^+ conditions significantly impacted spiking. Strikingly, RGCs in the 4wk IOP group were less impacted by high K^+, maintaining sustained spiking at greater magnitudes of depolarizing current before reaching the threshold for depolarization block. These findings support the notion that decreased RGC excitability and altered K^+ sensitivity are related to RGC-intrinsic changes.

To further probe these effects, we measured AP half-width during evoked spiking (**Fig. 3.5**). Differences in this measure may reflect changes to the mechanisms of AP generation, as AP shape is impacted by K^+ currents (Geiger and Jonas, 2000; Kole et al., 2007; Kuznetsov et al., 2012; Gonzalez Sabater et al., 2021; Alexander et al., 2022). Again, there was a dramatic difference in the effect of K^+ between the 4wk IOP and control groups: for both αON-S and αOFF-S, APs were less widened by high K^+. This further supports the hypothesis that elevated IOP is affecting RGC-intrinsic excitability and suggests that there may be altered structure or function of voltage gated K^+ channels. Interestingly,

however, there was cell type specificity in how AP widths differed with IOP exposure and K^+ conditions. αON-S cells exhibited a widening of APs following 4wk IOP elevation, even in baseline, normal K^+ conditions. On the contrary, αOFF-S AP widths were similar for both the 4wk IOP and the control groups under normal K^+. Both cell types had less change in AP width following high K^+ wash on, but this difference was driven largely by the IOP-induced baseline shift for the αON-S RGCs. This is perhaps a function of cell type-specific responses to stress, paralleling the differences seen in **Fig. 3.2**. αON-S RGCs had significantly diminished light-evoked spiking, while αOFF-S light spiking was mostly preserved. It remains to be determined whether these changes prove to be protective or maladaptive for the RGCs with continued stress.

3.4.2 Retinal ganglion cell adaptation to prolonged stress

The significant differences in the impact of high K^+ conditions on RGC responses are suggestive of an adaptive process, whereby RGCs alter their physiology to preserve function and/or mitigate further degenerative stress. Hyperexcitability at 2 wks following IOP elevation is driven by axogenic processes (Risner et al., 2018; Risner et al., 2020b), and these studies further support evidence of axonal changes at 4wks. RGC axonal excitability and AP generation is dependent upon and shaped by the AIS, a dynamic structure, thus we focused our mechanistic exploration on alterations to the AIS dimensions. We hypothesized that, similar to *in vitro* chronic depolarization (Grubb and Burrone, 2010), prolonged glaucomatous stress from K^+ dysregulation and early hyperexcitability would lead to a distal shift in the AIS away from the soma. Yet, the results shown in **Fig. 3.6** do not demonstrate any differences in AIS dimensions between 4wk IOP cells and controls. Though this interpretation is limited by sample size and the lack of topographic location of cells, since AIS dimensions scale with retinal topography (Raghuram et al., 2019), this finding indicates that our observed differences in excitability and K^+ sensitivity are likely not solely reflective of AIS structural plasticity.

Rather, changes in voltage-gated ion channel and interacting protein expression, alongside larger scale alterations in glial regulation of the extracellular milieu (Nwaobi et al., 2016; Murphy-Royal et al.,

2017; Fischer et al., 2019b; Theparambil et al., 2020; Boal et al., 2021), may underly a multifactorial adaptive process to minimize metabolic and excitotoxic stress. Retinal regulation of extracellular K^+ is largely accomplished by Müller glia (Newman et al., 1984; Karwoski et al., 1989; Kofuji and Newman, 2004), which undergo reactive changes in glaucoma and exhibit physiologic deficits in K^+ buffering capacity (Bolz et al., 2008; Fischer et al., 2019b). RGC hyperexcitability driving increased K^+ flux may compound with impaired glial buffering capacity, amplifying axonal stress. Furthermore, depressed excitability may reflect interactions between dysregulated potassium and alterations in other ions, such as calcium, which modulates neuronal excitability and can contribute to cell death (Jones and Smith, 2016; Segal, 2018). Investigation of changes to expression and function of calcium-activated potassium channels in this model may further elucidate ion-mediated mechanisms of glaucomatous degeneration (Stirling and Stys, 2010; Crish and Calkins, 2011; Van Hook et al., 2019).

Glaucoma is a chronic and insidious disease, where the interaction between vulnerable RGCs and physiologic stress can to dysfunction and cell death over the course of many years. It often takes a significant degree of axon degeneration for many patients notice the resultant vision changes (Hu et al., 2014). While this emphasizes the importance of early diagnosis, it also suggests a resilience of visual function in the face of prolonged stress. Discoveries in animal models of glaucoma have illuminated the variety of adaptive responses that RGCs undergo in the face of oxidative, metabolic, and inflammatory challenges (Calkins, 2021). The experiments presented here explore an important facet of RGC adaptation, giving insight into the modulation of RGC excitability, and lay the groundwork for mechanistic investigation into potential diagnostic and therapeutic targets in early glaucomatous neurodegeneration.

CHAPTER 4

MICROFLUIDIC PLATFORMS PROMOTE POLARIZATION OF HUMAN DERIVED RETINAL GANGLION CELLS THAT MODEL AXONOPATHY

4.1 Introduction

Human pluripotent stem cells differentiated into specialized cells of the CNS are used to model several neurodegenerative diseases, including glaucoma (Sluch et al., 2017; Welsbie et al., 2017; Coccia and Ahfeldt, 2021; Ahmad et al., 2022; Dräger et al., 2022; Gomes et al., 2022). Glaucoma is an age-related neurodegenerative disease exacerbated by increased sensitivity of visual tissues to translaminar pressure gradients at the optic nerve head, a transition zone where unmyelinated RGC axons project through the optic nerve (Burgoyne, 2011). Stress transduced at the optic nerve head piques distal nerve fibers, activating mechanisms that promote retrograde axonopathy (Crish et al., 2010; Calkins, 2012).

Previously, we generated model RGCs from human embryonic stem cells (hESC), using CRISPR Cas9 to express tdTomato and THY1.2 under the control of BRN3B, a gene enriched in RGCs. We differentiated BRN3B-tdTomato-THY1.2 hESCs toward a RGC fate by chemical induction and immunopurified cells by targeting the surface protein, THY1.2 (Sluch et al., 2017). During differentiation, hESC derived RGCs (hRGC) recapitulated developmental milestones similar to endogenous RGCs, including increased expression of ATOH7, BRN3B, ISL1, and SOX4 transcripts and RBPMS and TUJ1 proteins (Sluch et al., 2015; Sluch et al., 2017).

Recently, we investigated the morphologic and physiologic differentiation of hRGCs *in vitro*. We confirmed hRGCs to be highly pure - 98.5% of tdTomato-positive cells expressed RBPMS (Rodriguez et al., 2014; Risner et al., 2021a). *In vitro,* hRGC neurites continually grew up to at least four weeks, and as neuritic fields expanded, postsynaptic densities localized to neurites. In addition to dendrite-specific proteins, hRGCs expressed genes encoding axon-related proteins, including ankyrin G (AnkG) (Risner et al., 2021a). AnkG is a scaffolding protein that organizes constituent proteins composing the axon initial

segment (AIS). AnkG serves several functions, including maintaining neuron polarity, recruitment of voltage-gated channels essential for electrogenesis, and scaling geometry to adapt to changes in excitability (Zhou et al., 1998; Hedstrom et al., 2008; Galiano et al., 2012; Gasser et al., 2012; Huang and Rasband, 2018; Leterrier, 2018). AnkG expression is targeted by axonopathies, yet AnkG is required for regeneration and reinnervation following axon injury (Sun et al., 2014a; Teliska et al., 2022). Therefore, AnkG is a prime indicator of neuronal differentiation, degeneration, and target for repair.

Although we previously found hRGCs expressed the gene (*ANK3*) encoding AnkG, hRGCs plated on coverslips without supplementation with growth factors, weakly expressed AnkG protein early during differentiation, and AnkG appeared irregularly localized during later time points. In agreement with other reports in human pluripotential stem RGCs (Teotia et al., 2019; VanderWall et al., 2019), we found hRGC current-clamp responses sensitive to depolarization block, indicative of immature neurons (Chaunsali et al., 2020; Risner et al., 2021a). Based on protein and physiologic measurements, hRGCs cultured on coverslips without supplementation with growth factors appear not to polarize robustly intrinsically.

Here, we first demonstrated hRGC axon specification is enhanced by microfluidic platforms compared to coverslip cultures (Taylor et al., 2005; Taylor and Jeon, 2010; 2011). hRGCs plated on coverslips and microfluidic platforms possessed three distinct AIS localizations based on AnkG immunolabeling: AnkG localized to a neurite directly stemming from the soma (direct), AnkG accumulated on an axon-carrying dendrite (AcD) (Thome et al., 2014; Raghuram et al., 2019), or possessed multiple AnkG-positive processes (multi). Twenty-five percent of cells plated on coverslips contained multiple AnkG-labeled neurites, whereas only five percent of cells contained multiple AISs in microfluidic platforms. We then quantified AIS length and distance from the soma, as these dimensional variables correlate with voltage-gated channel conductance (Jørgensen et al., 2021; Rotterman et al., 2021) and altered in models of degeneration (Sohn et al., 2019; Chang et al., 2021; Jørgensen et al., 2021). We found microfluidic platforms normalized hRGC AIS length and distance compared to coverslip cultures relative to AIS morphologies of mouse RGCs from whole-mount retinas.

We then leveraged our hRGCs microfluidic culture system to model axonopathy induced by colchicine, an agent that inhibits microtubule polymerization and has been previously used to model RGC degeneration (Sluch et al., 2017; Welsbie et al., 2017; Patel et al., 2020). Following three days of colchicine treatment to the axon chamber, we found colchicine degraded hRGC axons as indicated by increased varicosities, loss of anterograde transport of cholera toxin subunit B (CTB), and axon retraction. We found hRGCs with AISs located on AcDs sensitive to colchicine treatment versus direct AISs. For cells with AcDs, colchicine reduced AIS distance from the soma and increased length, suggesting reduced excitability. Overall, our findings indicate compartmentalized microenvironments promote polarization of stem cell derived neurons that enable *in vitro* modeling of axonopathies, such as glaucoma.

4.2 Materials and methods

4.2.1 Animals

All experimental procedures were approved by the Institutional Animal Care and Use Committee of Vanderbilt University Medical Center and aligned with the ARVO Statement for the Use of Animals in Ophthalmic and Vision Research. B6.Cg-Tg(Thy1-YFP)16Jrs/J (Strain #003709) mice were purchased from The Jackson Laboratory. Upon delivery, mice were housed at the Division of Animal Care facilities at Vanderbilt and provided water and standard chow *ad libitum*. The strain was maintained in house by breeding homozygotes with wild type C57Bl/6J. For this study, we used heterozygous five-month-old female mice. We used female mice for comparison because H9 human embryonic stem cells are of female origin.

4.2.2 Cell culture

We obtained H9 BRN3B-P2A-tdTomato-P2A-THY1.2 human embryonic stem (hES) cells differentiated by chemical induction for 40 days toward a retinal ganglion cell (RGC) fate from Dr. Donald Zack (Sluch et al., 2017; Risner et al., 2021a). hES-RGCs (hRGC) were shipped frozen overnight from The Johns Hopkins University to Vanderbilt University Medical Center, and upon arrival, we immediately stored hRGCs in liquid nitrogen. hRGCs were thawed, suspended in culture medium, and

centrifuged at 120 x g for 5 mins. Culture medium consisted of BrainPhys (Catalog #05790, STEMCELL Technologies), N2 Supplement-A (Catalog #07152, STEMCELL Technologies), NeuroCult SMI1 Neuronal Supplement (Catalog #05711, STEMCELL Technologies), 20 ng/mL human recombinant brain-derived neurotrophic factor (Catalog #78005, STEMCELL Technologies), 20 ng/mL human recombinant glia-derived neurotrophic factor (Catalog #78058, STEMCELL Technologies), 200 nM ascorbic acid (Catalog #72132, STEMCELL Technologies), 1 mM adenosine 3',5'-cyclic monophosphate, N^6. O^2-dibutyryrl (Catalog #28745, Millipore-Sigma), and 1% gentamicin (Catalog #15750060, Gibco). Following centrifugation, we removed the supernatant, which included DMSO-based cryopreservation medium, and resuspended the cell pellet in fresh culture medium.

We plated hRGCs on 18 mm glass coverslips (Catalog #72222-01, Electron Microscopy Sciences) contained in 12-well plates (Catalog #665180, Greiner bio-one) or XC450 microfluidic platforms (Xona Microfluidics). Coverslips and microfluidic were coated with 50 µg/mL poly-d-lysine (PDL, Catalog #354210, Corning) diluted in sterile DPBS overnight at 37ºC and 10 µg/mL mouse laminin (Catalog #23017015, Thermo Fisher Scientific) diluted in DPBS for four hrs at 37ºC. For microfluidic platforms, we added 75K cells per somal port. However, only about 75% of these cells were drawn into the somal chamber. We plated hRGCs on coverslips at a density of 60K/cm^2. Samples were incubated at 37ºC with 5% CO_2. On the following day after plating cells, we exchanged half of the medium, adding an addition 30 ng/mL BDNF to coverslip cultures and to the axon chambers of microfluidic cultures. For microfluidic cultures we maintained a volume difference between the somal (160 µL) and axonal chambers (120 µL) to drive neurite outgrowth towards the axonal chambers. Subsequently, we exchanged half of the medium every two to three days for the duration. Cultures were maintained for 10 to 15 days. Following each endpoint, we fixed samples in 4% paraformaldehyde (PFA).

For a subset of experiments, we induced degeneration by administering 30 nM colchicine (Catalog #C97754, Millipore-Sigma), which was diluted in sterile DPBS for stocks and culture medium for working solutions. Colchicine was added to the axonal chambers of microfluidic cultures, and samples were incubated for three days (Welsbie et al., 2017). Twelve hrs prior to the endpoint, we added 1%

cholera toxin subunit B (CTB, Catalog #C34778, Thermo Fisher Scientific) in microfluidic somal chambers to track anterograde axonal transport. Afterwards, we fixed samples for 30 min in 4% PFA diluted in PBS.

4.2.3 Immunohistochemistry and imaging

Following fixation, we washed samples three times with PBS and blocked with 0.1% Triton-X and 5% normal donkey serum (NDS) at room temperature for two hrs. After blocking, we incubated samples overnight at 4ºC in primary antibodies including postsynaptic density 95 (PSD-95, 1:300, Catalog #51-6900, Invitrogen), ankyrin G (AnkG, 1:200, Catalog #75-146, Neuromab), cleaved caspase 3 (CC3, 1:400, Catalog #9661, Cell Signaling Technologies), phosphorylated neurofilament H (SMI-34, 1:1000, Catalog #835501, Biolegend) in addition to 0.1% Triton-X and 5% NDS. The following day, we washed samples three times with PBS and incubated samples in 0.1% Triton-X, 5% NDS, and appropriate secondary antibodies (Jackson Immunoresearch) for two hrs at room temperature. Afterwards, samples were washed three times with PBS, and we applied Fluoromount-G (Catalog #0100-20, Southern Biotech). We imaged samples at the Vanderbilt University Shared Imaging Shared Resource. We used a Nikon spinning disk confocal microscope with 40 or 60x oil-immersion objectives (Plan Apo Lambda 1.4 NA WD 0.13 mm) equipped with a Yokogawa CSU-X1 spinning disk head, Photometrics Prime 95B sCMOS camera, automated stage driver, and four laser lines (405, 488. 561, and 647 nm). Exposure and laser power settings were kept constant across independent variables (tissue preparation) for each dependent variable (*e.g.*, AnkG secondary antibody).

4.2.4 Image analysis

PSD-95 fluorescence and colocalization with tdTomato expression was determined using ImageJ plugins (NIH, Bethesda, MD). For AIS bounds determination, hRGC neurites containing AnkG labeling were hand traced in ImageJ using the freehand line tool from the edge of the soma and past the bounds of visible AnkG labeling. For each trace the fluorescence profile from the AnkG channel was exported and AIS localization (i.e., direct, AcD, or multi) was noted. AnkG profiles were analyzed in Python 3.9 using

the SciPy 1.7.1 module (Virtanen et al., 2020). Background fluorescence was subtracted from AnkG intensity profiles using a rolling ball filter with a radius of 50. Smoothed AnkG profiles were generated using a Savitzky-Golay filter with a first order polynomial fit. AIS bounds were systematically defined as the extent where smoothed AnkG values were greater than 50% of the difference between baseline and maximum intensity. Colocalization analysis was performed using the Coloc2 plugin. For representative images we enhanced immunofluorescence by subtracting background intensity, smoothing the intensity values, and increasing the contrast of the image.

4.2.5 Statistical analyses

All data are reported as mean ± standard error of the mean. All statistical tests were performed in GraphPad Prism 9 (GraphPad Software, San Diego, CA). All data sets were checked for normality. Two outliers for PSD-95 labeling data, one from each chamber as identified by Grubb's test with an alpha of 0.05, were excluded. There were a few instances (0% of mouse, 6% of coverslip, 1.5% of microfluidic) where AIS bounds could not be determined algorithmically due to weak antibody labeling, and these values were included for localization analysis but not distance/length analyses. Cells with multiple AISs were also excluded from dimension analysis since a primary axon could not be determined. For colchicine treated microfluidic devices, 2 of 6 devices were excluded from dimension analysis because they contained too few identifiable AISs of each localization. Otherwise, all data were included in analyses. For statistical tests on PSD-95 labeling, AIS dimension analysis, and colchicine degeneration assays, we used the average value from each independent replicate/sample for statistical tests. We defined statistical significance as a p-value of 0.05 or less. Exact p-values and sample sizes are indicated in figure legends, alongside the specific details of the statistical test used for each analysis.

4.3 Results

4.3.1 Microfluidic Platforms Promote Normalization of hRGC Axon Initial Segment Morphology

We established a foundation for investigating AIS morphology in hRGCs by first demonstrating mouse retinal ganglion cell (mRGC) AIS localization. We immunolabeled whole-mount retinas from

Thy1-YFP mice (female, 5 months of age, n = 3) against AnkG. For the majority of mRGCs, we observed AnkG localized to a single process emanating directly from a YFP-positive cell body (**Fig. 4.1A**). For a few mRGCs, AnkG accumulated on a process distal to a bifurcation in a primary neurite (**Fig. 4.1B**). This

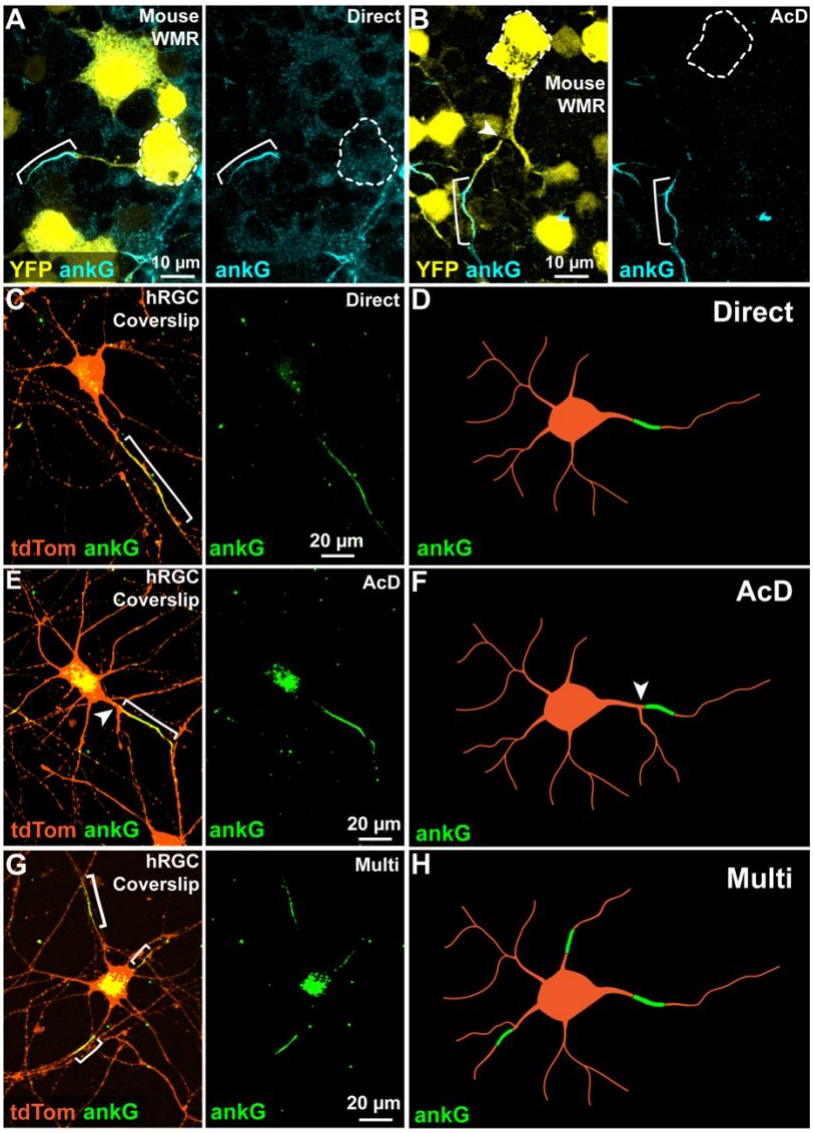

Figure 4.1 Mouse and human-derived RGCs exhibit heterogeneity in AIS localization
(**A-B**) Representative micrographs of whole mount retinas from B6.Cg-Tg(Thy1-YFP)16Jrs/J mice labeled for ankyrin-G (ankG) demonstrate two distinct patterns of retinal ganglion cell (RGC) axon initial segment (AIS) localization. (**A**) The majority of RGCs had a single ankG-labeled AIS (cyan) located on a process emanating directly from the YFP-labeled soma (yellow, with white dotted outline). (**B**) A small subset of mouse RGCs had an AIS located on a process distal to a bifurcation in a primary dendrite (white arrowhead), defined as an axon-carrying dendrite (AcD). (**C-H**) Example micrographs of tdTomato (tdTom, orange) expressing RGCs derived from human embryonic stem cells (hRGC) cultured on coverslips demonstrate greater heterogeneity in ankG-labeled (green) AIS localization. As seen in mouse retina, hRGCs had single AISs localized on a process emanating directly from the soma (direct, **C**, diagrammed in **D**) as well as on an AcD (**E**, diagrammed in **F**). There was also a subset of hRGCs that possessed contained multiple AISs (Multi, **G**, diagrammed in **H**).

previously described AIS localization is referred to as an axon-carrying dendrite (AcD) (Thome et al., 2014; Hamada et al., 2016; Raghuram et al., 2019).

Next, we defined AIS localization in hRGCs plated onto coverslips supplemented with brain- and glia-derived neurotrophic factors (BDNF, GDNF) and cultured for 10-15 days. We observed three distinct AIS localizations defined by AnkG immunolabeling. Similar to mRGCs, many hRGCs accumulated AnkG within neurites extending directly from cell somas (**Fig. 4.1C,D**) or from AcDs (**Fig. 4.1E,F**). However, in addition to these two profiles, we also observed many instances of AnkG localized to multiple neurites originating from a single hRGC soma (**Fig. 4.1G,H**).

We then determined the effect of microfluidic platforms on AIS localization and polarization. hRGCs were plated onto microfluidic platforms supplemented with BDNF and GDNF and cultured for 10 to 15 days. These platforms consisted of two primary chambers, soma and axon, connected by a microgroove barrier (**Fig. 4.2A**). Following 10 to 15 days *in vitro* (DIV), we observed neurites extending through the microgroove section and into the axon chamber (**Fig. 4.2B**). After performing immunohistochemistry and confocal microscopy, we found hRGCs cultured in microfluidic devices exhibited two principal AIS localizations: direct and AcD (**Fig. 4.2C,D**). Importantly, we did not observe AnkG accumulation within putative axons projecting into the axon chamber (**Fig. 4.2E**), indicating restriction of AnkG localization near the somas and not in distal axons (Galiano et al., 2012). To further investigate hRGC dendritic and axonal specification, we immunolabeled cells against the excitatory postsynaptic marker, PSD-95, and determined PSD-95 integrated intensity and colocalization with tdTomato in the soma (**Fig. 4.2F**) and axon (**Fig. 4.2G**) chambers. PSD-95 immunolabeling was significantly stronger, accounting for area, in the soma chamber (**Fig. 4.2H**, $p = 0.0281$), and there was greater colocalization of PSD-95 labeling with tdTomato+ hRGC processes in the soma chamber than in the axon chamber (**Fig. 4.2I**, $p = 0.0003$). Although PSD-95 did not heavily accumulate within fibers projecting into the axon chamber, similar to other reports, we observed PSD-95 localized within distal axon growth cones (**Fig. 4.2G**) (Fletcher et al., 1991; Sabo and McAllister, 2003).

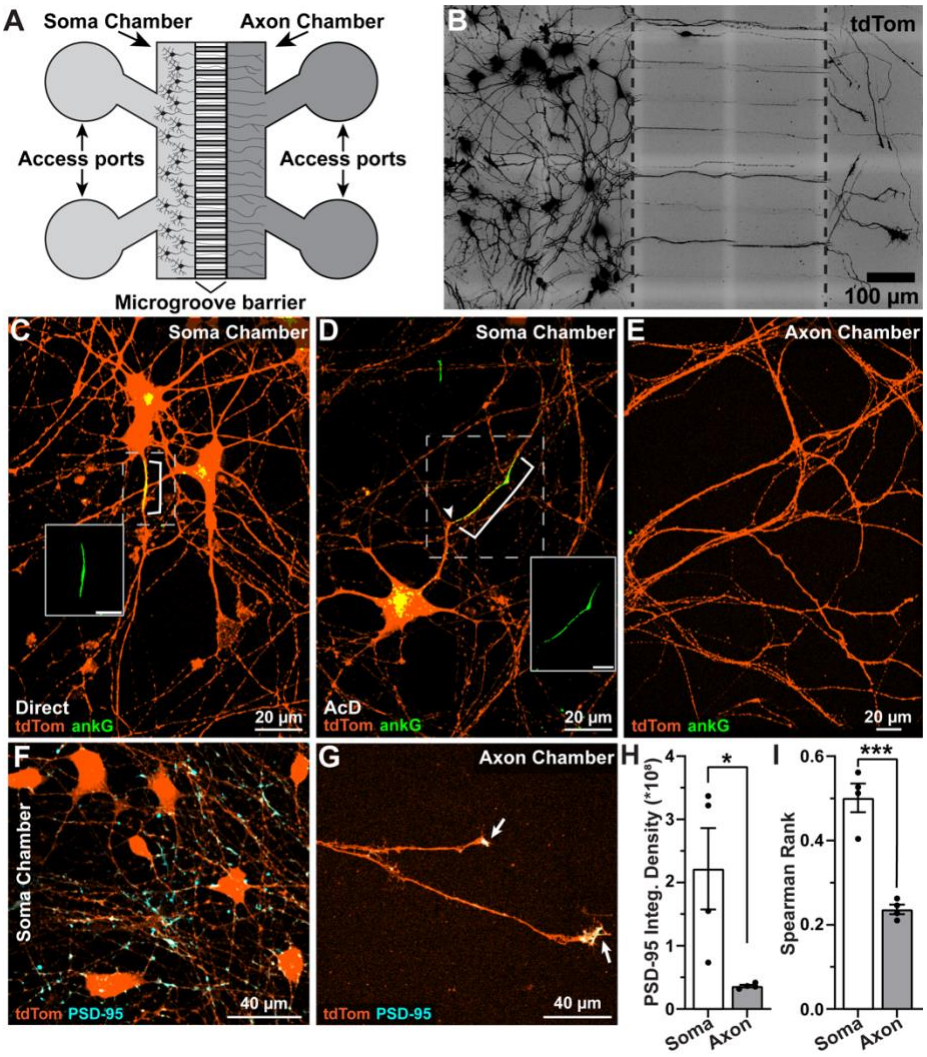

Figure 4.2 hRGCs plated on microfluidic platforms are polarized into somato-dendritic and axonal compartments

(**A**) Schematic of Xona XC450 microfluidic platform (compartments are not illustrated to scale). (**B**) When plated on XC450 for 8-10 d, hRGC projections extend through the microgroove chamber and into the axon chamber. (**C**) When hRGCS are cultured in microfluidic platforms, ankG (green) typically localizes to an axon extending directly from the soma (Direct) or (**D**) on an axon-carrying dendrite (AcD) within the soma chamber. Insets in C and D show ankG channel only. Scale bars in insets = 10 µm. (**E**) ankG does not accumulate within putative axons in the axon chamber. (**F-G**) Representative micrographs of PSD-95-labeled (cyan) hRGCs cultured in microfluidic devices demonstrate evidence of post-synaptic specification in the soma chamber (**F**) and localization to putative axon growth cones in the axon chamber (**G**). Arrows indicate PSD-95 colocalized with tdTom-positive putative axon growth cones. (**H**) Quantification of PSD-95 immunofluorescence suggests significantly greater expression in the soma chamber than the axon chamber ($p = 0.0281$, unpaired *t*-test). Integrated (Integ) density is the summed pixel values multiplied by area. (**I**) The soma chamber exhibits significantly greater colocalization of PSD-95 labeling and tdTom expression than in the axon chamber ($p = 0.0003$, unpaired *t*-test). n = 4 independent devices. Error bars: ± standard error of the mean. *$p < 0.05$, ***$p < 0.001$.

We then established a systematic method for measuring AIS dimensions by tracing AnkG fluorescence profiles along neurites and computationally determining AIS bounds (**Fig. 4.3**). We used this method to compare AIS dimensions between AnkG localizations across mRGCs and hRGCs coverslip

and microfluidic platform cultures (**Fig. 4.4**). For mRGCs we found 97% (131/135) of cells possessed an AIS stemming directly from the soma and the remaining 3% (4/135) localized to axons emanating from an AcD (**Fig. 4.4A**). Of the hRGCs plated on coverslips with an AIS that could be directly traced back to its soma of origin, 40% (63/156) stemmed directly from the soma, 34% (53/156) localized to an AcD, and 26% (40/156) possessed multiple AISs (**Fig. 4.4A**). For hRGCs cultured on microfluidic platforms, we found 59% (121/204) of AISs localized to axons projecting directly from the soma, 35% (72/204) stemmed from AcDs, and the remaining 5% (11/204) contained multiple AISs (**Fig. 4.4A**).

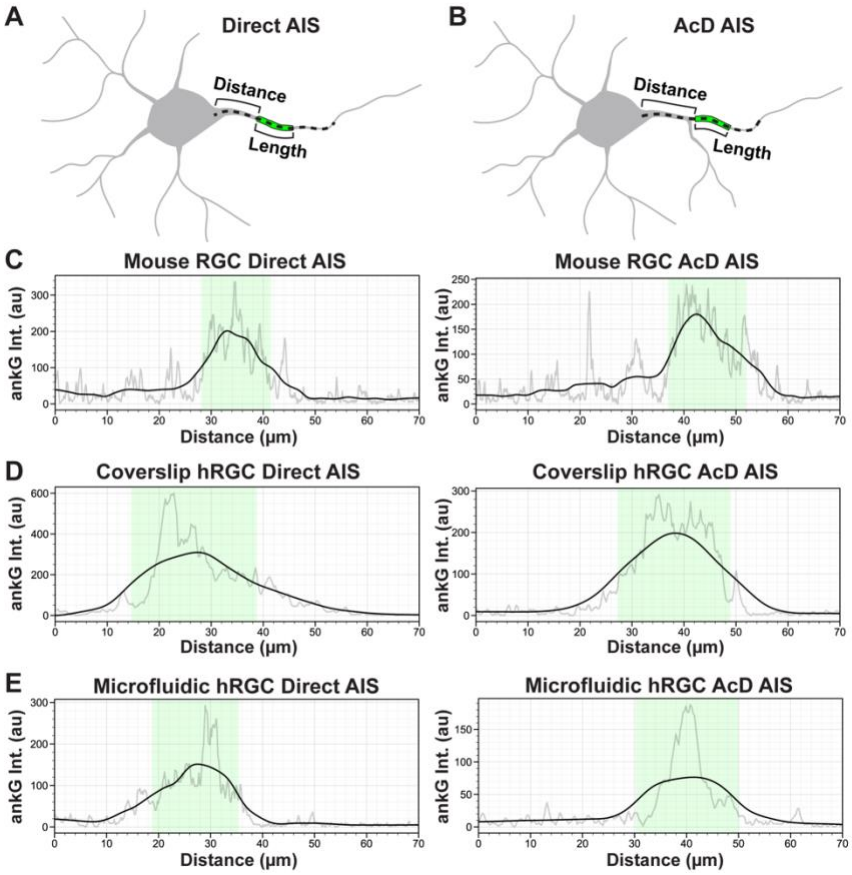

Figure 4.3 Systematic quantification of AIS length and distance from soma
(**A**-**B**) To determine AIS distance from soma and length, intensity profiles of ankG immunofluorescence were determined from hand traces (shown as dashed line) extending from the soma edge along the ankG-containing process for direct (**A**) and axon-carrying dendrite (AcD, **B**) morphologies. ankG illustrated as green span along the neuronal process. (**C**-**E**) Representative ankG intensity profiles from mouse RGCs (**C**), coverslip hRGCs (**D**), and hRGCs plated on microfluidic platforms (**E**). From raw traces (light gray lines), background fluorescence was subtracted, ankG intensity profiles were smoothed (black lines), and we defined the AIS length as the extent where the smoothed ankG intensity was greater than 50% of the difference between baseline and maximum intensity (green shaded region). au = arbitrary units, Int = mean intensity.

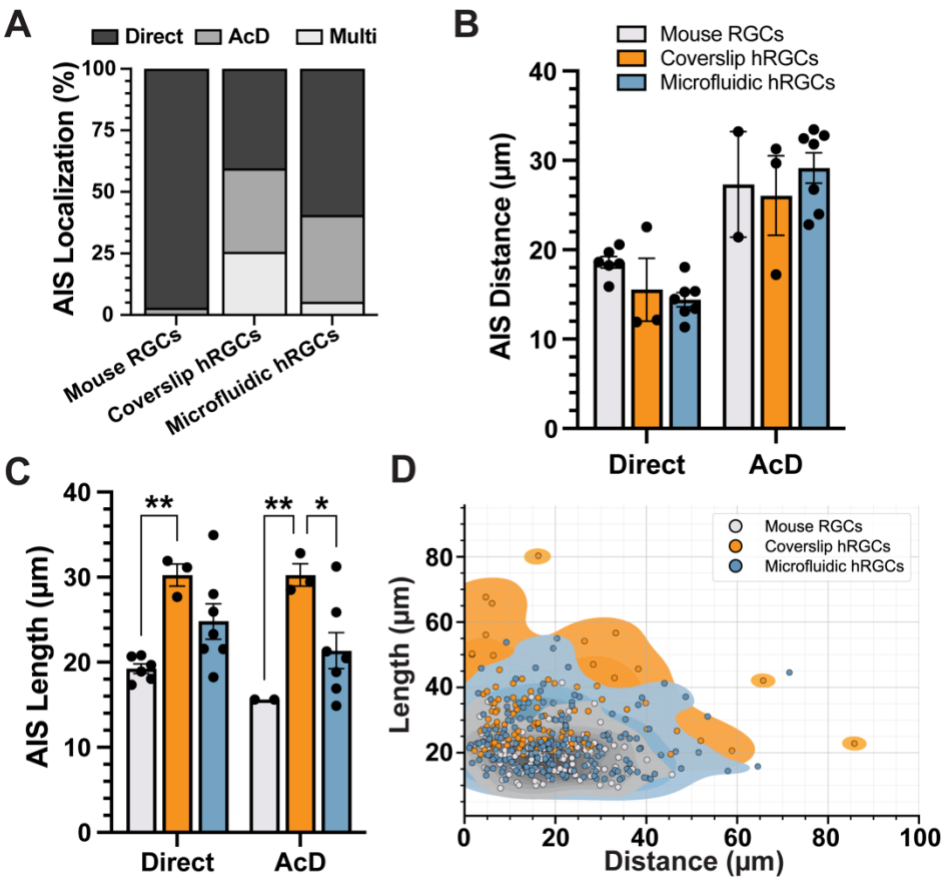

Figure 4.4 Microfluidic platforms promote normalization of AIS morphology in hRGCs
(**A**) Cumulative percentages of AIS localizations observed in mouse RGCs, hRGCs plated on coverslips, and hRGCs cultured in microfluidic platforms. (**B**) AIS distance from soma is significantly longer for AcD than direct AISs ($p < 0.0001$), but largely the same across cell types/culture platforms ($p = 0.6999$). (**C**) hRGCs cultured on coverslips possessed direct ($p = 0.0041$) and AcD ($p = 0.0031$) AISs significantly longer than mouse RGC direct and AcD AISs, respectively. hRGCs plated on microfluidic platformed contained AcD AISs significantly shorter than hRGCs cultured on coverslips ($p = 0.0182$). hRGCs plated on microfluidics possessed AISs of similar length to mouse RGCs ($p \geq 0.083$). (**D**) Distribution of AIS distance vs. length scatterplots for each of the cell types/culture platforms as determined by kernel density estimates. Coverslip hRGC (orange) AIS dimensions appear to have a more variable distribution than microfluidic hRGCs (blue) or mouse RGCs (gray). Sample sizes (excluding multi) - Mouse RGC group: 135 cells, 6 retinas (only 2 retinas contained AcD); coverslip hRGC group: 109 cells from 3 independent samples; microfluidic hRGC group: 190 cells, 7 independent devices. Statistics: Two-way ANOVA, Tukey post-hoc test (B,C); Kernel density estimate (D). Error bars: ± standard error of the mean. *$p < 0.05$, **$p < 0.01$.

We then compared AIS dimensions for all cells possessing a single AnkG-positive neurite (i.e., direct or AcD localizations). The distance from the edge of the soma to the beginning of the AnkG labeling was significantly longer for AcD AISs than direct (**Fig. 4.4B**, $p < 0.0001$). However, culture condition did not significantly impact the AIS distance ($p = 0.6999$). Compared to mouse RGCs, hRGCs plated on coverslips possessed significantly longer direct and AcD AISs (**Fig. 4.4C**; $p = 0.0041$ direct, $p = 0.0031$ AcD). hRGCs plated onto microfluidic platforms possessed significantly shorter AcD AISs

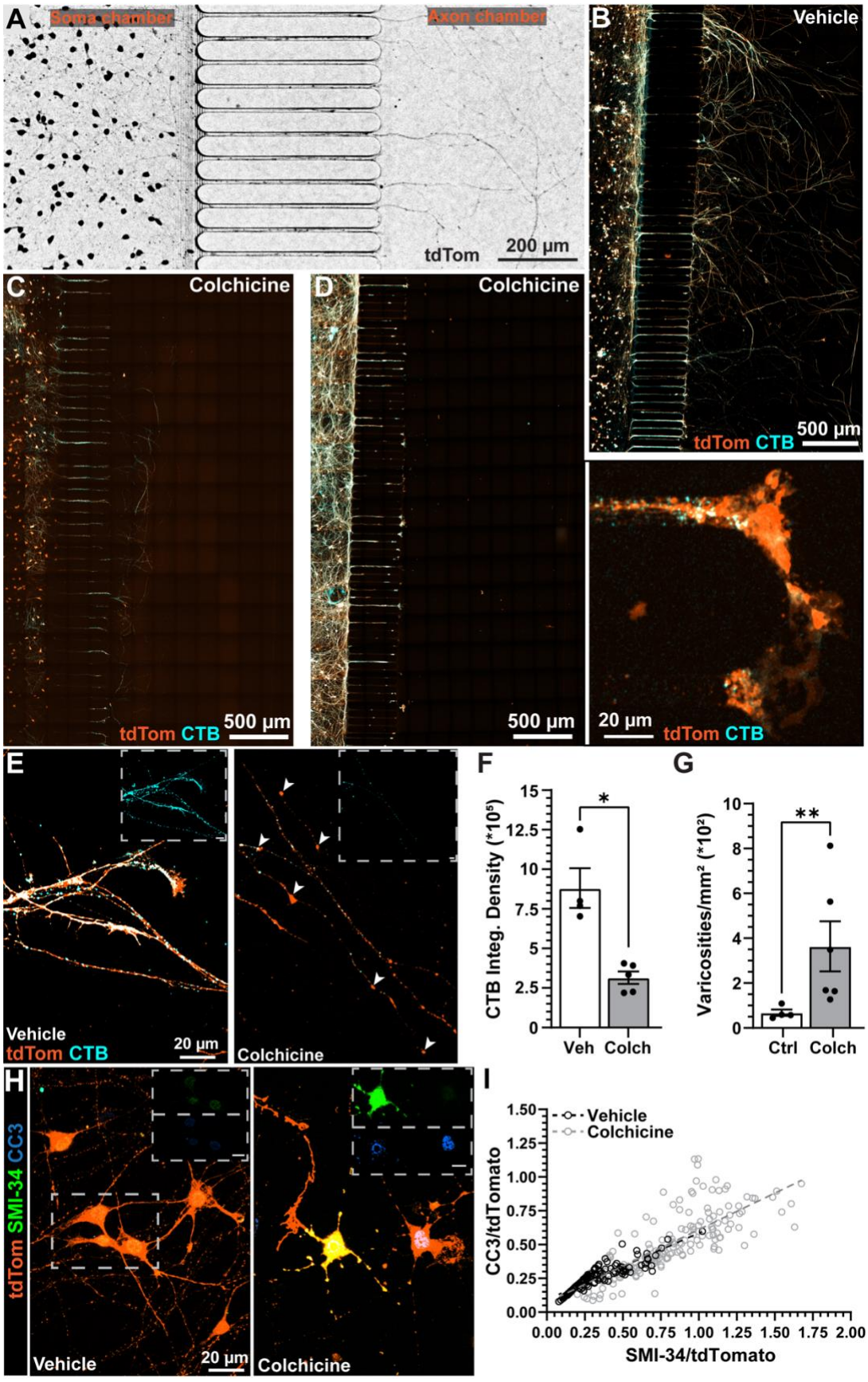
A
Soma chamber
Axon chamber
tdTom
200 µm
B
Vehicle
tdTom CTB
500 µm
C
Colchicine
tdTom CTB
500 µm
D
Colchicine
500 µm
20 µm
tdTom CTB
E
Vehicle
tdTom CTB
20 µm
Colchicine
F
CTB Integ. Density (*10⁵)
15
12.5
10
7.5
5
2.5
0
*
Veh
Colch
G
Varicosities/mm² (*10²)
10
8
6
4
2
0
**
Ctrl
Colch
H
tdTom SMI-34 CC3
Vehicle
20 µm
Colchicine
I
Vehicle
Colchicine
CC3/tdTomato
1.50
1.25
1.00
0.75
0.50
0.25
0.00
0.00 0.25 0.50 0.75 1.00 1.25 1.50 1.75 2.00
SMI-34/tdTomato

Figure 4.5 Colchicine application models axonopathy in hRGCs cultured on microfluidic platforms
(**A**) Micrograph of live tdTomato-positive (black) hRGCs following 8 DIV, demonstrating extension of putative axons into the axon chamber prior to application of colchicine. (**B-D**) Representative images of tdTomato-positive hRGCs (orange) cultured in microfluidic devices after the addition of either vehicle (**B**) or colchicine (30 nM, 3 d) to the axon chamber (**C,D**). Colchicine caused axon retraction (**C**) in some samples and outright axon degeneration in other samples (**D**). (**D**, right) Example degenerative axon located within the microgroove section of the microfluidic platform following colchicine treatment. Fluorescently conjugated cholera toxin subunit B (CTB, cyan) added to the soma chamber (left side of images) is transported anterogradely to distal putative axons in the axon chamber. Colchicine appeared to reduce the transport of CTB to spared axons in the axon chamber (**C-E**). (**E**) Higher-magnification example images of the axon chambers in vehicle- and colchicine-treated cells. CTB fluorescence (cyan) is evident in vehicle samples but reduced following colchicine treatment. In colchicine-treated cultures, spared axons exhibit degenerative varicosities (**E**, right, white arrowheads,). (**F-G**) Following colchicine treatment CTB fluorescence in the axon chamber is reduced ($p = 0.0159$), and varicosity density significantly increased ($p = 0.0095$). Vehicle group = 4 independent samples, Colchicine group = 5-6 independent samples. (**H**) Example confocal images of hRGCs (orange) following vehicle (left) or colchicine (right) treatment and immunolabeled against SMI-34 (green) and cleaved caspase 3 (CC3, blue). Scale bars in insets of E and H subpanels = 10 µm. (**I**) We found significant positive correlations between CC3 and SMI-34 for both vehicle ($R^2 = 0.80$, $p < 0.001$) and colchicine ($R^2 = 0.72$, $p < 0.001$) treated cells. CC3 and SMI-34 integrated density was normalized by tdTomato fluorescence integrated density. Vehicle: n = 123 cells from 2 devices. Colchicine: n = 214 cells from 4 devices. Statistics: Mann-Whitney test (F,G), Linear regression (I). Error bars: ± standard error of the mean. *$p < 0.05$, **$p < 0.01$.

versus hRGCs plated onto coverslips ($p = 0.0182$). We found microfluidic hRGC AIS length similar to mRGCs for both direct ($p = 0.0830$) and AcD AISs ($p = 0.2861$; **Fig. 4.4C**). Finally, we noted differences in the variability in AIS dimensions between mRGCs, hRGCs plated on coverslips, and hRGC plated on microfluidic platforms. hRGCs plated on coverslips appeared to have a highly variable distribution of the AIS distance versus length relationship, whereas microfluidic hRGC and mRGC AISs dimensions demonstrated less variability (**Fig.4. 4D**).

4.3.2 Colchicine-induced hRGC Axonopathy Disrupts AIS Structure

Next, we sought to develop an *in vitro* model of axonopathy in hRGCs cultured in microfluidic platforms. We noted that neurites extended through the microgroove barrier and into the axon chamber within 8 to 12 DIV (**Fig. 4.5A**). Following 10 to 12 DIV, we administered either vehicle (culture medium) or 30 nM colchicine into the axon chamber. Two days after the treatment with vehicle or colchicine, we added 1% CTB 647 into the soma chamber of the microfluidic platform to evaluate anterograde axonal transport. Previous investigations on anterograde axonal transport using neural tracers have demonstrated similar microfluidic platforms maintain fluidic isolation between chambers for at least 20 hrs (Taylor et al., 2005). The next day, we prepared samples for immunocytochemistry and confocal microscopy.

In vehicle conditions, we observed tdTomato-positive axon-like processes labeled with CTB extending into the axon chamber up to 2 mm from the soma chamber (**Fig. 4.5B**). Following treatment with colchicine, axons appeared retracted or outright degenerated (**Fig. 4.5C-D**). We observed enlarged varicosities along colchicine-treated hRGC axons and ostensibly diminished CTB transport relative to vehicle-treated hRGCs (**Fig. 4.5E**). Quantification of CTB fluorescence within remaining fibers in the axon chamber indicated colchicine treatment significantly reduced anterograde transport by 64% ($p = 0.0159$, **Fig. 4.5F**). In addition to axon transport deficits, we found colchicine significantly increased the density of axonal varicosities by 438% ($p < 0.0095$, **Fig. 4.5G**). Finally, we probed hRGCs for additional indicators of degeneration, including expression of phosphorylated neurofilament H (SMI-34) and cleaved caspase 3 (CC3) in the soma chamber (Noristani et al., 2016; Bernardo-Colon et al., 2019). As expected, based on our results from axon transport assays, we found Colchicine treatment appeared to increase accumulation of both SMI34 and CC3 within hRGC somas (**Fig 4.5H**). We normalized SMI-34 and CC3 immunofluorescence to tdTomato fluorescence and plotted the values for each cell. Colchicine did not significantly affect tdTomato fluorescence (Vehicle = 155,580 ± 49,457, Colchicine = 83,172 ± 33,006 integrated intensity; $p = 0.228$). Following normalization, we found significant ($p < 0.001$) positive correlations between SMI-34 and CC3 for both vehicle and colchicine conditions. We found 0.8 and 0.74 of the variation in CC3 immunofluorescence accounted for by SMI-34 immunolabeling in vehicle and colchicine samples, respectively. Notably, we observed colchicine increased both SMI-34 and CC3 intensity compared to vehicle (**Fig. 4.5I**).

Finally, we sought to determine the influence of colchicine on AIS morphology. However, we found colchicine degraded AnkG immunofluorescence, and therefore, we could not identify an AIS for many hRGCs. However, we evaluated AIS localization and dimension on cells with visible AnkG labeling that we could trace its somatic origin, and we found axons localized both directly from the soma and from AcDs (**Fig. 4.6A,B**). We did not observe any colchicine-treated hRGCs possessing multiple AISs projecting from a single soma, however, the overall distribution of AIS localizations was not statistically different between vehicle and colchicine-treated cells (**Fig. 4.6C**, $p = 0.1041$). As described

above (**Fig. 4.3**), we then measured the distance from soma and length of each AIS. We found the AISs remaining after colchicine treatment tended to be closer to the soma overall than vehicle conditions (**Fig. 4.6D**, p = 0.0063). AISs localized to AcDs appeared to be more strongly impacted by colchicine treatment (**Fig. 4.6D**, p = 0.0179) than direct AISs (**Fig. 4.6C**, p = 0.3041). However, colchicine did not impact AIS length (**Fig. 4.6E**, p = 0.3066). These findings suggest that during degeneration axon molecular identity is disrupted prior to structural degradation and eventual cell death, and that AIS localization may be correlated to susceptibility to degeneration.

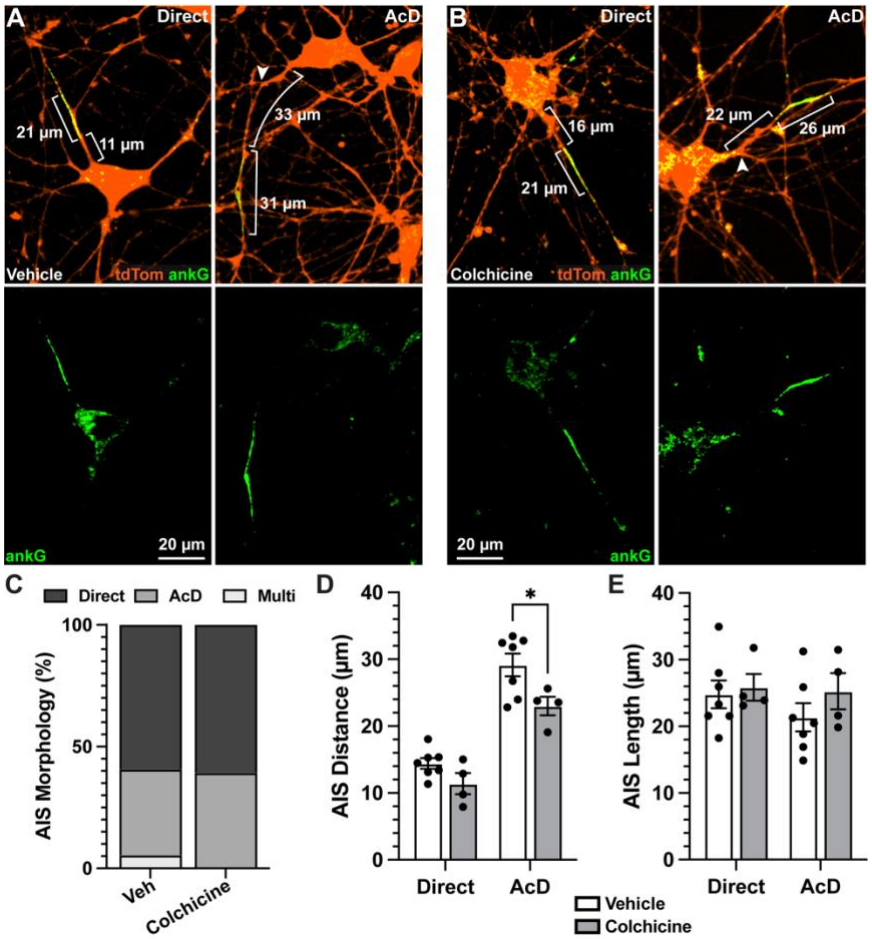

Figure 4.6 AcD axon initial segments are preferentially susceptible to colchicine-induced changes in morphology

(**A-B**) Example images of ankG labeling (green) in hRGCs (orange) treated with vehicle (**A**) or colchicine (**B**). (**C**) Cumulative percentages of AIS localizations for both treatment groups. No multi-AIS cells were seen in the colchicine group, although there was not a significant difference in the distribution of localizations between groups (p = 0.104). (**D**) Colchicine treatment significantly decreased AIS distance from soma (p = 0.0063), with a greater decrease seen in AcD AISs (p = 0.0179) than in direct AISs (p = 0.3041). (**E**) Colchicine treatment did not significantly affect AIS length (p = 0.3066). Vehicle group: n = 190 cells from 7 independent devices. Colchicine group: n = 76 cells from 4 independent devices. Statistics: chi-squared test (C), Two-way ANOVA with Šídák's multiple comparisons test (D,E). Error bars: ± standard error of the mean. *p < 0.05.

4.4 Discussion

Previously we found hRGCs cultured on glass coverslips without growth factor supplementation do not form well-defined AISs (Risner et al., 2021a). Here, we sought to develop an *in vitro* model to drive hRGC axon specification. We demonstrated that microfluidic platform promote polarization based on AnkG and PSD-95 localization. Using this microfluidic platform, next, we sought to develop and validate a model of axonopathy and test the influence of injury on AIS morphology. We chemically lesioned hRGC axons by adding colchicine, and we found axon-carrying dendrite (AcD) AISs respond to insult through changes in morphology.

We demonstrated a foundation for characterizing hRGC AIS morphology by first examining mouse RGC AIS morphology. Our characterization of mouse RGCs AIS morphologies demonstrated similar direct and AcD profiles as previously observed in hippocampal pyramidal, cortical, and RGCs (**Fig. 4.1A,B**) (Thome et al., 2014; Hamada et al., 2016; Raghuram et al., 2019; Boal et al., 2022; Hodapp et al., 2022; Wahle et al., 2022). Moreover, our AIS geometry measurements of mouse RGCs were consistent with previously reported values (Raghuram et al., 2019; Werginz et al., 2020; Boal et al., 2022; Wienbar and Schwartz, 2022).

Compared to mouse RGCs, hRGCs plated on coverslips exhibited marked heterogeneity in AIS localization as evidenced by morphologic type and variability (**Figs. 4.1C-H; 4.4A,D**). Importantly, one-fourth of these cells contained multiple AnkG-positive putative axons originating from a single soma (**Figs. 4.1G, 4.4A**). This multi-AIS phenotype can be induced by systemic pharmacologic enhancement of microtubule stability or disrupting the binding of AnkG to the cytoskeleton (Witte et al., 2008; Dorrego-Rivas et al., 2022), suggesting multi-AIS cells lack axon specification. Culturing hRGCs on microfluidic platforms reduced the number of multi-AIS cells, and increased the proportion of cells with direct AISs (**Figs. 4.2C; 4.4A,D**). Notably, the AIS morphology appears dependent on culture platform as the extracellular matrix and medium was the same for coverslip and microfluidic samples. Together, these finding suggests microfluidic platforms promote axon specification.

Based solely on this study, the mechanisms underlying the increase in the number of polarized neurons in microfluidic devices is unclear. However, evidence suggest axon specification may be enhanced by promoting long-ranged neurite outgrowth through the restricted confines of the microgroove section of microfluidic devices, which inhibit neurites from turning back toward the soma chamber and growth factor gradients generated through hydrostatic pressure (Taylor et al., 2005; Fligor et al., 2021). The initial group of cells containing pioneering axons may increase polarization of neighboring neurons (Namba et al., 2014). Future studies will test this notion directly by comparing AIS morphology of cell extending long-ranged axons versus cells that do not.

AIS geometry is an indicator of neuronal development, synaptic strength, and intrinsic excitability (Gutzmann et al., 2014; Hamada et al., 2016; Yamada and Kuba, 2016a; Schluter et al., 2019; Booker et al., 2020; Goethals and Brette, 2020; Werginz et al., 2020; Fekete et al., 2021; Jamann et al., 2021). Considering results from others, the AIS geometry of hRGCs, regardless of culture platform, predicts hyperexcitability compared to the AIS geometry of mouse RGCs (Grubb and Burrone, 2010; Rotterman et al., 2021). Our earlier findings support this estimate. We found hRGCs sensitive to small depolarizing currents (10 pA), but hRGCs produced depolarization block when depolarizing current strength modestly increased (20-60 pA) (Risner et al., 2021a). This small dynamic range for repetitive firing may be due to weak synaptic input, reduced expression of voltage-sensitive channels, or improper localization of voltage-gated channels along the AIS (Van Wart and Matthews, 2006; Booker et al., 2020). Regarding synapses, evidence suggests coculturing human stem cell derived RGCs with astrocytes, increases localization of postsynaptic densities and repetitive firing, yet cells remained sensitive to depolarization block (VanderWall et al., 2019). As depolarization block is primarily due to accumulation of inactivation of voltage-gated Na^+ (Na_V) channels (Catterall et al., 2007), future investigations will probe the influence of culture platform on expression and localization of $Na_V1.2$ and $Na_V1.6$ channels relative to AnkG in hRGCs.

Next, we sought to develop and validate an *in vitro* model of hRGC axonopathy by chemically lesioning axons, using colchicine, and testing the influence of injury on AIS morphology. Here, we found

colchicine produced remarkable axon retraction and degeneration (**Fig. 4.5B-D**). This variability in the responses of axons to colchicine between cultures may be due to modest volume differences between the soma and axon chambers that led to dilution of the colchicine in the axon chamber. In future experiments, application of culture membranes that cover the access ports of the microfluidic platforms may prevent evaporation that might produce slight differences in volume between chambers. In samples that contained neurites in the axon chamber, we found colchicine reduced anterograde axonal transport of CTB and increased density of enlarged varicosities (**Fig. 4.5E-G**). In corroboration with these results, several studies have shown axonopathy produces deficits in anterograde axonal transport and induces formation of varicosities (Wang et al., 2003; Calkins et al., 2017; Gu et al., 2017; Risner et al., 2018).

Deficits in axonal transport and varicosity growth are two interrelated markers of degeneration: axonal transport of mitochondria ceases during varicosity formation (Gu et al., 2017). However, evidence from both *in vitro* and *in vivo* preparations suggest varicosity development is partially reversible, suggesting that varicosity formation and underlying mechanisms may be a target for neuronal repair (Yang et al., 2013; Gu et al., 2017; Marion et al., 2018). Based on our findings from axonal transport and morphologic assays, we were not surprised to find that colchicine increased expression of other indicators of degeneration, including phosphorylated neurofilament H (SMI-34) and cleaved caspase 3 (CC3) (**Fig. 4.5H,I**) (Noristani et al., 2016; Bernardo-Colon et al., 2019). Overall, our results suggest microfluidic platforms provide a system to model axonopathy and test mechanisms for neuronal repair.

Finally, we examined if colchicine-induced axonopathy altered AIS morphology in hRGCs (**Fig. 4.6A,B**). Interestingly, hRGC AISs on AcDs appeared to be more susceptible to colchicine than direct AISs. Following colchicine treatment, AcDs exhibited a proximal shift towards the soma (**Fig. 4.6D**). This finding suggests at least two possibilities: our sample is biased towards hRGCs that remained intact following colchicine treatment or AcDs respond to colchicine through changes in geometry. Of course, evidence exists supporting both possibilities. The murine retina contains over 40 different RGC types, and some RGC types appear more sensitive to stress (Sanes and Masland, 2015; Ou et al., 2016; Risner et al., 2021b; Shekhar and Sanes, 2021; Boal et al., 2022; McGrady et al., 2022). Of note, RGCs that possess

large somas, expressing modest amounts of melanopsin, that produce a sustained response to light onset (i.e., αON-Sustained/M4 RGCs) seem to be less vulnerable to stress (Schmidt et al., 2014; Duan et al., 2015; Risner et al., 2021b; McGrady et al., 2022). However, in a similar cell line to the one used in these studies, melanopsin-positive cells are sparse (Daniszewski et al., 2018). Alternatively, several studies have indicated AIS geometry is plastic, changing in an activity-dependent manner (Grubb and Burrone, 2010; Evans et al., 2015; Yamada and Kuba, 2016a; Jamann et al., 2021) and altered in degenerative disease (Sohn et al., 2019; Chang et al., 2021). Future studies will test local stabilization of AnkG-associated microtubules during axonopathy towards regenerating axons (Witte et al., 2008; Teliska et al., 2022).

CHAPTER 5

DISCUSSION AND CONCLUSIONS

5.1 Aim 1

As we navigate the world our visual system must be able to encode a detailed and ever-changing visual environment both quickly and efficiently. Much of this processing occurs at the level of the retina, which encodes light energy as electrochemical signals and, through complex circuitry within its multilayered cellular network, begins to interpret features of the visual scene. These signals are integrated and conveyed to the brain by retinal ganglion cells (RGCs). These cells are diverse and have highly varied physiologic properties that underly their ability to encode detailed visual information (Sanes and Masland, 2015; Baden et al., 2016; Bae et al., 2018; Tran et al., 2019; Goetz et al., 2022). The purpose of this aim was to expand upon the growing body of evidence that intrinsic properties of RGCs, particularly those governing their excitability, contribute significantly to their response properties (Emanuel et al., 2017; Werginz et al., 2020; Wienbar and Schwartz, 2022). Specifically, this aim sought to test the hypothesis that *intrinsic physiologic differences between RGCs are driven in part by the sensitivity of the cells to the extracellular potassium concentration*.

5.1.1 Summary of outcomes

We began by characterizing some physiologic differences between two alpha type RGCs, αON-S and αOFF-S, which have similar sustained responses but differing preferred stimulus. Our goal was to determine intrinsic factors, beyond differences in synaptic input, which may differentiate the cells. Through our experiments, we observed that αON-S and αOFF-S RGCs exhibit unique resting membrane potentials and voltage-gated responses to depolarizing currents, as well as variations in their light-evoked activity (**Figs. 2.1, 2.2**). Interestingly, we found that αOFF-S RGCs generated more robust responses to small depolarizing currents compared to αON-S RGCs (**Fig. 2.2**). We also noticed that this difference could not solely be attributed to the higher spontaneous activity of αOFF-S cells, as the slope of the

increase in rate was greater for αOFF-S than αON-S cells (**Fig. 2.2B**). Notably, in response to larger current injections, αOFF-S RGCs often produced few full spikes, followed by aborted action potentials, and sustained membrane potential, which indicated depolarization block, an important physiologic phenomenon which has been shown to underly light encoding in other RGCs (Wienbar and Schwartz, 2022). Conversely, αON-S RGC responses remained steady even with large current injections (**Fig. 2.2**). These differences persisted even when controlling for RMP (**Fig. 2.2C,D**), which suggests that RGC-intrinsic mechanisms contributed to these differences in spike rate and depolarization block. Our findings corroborate and expand on previous evidence indicating that ON and OFF RGC responses are differentially influenced by stimulus amplitude (Twyford et al., 2014; Kameneva et al., 2016).

Further analysis revealed that in addition to spike rate, the width of αON-S and αOFF-S RGC action potentials (APs) also varied with stimulus strength. Specifically, as depolarizing current increased, αOFF-S RGC AP half-width increased dramatically, while αON-S RGC AP half-width increased only moderately (**Fig. 2.3A-D**). This widening of APs aligns with previous reports in RGCs (Goethals et al., 2021). Stronger depolarizing currents also led to increased variability in AP half-width in αOFF-S RGCs, while αON-S RGC half-width variability remained steady across test currents (**Fig. 2.3E**). Interestingly, AP width variability in αOFF-S RGCs increased before the onset of depolarization block (**Fig. 2.2B**), suggesting a link between mechanisms generating depolarization block and maintaining AP half-width. We explored this connection by comparing AP half-width to spike rate for each test current (**Fig. 2.3F**). Our analysis revealed a significant correlation between αOFF-S RGC AP half-width and spike rate, but not for αON-S RGCs. Overall, our findings imply that the mechanisms responsible for depolarization block and regulating AP half-width are interconnected, highlighting a fundamental physiological difference between αON-S and αOFF-S RGCs.

Our next goal was to investigate a potential mechanism for this link. Research suggests that rate-dependent spike widening is caused by K^+ currents (Ma and Koester, 1996; Kasten et al., 2007). Furthermore, evidence from computational modeling has linked differences in K^+ permeability to the unique stimulation thresholds for AP failure and depolarization block in ON versus OFF RGCs

(Kameneva et al., 2016). Building on this understanding, we investigated the sensitivity of αON-S and αOFF-S cells to K^+ gradients as a possible physiological explanation linking the distinctive excitability profiles and AP widths we observed.

We tested this premise by applying high K^+ medium to both αON-S and αOFF-S RGCs, which resulted in the expected depolarization of their RMPs. However, we observed a significantly greater impact on the RMP of αOFF-S RGCs compared to αON-S RGCs (**Fig. 2.4B,C**). Additionally, the relationship between current input and spiking activity for both cell types was altered, with αOFF-S cells unable to maintain spiking activity in response to additional depolarizing current input (**Fig. 2.5**). These findings suggest αON-S and αOFF-S RGCs exhibit different sensitivities to K^+ concentration gradients across their membranes. Interestingly, under high K^+ conditions, the current-spiking relationship and AP shapes of αON-S cells closely resembled those of αOFF-S cells under baseline conditions (**Fig. 2.6**). Specifically, we observed an increase in AP failure and decrease in firing rate in αON-S cells in response to stronger depolarizing stimulation, suggesting depolarization block, which mirrored the changes seen in αOFF-S cells.

5.1.2 Significance

The findings suggest that the differential sensitivity of αON-S and αOFF-S RGCs to extracellular K^+ plays an important role in shaping their distinct response properties. By demonstrating this, we shed light on the mechanisms that shape visual encoding in the retina and add evidence that axogenic processes of action potential generation, in addition to a diversity in synaptic input, contribute significantly to this process.

The results also highlight the importance of understanding how intrinsic properties of neurons contribute to their functional diversity, with potential implications for developing therapeutic strategies that target specific types of neurons in various neurological diseases. One challenge to developing neuroprotective therapies for degenerative disease is understanding how to navigate cellular heterogeneity. Though there are shared glaucomatous stressors, including metabolic restriction,

inflammation, and oxidative stress, the same features of RGCs that distinguish their encoding properties may also leave them differentially sensitive to the stress.

This is particularly relevant when considering our finding that different RGCs have different sensitivities to the concentration of extracellular potassium. As we have demonstrated, maintaining a normal K^+ concentration is critical for the physiological function of RGCs. Under typical conditions there is minimal fluctuation in extracellular K^+ (Heinemann and Lux, 1977). However, disruptions in the mechanisms that control extracellular K^+ concentration have been demonstrated in experimental glaucoma (Fischer et al., 2019a; Fischer et al., 2019b). Dysfunctional K^+ homeostasis may affect different RGC types to varying degrees, impacting excitability, AP generation, and sustained firing. Stressed RGCs display increased excitability early in the disease, which may contribute to their vulnerability (Risner et al., 2018). The interaction between K^+ channels and apoptotic pathways may further contribute to RGC degeneration. Disruption of proper physiologic function can predispose a neuron to die in pathologic conditions (Zhao et al., 2022). Thus, the type-specific differences in sensitivity to K^+ as demonstrated here, in the context of ionic dysregulation, may influence type-specific susceptibility to disease. This hypothesis is supported by evidence that certain types of RGCs, such as OFF RGCs, may be more susceptible to degeneration (Della Santina et al., 2013; El-Danaf and Huberman, 2015; Ou et al., 2016; Risner et al., 2021b). Exploration of this hypothesis and evaluation of how RGC sensitivity to K^+ stress changes in glaucoma forms the basis for Aim 2.

5.2 Aim 2

Understanding the ways in which neurons adapt to and cope with stress is crucial for developing effective treatments for neurodegenerative diseases. In the case of glaucoma, sensitivity to the mechanical stress conveyed by intraocular pressure (IOP) results in pathophysiologic processes that disrupt normal neuronal physiology. Furthermore, these internal stressors are amplified by the additional disruption of external homeostatic support provided by glia. Of particular interest to this work, regulation of the extracellular milieu by astrocytes and Müller glia becomes altered in glaucoma (Fischer et al., 2019a;

Fischer et al., 2019b). As introduced in Aim 1, different RGC subtypes display varying degrees of sensitivity to extracellular K^+ levels, and there is evidence that certain subtypes are more susceptible to glaucomatous degeneration than others (Della Santina et al., 2013; El-Danaf and Huberman, 2015; Ou et al., 2016; Risner et al., 2021b). This aim sought to link these concepts and explore how the sensitivities identified in Aim 1 change in the context of disease. Leveraging an inducible mouse model of experimental glaucoma, this aim tests the hypothesis that *retinal ganglion cells undergo adaptive changes in response to glaucomatous stress to lessen the impact of dysregulation of the extracellular milieu.*

5.2.1 Summary of outcomes

The work in this aim began by expanding upon the differences between αON-S and αOFF-S RGCs demonstrated in chapter 2, evaluating how excitability and sensitivity to acutely elevated extracellular K^+ change with prolonged exposure to elevated IOP. We hypothesized that intrinsic differences in K^+ sensitivity between αON-S and αOFF-S RGCs may drive a preferential susceptibility to elevated IOP-induced degeneration. As in previous experiments at the four-week time point (Risner et al., 2021b; Risner et al., 2022) we observed IOP-related reduction in light spiking (**Fig. 3.2**) and reduced excitability as indicated by blunted current-evoked spiking (**Fig. 3.4)** in αON-S cells and a trend towards alterations for αOFF-S cells. Though both αRGC types were affected by the prolonged IOP elevation, there appeared to be a marginally larger effect on the αON-S cells. While this difference could represent a preferential susceptibility to IOP-related stress, such excitability changes may also be an adaptive response to the prolonged stress of hyperexcitability and ionic dysregulation.

To test this hypothesis, we utilized a similar acute ionic stress approach as employed in chapter 2. Our results showed that acute exposure to high extracellular K^+ depolarized membranes of both αON-S and αOFF-S RGCs, regardless of IOP exposure. However, notably, prolonged exposure to elevated IOP significantly reduced this effect, suggesting there may be a decreased sensitivity of RGCs to acute ionic stress (**Fig 3.3**). We further examined the impact of acute K^+ stress on RGC excitability to assess whether this IOP-induced difference was related to intrinsic changes in RGCs or simply related to altered synaptic

tone. Our findings indicated that RGCs in the 4wk IOP group were less affected by high K^+ and maintained sustained spiking at greater magnitudes of depolarizing current before reaching the threshold for depolarization block (**Fig. 3.4**). These results suggest that altered K^+ sensitivity and decreased RGC excitability may be related to RGC-intrinsic changes due to prolonged IOP elevation.

To further explore this possibility, we measured AP half-width during evoked spiking (**Fig. 3.5**). This measure reflects changes to the mechanisms of AP generation and is affected by K^+ currents (Geiger and Jonas, 2000; Kole et al., 2007; Kuznetsov et al., 2012; Gonzalez Sabater et al., 2021; Alexander et al., 2022). Consistent with RMP effects, we found a significant difference in the effect of K^+ between the 4wk IOP and control groups for both αON-S and αOFF-S, with APs less widened by high K^+. This provides further support for the notion that elevated IOP is affecting RGC-intrinsic excitability and suggests there may be altered structure or function of voltage-gated K^+ channels. Relevant to our hypothesis of possible cell type specificity, we also found differences in how AP widths were affected by IOP exposure and K^+ conditions. αON-S cells exhibited a widening of APs following 4wk IOP elevation, even under normal K^+ conditions, while αOFF-S AP widths were similar for both groups under normal K^+. Both cell types exposed to IOP showed less change in AP width following high K^+ wash on, but this difference was largely driven by the IOP-induced baseline shift for αON-S RGCs. These findings are consistent with the cell type-specific differences seen in **Fig. 3.2**, where αON-S RGCs exhibited significantly diminished light-evoked spiking, while αOFF-S light spiking was mostly preserved.

5.2.2 Significance

The findings presented in this aim expand upon the concepts of Aim 1, exploring RGC sensitivity to extracellular potassium in the context of experimental glaucoma. The key finding is that after prolonged exposure to elevated IOP, RGCs undergo an adaptive response that results in a decreased sensitivity to acute ionic stress in the form of elevated extracellular K^+.

An important point to consider is whether these changes represent a protective or maladaptive response to continued stress on the RGCs. Early in disease, RGC hyperexcitability driving increased K^+

flux may compound with impaired glial buffering capacity, amplifying axonal stress. Attempts to manage membrane potential to maintain spiking ability may further stress already metabolically restricted neurons. Hyperexcitable cells require higher energy supplies to maintain ionic balance across their membrane and generate action potentials. Thus, in a pathological context hyperexcitability may push the metabolic demand of these cells beyond the available supply, worsening the degree of stress. A decrease RGC excitability and blunted sensitivity to extracellular ionic changes could be an attempt by the cell to decrease its metabolic load and oxidative stress, in order to preserve some degree of function in the face of progressively worsening conditions.

However, these changes may alternatively represent neurons that have exhausted their adaptive capacity and are at their final stage before outright degeneration. In this case, depressed excitability may reflect pathologic interactions between dysregulated potassium homeostasis and alterations in other ions, such as calcium, which is a key modulator of neuronal excitability but can also contribute to cell death (Diem et al., 2001a; Jones and Smith, 2016; Segal, 2018). This conclusion is limited by evidence that at the 4wk timepoint in this model, there is pathologic evidence of some axonal damage but minimal loss of RGC somas in the retina (Ward et al., 2014; Bond et al., 2016; Risner et al., 2021b; Risner et al., 2022), suggesting that this altered excitability may not be occurring in the immediate context of cell death.

The findings in this aim elucidate some key targets that can be further explored for future neuroprotective therapies. There is a wide diversity of K^+ channels expressed in RGCs (Zhong et al., 2013), many of which could be related to the relationship between neuronal excitability, AP generation, and K^+ sensitivity. Channels mediating A-type voltage-gated K^+ currents (Ma and Koester, 1996; Holmqvist et al., 2002), or the Ca^{2+}-activated BK channels (Wang et al., 1998; Gu et al., 2007) may be promising for future investigation. RGC type-specific expression data (Tran et al., 2019; Goetz et al., 2022) present an opportunity to gain a detailed understanding of which channels may contribute to these physiological differences and could be leveraged in models of glaucoma.

5.3 Aim 3

As evident from the body of work presented thus far, there are numerous factors that contribute to a neuron's encoding and transmission of information as action potentials. Experiments from chapters 2 and 3 emphasize the importance of the axon in determining differences in neuronal excitability and response to degenerative stress. An important structural component shaping these contributions is the axon initial segment (AIS), a protein-rich scaffold that is responsible for the generation of action potentials in the axon. The dimensions of the AIS have a significant impact on the neuron's excitability and are tightly regulated during development to ensure appropriate light encoding properties of distinct RGC subtypes (Raghuram et al., 2019; Wienbar and Schwartz, 2022). However, recent studies have shown that the AIS is a dynamic structure that can adapt to changing physiological and pathological stimuli, enabling the maintenance of appropriate action potential generation (Grubb and Burrone, 2010; Jamann et al., 2021). This aim sought to leverage both in vivo and in vitro approaches to investigate the underlying mechanisms governing AIS development and its resilience to degeneration. In particular, it tests the hypotheses that (1) *in vitro models can simulate axon development and degeneration* and (2) *alterations to the AIS structure can explain the physiological differences in neuronal excitability and underlie degenerative changes in axonopathy*.

5.3.1 Summary of outcomes

Work supporting this aim unites concepts from chapters 2, 3, and 4. We explored the relationships between AIS structure and RGC excitability and evaluated AIS plasticity as a potential mechanism for neuronal adaptation in glaucoma. We expanded this line of investigation by modeling RGC development and axonopathy *in vitro*, allowing a high throughput evaluation of factors influencing AIS dimensions. These results provide important insights into the link between AIS structure and the intrinsic electrical properties of RGCs in health and disease.

We began by trying to distinguish αON-S and αOFF-S RGCs by investigating the relationship between AIS dimensions and action potential generation. We hypothesized that AIS scaling could be a

potential contributor to differences in spike rate and depolarization block between the two RGC types. Although we did not detect significant differences in AIS dimensions between the two subtypes of RGCs, when correlating dimensions with current-evoked spiking we found that the relationship between AIS length and spike rate varied by both cell type and by the strength of stimulation (**Fig. 2.7**). Intriguingly, we found that longer AISs were associated with higher evoked spike rates in αOFF-S RGCs at low currents, indicating that AIS length is a driver of AP generation threshold in that range (Jamann et al., 2021). However, with stronger stimulation, the relationship flipped, and cells with longer AISs had lower spike rates. Such a relationship was not seen for αON-S, further complicating things. These results suggest that the contributions of the AIS to spiking output vary by cell type and suggest that AIS structure alone cannot explain RGC excitability and threshold for depolarization block.

Expanding upon these findings, we next set out to establish how the AIS changes in response to prolonged glaucomatous stress. Specifically, we were searching for a mechanism for the adaptive process delineated in Aim 2. There is strong evidence that axon specific alterations occur throughout the progression of glaucomatous damage, underlying RGC hyperexcitability at 2 weeks in the microbead occlusion model (Risner et al., 2018; Risner et al., 2020b), and now underlying decreased excitability and potassium sensitivity at 4 weeks (**Figs. 3.2, 3.4, 3.5**). Since RGC axonal excitability and AP generation depend on the AIS, we hypothesized that prolonged glaucomatous stress from K^+ dysregulation and early hyperexcitability would lead to a distal shift in the AIS away from the soma (Grubb and Burrone, 2010). However, we did not observe any significant differences in AIS dimensions between the 4-week IOP cells and controls.

Taking a step back, we next endeavored to apply an *in vitro* approach to gain greater throughput in evaluating factors governing AIS development and susceptibility to changes in a model of axonopathy. Previously we observed that human embryonic stem cell derived retinal ganglion cells (hRGCs) cultured on glass coverslips without growth factor supplementation lacked well-defined axon initial segments (AISs) (Risner et al., 2021a). This structural deficit correlated with an immature excitability phenotype. This finding prompted us to develop an in vitro model to drive hRGC axon specification. We achieved

this model using a microfluidic platform that promoted polarization and used mouse RGC AIS morphology to establish an *in vivo* basis for comparison.

Our experiments revealed marked heterogeneity in AIS localization and morphologic type in hRGCs plated on coverslips compared to mouse RGCs (**Figs. 4.1C-H; 4.4A,D**). A sizeable portion of these cells had multiple AnkG-positive putative axons originating from a single soma, suggesting a lack of well-regulated axon specification. However, culturing hRGCs on microfluidic platforms reduced the number of multi-AIS cells and increased the proportion of cells with direct AISs (**Figs. 4.2C, 4.4A,D**). These findings suggest that the polarized environment of the microfluidic platform plays a critical role in promoting axon specification and proper AIS morphology.

We next aimed to establish an in vitro model of hRGC axonopathy using colchicine to chemically lesion axons and observe the effects of injury on AIS morphology (**Fig 4.5**). Colchicine treatment caused significant axon degeneration and retraction. We also observed a reduction in anterograde axonal transport of CTB, an increase in enlarged varicosities, and increased expression of other indicators of degeneration. These results are consistent with established markers of axonopathy and neurodegeneration, supporting this approach as an appropriate *in vitro* model of the disease (Wang et al., 2003; Noristani et al., 2016; Calkins et al., 2017; Gu et al., 2017; Risner et al., 2018; Bernardo-Colon et al., 2019). Finally, we used this model to investigate changes to AIS structure in axonopathy (**Fig. 4.6**). Interestingly, we found that not all axons were equally affected. Cells in which the AIS was located on an axon-carrying dendrite (AcD) appeared to be more susceptible to colchicine. Elsewhere in the central nervous system, cells with AcDs occupy a specific functional niche and exhibit different excitability properties (Thome et al., 2014; Hodapp et al., 2022). These findings that the AIS geometry is preferentially altered in AcD-containing RGCs further corroborates evidence of RGC type-specific susceptibility and suggests that AIS structure may indeed be altered by glaucomatous stress in certain cases.

5.3.2 Significance

The findings related to this aim offer mechanistic insight into some of the structural components of an axon that govern RGC excitability but complicate the notion that the structure of the AIS can explain cell-cell differences and predict resilience to glaucomatous stress. Rather, it supports key findings from Aims 1 and 2 that more nuanced ion channel-level differences interact with larger scale structural components, offering promising potential for molecular therapies.

The combined evidence from prior studies describing the influence of the AIS on RGC light encoding (Werginz et al., 2020; Wienbar and Schwartz, 2022) alongside our *in vitro* studies emphasizing the importance in proper development of the AIS for regulating spiking output within tight margins. Indeed, poorly matured hRGCs with abnormal AIS localization and dimensions do not exhibit well-developed responses to electrical stimulation (Risner et al., 2021a). Still, our findings that the relationship between AIS structure and RGC spiking output is dependent upon the magnitude of stimulation demonstrate that excitability is not static. Reconciling these results with those supporting Aim 1, we can hypothesize that AIS structure influences the clustering of specific voltage gated sodium and potassium channels on different RGC types, which dynamically interact with the internal and external states of the neuron to adjust the properties of action potential generation to physiologic ranges. Thus, action potential initiation and repetitive firing can be influenced by the degree of membrane depolarization and the state of extracellular milieu, perhaps even adjusting to balance the metabolic demands of the neuron with the need for proper signal encoding.

Our *in vivo* and *in vitro* models of glaucomatous degeneration presented an opportunity to investigate this hypothesis, examining changes to AIS structure and neuronal excitability after axonal stress. Given the prolonged alterations to RGC excitability and dysregulation of extracellular potassium homeostasis in glaucoma, we anticipated that we may see plasticity in the AIS to adapt to these conditions. However, in our inducible mouse model of glaucoma we did not see such a change following elevated IOP exposure. This suggests that our observed differences in excitability and K^+ sensitivity are likely not solely reflective of AIS structural plasticity. Rather, more pathologic changes in voltage-gated

ion channel and interacting protein expression, as well as alterations in glial regulation of the extracellular milieu, may contribute to a multifactorial adaptive process aimed at minimizing metabolic and excitotoxic stress. Conversely, in our *in vitro* model of axonopathy we did observe alterations to AIS structure, albeit in a specific subset of cells. This could possibly reflect RGC type-specific susceptibility, especially considering that the AIS morphology of the affected subtype is linked to more excitable cells which require greater metabolic support. Given the sample size limitations of our *ex vivo* patch clamp recording approach, further work linking axonal structure with cell type-specific alterations in neurodegeneration is warranted.

5.4 Conclusions

Neurodegenerative diseases are complex and multifactorial disorders that affect a wide variety of central nervous system regions and cell types. While the etiologies and pathophysiologic processes of these diseases may differ, they share many common hallmark features of progression. The work presented here explores the central question of understanding how fundamental neurodegenerative stressors, both intrinsic processes related to genetics and aging as well as extrinsic stressors like mechanical stress, lead to shared features of dysfunction and ultimately the death of vulnerable neurons. The focus here was on linking disruptions in ion homeostasis, neuronal hyperexcitability, and cell type specific susceptibility to degeneration, all of which can be seen across a variety of distinct neurodegenerative conditions.

In Aim 1, we examined intrinsic features that distinguish the firing properties of two different subtypes of RGCs. We found that there was a remarkable difference in the sensitivity of these RGCs to the concentration of extracellular potassium, which significantly contributed to their excitability behavior under homeostatic conditions. During periods of pathologic stress, however, extracellular potassium can become dysregulated. We hypothesized that this may represent a link between glaucomatous stress and the propensity for certain RGCs to succumb more quickly to the stress than others. Following this line of investigation, in Aim 2 we evaluated how the effects of potassium delineated in Aim 1 changed with prolonged exposure to elevated intraocular pressure, an important glaucoma-relevant stressor.

Remarkably, we found that RGCs underwent an adaptive process that made them more resilient to an acute ionic stressor. Independent of subtype, RGC firing was less impacted by elevated extracellular potassium after prolonged glaucomatous stress.

While there was evidence for cell type specific differences in this adaptation, the results of Aim 2 add some nuance to the original hypothesis following Aim 1 that potassium sensitivity was a key link between degenerative stress and cell type susceptibility. Rather, it suggests a remarkable degree of resilience supported by neuronal adaptations to stress. In Aim 3, we endeavored to mechanistically investigate one key structure regulating neuronal excitability that could be linked to this adaptive process, the axon initial segment (AIS). Aim 3 links findings from Aims 1 and 2, and is supported by data from Chapters 2, 3, and 4. We found in chapter 3 that there wasn't a large-scale shift in AIS structure following prolonged IOP exposure, despite evidence from *in vitro* studies of prolonged potassium elevation. This challenged the notion that axonal plasticity alone could be responsible for this adaptation. Rather, evidence from chapter 2 suggesting that the impact of AIS structure of neuronal excitability is dependent upon cell type and context, such as stimulation level, supports a more nuanced interpretation that this adaptation is likely due to ion channel-level differences interact with larger scale structural components. This nuanced approach was further supported by evidence from chapter 4, where in our in vitro model of axonopathy we saw differential susceptibility of hRGCs to our stressor based upon axonal factors linked to neuronal excitability.

Together, the results of this work offer further insight into processes linking neuronal hyperexcitability, glial dysfunction, and other common stressors seen in neurodegenerative diseases to factors that predispose certain neurons to succumb to disease while others remain resilient. Furthermore, they add to the body of evidence that there are endogenous neuroprotective processes employed by neurons and glia to maintain function in the face of prolonged stress. This offers important insight into the relationship between dysregulated extracellular milieu and neuronal stress in degenerative disease and suggests possible targets for developing neuroprotective therapies. To further develop this understanding, future lines of investigation should evaluate in more depth the points of contradiction and nuance

established with the interpretation of these results. First, a more detailed timeline of RGC adaptation to potassium stress across multiple time points of disease should be established. It remains unclear how soon into the disease process RGCs exhibit decreased potassium sensitivity. Establishing this time point may further elucidate the protective vs. maladaptive consequences of this changes. Similarly, it may help in establishing whether cell type specific differences in potassium sensitivity are truly linked to susceptibility to degeneration. Next, a detailed investigation of potassium channel expression should be conducted, determining differences between cell types and disease states. Altered channel expression is seen across a variety of degenerative diseases and could offer further insight into specific mechanisms and potential molecular targets for neuroprotective therapy. Another future avenue for exploration of these mechanisms is expanding the measurement of AIS dimensions in models of glaucoma. Our mouse model was limited by a low sample size of measured RGCs, while our *in vitro* model was limited by translatability despite the improvements offered by the microfluidic culture platform. A large-scale in vivo study could help bridge this gap, using mice with fluorescently tagged RGCs to increase the amount of AISs to measure. This could allow for greater power to detect subtle changes to AIS structure, but would be limited by difficulty in distinguishing different RGC types as we did in this work. Finally, future studies could investigate additional RGC types. Here, we focused on αON-S and αOFF-S cells, a small subset of the total diversity of RGCs in mice. Of particular interest would be αOFF-T RGCs, which are nearly as easy to locate and record as the cells in this work and appear to be both more susceptible to glaucomatous stress (Della Santina et al., 2013; Ou et al., 2016) while also having excitability that is more highly dependent on AIS structure (Werginz et al., 2020).

Glaucoma is a complex and chronic disease that can lead to insidious vision loss over time, often without noticeable symptoms until significant degeneration has already occurred. The pathogenesis of glaucoma involves the interaction between vulnerable retinal ganglion cells and various types of physiological stress, such as oxidative stress, metabolic stress, and inflammation. One of the key features observed in many neurodegenerative diseases in addition to glaucoma, including Alzheimer's Disease, Parkinson's Disease, and Amyotrophic Lateral Sclerosis, is neuronal hyperexcitability early in their

progression. This phenomenon is particularly noteworthy as it is thought to exert significant stress on neurons, affecting metabolic demand and calcium load, pushing neurons beyond their threshold for cellular damage towards death.

Moreover, the vulnerability of different cell types in the face of these pathologies is not uniform, and it may be influenced by intrinsic morphologic, physiologic, and biochemical properties that underpin the increased sensitivity to degeneration during stress. Despite the challenges posed by these stressors, research has shown that RGCs have the capacity to undergo a variety of adaptive responses in order to protect themselves against further damage (Calkins, 2021). Animal models of glaucoma have been crucial in uncovering the mechanisms by which RGCs adapt to stress. The findings presented in this body of work offer valuable insights into how RGCs modulate their excitability in the face of prolonged stress induced by elevated intraocular pressure. Such modulation is believed to play an important role in preserving visual function, and may offer potential diagnostic and therapeutic targets for early glaucomatous neurodegeneration.

In light of these discoveries, it is becoming increasingly clear that RGCs possess a remarkable degree of resilience in the face of sustained stress. This may explain why patients with glaucoma can maintain relatively good vision for extended periods of time, despite ongoing degenerative stress. While early diagnosis and treatment of glaucoma are crucial, the ability of RGCs to adapt and respond to various types of stress offers hope that novel interventions could be developed to protect and preserve visual function in patients. Moving forward, it will be important to continue exploring the various mechanisms by which RGCs adapt to stress, in order to uncover potential therapeutic targets. Furthermore, identifying the specific intrinsic factors that contribute to cell type-specific vulnerability in glaucoma could be key to developing effective targeted therapies. In particular, the findings presented in this study suggest that the modulation of RGC excitability may be a promising avenue for further investigation. By understanding how RGCs modulate their excitability in response to stress, it may be possible to identify specific targets for interventions aimed at preserving visual function in patients with glaucoma.

REFERENCES

Abudara, V., Retamal, M.A., Del Rio, R., and Orellana, J.A. (2018). Synaptic Functions of Hemichannels and Pannexons: A Double-Edged Sword. *Front Mol Neurosci* 11**,** 435. doi: 10.3389/fnmol.2018.00435.

Agostinone, J., and Di Polo, A. (2015). Retinal ganglion cell dendrite pathology and synapse loss: Implications for glaucoma. *Prog Brain Res* 220**,** 199-216. doi: 10.1016/bs.pbr.2015.04.012.

Ahmad, I., Goel, D., Ghosh, A., Kapoor, H., Kumar, D., Srivastava, A.K., et al. (2022). Lab resource: Single cell line generation and characterization of a human-derived induced pluripotent stem cell line (IGIBi005-A) from a patient with spastic paraplegia/ataxia/ALS phenotype due to the mutation of the gene Kinesin Family Member 5A (KIF5A). *Stem Cell Res* 64**,** 102904. doi: 10.1016/j.scr.2022.102904.

Aihara, M., Lindsey, J.D., and Weinreb, R.N. (2003). Experimental mouse ocular hypertension: establishment of the model. *Invest Ophthalmol Vis Sci* 44(10)**,** 4314-4320. doi: 10.1167/iovs.03-0137.

Akin, E.J., Sole, L., Dib-Hajj, S.D., Waxman, S.G., and Tamkun, M.M. (2015). Preferential targeting of Nav1.6 voltage-gated Na+ Channels to the axon initial segment during development. *PLoS One* 10(4)**,** e0124397. doi: 10.1371/journal.pone.0124397.

Alexander, T.D., Muqeem, T., Zhi, L., Tymanskyj, S.R., and Covarrubias, M.L. (2022). Tunable Action Potential Repolarization Governed by Kv3.4 Channels in Dorsal Root Ganglion Neurons. *J Neurosci* 42(46)**,** 8647-8657. doi: 10.1523/JNEUROSCI.1210-22.2022.

Aloisi, F. (2001). Immune function of microglia. *Glia* 36(2)**,** 165-179. doi: 10.1002/glia.1106.

Ames, A., 3rd, Li, Y.Y., Heher, E.C., and Kimble, C.R. (1992). Energy metabolism of rabbit retina as related to function: high cost of Na+ transport. *J Neurosci* 12(3)**,** 840-853. doi: 10.1523/JNEUROSCI.12-03-00840.1992.

Anderson, C.M., and Swanson, R.A. (2000). Astrocyte glutamate transport: review of properties, regulation, and physiological functions. *Glia* 32(1)**,** 1-14. doi: https://doi.org/10.1002/1098-1136(200010)32:1<1::AID-GLIA10>3.0.CO;2-W.

Anderson, D.R., and Normal Tension Glaucoma, S. (2003). Collaborative normal tension glaucoma study. *Curr Opin Ophthalmol* 14(2)**,** 86-90. doi: 10.1097/00055735-200304000-00006.

Anderson, M.G., Smith, R.S., Hawes, N.L., Zabaleta, A., Chang, B., Wiggs, J.L., et al. (2002). Mutations in genes encoding melanosomal proteins cause pigmentary glaucoma in DBA/2J mice. *Nat Genet* 30(1)**,** 81-85. doi: 10.1038/ng794.

Asari, H., and Meister, M. (2012). Divergence of visual channels in the inner retina. *Nat Neurosci* 15(11)**,** 1581-1589. doi: 10.1038/nn.3241.

Attwell, D., and Laughlin, S.B. (2001). An energy budget for signaling in the grey matter of the brain. *J Cereb Blood Flow Metab* 21(10)**,** 1133-1145. doi: 10.1097/00004647-200110000-00001.

Baden, T., Berens, P., Franke, K., Roman Roson, M., Bethge, M., and Euler, T. (2016). The functional diversity of retinal ganglion cells in the mouse. *Nature* 529(7586)**,** 345-350. doi: 10.1038/nature16468.

Bae, J.A., Mu, S., Kim, J.S., Turner, N.L., Tartavull, I., Kemnitz, N., et al. (2018). Digital Museum of Retinal Ganglion Cells with Dense Anatomy and Physiology. *Cell* 173(5)**,** 1293-1306 e1219. doi: 10.1016/j.cell.2018.04.040.

Barlow, H.B. (1953). Summation and inhibition in the frog's retina. *J Physiol* 119(1)**,** 69-88. doi: 10.1113/jphysiol.1953.sp004829.

Bataveljic, D., Nikolic, L., Milosevic, M., Todorovic, N., and Andjus, P.R. (2012). Changes in the astrocytic aquaporin-4 and inwardly rectifying potassium channel expression in the brain of the amyotrophic lateral sclerosis SOD1(G93A) rat model. *Glia* 60(12)**,** 1991-2003. doi: 10.1002/glia.22414.

Bazargani, N., and Attwell, D. (2016). Astrocyte calcium signaling: the third wave. *Nat Neurosci* 19(2)**,** 182-189. doi: 10.1038/nn.4201.

Bean, B.P. (2007). The action potential in mammalian central neurons. *Nat Rev Neurosci* 8(6)**,** 451-465. doi: 10.1038/nrn2148.
Beck, R.W., and Gal, R.L. (2008). Treatment of acute optic neuritis: a summary of findings from the optic neuritis treatment trial. *Arch Ophthalmol* 126(7)**,** 994-995. doi: 10.1001/archopht.126.7.994.
Bender, K.J., and Trussell, L.O. (2012). The physiology of the axon initial segment. *Annu Rev Neurosci* 35(1)**,** 249-265. doi: 10.1146/annurev-neuro-062111-150339.
Benozzi, J., Nahum, L.P., Campanelli, J.L., and Rosenstein, R.E. (2002). Effect of hyaluronic acid on intraocular pressure in rats. *Invest Ophthalmol Vis Sci* 43(7)**,** 2196-2200.
Bergles, D.E., and Jahr, C.E. (1998). Glial contribution to glutamate uptake at Schaffer collateral-commissural synapses in the hippocampus. *J Neurosci* 18(19)**,** 7709-7716. doi: 10.1523/JNEUROSCI.18-19-07709.1998.
Bernardo-Colon, A., Vest, V., Cooper, M.L., Naguib, S.A., Calkins, D.J., and Rex, T.S. (2019). Progression and Pathology of Traumatic Optic Neuropathy From Repeated Primary Blast Exposure. *Front Neurosci* 13**,** 719. doi: 10.3389/fnins.2019.00719.
Berry, R.H., Qu, J., John, S.W., Howell, G.R., and Jakobs, T.C. (2015). Synapse Loss and Dendrite Remodeling in a Mouse Model of Glaucoma. *PLoS One* 10(12)**,** e0144341. doi: 10.1371/journal.pone.0144341.
Boal, A., McGrady, N.R., Lambert, W.S., Risner, M.L., and Calkins, D.J. (2020). Influence of intraocular pressure on retinal ganglion cells separated by retinal quadrant. *Investigative Ophthalmology & Visual Science* 61(7)**,** 1995-1995.
Boal, A.M., McGrady, N.R., Risner, M.L., and Calkins, D.J. (2022). Sensitivity to extracellular potassium underlies type-intrinsic differences in retinal ganglion cell excitability. *Front Cell Neurosci* 16**,** 966425. doi: 10.3389/fncel.2022.966425.
Boal, A.M., Risner, M.L., Cooper, M.L., Wareham, L.K., and Calkins, D.J. (2021). Astrocyte Networks as Therapeutic Targets in Glaucomatous Neurodegeneration. *Cells* 10(6). doi: 10.3390/cells10061368.
Bodeutsch, N., Siebert, H., Dermon, C., and Thanos, S. (1999). Unilateral injury to the adult rat optic nerve causes multiple cellular responses in the contralateral site. *J Neurobiol* 38(1)**,** 116-128. doi: 10.1002/(sici)1097-4695(199901)38:1<116::aid-neu9>3.0.co;2-f.
Boije, H., Shirazi Fard, S., Edqvist, P.H., and Hallbook, F. (2016). Horizontal Cells, the Odd Ones Out in the Retina, Give Insights into Development and Disease. *Front Neuroanat* 10**,** 77. doi: 10.3389/fnana.2016.00077.
Boiko, T., Van Wart, A., Caldwell, J.H., Levinson, S.R., Trimmer, J.S., and Matthews, G. (2003). Functional specialization of the axon initial segment by isoform-specific sodium channel targeting. *J Neurosci* 23(6)**,** 2306-2313. doi: 10.1523/JNEUROSCI.23-06-02306.2003.
Bolz, S., Schuettauf, F., Fries, J.E., Thaler, S., Reichenbach, A., and Pannicke, T. (2008). K(+) currents fail to change in reactive retinal glial cells in a mouse model of glaucoma. *Graefes Arch Clin Exp Ophthalmol* 246(9)**,** 1249-1254. doi: 10.1007/s00417-008-0872-x.
Bond, W.S., Hines-Beard, J., GoldenMerry, Y.L., Davis, M., Farooque, A., Sappington, R.M., et al. (2016). Virus-mediated EpoR76E Therapy Slows Optic Nerve Axonopathy in Experimental Glaucoma. *Mol Ther* 24(2)**,** 230-239. doi: 10.1038/mt.2015.198.
Booker, S.A., Simões de Oliveira, L., Anstey, N.J., Kozic, Z., Dando, O.R., Jackson, A.D., et al. (2020). Input-Output Relationship of CA1 Pyramidal Neurons Reveals Intact Homeostatic Mechanisms in a Mouse Model of Fragile X Syndrome. *Cell Rep* 32(6)**,** 107988. doi: 10.1016/j.celrep.2020.107988.
Borg-Graham, L.J. (2001). The computation of directional selectivity in the retina occurs presynaptic to the ganglion cell. *Nat Neurosci* 4(2)**,** 176-183. doi: 10.1038/84007.
Briggman, K.L., Helmstaedter, M., and Denk, W. (2011). Wiring specificity in the direction-selectivity circuit of the retina. *Nature* 471(7337)**,** 183-188. doi: 10.1038/nature09818.
Broadway, D.C. (2012). Visual field testing for glaucoma - a practical guide. *Community Eye Health* 25(79-80)**,** 66-70.

Brown, A.M. (2004). Brain glycogen re-awakened. *J Neurochem* 89(3)**,** 537-552. doi: 10.1111/j.1471-4159.2004.02421.x.
Brown, A.M., Tekkok, S.B., and Ransom, B.R. (2003). Glycogen regulation and functional role in mouse white matter. *J Physiol* 549(Pt 2)**,** 501-512. doi: 10.1113/jphysiol.2003.042416.
Brymer, K.J., Hurley, E.P., Barron, J.C., Mukherjee, B., Barnes, J.R., Nafar, F., et al. (2023). Asymmetric dysregulation of glutamate dynamics across the synaptic cleft in a mouse model of Alzheimer's disease. *Acta Neuropathol Commun* 11(1)**,** 27. doi: 10.1186/s40478-023-01524-x.
Budenz, D.L., Barton, K., Whiteside-de Vos, J., Schiffman, J., Bandi, J., Nolan, W., et al. (2013). Prevalence of glaucoma in an urban West African population: the Tema Eye Survey. *JAMA Ophthalmol* 131(5)**,** 651-658. doi: 10.1001/jamaophthalmol.2013.1686.
Burgoyne, C.F. (2011). A biomechanical paradigm for axonal insult within the optic nerve head in aging and glaucoma. *Exp Eye Res* 93(2)**,** 120-132. doi: 10.1016/j.exer.2010.09.005.
Burgoyne, C.F. (2015). The non-human primate experimental glaucoma model. *Exp Eye Res* 141**,** 57-73. doi: 10.1016/j.exer.2015.06.005.
Bushong, E.A., Martone, M.E., Jones, Y.Z., and Ellisman, M.H. (2002). Protoplasmic astrocytes in CA1 stratum radiatum occupy separate anatomical domains. *J Neurosci* 22(1)**,** 183-192. doi: 10.1523/JNEUROSCI.22-01-00183.2002.
Bussel, II, Wollstein, G., and Schuman, J.S. (2014). OCT for glaucoma diagnosis, screening and detection of glaucoma progression. *Br J Ophthalmol* 98 Suppl 2(Suppl 2)**,** ii15-19. doi: 10.1136/bjophthalmol-2013-304326.
Cabezas, R., Avila, M., Gonzalez, J., El-Bacha, R.S., Baez, E., Garcia-Segura, L.M., et al. (2014). Astrocytic modulation of blood brain barrier: perspectives on Parkinson's disease. *Front Cell Neurosci* 8**,** 211. doi: 10.3389/fncel.2014.00211.
Cacace, R., Heeman, B., Van Mossevelde, S., De Roeck, A., Hoogmartens, J., De Rijk, P., et al. (2019). Loss of DPP6 in neurodegenerative dementia: a genetic player in the dysfunction of neuronal excitability. *Acta Neuropathol* 137(6)**,** 901-918. doi: 10.1007/s00401-019-01976-3.
Cai, C., Ren, Q., Desai, N.J., Rizzo, J.F., 3rd, and Fried, S.I. (2011). Response variability to high rates of electric stimulation in retinal ganglion cells. *J Neurophysiol* 106(1)**,** 153-162. doi: 10.1152/jn.00956.2010.
Caldwell, J.H., Schaller, K.L., Lasher, R.S., Peles, E., and Levinson, S.R. (2000). Sodium channel Nav1. 6 is localized at nodes of Ranvier, dendrites, and synapses. *Proceedings of the National Academy of Sciences* 97(10)**,** 5616-5620.
Cali, C., Tauffenberger, A., and Magistretti, P. (2019). The Strategic Location of Glycogen and Lactate: From Body Energy Reserve to Brain Plasticity. *Front Cell Neurosci* 13**,** 82. doi: 10.3389/fncel.2019.00082.
Calkins, D.J. (2012). Critical pathogenic events underlying progression of neurodegeneration in glaucoma. *Prog Retin Eye Res* 31(6)**,** 702-719. doi: 10.1016/j.preteyeres.2012.07.001.
Calkins, D.J. (2021). Adaptive responses to neurodegenerative stress in glaucoma. *Prog Retin Eye Res* 84**,** 100953. doi: 10.1016/j.preteyeres.2021.100953.
Calkins, D.J., and Horner, P.J. (2012). The cell and molecular biology of glaucoma: axonopathy and the brain. *Invest Ophthalmol Vis Sci* 53(5)**,** 2482-2484. doi: 10.1167/iovs.12-9483i.
Calkins, D.J., Lambert, W.S., Formichella, C.R., McLaughlin, W.M., and Sappington, R.M. (2018). The Microbead Occlusion Model of Ocular Hypertension in Mice. *Methods Mol Biol* 1695**,** 23-39. doi: 10.1007/978-1-4939-7407-8_3.
Calkins, D.J., Pekny, M., Cooper, M.L., Benowitz, L., Lasker, I.I.o.A., and Glaucomatous Neurodegeneration, P. (2017). The challenge of regenerative therapies for the optic nerve in glaucoma. *Exp Eye Res* 157**,** 28-33. doi: 10.1016/j.exer.2017.01.007.
Casson, R.J., Chidlow, G., Crowston, J.G., Williams, P.A., and Wood, J.P.M. (2021). Retinal energy metabolism in health and glaucoma. *Prog Retin Eye Res* 81**,** 100881. doi: 10.1016/j.preteyeres.2020.100881.

Catterall, W.A. (2010). Ion channel voltage sensors: structure, function, and pathophysiology. *Neuron* 67(6)**,** 915-928. doi: 10.1016/j.neuron.2010.08.021.
Catterall, W.A. (2012). Voltage-gated sodium channels at 60: structure, function and pathophysiology. *The Journal of physiology* 590(11)**,** 2577-2589.
Catterall, W.A., Cestèle, S., Yarov-Yarovoy, V., Yu, F.H., Konoki, K., and Scheuer, T. (2007). Voltage-gated ion channels and gating modifier toxins. *Toxicon* 49(2)**,** 124-141. doi: 10.1016/j.toxicon.2006.09.022.
Catterall, W.A., Goldin, A.L., and Waxman, S.G. (2005). International Union of Pharmacology. XLVII. Nomenclature and structure-function relationships of voltage-gated sodium channels. *Pharmacol Rev* 57(4)**,** 397-409. doi: 10.1124/pr.57.4.4.
Catterall, W.A., Kalume, F., and Oakley, J.C. (2010). NaV1.1 channels and epilepsy. *J Physiol* 588(Pt 11)**,** 1849-1859. doi: 10.1113/jphysiol.2010.187484.
Chang, C.W., Evans, M.D., Yu, X., Yu, G.Q., and Mucke, L. (2021). Tau reduction affects excitatory and inhibitory neurons differently, reduces excitation/inhibition ratios, and counteracts network hypersynchrony. *Cell Rep* 37(3)**,** 109855. doi: 10.1016/j.celrep.2021.109855.
Chang, D.T., Rintoul, G.L., Pandipati, S., and Reynolds, I.J. (2006). Mutant huntingtin aggregates impair mitochondrial movement and trafficking in cortical neurons. *Neurobiol Dis* 22(2)**,** 388-400. doi: 10.1016/j.nbd.2005.12.007.
Charvériat, M., Naus, C.C., Leybaert, L., Sáez, J.C., and Giaume, C. (2017). Connexin-Dependent Neuroglial Networking as a New Therapeutic Target. *Frontiers in Cellular Neuroscience* 11.
Chaunsali, L., Tewari, B.P., Gallucci, A., Thompson, E.G., Savoia, A., Feld, N., et al. (2020). Glioma-induced peritumoral hyperexcitability in a pediatric glioma model. *Physiol Rep* 8(19)**,** e14567. doi: 10.14814/phy2.14567.
Chen, L., Yang, P., and Kijlstra, A. (2002). Distribution, markers, and functions of retinal microglia. *Ocul Immunol Inflamm* 10(1)**,** 27-39. doi: 10.1076/ocii.10.1.27.10328.
Chen, Y., Hughes, G., Chen, X., Qian, S., Cao, W., Wang, L., et al. (2015). Genetic Variants Associated With Different Risks for High Tension Glaucoma and Normal Tension Glaucoma in a Chinese Population. *Invest Ophthalmol Vis Sci* 56(4)**,** 2595-2600. doi: 10.1167/iovs.14-16269.
Chen, Y., Wang, L., Zhang, L., Chen, B., Yang, L., Li, X., et al. (2018). Inhibition of Connexin 43 Hemichannels Alleviates Cerebral Ischemia/Reperfusion Injury via the TLR4 Signaling Pathway. *Front Cell Neurosci* 12**,** 372. doi: 10.3389/fncel.2018.00372.
Chever, O., Lee, C.Y., and Rouach, N. (2014). Astroglial connexin43 hemichannels tune basal excitatory synaptic transmission. *J Neurosci* 34(34)**,** 11228-11232. doi: 10.1523/JNEUROSCI.0015-14.2014.
Chrysostomou, V., Rezania, F., Trounce, I.A., and Crowston, J.G. (2013). Oxidative stress and mitochondrial dysfunction in glaucoma. *Curr Opin Pharmacol* 13(1)**,** 12-15. doi: 10.1016/j.coph.2012.09.008.
Clausen, M.V., Hilbers, F., and Poulsen, H. (2017). The Structure and Function of the Na,K-ATPase Isoforms in Health and Disease. *Front Physiol* 8**,** 371. doi: 10.3389/fphys.2017.00371.
Coccia, E., and Ahfeldt, T. (2021). Towards physiologically relevant human pluripotent stem cell (hPSC) models of Parkinson's disease. *Stem Cell Res Ther* 12(1)**,** 253. doi: 10.1186/s13287-021-02326-5.
Cohen, E., and Sterling, P. (1990). Convergence and divergence of cones onto bipolar cells in the central area of cat retina. *Philos Trans R Soc Lond B Biol Sci* 330(1258)**,** 323-328. doi: 10.1098/rstb.1990.0202.
Cohen, L.P., and Pasquale, L.R. (2014). Clinical characteristics and current treatment of glaucoma. *Cold Spring Harb Perspect Med* 4(6). doi: 10.1101/cshperspect.a017236.
Contreras, J.E., Sanchez, H.A., Eugenin, E.A., Speidel, D., Theis, M., Willecke, K., et al. (2002). Metabolic inhibition induces opening of unapposed connexin 43 gap junction hemichannels and reduces gap junctional communication in cortical astrocytes in culture. *Proc Natl Acad Sci U S A* 99(1)**,** 495-500. doi: 10.1073/pnas.012589799.

Cooper, M.L., Collyer, J.W., and Calkins, D.J. (2018). Astrocyte remodeling without gliosis precedes optic nerve Axonopathy. *Acta Neuropathol Commun* 6(1)**,** 38. doi: 10.1186/s40478-018-0542-0.

Cooper, M.L., Pasini, S., Lambert, W.S., D'Alessandro, K.B., Yao, V., Risner, M.L., et al. (2020). Redistribution of metabolic resources through astrocyte networks mitigates neurodegenerative stress. *Proc Natl Acad Sci U S A* 117(31)**,** 18810-18821. doi: 10.1073/pnas.2009425117.

Copenhagen, D.R., Hemila, S., and Reuter, T. (1990). Signal transmission through the dark-adapted retina of the toad (Bufo marinus). Gain, convergence, and signal/noise. *J Gen Physiol* 95(4)**,** 717-732. doi: 10.1085/jgp.95.4.717.

Crish, S.D., and Calkins, D.J. (2011). Neurodegeneration in glaucoma: progression and calcium-dependent intracellular mechanisms. *Neuroscience* 176**,** 1-11. doi: 10.1016/j.neuroscience.2010.12.036.

Crish, S.D., and Calkins, D.J. (2015). Central visual pathways in glaucoma: evidence for distal mechanisms of neuronal self-repair. *J Neuroophthalmol* 35 Suppl 1**,** S29-37. doi: 10.1097/WNO.0000000000000291.

Crish, S.D., Sappington, R.M., Inman, D.M., Horner, P.J., and Calkins, D.J. (2010). Distal axonopathy with structural persistence in glaucomatous neurodegeneration. *Proc Natl Acad Sci U S A* 107(11)**,** 5196-5201. doi: 0913141107 [pii]
10.1073/pnas.0913141107.

Dacey, D.M. (1993). The mosaic of midget ganglion cells in the human retina. *J Neurosci* 13(12)**,** 5334-5355. doi: 10.1523/JNEUROSCI.13-12-05334.1993.

Danesh-Meyer, H.V., Zhang, J., Acosta, M.L., Rupenthal, I.D., and Green, C.R. (2016). Connexin43 in retinal injury and disease. *Prog Retin Eye Res* 51**,** 41-68. doi: 10.1016/j.preteyeres.2015.09.004.

Daniszewski, M., Senabouth, A., Nguyen, Q.H., Crombie, D.E., Lukowski, S.W., Kulkarni, T., et al. (2018). Single cell RNA sequencing of stem cell-derived retinal ganglion cells. *Sci Data* 5**,** 180013. doi: 10.1038/sdata.2018.13.

Day, A.C., Baio, G., Gazzard, G., Bunce, C., Azuara-Blanco, A., Munoz, B., et al. (2012). The prevalence of primary angle closure glaucoma in European derived populations: a systematic review. *Br J Ophthalmol* 96(9)**,** 1162-1167. doi: 10.1136/bjophthalmol-2011-301189.

De la Huerta, I., Kim, I.J., Voinescu, P.E., and Sanes, J.R. (2012). Direction-selective retinal ganglion cells arise from molecularly specified multipotential progenitors. *Proc Natl Acad Sci U S A* 109(43)**,** 17663-17668. doi: 10.1073/pnas.1215806109.

De Leon-Ortega, J.E., and Girkin, C.A. (2002). Ocular trauma-related glaucoma. *Ophthalmol Clin North Am* 15(2)**,** 215-223. doi: 10.1016/s0896-1549(02)00011-1.

de Lera Ruiz, M., and Kraus, R.L. (2015). Voltage-Gated Sodium Channels: Structure, Function, Pharmacology, and Clinical Indications. *J Med Chem* 58(18)**,** 7093-7118. doi: 10.1021/jm501981g.

De Pina-Benabou, M.H., Srinivas, M., Spray, D.C., and Scemes, E. (2001). Calmodulin kinase pathway mediates the K+-induced increase in Gap junctional communication between mouse spinal cord astrocytes. *J Neurosci* 21(17)**,** 6635-6643. doi: 10.1523/JNEUROSCI.21-17-06635.2001.

de Polavieja, G.G., Harsch, A., Kleppe, I., Robinson, H.P., and Juusola, M. (2005). Stimulus history reliably shapes action potential waveforms of cortical neurons. *J Neurosci* 25(23)**,** 5657-5665. doi: 10.1523/JNEUROSCI.0242-05.2005.

De Vos, K.J., Grierson, A.J., Ackerley, S., and Miller, C.C. (2008). Role of axonal transport in neurodegenerative diseases. *Annu Rev Neurosci* 31**,** 151-173. doi: 10.1146/annurev.neuro.31.061307.090711.

Della Santina, L., Inman, D.M., Lupien, C.B., Horner, P.J., and Wong, R.O. (2013). Differential progression of structural and functional alterations in distinct retinal ganglion cell types in a mouse model of glaucoma. *J Neurosci* 33(44)**,** 17444-17457. doi: 10.1523/JNEUROSCI.5461-12.2013.

Demb, J.B. (2007). Cellular mechanisms for direction selectivity in the retina. *Neuron* 55(2)**,** 179-186. doi: 10.1016/j.neuron.2007.07.001.

Dengler-Crish, C.M., Smith, M.A., Inman, D.M., Wilson, G.N., Young, J.W., and Crish, S.D. (2014). Anterograde transport blockade precedes deficits in retrograde transport in the visual projection of the DBA/2J mouse model of glaucoma. *Front Neurosci* 8**,** 290. doi: 10.3389/fnins.2014.00290.

Diaz-Coranguez, M., Ramos, C., and Antonetti, D.A. (2017). The inner blood-retinal barrier: Cellular basis and development. *Vision Res* 139**,** 123-137. doi: 10.1016/j.visres.2017.05.009.

Diem, R., Meyer, R., Weishaupt, J.H., and Bahr, M. (2001a). Reduction of potassium currents and phosphatidylinositol 3-kinase-dependent AKT phosphorylation by tumor necrosis factor-(alpha) rescues axotomized retinal ganglion cells from retrograde cell death in vivo. *J Neurosci* 21(6)**,** 2058-2066.

Diem, R., Meyer, R., Weishaupt, J.H., and Bähr, M. (2001b). Reduction of Potassium Currents and Phosphatidylinositol 3-Kinase-Dependent Akt Phosphorylation by Tumor Necrosis Factor-α Rescues Axotomized Retinal Ganglion Cells from Retrograde Cell DeathIn Vivo. *The Journal of Neuroscience* 21(6)**,** 2058-2066. doi: 10.1523/jneurosci.21-06-02058.2001.

Diogenes, M.J., Dias, R.B., Rombo, D.M., Vicente Miranda, H., Maiolino, F., Guerreiro, P., et al. (2012). Extracellular alpha-synuclein oligomers modulate synaptic transmission and impair LTP via NMDA-receptor activation. *J Neurosci* 32(34)**,** 11750-11762. doi: 10.1523/JNEUROSCI.0234-12.2012.

Dong, X.X., Wang, Y., and Qin, Z.H. (2009). Molecular mechanisms of excitotoxicity and their relevance to pathogenesis of neurodegenerative diseases. *Acta Pharmacol Sin* 30(4)**,** 379-387. doi: 10.1038/aps.2009.24.

Dorrego-Rivas, A., Ezan, J., Moreau, M.M., Poirault-Chassac, S., Aubailly, N., De Neve, J., et al. (2022). The core PCP protein Prickle2 regulates axon number and AIS maturation by binding to AnkG and modulating microtubule bundling. *Sci Adv* 8(36)**,** eabo6333. doi: 10.1126/sciadv.abo6333.

Downs, J.C. (2015). Optic nerve head biomechanics in aging and disease. *Exp Eye Res* 133**,** 19-29. doi: 10.1016/j.exer.2015.02.011.

Downs, M., Sethi, M.K., Raghunathan, R., Layne, M.D., and Zaia, J. (2022). Matrisome changes in Parkinson's disease. *Anal Bioanal Chem* 414(9)**,** 3005-3015. doi: 10.1007/s00216-022-03929-4.

Dräger, N.M., Sattler, S.M., Huang, C.T., Teter, O.M., Leng, K., Hashemi, S.H., et al. (2022). A CRISPRi/a platform in human iPSC-derived microglia uncovers regulators of disease states. *Nat Neurosci* 25(9)**,** 1149-1162. doi: 10.1038/s41593-022-01131-4.

Duan, X., Qiao, M., Bei, F., Kim, I.-J., He, Z., and Sanes, J.R. (2015). Subtype-specific regeneration of retinal ganglion cells following axotomy: effects of osteopontin and mTOR signaling. *Neuron* 85(6)**,** 1244-1256. doi: 10.1016/j.neuron.2015.02.017.

Duchen, M.R. (2004). Roles of mitochondria in health and disease. *Diabetes* 53 Suppl 1(suppl_1)**,** S96-102. doi: 10.2337/diabetes.53.2007.s96.

Ek-Vitorin, J.F., Pontifex, T.K., and Burt, J.M. (2018). Cx43 Channel Gating and Permeation: Multiple Phosphorylation-Dependent Roles of the Carboxyl Terminus. *Int J Mol Sci* 19(6). doi: 10.3390/ijms19061659.

El-Danaf, R.N., and Huberman, A.D. (2015). Characteristic patterns of dendritic remodeling in early-stage glaucoma: evidence from genetically identified retinal ganglion cell types. *J Neurosci* 35(6)**,** 2329-2343. doi: 10.1523/JNEUROSCI.1419-14.2015.

Elkington, A.R., Inman, C.B., Steart, P.V., and Weller, R.O. (1990). The structure of the lamina cribrosa of the human eye: an immunocytochemical and electron microscopical study. *Eye (Lond)* 4 (Pt 1)(1)**,** 42-57. doi: 10.1038/eye.1990.5.

Emanuel, A.J., Kapur, K., and Do, M.T.H. (2017). Biophysical Variation within the M1 Type of Ganglion Cell Photoreceptor. *Cell Rep* 21(4)**,** 1048-1062. doi: 10.1016/j.celrep.2017.09.095.

Engelmann, J., van den Burg, E., Bacelo, J., de Ruijters, M., Kuwana, S., Sugawara, Y., et al. (2008). Dendritic backpropagation and synaptic plasticity in the mormyrid electrosensory lobe. *J Physiol Paris* 102(4-6)**,** 233-245. doi: 10.1016/j.jphysparis.2008.10.004.

Enkvist, M.O., and McCarthy, K.D. (1994). Astroglial gap junction communication is increased by treatment with either glutamate or high K+ concentration. *J Neurochem* 62(2)**,** 489-495. doi: 10.1046/j.1471-4159.1994.62020489.x.

Evans, M.D., Dumitrescu, A.S., Kruijssen, D.L.H., Taylor, S.E., and Grubb, M.S. (2015). Rapid Modulation of Axon Initial Segment Length Influences Repetitive Spike Firing. *Cell Rep* 13(6)**,** 1233-1245. doi: 10.1016/j.celrep.2015.09.066.

Famiglietti, E.V., Jr., and Kolb, H. (1976). Structural basis for ON-and OFF-center responses in retinal ganglion cells. *Science* 194(4261)**,** 193-195. doi: 10.1126/science.959847.

Fekete, A., Ankri, N., Brette, R., and Debanne, D. (2021). Neural excitability increases with axonal resistance between soma and axon initial segment. *Proc Natl Acad Sci U S A* 118(33)**,** e2102217118. doi: 10.1073/pnas.2102217118.

Feldman, B.H., Fantin, A., Lee, A.G., Kedar, S., Othman, B.A., and FitzGibbon, E.J. (2022). *Optic Atrophy* [Online]. American Academy of Ophthalmology. Available: https://eyewiki.aao.org/Optic_Atrophy [Accessed February 2, 2023 2023].

Feldman, D.E. (2012). The spike-timing dependence of plasticity. *Neuron* 75(4)**,** 556-571. doi: 10.1016/j.neuron.2012.08.001.

Fellman, R.L., Mattox, C., Singh, K., Flowers, B., Francis, B.A., Robin, A.L., et al. (2020). American Glaucoma Society Position Paper: Microinvasive Glaucoma Surgery. *Ophthalmol Glaucoma* 3(1)**,** 1-6. doi: 10.1016/j.ogla.2019.12.003.

Fischer, R.A., Risner, M.L., Roux, A.L., Wareham, L.K., and Sappington, R.M. (2019a). Impairment of Membrane Repolarization Accompanies Axon Transport Deficits in Glaucoma. *Front Neurosci* 13**,** 1139. doi: 10.3389/fnins.2019.01139.

Fischer, R.A., Roux, A.L., Wareham, L.K., and Sappington, R.M. (2019b). Pressure-dependent modulation of inward-rectifying K(+) channels: implications for cation homeostasis and K(+) dynamics in glaucoma. *Am J Physiol Cell Physiol* 317(2)**,** C375-C389. doi: 10.1152/ajpcell.00444.2018.

Fjell, J., Dib-Hajj, S., Fried, K., Black, J.A., and Waxman, S.G. (1997). Differential expression of sodium channel genes in retinal ganglion cells. *Brain Res Mol Brain Res* 50(1-2)**,** 197-204. doi: 10.1016/s0169-328x(97)00187-3.

Flammer, J. (1994). The vascular concept of glaucoma. *Surv Ophthalmol* 38 Suppl**,** S3-6. doi: 10.1016/0039-6257(94)90041-8.

Fletcher, T.L., Cameron, P., De Camilli, P., and Banker, G. (1991). The distribution of synapsin I and synaptophysin in hippocampal neurons developing in culture. *J Neurosci* 11(6)**,** 1617-1626. doi: 10.1523/jneurosci.11-06-01617.1991.

Fligor, C.M., Lavekar, S.S., Harkin, J., Shields, P.K., VanderWall, K.B., Huang, K.C., et al. (2021). Extension of retinofugal projections in an assembled model of human pluripotent stem cell-derived organoids. *Stem Cell Reports* 16(9)**,** 2228-2241. doi: 10.1016/j.stemcr.2021.05.009.

Frazzini, V., Guarnieri, S., Bomba, M., Navarra, R., Morabito, C., Mariggio, M.A., et al. (2016). Altered Kv2.1 functioning promotes increased excitability in hippocampal neurons of an Alzheimer's disease mouse model. *Cell Death Dis* 7(2)**,** e2100. doi: 10.1038/cddis.2016.18.

Freitas-Andrade, M., Bechberger, J., Wang, J., Yeung, K.K.C., Whitehead, S.N., Hansen, R.S., et al. (2020). Danegaptide Enhances Astrocyte Gap Junctional Coupling and Reduces Ischemic Reperfusion Brain Injury in Mice. *Biomolecules* 10(3). doi: 10.3390/biom10030353.

Friedman, D.S., Wolfs, R.C., O'Colmain, B.J., Klein, B.E., Taylor, H.R., West, S., et al. (2004). Prevalence of open-angle glaucoma among adults in the United States. *Arch Ophthalmol* 122(4)**,** 532-538. doi: 10.1001/archopht.122.4.532.

Friedman, L.K. (2006). Calcium: a role for neuroprotection and sustained adaptation. *Mol Interv* 6(6)**,** 315-329. doi: 10.1124/mi.6.6.5.

Fu, H., Hardy, J., and Duff, K.E. (2018). Selective vulnerability in neurodegenerative diseases. *Nat Neurosci* 21(10)**,** 1350-1358. doi: 10.1038/s41593-018-0221-2.

Fu, Y. (2018). *Phototransduction in Rods and Cones* [Online]. Webvision: Moran Eye Institute. Available: https://webvision.med.utah.edu/book/part-v-phototransduction-in-rods-and-cones/phototransduction-in-rods-and-cones/ [Accessed January 23, 2023 2023].

Galiano, M.R., Jha, S., Ho, T.S., Zhang, C., Ogawa, Y., Chang, K.J., et al. (2012). A distal axonal cytoskeleton forms an intra-axonal boundary that controls axon initial segment assembly. *Cell* 149(5)**,** 1125-1139. doi: 10.1016/j.cell.2012.03.039.

Galinsky, R., Davidson, J.O., Lear, C.A., Bennet, L., Green, C.R., and Gunn, A.J. (2017). Connexin hemichannel blockade improves survival of striatal GABA-ergic neurons after global cerebral ischaemia in term-equivalent fetal sheep. *Sci Rep* 7(1)**,** 6304. doi: 10.1038/s41598-017-06683-1.

Galli-Resta, L., Novelli, E., Volpini, M., and Strettoi, E. (2000). The spatial organization of cholinergic mosaics in the adult mouse retina. *Eur J Neurosci* 12(10)**,** 3819-3822. doi: 10.1046/j.1460-9568.2000.00280.x.

Gao, V., Suzuki, A., Magistretti, P.J., Lengacher, S., Pollonini, G., Steinman, M.Q., et al. (2016). Astrocytic beta2-adrenergic receptors mediate hippocampal long-term memory consolidation. *Proc Natl Acad Sci U S A* 113(30)**,** 8526-8531. doi: 10.1073/pnas.1605063113.

Gasser, A., Ho, T.S., Cheng, X., Chang, K.J., Waxman, S.G., Rasband, M.N., et al. (2012). An ankyrinG-binding motif is necessary and sufficient for targeting Nav1.6 sodium channels to axon initial segments and nodes of Ranvier. *J Neurosci* 32(21)**,** 7232-7243. doi: 10.1523/JNEUROSCI.5434-11.2012.

Gasser, H.S., and Erlanger, J. (1927). The role played by the sizes of the constituent fibers of a nerve trunk in determining the form of its action potential wave. *American Journal of Physiology* 80(3)**,** 522-547. doi: DOI 10.1152/ajplegacy.1927.80.3.522.

Geiger, J.R., and Jonas, P. (2000). Dynamic control of presynaptic Ca(2+) inflow by fast-inactivating K(+) channels in hippocampal mossy fiber boutons. *Neuron* 28(3)**,** 927-939. doi: 10.1016/s0896-6273(00)00164-1.

Gerometta, R., Podos, S.M., Candia, O.A., Wu, B., Malgor, L.A., Mittag, T., et al. (2004). Steroid-induced ocular hypertension in normal cattle. *Arch Ophthalmol* 122(10)**,** 1492-1497. doi: 10.1001/archopht.122.10.1492.

Giaume, C., Naus, C.C., Saez, J.C., and Leybaert, L. (2021). Glial Connexins and Pannexins in the Healthy and Diseased Brain. *Physiol Rev* 101(1)**,** 93-145. doi: 10.1152/physrev.00043.2018.

Goel, M., Picciani, R.G., Lee, R.K., and Bhattacharya, S.K. (2010). Aqueous humor dynamics: a review. *Open Ophthalmol J* 4**,** 52-59. doi: 10.2174/1874364101004010052.

Goethals, S., and Brette, R. (2020). Theoretical relation between axon initial segment geometry and excitability. *Elife* 9. doi: 10.7554/eLife.53432.

Goethals, S., Sierksma, M.C., Nicol, X., Reaux-Le Goazigo, A., and Brette, R. (2021). Electrical match between initial segment and somatodendritic compartment for action potential backpropagation in retinal ganglion cells. *J Neurophysiol* 126(1)**,** 28-46. doi: 10.1152/jn.00005.2021.

Goetz, J., Jessen, Z.F., Jacobi, A., Mani, A., Cooler, S., Greer, D., et al. (2022). Unified classification of mouse retinal ganglion cells using function, morphology, and gene expression. *bioRxiv***,** 2021.2006.2010.447922. doi: 10.1101/2021.06.10.447922.

Goldman, D.E. (1943). Potential, Impedance, and Rectification in Membranes. *J Gen Physiol* 27(1)**,** 37-60. doi: 10.1085/jgp.27.1.37.

Gomes, C., VanderWall, K.B., Pan, Y., Lu, X., Lavekar, S.S., Huang, K.C., et al. (2022). Astrocytes modulate neurodegenerative phenotypes associated with glaucoma in OPTN(E50K) human stem cell-derived retinal ganglion cells. *Stem Cell Reports* 17(7)**,** 1636-1649. doi: 10.1016/j.stemcr.2022.05.006.

Gonzalez Sabater, V., Rigby, M., and Burrone, J. (2021). Voltage-Gated Potassium Channels Ensure Action Potential Shape Fidelity in Distal Axons. *J Neurosci* 41(25)**,** 5372-5385. doi: 10.1523/jneurosci.2765-20.2021.

Griemsmann, S., Hoft, S.P., Bedner, P., Zhang, J., von Staden, E., Beinhauer, A., et al. (2015). Characterization of Panglial Gap Junction Networks in the Thalamus, Neocortex, and

Hippocampus Reveals a Unique Population of Glial Cells. *Cereb Cortex* 25(10)**,** 3420-3433. doi: 10.1093/cercor/bhu157.
Grozdanic, S.D., Betts, D.M., Sakaguchi, D.S., Allbaugh, R.A., Kwon, Y.H., and Kardon, R.H. (2003). Laser-induced mouse model of chronic ocular hypertension. *Invest Ophthalmol Vis Sci* 44(10)**,** 4337-4346. doi: 10.1167/iovs.03-0015.
Grubb, M.S., and Burrone, J. (2010). Activity-dependent relocation of the axon initial segment fine-tunes neuronal excitability. *Nature* 465(7301)**,** 1070-1074. doi: 10.1038/nature09160.
Grubman, A., Choo, X.Y., Chew, G., Ouyang, J.F., Sun, G., Croft, N.P., et al. (2021). Transcriptional signature in microglia associated with Abeta plaque phagocytosis. *Nat Commun* 12(1)**,** 3015. doi: 10.1038/s41467-021-23111-1.
Gu, N., Vervaeke, K., and Storm, J.F. (2007). BK potassium channels facilitate high-frequency firing and cause early spike frequency adaptation in rat CA1 hippocampal pyramidal cells. *J Physiol* 580(Pt.3)**,** 859-882. doi: 10.1113/jphysiol.2006.126367.
Gu, Y., Jukkola, P., Wang, Q., Esparza, T., Zhao, Y., Brody, D., et al. (2017). Polarity of varicosity initiation in central neuron mechanosensation. *J Cell Biol* 216(7)**,** 2179-2199. doi: 10.1083/jcb.201606065.
Guttenplan, K.A., Stafford, B.K., El-Danaf, R.N., Adler, D.I., Munch, A.E., Weigel, M.K., et al. (2020). Neurotoxic Reactive Astrocytes Drive Neuronal Death after Retinal Injury. *Cell Rep* 31(12)**,** 107776. doi: 10.1016/j.celrep.2020.107776.
Gutzmann, A., Ergül, N., Grossmann, R., Schultz, C., Wahle, P., and Engelhardt, M. (2014). A period of structural plasticity at the axon initial segment in developing visual cortex. *Front Neuroanat* 8**,** 11. doi: 10.3389/fnana.2014.00011.
Hall, A.M., Throesch, B.T., Buckingham, S.C., Markwardt, S.J., Peng, Y., Wang, Q., et al. (2015). Tau-dependent Kv4.2 depletion and dendritic hyperexcitability in a mouse model of Alzheimer's disease. *J Neurosci* 35(15)**,** 6221-6230. doi: 10.1523/JNEUROSCI.2552-14.2015.
Hamada, M.S., Goethals, S., de Vries, S.I., Brette, R., and Kole, M.H. (2016). Covariation of axon initial segment location and dendritic tree normalizes the somatic action potential. *Proc Natl Acad Sci U S A* 113(51)**,** 14841-14846. doi: 10.1073/pnas.1607548113.
Harden, S.W. (2022). *pyABF 2.3.5* [Online]. Available: https://swharden.com/pyabf/ [Accessed 12/3/22 2022].
Hargrave, P.A., and McDowell, J.H. (1993). "Rhodopsin and Phototransduction," in *International Review of Cytology*, eds. M. Friedlander & M. Mueckler. Academic Press), 49-97.
Harris, A.L. (2007). Connexin channel permeability to cytoplasmic molecules. *Prog Biophys Mol Biol* 94(1-2)**,** 120-143. doi: 10.1016/j.pbiomolbio.2007.03.011.
Harun-Or-Rashid, M., Pappenhagen, N., Palmer, P.G., Smith, M.A., Gevorgyan, V., Wilson, G.N., et al. (2018). Structural and Functional Rescue of Chronic Metabolically Stressed Optic Nerves through Respiration. *J Neurosci* 38(22)**,** 5122-5139. doi: 10.1523/JNEUROSCI.3652-17.2018.
Hasel, P., Dando, O., Jiwaji, Z., Baxter, P., Todd, A.C., Heron, S., et al. (2017). Neurons and neuronal activity control gene expression in astrocytes to regulate their development and metabolism. *Nat Commun* 8(1)**,** 15132. doi: 10.1038/ncomms15132.
Hatch, R.J., Wei, Y., Xia, D., and Gotz, J. (2017). Hyperphosphorylated tau causes reduced hippocampal CA1 excitability by relocating the axon initial segment. *Acta Neuropathol* 133(5)**,** 717-730. doi: 10.1007/s00401-017-1674-1.
Hayreh, S.S. (2001). The blood supply of the optic nerve head and the evaluation of it - myth and reality. *Prog Retin Eye Res* 20(5)**,** 563-593. doi: 10.1016/s1350-9462(01)00004-0.
Hayreh, S.S. (2004). Posterior ciliary artery circulation in health and disease: the Weisenfeld lecture. *Invest Ophthalmol Vis Sci* 45(3)**,** 749-757; 748. doi: 10.1167/iovs.03-0469.
Hayreh, S.S. (2009). Ischemic optic neuropathy. *Prog Retin Eye Res* 28(1)**,** 34-62. doi: 10.1016/j.preteyeres.2008.11.002.
Hayreh, S.S., Podhajsky, P.A., and Zimmerman, B. (1998). Ocular manifestations of giant cell arteritis. *American journal of ophthalmology* 125(4)**,** 509-520.

Heavner, W., and Pevny, L. (2012). Eye development and retinogenesis. *Cold Spring Harb Perspect Biol* 4(12). doi: 10.1101/cshperspect.a008391.
Hedstrom, K.L., Ogawa, Y., and Rasband, M.N. (2008). AnkyrinG is required for maintenance of the axon initial segment and neuronal polarity. *J Cell Biol* 183(4)**,** 635-640. doi: 10.1083/jcb.200806112.
Heijl, A., Leske, M.C., Bengtsson, B., Hyman, L., Bengtsson, B., Hussein, M., et al. (2002). Reduction of intraocular pressure and glaucoma progression: results from the Early Manifest Glaucoma Trial. *Arch Ophthalmol* 120(10)**,** 1268-1279. doi: 10.1001/archopht.120.10.1268.
Heinemann, U., and Lux, H.D. (1977). Ceiling of stimulus induced rises in extracellular potassium concentration in the cerebral cortex of cat. *Brain Res* 120(2)**,** 231-249. doi: 10.1016/0006-8993(77)90903-9.
Hennis, A., Wu, S.Y., Nemesure, B., Honkanen, R., Leske, M.C., and Barbados Eye Studies, G. (2007). Awareness of incident open-angle glaucoma in a population study: the Barbados Eye Studies. *Ophthalmology* 114(10)**,** 1816-1821. doi: 10.1016/j.ophtha.2007.06.013.
Hernandez, M.R., Miao, H., and Lukas, T. (2008). Astrocytes in glaucomatous optic neuropathy. *Prog Brain Res* 173**,** 353-373. doi: 10.1016/S0079-6123(08)01125-4.
Herrero-Mendez, A., Almeida, A., Fernandez, E., Maestre, C., Moncada, S., and Bolanos, J.P. (2009). The bioenergetic and antioxidant status of neurons is controlled by continuous degradation of a key glycolytic enzyme by APC/C-Cdh1. *Nat Cell Biol* 11(6)**,** 747-752. doi: 10.1038/ncb1881.
Hickman, S.J., Dalton, C.M., Miller, D.H., and Plant, G.T. (2002). Management of acute optic neuritis. *Lancet* 360(9349)**,** 1953-1962. doi: 10.1016/s0140-6736(02)11919-2.
Hodapp, A., Kaiser, M.E., Thome, C., Ding, L., Rozov, A., Klumpp, M., et al. (2022). Dendritic axon origin enables information gating by perisomatic inhibition in pyramidal neurons. *Science* 377(6613)**,** 1448-1452. doi: 10.1126/science.abj1861.
Hodgkin, A.L., and Huxley, A.F. (1947). Potassium leakage from an active nerve fibre. *J Physiol* 106(3)**,** 341-367. doi: 10.1113/jphysiol.1947.sp004216.
Hodgkin, A.L., and Huxley, A.F. (1952a). The components of membrane conductance in the giant axon of Loligo. *J Physiol* 116(4)**,** 473-496. doi: 10.1113/jphysiol.1952.sp004718.
Hodgkin, A.L., and Huxley, A.F. (1952b). Currents carried by sodium and potassium ions through the membrane of the giant axon of Loligo. *J Physiol* 116(4)**,** 449-472. doi: 10.1113/jphysiol.1952.sp004717.
Hodgkin, A.L., and Huxley, A.F. (1952c). The dual effect of membrane potential on sodium conductance in the giant axon of Loligo. *J Physiol* 116(4)**,** 497-506. doi: 10.1113/jphysiol.1952.sp004719.
Hodgkin, A.L., and Katz, B. (1949). The effect of sodium ions on the electrical activity of giant axon of the squid. *J Physiol* 108(1)**,** 37-77. doi: 10.1113/jphysiol.1949.sp004310.
Hollander, H., Makarov, F., Dreher, Z., van Driel, D., Chan-Ling, T.L., and Stone, J. (1991). Structure of the macroglia of the retina: sharing and division of labour between astrocytes and Muller cells. *J Comp Neurol* 313(4)**,** 587-603. doi: 10.1002/cne.903130405.
Holmqvist, M.H., Cao, J., Hernandez-Pineda, R., Jacobson, M.D., Carroll, K.I., Sung, M.A., et al. (2002). Elimination of fast inactivation in Kv4 A-type potassium channels by an auxiliary subunit domain. *Proc Natl Acad Sci U S A* 99(2)**,** 1035-1040. doi: 10.1073/pnas.022509299.
Hu, C.X., Zangalli, C., Hsieh, M., Gupta, L., Williams, A.L., Richman, J., et al. (2014). What do patients with glaucoma see? Visual symptoms reported by patients with glaucoma. *Am J Med Sci* 348(5)**,** 403-409. doi: 10.1097/MAJ.0000000000000319.
Huang, C.Y., and Rasband, M.N. (2018). Axon initial segments: structure, function, and disease. *Ann N Y Acad Sci* 1420(1)**,** 46-61. doi: 10.1111/nyas.13718.
Huberman, A.D., Wei, W., Elstrott, J., Stafford, B.K., Feller, M.B., and Barres, B.A. (2009). Genetic identification of an On-Off direction-selective retinal ganglion cell subtype reveals a layer-specific subcortical map of posterior motion. *Neuron* 62(3)**,** 327-334. doi: 10.1016/j.neuron.2009.04.014.

Inman, D.M., and Harun-Or-Rashid, M. (2017). Metabolic Vulnerability in the Neurodegenerative Disease Glaucoma. *Front Neurosci* 11**,** 146. doi: 10.3389/fnins.2017.00146.

Inman, D.M., Sappington, R.M., Horner, P.J., and Calkins, D.J. (2006). Quantitative correlation of optic nerve pathology with ocular pressure and corneal thickness in the DBA/2 mouse model of glaucoma. *Invest Ophthalmol Vis Sci* 47(3)**,** 986-996. doi: 10.1167/iovs.05-0925.

Inoue, T., and Tanihara, H. (2013). Rho-associated kinase inhibitors: a novel glaucoma therapy. *Prog Retin Eye Res* 37**,** 1-12. doi: 10.1016/j.preteyeres.2013.05.002.

Investigators, T.A. (2000). The Advanced Glaucoma Intervention Study (AGIS): 7. The relationship between control of intraocular pressure and visual field deterioration.The AGIS Investigators. *Am J Ophthalmol* 130(4)**,** 429-440. doi: 10.1016/s0002-9394(00)00538-9.

Ito, Y.A., Belforte, N., Cueva Vargas, J.L., and Di Polo, A. (2016). A Magnetic Microbead Occlusion Model to Induce Ocular Hypertension-Dependent Glaucoma in Mice. *J Vis Exp* (109)**,** e53731. doi: 10.3791/53731.

Jakoby, P., Schmidt, E., Ruminot, I., Gutierrez, R., Barros, L.F., and Deitmer, J.W. (2014). Higher transport and metabolism of glucose in astrocytes compared with neurons: a multiphoton study of hippocampal and cerebellar tissue slices. *Cereb Cortex* 24(1)**,** 222-231. doi: 10.1093/cercor/bhs309.

Jamann, N., Dannehl, D., Lehmann, N., Wagener, R., Thielemann, C., Schultz, C., et al. (2021). Sensory input drives rapid homeostatic scaling of the axon initial segment in mouse barrel cortex. *Nat Commun* 12(1)**,** 23. doi: 10.1038/s41467-020-20232-x.

Johnson, E.C., Carter, E.K., Dammer, E.B., Duong, D.M., Gerasimov, E.S., Liu, Y., et al. (2022). Large-scale deep multi-layer analysis of Alzheimer's disease brain reveals strong proteomic disease-related changes not observed at the RNA level. *Nature neuroscience* 25(2)**,** 213-225.

Jones, B.L., and Smith, S.M. (2016). Calcium-Sensing Receptor: A Key Target for Extracellular Calcium Signaling in Neurons. *Front Physiol* 7**,** 116. doi: 10.3389/fphys.2016.00116.

Jørgensen, H.S., Jensen, D.B., Dimintiyanova, K.P., Bonnevie, V.S., Hedegaard, A., Lehnhoff, J., et al. (2021). Increased Axon Initial Segment Length Results in Increased Na(+) Currents in Spinal Motoneurones at Symptom Onset in the G127X SOD1 Mouse Model of Amyotrophic Lateral Sclerosis. *Neuroscience* 468**,** 247-264. doi: 10.1016/j.neuroscience.2020.11.016.

Kameneva, T., Maturana, M.I., Hadjinicolaou, A.E., Cloherty, S.L., Ibbotson, M.R., Grayden, D.B., et al. (2016). Retinal ganglion cells: mechanisms underlying depolarization block and differential responses to high frequency electrical stimulation of ON and OFF cells. *J Neural Eng* 13(1)**,** 016017. doi: 10.1088/1741-2560/13/1/016017.

Kanamori, A., Nakamura, M., Nakanishi, Y., Yamada, Y., and Negi, A. (2005). Long-term glial reactivity in rat retinas ipsilateral and contralateral to experimental glaucoma. *Exp Eye Res* 81(1)**,** 48-56. doi: 10.1016/j.exer.2005.01.012.

Kar, R., Riquelme, M.A., Werner, S., and Jiang, J.X. (2013). Connexin 43 channels protect osteocytes against oxidative stress-induced cell death. *J Bone Miner Res* 28(7)**,** 1611-1621. doi: 10.1002/jbmr.1917.

Karwoski, C.J., Lu, H.K., and Newman, E.A. (1989). Spatial buffering of light-evoked potassium increases by retinal Muller (glial) cells. *Science* 244(4904)**,** 578-580. doi: 10.1126/science.2785716.

Kasischke, K.A., Vishwasrao, H.D., Fisher, P.J., Zipfel, W.R., and Webb, W.W. (2004). Neural activity triggers neuronal oxidative metabolism followed by astrocytic glycolysis. *Science* 305(5680)**,** 99-103. doi: 10.1126/science.1096485.

Kass, M.A., Heuer, D.K., Higginbotham, E.J., Johnson, C.A., Keltner, J.L., Miller, J.P., et al. (2002). The Ocular Hypertension Treatment Study: a randomized trial determines that topical ocular hypotensive medication delays or prevents the onset of primary open-angle glaucoma. *Arch Ophthalmol* 120(6)**,** 701-713; discussion 829-730. doi: 10.1001/archopht.120.6.701.

Kasten, M.R., Rudy, B., and Anderson, M.P. (2007). Differential regulation of action potential firing in adult murine thalamocortical neurons by Kv3.2, Kv1, and SK potassium and N-type calcium channels. *J Physiol* 584(Pt 2)**,** 565-582. doi: 10.1113/jphysiol.2007.141135.

Kay, J.N., De la Huerta, I., Kim, I.J., Zhang, Y., Yamagata, M., Chu, M.W., et al. (2011). Retinal ganglion cells with distinct directional preferences differ in molecular identity, structure, and central projections. *J Neurosci* 31(21)**,** 7753-7762. doi: 10.1523/JNEUROSCI.0907-11.2011.

Kerr, N.M., Johnson, C.S., de Souza, C.F., Chee, K.S., Good, W.R., Green, C.R., et al. (2010). Immunolocalization of gap junction protein connexin43 (GJA1) in the human retina and optic nerve. *Invest Ophthalmol Vis Sci* 51(8)**,** 4028-4034. doi: 10.1167/iovs.09-4847.

Kerr, N.M., Johnson, C.S., Green, C.R., and Danesh-Meyer, H.V. (2011). Gap junction protein connexin43 (GJA1) in the human glaucomatous optic nerve head and retina. *J Clin Neurosci* 18(1)**,** 102-108. doi: 10.1016/j.jocn.2010.06.002.

Kerr, N.M., Johnson, C.S., Zhang, J., Eady, E.K., Green, C.R., and Danesh-Meyer, H.V. (2012). High pressure-induced retinal ischaemia reperfusion causes upregulation of gap junction protein connexin43 prior to retinal ganglion cell loss. *Exp Neurol* 234(1)**,** 144-152. doi: 10.1016/j.expneurol.2011.12.027.

Kerrigan-Baumrind, L.A., Quigley, H.A., Pease, M.E., Kerrigan, D.F., and Mitchell, R.S. (2000). Number of ganglion cells in glaucoma eyes compared with threshold visual field tests in the same persons. *Invest Ophthalmol Vis Sci* 41(3)**,** 741-748.

Kersey, J.P., and Broadway, D.C. (2006). Corticosteroid-induced glaucoma: a review of the literature. *Eye (Lond)* 20(4)**,** 407-416. doi: 10.1038/sj.eye.6701895.

Kielian, T. (2008). Glial connexins and gap junctions in CNS inflammation and disease. *J Neurochem* 106(3)**,** 1000-1016. doi: 10.1111/j.1471-4159.2008.05405.x.

Killer, H.E., and Pircher, A. (2018). Normal tension glaucoma: review of current understanding and mechanisms of the pathogenesis. *Eye (Lond)* 32(5)**,** 924-930. doi: 10.1038/s41433-018-0042-2.

Kim, D., Mouritzen, U., Larsen, B.D., and Roy, S. (2018). Inhibition of Cx43 gap junction uncoupling prevents high glucose-induced apoptosis and reduces excess cell monolayer permeability in retinal vascular endothelial cells. *Exp Eye Res* 173**,** 85-90. doi: 10.1016/j.exer.2018.05.003.

Kim, D.M., and Nimigean, C.M. (2016). Voltage-Gated Potassium Channels: A Structural Examination of Selectivity and Gating. *Cold Spring Harb Perspect Biol* 8(5). doi: 10.1101/cshperspect.a029231.

Kim, K.R., Kim, Y., Jeong, H.J., Kang, J.S., Lee, S.H., Kim, Y., et al. (2021). Impaired pattern separation in Tg2576 mice is associated with hyperexcitable dentate gyrus caused by Kv4.1 downregulation. *Mol Brain* 14(1)**,** 62. doi: 10.1186/s13041-021-00774-x.

Kocsis, J.D., Malenka, R.C., and Waxman, S.G. (1983). Effects of extracellular potassium concentration on the excitability of the parallel fibres of the rat cerebellum. *J Physiol* 334(1)**,** 225-244. doi: 10.1113/jphysiol.1983.sp014491.

Koeberle, P.D., Wang, Y., and Schlichter, L.C. (2010). Kv1.1 and Kv1.3 channels contribute to the degeneration of retinal ganglion cells after optic nerve transection in vivo. *Cell Death Differ* 17(1)**,** 134-144. doi: 10.1038/cdd.2009.113.

Kofuji, P., and Newman, E.A. (2004). Potassium buffering in the central nervous system. *Neuroscience* 129(4)**,** 1045-1056. doi: 10.1016/j.neuroscience.2004.06.008.

Kolb, H. (1997). Amacrine cells of the mammalian retina: neurocircuitry and functional roles. *Eye (Lond)* 11 (Pt 6)(6)**,** 904-923. doi: 10.1038/eye.1997.230.

Kolb, H. (2011). *Simple Anatonmy of the Retina* [Online]. Webvision: Moran Eye Institute. Available: https://webvision.med.utah.edu/book/part-i-foundations/simple-anatomy-of-the-retina/ [Accessed January 23, 2023 2023].

Kolb, H. (2012). *Inner Plexiform Layer* [Online]. Webvision: Moran Eye Institute. Available: https://webvision.med.utah.edu/book/part-ii-anatomy-and-physiology-of-the-retina/inner-plexiform-laye/ [Accessed January 23, 2023 2023].

Kolb, H. (2013). *Photoreceptors* [Online]. Webvision: Moran Eye Institute. Available: https://webvision.med.utah.edu/book/part-ii-anatomy-and-physiology-of-the-retina/photoreceptors/ [Accessed January 23, 2023 2023].
Kole, M.H., Letzkus, J.J., and Stuart, G.J. (2007). Axon initial segment Kv1 channels control axonal action potential waveform and synaptic efficacy. *Neuron* 55(4)**,** 633-647. doi: 10.1016/j.neuron.2007.07.031.
Kong, A.W., Turner, M.L., Chan, H., Stamper, R.L., Arnold, B.F., Della Santina, L., et al. (2021). Asymmetric Functional Impairment of ON and OFF Retinal Pathways in Glaucoma. *Ophthalmology Science* 1(2). doi: 10.1016/j.xops.2021.100026.
Kordeli, E., Lambert, S., and Bennett, V. (1995). AnkyrinG. A new ankyrin gene with neural-specific isoforms localized at the axonal initial segment and node of Ranvier. *J Biol Chem* 270(5)**,** 2352-2359. doi: 10.1074/jbc.270.5.2352.
Koulakoff, A., Ezan, P., and Giaume, C. (2008). Neurons control the expression of connexin 30 and connexin 43 in mouse cortical astrocytes. *Glia* 56(12)**,** 1299-1311. doi: 10.1002/glia.20698.
Koval, M., Molina, S.A., and Burt, J.M. (2014). Mix and match: investigating heteromeric and heterotypic gap junction channels in model systems and native tissues. *FEBS Lett* 588(8)**,** 1193-1204. doi: 10.1016/j.febslet.2014.02.025.
Kress, G.J., and Mennerick, S. (2009). Action potential initiation and propagation: upstream influences on neurotransmission. *Neuroscience* 158(1)**,** 211-222. doi: 10.1016/j.neuroscience.2008.03.021.
Krieger, B., Qiao, M., Rousso, D.L., Sanes, J.R., and Meister, M. (2017). Four alpha ganglion cell types in mouse retina: Function, structure, and molecular signatures. *PLoS One* 12(7)**,** e0180091. doi: 10.1371/journal.pone.0180091.
Kuchtey, J., Olson, L.M., Rinkoski, T., Mackay, E.O., Iverson, T.M., Gelatt, K.N., et al. (2011). Mapping of the disease locus and identification of ADAMTS10 as a candidate gene in a canine model of primary open angle glaucoma. *PLoS Genet* 7(2)**,** e1001306. doi: 10.1371/journal.pgen.1001306.
Kuo, C., Green, C.R., Rupenthal, I.D., and Mugisho, O.O. (2020). Connexin43 hemichannel block protects against retinal pigment epithelial cell barrier breakdown. *Acta Diabetol* 57(1)**,** 13-22. doi: 10.1007/s00592-019-01352-3.
Kuznetsov, K.I., Grygorov, O.O., Maslov, V.Y., Veselovsky, N.S., and Fedulova, S.A. (2012). Kv3 channels modulate calcium signals induced by fast firing patterns in the rat retinal ganglion cells. *Cell Calcium* 52(5)**,** 405-411. doi: 10.1016/j.ceca.2012.06.007.
Kwon, Y.H., Fingert, J.H., Kuehn, M.H., and Alward, W.L. (2009). Primary open-angle glaucoma. *N Engl J Med* 360(11)**,** 1113-1124. doi: 10.1056/NEJMra0804630.
Lafuente, M.P., Villegas-Perez, M.P., Mayor, S., Aguilera, M.E., Miralles de Imperial, J., and Vidal-Sanz, M. (2002). Neuroprotective effects of brimonidine against transient ischemia-induced retinal ganglion cell death: a dose response in vivo study. *Exp Eye Res* 74(2)**,** 181-189. doi: 10.1006/exer.2001.1122.
Lampe, P.D., and Lau, A.F. (2004). The effects of connexin phosphorylation on gap junctional communication. *Int J Biochem Cell Biol* 36(7)**,** 1171-1186. doi: 10.1016/S1357-2725(03)00264-4.
Larsen, B.R., Assentoft, M., Cotrina, M.L., Hua, S.Z., Nedergaard, M., Kaila, K., et al. (2014). Contributions of the Na(+)/K(+)-ATPase, NKCC1, and Kir4.1 to hippocampal K(+) clearance and volume responses. *Glia* 62(4)**,** 608-622. doi: 10.1002/glia.22629.
Larsen, B.R., Stoica, A., and MacAulay, N. (2016). Managing Brain Extracellular K(+) during Neuronal Activity: The Physiological Role of the Na(+)/K(+)-ATPase Subunit Isoforms. *Front Physiol* 7**,** 141. doi: 10.3389/fphys.2016.00141.
Lee, C.Y., Dallerac, G., Ezan, P., Anderova, M., and Rouach, N. (2016). Glucose Tightly Controls Morphological and Functional Properties of Astrocytes. *Front Aging Neurosci* 8**,** 82. doi: 10.3389/fnagi.2016.00082.
Leite, M.T., Sakata, L.M., and Medeiros, F.A. (2011). Managing glaucoma in developing countries. *Arq Bras Oftalmol* 74(2)**,** 83-84. doi: 10.1590/s0004-27492011000200001.

Lena, I., and Mantegazza, M. (2019). Na(V)1.2 haploinsufficiency in Scn2a knock-out mice causes an autistic-like phenotype attenuated with age. *Sci Rep* 9(1)**,** 12886. doi: 10.1038/s41598-019-49392-7.

Leske, M.C., Heijl, A., Hyman, L., Bengtsson, B., Dong, L., Yang, Z., et al. (2007). Predictors of long-term progression in the early manifest glaucoma trial. *Ophthalmology* 114(11)**,** 1965-1972. doi: 10.1016/j.ophtha.2007.03.016.

Leterrier, C. (2016). "Chapter Six - The Axon Initial Segment, 50Years Later: A Nexus for Neuronal Organization and Function," in *Current Topics in Membranes*, ed. V. Bennett. Academic Press), 185-233.

Leterrier, C. (2018). The Axon Initial Segment: An Updated Viewpoint. *J Neurosci* 38(9)**,** 2135-2145. doi: 10.1523/JNEUROSCI.1922-17.2018.

Levkovitch-Verbin, H., Quigley, H.A., Martin, K.R.G., Valenta, D., Baumrind, L.A., and Pease, M.E. (2002). Translimbal Laser Photocoagulation to the Trabecular Meshwork as a Model of Glaucoma in Rats. *Investigative Ophthalmology & Visual Science* 43(2)**,** 402-410.

Levy, L.M., Warr, O., and Attwell, D. (1998). Stoichiometry of the glial glutamate transporter GLT-1 expressed inducibly in a Chinese hamster ovary cell line selected for low endogenous Na+-dependent glutamate uptake. *J Neurosci* 18(23)**,** 9620-9628. doi: 10.1523/JNEUROSCI.18-23-09620.1998.

Li, Q., and Barres, B.A. (2018). Microglia and macrophages in brain homeostasis and disease. *Nat Rev Immunol* 18(4)**,** 225-242. doi: 10.1038/nri.2017.125.

Liao, C.K., Wang, S.M., Chen, Y.L., Wang, H.S., and Wu, J.C. (2010). Lipopolysaccharide-induced inhibition of connexin43 gap junction communication in astrocytes is mediated by downregulation of caveolin-3. *Int J Biochem Cell Biol* 42(5)**,** 762-770. doi: 10.1016/j.biocel.2010.01.016.

Libby, R.T., Anderson, M.G., Pang, I.H., Robinson, Z.H., Savinova, O.V., Cosma, I.M., et al. (2005). Inherited glaucoma in DBA/2J mice: pertinent disease features for studying the neurodegeneration. *Vis Neurosci* 22(5)**,** 637-648. doi: 10.1017/S0952523805225130.

Liddelow, S.A., Guttenplan, K.A., Clarke, L.E., Bennett, F.C., Bohlen, C.J., Schirmer, L., et al. (2017). Neurotoxic reactive astrocytes are induced by activated microglia. *Nature* 541(7638)**,** 481-487. doi: 10.1038/nature21029.

Lieberman, M.F., Shahi, A., and Green, W.R. (1978). Embolic ischemic optic neuropathy. *Am J Ophthalmol* 86(2)**,** 206-210. doi: 10.1016/s0002-9394(14)76813-8.

Lievens, J.C., Woodman, B., Mahal, A., Spasic-Boscovic, O., Samuel, D., Kerkerian-Le Goff, L., et al. (2001). Impaired glutamate uptake in the R6 Huntington's disease transgenic mice. *Neurobiol Dis* 8(5)**,** 807-821. doi: 10.1006/nbdi.2001.0430.

Lin, J.H., Weigel, H., Cotrina, M.L., Liu, S., Bueno, E., Hansen, A.J., et al. (1998). Gap-junction-mediated propagation and amplification of cell injury. *Nat Neurosci* 1(6)**,** 494-500. doi: 10.1038/2210.

Liu, G., Li, H., Cull, G., Wilsey, L., Yang, H., Reemmer, J., et al. (2021). Downregulation of Retinal Connexin 43 in GFAP-Expressing Cells Modifies Vasoreactivity Induced by Perfusion Ocular Pressure Changes. *Invest Ophthalmol Vis Sci* 62(1)**,** 26. doi: 10.1167/iovs.62.1.26.

Louie, H.H., Shome, A., Kuo, C.Y., Rupenthal, I.D., Green, C.R., and Mugisho, O.O. (2021). Connexin43 hemichannel block inhibits NLRP3 inflammasome activation in a human retinal explant model of diabetic retinopathy. *Exp Eye Res* 202**,** 108384. doi: 10.1016/j.exer.2020.108384.

Ma, B., Buckalew, R., Du, Y., Kiyoshi, C.M., Alford, C.C., Wang, W., et al. (2016). Gap junction coupling confers isopotentiality on astrocyte syncytium. *Glia* 64(2)**,** 214-226. doi: 10.1002/glia.22924.

Ma, M., and Koester, J. (1996). The role of K+ currents in frequency-dependent spike broadening in Aplysia R20 neurons: a dynamic-clamp analysis. *J Neurosci* 16(13)**,** 4089-4101. doi: 10.1523/JNEUROSCI.16-13-04089.1996.

Macharadze, T., Goldschmidt, J., Marunde, M., Wanger, T., Scheich, H., Zuschratter, W., et al. (2009). Interretinal transduction of injury signals after unilateral optic nerve crush. *Neuroreport* 20(3)**,** 301-305. doi: 10.1097/WNR.0b013e32832027e6.

Machler, P., Wyss, M.T., Elsayed, M., Stobart, J., Gutierrez, R., von Faber-Castell, A., et al. (2016). In Vivo Evidence for a Lactate Gradient from Astrocytes to Neurons. *Cell Metab* 23(1)**,** 94-102. doi: 10.1016/j.cmet.2015.10.010.

Mahmoud, S., Gharagozloo, M., Simard, C., and Gris, D. 2019. Astrocytes Maintain Glutamate Homeostasis in the CNS by Controlling the Balance between Glutamate Uptake and Release. *Cells* [Online], 8(2).

Malone, P., Miao, H., Parker, A., Juarez, S., and Hernandez, M.R. (2007). Pressure induces loss of gap junction communication and redistribution of connexin 43 in astrocytes. *Glia* 55(10)**,** 1085-1098. doi: 10.1002/glia.20527.

Mao, Y., Nguyen, T., Tonkin, R.S., Lees, J.G., Warren, C., O'Carroll, S.J., et al. (2017). Characterisation of Peptide5 systemic administration for treating traumatic spinal cord injured rats. *Exp Brain Res* 235(10)**,** 3033-3048. doi: 10.1007/s00221-017-5023-3.

Margolis, D.J., and Detwiler, P.B. (2007). Different mechanisms generate maintained activity in ON and OFF retinal ganglion cells. *J Neurosci* 27(22)**,** 5994-6005. doi: 10.1523/JNEUROSCI.0130-07.2007.

Margolis, D.J., Gartland, A.J., Euler, T., and Detwiler, P.B. (2010). Dendritic calcium signaling in ON and OFF mouse retinal ganglion cells. *The Journal of neuroscience : the official journal of the Society for Neuroscience* 30(21)**,** 7127-7138. doi: 10.1523/JNEUROSCI.5694-09.2010.

Marin, M.A., Ziburkus, J., Jankowsky, J., and Rasband, M.N. (2016). Amyloid-beta plaques disrupt axon initial segments. *Exp Neurol* 281**,** 93-98. doi: 10.1016/j.expneurol.2016.04.018.

Marion, C.M., Radomski, K.L., Cramer, N.P., Galdzicki, Z., and Armstrong, R.C. (2018). Experimental Traumatic Brain Injury Identifies Distinct Early and Late Phase Axonal Conduction Deficits of White Matter Pathophysiology, and Reveals Intervening Recovery. *J Neurosci* 38(41)**,** 8723-8736. doi: 10.1523/jneurosci.0819-18.2018.

Markram, H., Lubke, J., Frotscher, M., and Sakmann, B. (1997). Regulation of synaptic efficacy by coincidence of postsynaptic APs and EPSPs. *Science* 275(5297)**,** 213-215. doi: 10.1126/science.275.5297.213.

Mattson, M.P. (2007). Calcium and neurodegeneration. *Aging Cell* 6(3)**,** 337-350. doi: 10.1111/j.1474-9726.2007.00275.x.

May, C.A., and Lutjen-Drecoll, E. (2002). Morphology of the murine optic nerve. *Invest Ophthalmol Vis Sci* 43(7)**,** 2206-2212.

McGrady, N.R., Holden, J.M., Ribeiro, M., Boal, A.M., Risner, M.L., and Calkins, D.J. (2022). Axon hyperexcitability in the contralateral projection following unilateral optic nerve crush in mice. *Brain Commun* 4(5)**,** fcac251. doi: 10.1093/braincomms/fcac251.

McGrady, N.R., Pasini, S., Baratta, R.O., Del Buono, B.J., Schlumpf, E., and Calkins, D.J. (2021). Restoring the Extracellular Matrix: A Neuroprotective Role for Collagen Mimetic Peptides in Experimental Glaucoma. *Front Pharmacol* 12**,** 764709. doi: 10.3389/fphar.2021.764709.

McGrady, N.R., Risner, M.L., Vest, V., and Calkins, D.J. (2020). TRPV1 Tunes Optic Nerve Axon Excitability in Glaucoma. *Front Physiol* 11**,** 249. doi: 10.3389/fphys.2020.00249.

Merayo-Lloves, J., Power, W.J., Rodriguez, A., Pedroza-Seres, M., and Foster, C.S. (1999). Secondary glaucoma in patients with uveitis. *Ophthalmologica* 213(5)**,** 300-304. doi: 10.1159/000027443.

Meunier, C., Wang, N., Yi, C., Dallerac, G., Ezan, P., Koulakoff, A., et al. (2017). Contribution of Astroglial Cx43 Hemichannels to the Modulation of Glutamatergic Currents by D-Serine in the Mouse Prefrontal Cortex. *J Neurosci* 37(37)**,** 9064-9075. doi: 10.1523/JNEUROSCI.2204-16.2017.

Miller, K.E., and Sheetz, M.P. (2004). Axonal mitochondrial transport and potential are correlated. *J Cell Sci* 117(Pt 13)**,** 2791-2804. doi: 10.1242/jcs.01130.

Miller, S.J. (2018). Astrocyte Heterogeneity in the Adult Central Nervous System. *Front Cell Neurosci* 12**,** 401. doi: 10.3389/fncel.2018.00401.
Mitra, P., and Miller, R.F. (2007a). Mechanism underlying rebound excitation in retinal ganglion cells. *Vis Neurosci* 24(5)**,** 709-731. doi: 10.1017/S0952523807070654.
Mitra, P., and Miller, R.F. (2007b). Normal and rebound impulse firing in retinal ganglion cells. *Vis Neurosci* 24(1)**,** 79-90. doi: 10.1017/S0952523807070101.
Mojumder, D.K., Frishman, L.J., Otteson, D.C., and Sherry, D.M. (2007). Voltage-gated sodium channel alpha-subunits Na(v)1.1, Na(v)1.2, and Na(v)1.6 in the distal mammalian retina. *Mol Vis* 13**,** 2163-2182.
Monemi, S., Spaeth, G., DaSilva, A., Popinchalk, S., Ilitchev, E., Liebmann, J., et al. (2005). Identification of a novel adult-onset primary open-angle glaucoma (POAG) gene on 5q22.1. *Hum Mol Genet* 14(6)**,** 725-733. doi: 10.1093/hmg/ddi068.
Mongeon, R., Venkatachalam, V., and Yellen, G. (2016). Cytosolic NADH-NAD(+) Redox Visualized in Brain Slices by Two-Photon Fluorescence Lifetime Biosensor Imaging. *Antioxid Redox Signal* 25(10)**,** 553-563. doi: 10.1089/ars.2015.6593.
Moretto, E., Stuart, S., Surana, S., Vargas, J.N.S., and Schiavo, G. (2022). The Role of Extracellular Matrix Components in the Spreading of Pathological Protein Aggregates. *Front Cell Neurosci* 16**,** 844211. doi: 10.3389/fncel.2022.844211.
Morgan, J.E. (2000). Optic nerve head structure in glaucoma: astrocytes as mediators of axonal damage. *Eye (Lond)* 14 (Pt 3B)(3)**,** 437-444. doi: 10.1038/eye.2000.128.
Morrison, J.C., Cepurna Ying Guo, W.O., and Johnson, E.C. (2011). Pathophysiology of human glaucomatous optic nerve damage: insights from rodent models of glaucoma. *Exp Eye Res* 93(2)**,** 156-164. doi: 10.1016/j.exer.2010.08.005.
Morrison, J.C., Moore, C.G., Deppmeier, L.M., Gold, B.G., Meshul, C.K., and Johnson, E.C. (1997). A rat model of chronic pressure-induced optic nerve damage. *Exp Eye Res* 64(1)**,** 85-96. doi: 10.1006/exer.1996.0184.
Moyer, V.A., and Force, U.S.P.S.T. (2013). Screening for glaucoma: U.S. Preventive Services Task Force Recommendation Statement. *Ann Intern Med* 159(7)**,** 484-489. doi: 10.7326/0003-4819-159-6-201309170-00686.
Munoz, M.F., Puebla, M., and Figueroa, X.F. (2015). Control of the neurovascular coupling by nitric oxide-dependent regulation of astrocytic Ca(2+) signaling. *Front Cell Neurosci* 9**,** 59. doi: 10.3389/fncel.2015.00059.
Murphy-Royal, C., Dupuis, J., Groc, L., and Oliet, S.H.R. (2017). Astroglial glutamate transporters in the brain: Regulating neurotransmitter homeostasis and synaptic transmission. *J Neurosci Res* 95(11)**,** 2140-2151. doi: 10.1002/jnr.24029.
Murphy-Royal, C., Johnston, A.D., Boyce, A.K.J., Diaz-Castro, B., Institoris, A., Peringod, G., et al. (2020). Stress gates an astrocytic energy reservoir to impair synaptic plasticity. *Nat Commun* 11(1)**,** 2014. doi: 10.1038/s41467-020-15778-9.
Naguib, S., Backstrom, J.R., Gil, M., Calkins, D.J., and Rex, T.S. (2021). Retinal oxidative stress activates the NRF2/ARE pathway: An early endogenous protective response to ocular hypertension. *Redox Biol* 42**,** 101883. doi: 10.1016/j.redox.2021.101883.
Nagy, J.I., Patel, D., Ochalski, P.A., and Stelmack, G.L. (1999). Connexin30 in rodent, cat and human brain: selective expression in gray matter astrocytes, co-localization with connexin43 at gap junctions and late developmental appearance. *Neuroscience* 88(2)**,** 447-468. doi: 10.1016/s0306-4522(98)00191-2.
Nakajima, Y., Iwakabe, H., Akazawa, C., Nawa, H., Shigemoto, R., Mizuno, N., et al. (1993). Molecular characterization of a novel retinal metabotropic glutamate receptor mGluR6 with a high agonist selectivity for L-2-amino-4-phosphonobutyrate. *J Biol Chem* 268(16)**,** 11868-11873. doi: https://doi.org/10.1016/S0021-9258(19)50280-0.
Nam, M.H., Stankowska, D.L., Johnson, G.A., Nahomi, R.B., Pantcheva, M.B., and Nagaraj, R.H. (2022). Peptains block retinal ganglion cell death in animal models of ocular hypertension:

implications for neuroprotection in glaucoma. *Cell Death Dis* 13(11)**,** 958. doi: 10.1038/s41419-022-05407-2.
Namba, T., Kibe, Y., Funahashi, Y., Nakamuta, S., Takano, T., Ueno, T., et al. (2014). Pioneering axons regulate neuronal polarization in the developing cerebral cortex. *Neuron* 81(4)**,** 814-829. doi: 10.1016/j.neuron.2013.12.015.
Neher, E. (1992). Ion channels for communication between and within cells. *Science* 256(5056)**,** 498-502. doi: 10.1126/science.1373906.
Neishabouri, A.M., and Faisal, A.A. (2011). The metabolic efficiency of myelinated vs unmyelinated axons. *BMC Neuroscience* 12(S1)**,** P100. doi: 10.1186/1471-2202-12-s1-p100.
Nelson, R. (2007). *Ganglion Cell Physiology* [Online]. Webvision: Moran Eye Institute. Available: https://webvision.med.utah.edu/book/part-ii-anatomy-and-physiology-of-the-retina/ganglion-cell-physiology/ [Accessed January 24, 2023 2023].
Neveu, M.M., and Jeffery, G. (2007). Chiasm formation in man is fundamentally different from that in the mouse. *Eye (Lond)* 21(10)**,** 1264-1270. doi: 10.1038/sj.eye.6702839.
Newman, E.A. (2004). Glial modulation of synaptic transmission in the retina. *Glia* 47(3)**,** 268-274. doi: 10.1002/glia.20030.
Newman, E.A. (2015). Glial cell regulation of neuronal activity and blood flow in the retina by release of gliotransmitters. *Philos Trans R Soc Lond B Biol Sci* 370(1672). doi: 10.1098/rstb.2014.0195.
Newman, E.A., Frambach, D.A., and Odette, L.L. (1984). Control of extracellular potassium levels by retinal glial cell K+ siphoning. *Science* 225(4667)**,** 1174-1175. doi: 10.1126/science.6474173.
Nicholls, D.G. (2004). Mitochondrial dysfunction and glutamate excitotoxicity studied in primary neuronal cultures. *Curr Mol Med* 4(2)**,** 149-177. doi: 10.2174/1566524043479239.
Nickells, R.W., Howell, G.R., Soto, I., and John, S.W. (2012). Under pressure: cellular and molecular responses during glaucoma, a common neurodegeneration with axonopathy. *Annu Rev Neurosci* 35(1)**,** 153-179. doi: 10.1146/annurev.neuro.051508.135728.
Noristani, R., Kuehn, S., Stute, G., Reinehr, S., Stellbogen, M., Dick, H.B., et al. (2016). Retinal and Optic Nerve Damage is Associated with Early Glial Responses in an Experimental Autoimmune Glaucoma Model. *J Mol Neurosci* 58(4)**,** 470-482. doi: 10.1007/s12031-015-0707-2.
Nwaobi, S.E., Cuddapah, V.A., Patterson, K.C., Randolph, A.C., and Olsen, M.L. (2016). The role of glial-specific Kir4.1 in normal and pathological states of the CNS. *Acta Neuropathol* 132(1)**,** 1-21. doi: 10.1007/s00401-016-1553-1.
Odette, L.L., and Newman, E.A. (1988). Model of potassium dynamics in the central nervous system. *Glia* 1(3)**,** 198-210. doi: 10.1002/glia.440010305.
Orthmann-Murphy, J.L., Freidin, M., Fischer, E., Scherer, S.S., and Abrams, C.K. (2007). Two distinct heterotypic channels mediate gap junction coupling between astrocyte and oligodendrocyte connexins. *J Neurosci* 27(51)**,** 13949-13957. doi: 10.1523/JNEUROSCI.3395-07.2007.
Osborne, B., and Balcer, L.J. (2021). "Optic neuropathies," ed. P.W. Brazis. (UpToDate: Wolters Kluwer).
Ou, Y., Jo, R.E., Ullian, E.M., Wong, R.O., and Della Santina, L. (2016). Selective Vulnerability of Specific Retinal Ganglion Cell Types and Synapses after Transient Ocular Hypertension. *J Neurosci* 36(35)**,** 9240-9252. doi: 10.1523/JNEUROSCI.0940-16.2016.
Pacholko, A.G., Wotton, C.A., and Bekar, L.K. (2020). Astrocytes-The Ultimate Effectors of Long-Range Neuromodulatory Networks? *Front Cell Neurosci* 14**,** 581075. doi: 10.3389/fncel.2020.581075.
Palop, J.J., and Mucke, L. (2016). Network abnormalities and interneuron dysfunction in Alzheimer disease. *Nat Rev Neurosci* 17(12)**,** 777-792. doi: 10.1038/nrn.2016.141.
Panagis, L., Thanos, S., Fischer, D., and Dermon, C.R. (2005). Unilateral optic nerve crush induces bilateral retinal glial cell proliferation. *Eur J Neurosci* 21(8)**,** 2305-2309. doi: 10.1111/j.1460-9568.2005.04046.x.
Pang, I.H., and Clark, A.F. (2020). Inducible rodent models of glaucoma. *Prog Retin Eye Res* 75**,** 100799. doi: 10.1016/j.preteyeres.2019.100799.

Pang, J.J., Gao, F., and Wu, S.M. (2003). Light-evoked excitatory and inhibitory synaptic inputs to ON and OFF alpha ganglion cells in the mouse retina. *J Neurosci* 23(14)**,** 6063-6073.

Pannasch, U., Vargova, L., Reingruber, J., Ezan, P., Holcman, D., Giaume, C., et al. (2011). Astroglial networks scale synaptic activity and plasticity. *Proc Natl Acad Sci U S A* 108(20)**,** 8467-8472. doi: 10.1073/pnas.1016650108.

Patel, A.K., Broyer, R.M., Lee, C.D., Lu, T., Louie, M.J., La Torre, A., et al. (2020). Inhibition of GCK-IV kinases dissociates cell death and axon regeneration in CNS neurons. *Proc Natl Acad Sci U S A* 117(52)**,** 33597-33607. doi: 10.1073/pnas.2004683117.

Peichl, L., Ott, H., and Boycott, B.B. (1987). Alpha ganglion cells in mammalian retinae. *Proc R Soc Lond B Biol Sci* 231(1263)**,** 169-197. doi: 10.1098/rspb.1987.0040.

Pellerin, L., and Magistretti, P.J. (1994). Glutamate uptake into astrocytes stimulates aerobic glycolysis: a mechanism coupling neuronal activity to glucose utilization. *Proc Natl Acad Sci U S A* 91(22)**,** 10625-10629. doi: 10.1073/pnas.91.22.10625.

Perez De Sevilla Muller, L., Shelley, J., and Weiler, R. (2007). Displaced amacrine cells of the mouse retina. *J Comp Neurol* 505(2)**,** 177-189. doi: 10.1002/cne.21487.

Petzold, A., Wattjes, M.P., Costello, F., Flores-Rivera, J., Fraser, C.L., Fujihara, K., et al. (2014). The investigation of acute optic neuritis: a review and proposed protocol. *Nat Rev Neurol* 10(8)**,** 447-458. doi: 10.1038/nrneurol.2014.108.

Pillow, J.W., Paninski, L., Uzzell, V.J., Simoncelli, E.P., and Chichilnisky, E.J. (2005). Prediction and decoding of retinal ganglion cell responses with a probabilistic spiking model. *J Neurosci* 25(47)**,** 11003-11013. doi: 10.1523/JNEUROSCI.3305-05.2005.

Pinton, P., Giorgi, C., Siviero, R., Zecchini, E., and Rizzuto, R. (2008). Calcium and apoptosis: ER-mitochondria Ca2+ transfer in the control of apoptosis. *Oncogene* 27(50)**,** 6407-6418. doi: 10.1038/onc.2008.308.

Plateroti, P., Plateroti, A.M., Abdolrahimzadeh, S., and Scuderi, G. (2015). Pseudoexfoliation Syndrome and Pseudoexfoliation Glaucoma: A Review of the Literature with Updates on Surgical Management. *J Ophthalmol* 2015**,** 370371. doi: 10.1155/2015/370371.

Price, D.A., Harris, A., Siesky, B., and Mathew, S. (2020a). The Influence of Translaminar Pressure Gradient and Intracranial Pressure in Glaucoma: A Review. *J Glaucoma* 29(2)**,** 141-146. doi: 10.1097/IJG.0000000000001421.

Price, G.W., Chadjichristos, C.E., Kavvadas, P., Tang, S.C.W., Yiu, W.H., Green, C.R., et al. (2020b). Blocking Connexin-43 mediated hemichannel activity protects against early tubular injury in experimental chronic kidney disease. *Cell Commun Signal* 18(1)**,** 79. doi: 10.1186/s12964-020-00558-1.

Provis, J.M., Diaz, C.M., and Penfold, P.L. (1996). Microglia in human retina: a heterogeneous population with distinct ontogenies. *Perspect Dev Neurobiol* 3(3)**,** 213-222.

Quigley, H.A., Addicks, E.M., Green, W.R., and Maumenee, A.E. (1981). Optic nerve damage in human glaucoma. II. The site of injury and susceptibility to damage. *Arch Ophthalmol* 99(4)**,** 635-649. doi: 10.1001/archopht.1981.03930010635009.

Quigley, H.A., Katz, J., Derick, R.J., Gilbert, D., and Sommer, A. (1992). An evaluation of optic disc and nerve fiber layer examinations in monitoring progression of early glaucoma damage. *Ophthalmology* 99(1)**,** 19-28. doi: 10.1016/s0161-6420(92)32018-4.

Quist, A.P., Rhee, S.K., Lin, H., and Lal, R. (2000). Physiological role of gap-junctional hemichannels. Extracellular calcium-dependent isosmotic volume regulation. *J Cell Biol* 148(5)**,** 1063-1074. doi: 10.1083/jcb.148.5.1063.

Raghuram, V., Werginz, P., and Fried, S.I. (2019). Scaling of the AIS and Somatodendritic Compartments in alpha S RGCs. *Front Cell Neurosci* 13**,** 436. doi: 10.3389/fncel.2019.00436.

Rahman, M.M., and Lendel, C. (2021). Extracellular protein components of amyloid plaques and their roles in Alzheimer's disease pathology. *Mol Neurodegener* 16(1)**,** 59. doi: 10.1186/s13024-021-00465-0.

Rasband, M.N. (2010). The axon initial segment and the maintenance of neuronal polarity. *Nat Rev Neurosci* 11(8)**,** 552-562. doi: 10.1038/nrn2852.
Rasband, M.N., and Peles, E. (2015). The Nodes of Ranvier: Molecular Assembly and Maintenance. *Cold Spring Harb Perspect Biol* 8(3)**,** a020495. doi: 10.1101/cshperspect.a020495.
Reichenbach, A., and Bringmann, A. (2020). Glia of the human retina. *Glia* 68(4)**,** 768-796. doi: 10.1002/glia.23727.
Retamal, M.A., Froger, N., Palacios-Prado, N., Ezan, P., Saez, P.J., Saez, J.C., et al. (2007). Cx43 hemichannels and gap junction channels in astrocytes are regulated oppositely by proinflammatory cytokines released from activated microglia. *J Neurosci* 27(50)**,** 13781-13792. doi: 10.1523/JNEUROSCI.2042-07.2007.
Rezaie, T., Child, A., Hitchings, R., Brice, G., Miller, L., Coca-Prados, M., et al. (2002). Adult-onset primary open-angle glaucoma caused by mutations in optineurin. *Science* 295(5557)**,** 1077-1079. doi: 10.1126/science.1066901.
Risner, M.L., McGrady, N.R., Boal, A.M., Pasini, S., and Calkins, D.J. (2020a). TRPV1 Supports Axogenic Enhanced Excitability in Response to Neurodegenerative Stress. *Front Cell Neurosci* 14**,** 603419. doi: 10.3389/fncel.2020.603419.
Risner, M.L., McGrady, N.R., Pasini, S., Lambert, W.S., and Calkins, D.J. (2020b). Elevated ocular pressure reduces voltage-gated sodium channel NaV1.2 protein expression in retinal ganglion cell axons. *Exp Eye Res* 190**,** 107873. doi: 10.1016/j.exer.2019.107873.
Risner, M.L., Pasini, S., Chamling, X., McGrady, N.R., Goldberg, J.L., Zack, D.J., et al. (2021a). Intrinsic Morphologic and Physiologic Development of Human Derived Retinal Ganglion Cells In Vitro. *Transl Vis Sci Technol* 10(10)**,** 1. doi: 10.1167/tvst.10.10.1.
Risner, M.L., Pasini, S., Cooper, M.L., Lambert, W.S., and Calkins, D.J. (2018). Axogenic mechanism enhances retinal ganglion cell excitability during early progression in glaucoma. *Proc Natl Acad Sci U S A* 115(10)**,** E2393-E2402. doi: 10.1073/pnas.1714888115.
Risner, M.L., Pasini, S., McGrady, N.R., and Calkins, D.J. (2022). Bax Contributes to Retinal Ganglion Cell Dendritic Degeneration During Glaucoma. *Mol Neurobiol* 59(3)**,** 1366-1380. doi: 10.1007/s12035-021-02675-5.
Risner, M.L., Pasini, S., McGrady, N.R., D'Alessandro, K.B., Yao, V., Cooper, M.L., et al. (2021b). Neuroprotection by Wld(S) depends on retinal ganglion cell type and age in glaucoma. *Mol Neurodegener* 16(1)**,** 36. doi: 10.1186/s13024-021-00459-y.
Rockhill, R.L., Euler, T., and Masland, R.H. (2000). Spatial order within but not between types of retinal neurons. *Proc Natl Acad Sci U S A* 97(5)**,** 2303-2307. doi: 10.1073/pnas.030413497.
Rodriguez, A.R., de Sevilla Müller, L.P., and Brecha, N.C. (2014). The RNA binding protein RBPMS is a selective marker of ganglion cells in the mammalian retina. *The Journal of comparative neurology* 522(6)**,** 1411-1443. doi: 10.1002/cne.23521.
Rotchford, A.P., Kirwan, J.F., Muller, M.A., Johnson, G.J., and Roux, P. (2003). Temba glaucoma study: a population-based cross-sectional survey in urban South Africa. *Ophthalmology* 110(2)**,** 376-382. doi: 10.1016/S0161-6420(02)01568-3.
Rothstein, J.D., Dykes-Hoberg, M., Pardo, C.A., Bristol, L.A., Jin, L., Kuncl, R.W., et al. (1996). Knockout of glutamate transporters reveals a major role for astroglial transport in excitotoxicity and clearance of glutamate. *Neuron* 16(3)**,** 675-686. doi: 10.1016/s0896-6273(00)80086-0.
Rotterman, T.M., Carrasco, D.I., Housley, S.N., Nardelli, P., Powers, R.K., and Cope, T.C. (2021). Axon initial segment geometry in relation to motoneuron excitability. *PLoS One* 16(11)**,** e0259918. doi: 10.1371/journal.pone.0259918.
Rouach, N., Glowinski, J., and Giaume, C. (2000). Activity-dependent neuronal control of gap-junctional communication in astrocytes. *J Cell Biol* 149(7)**,** 1513-1526. doi: 10.1083/jcb.149.7.1513.
Rouach, N., Koulakoff, A., Abudara, V., Willecke, K., and Giaume, C. (2008). Astroglial metabolic networks sustain hippocampal synaptic transmission. *Science* 322(5907)**,** 1551-1555. doi: 10.1126/science.1164022.

Roy Chowdhury, U., Hann, C.R., Stamer, W.D., and Fautsch, M.P. (2015). Aqueous humor outflow: dynamics and disease. *Invest Ophthalmol Vis Sci* 56(5)**,** 2993-3003. doi: 10.1167/iovs.15-16744.

Rush, A.M., Dib-Hajj, S.D., and Waxman, S.G. (2005). Electrophysiological properties of two axonal sodium channels, Nav1.2 and Nav1.6, expressed in mouse spinal sensory neurones. *J Physiol* 564(Pt 3)**,** 803-815. doi: 10.1113/jphysiol.2005.083089.

Sabo, S.L., and McAllister, A.K. (2003). Mobility and cycling of synaptic protein–containing vesicles in axonal growth cone filopodia. *Nature Neuroscience* 6(12)**,** 1264-1269. doi: 10.1038/nn1149.

Sah, P., and Faber, E.S. (2002). Channels underlying neuronal calcium-activated potassium currents. *Prog Neurobiol* 66(5)**,** 345-353. doi: 10.1016/s0301-0082(02)00004-7.

Samsel, P.A., Kisiswa, L., Erichsen, J.T., Cross, S.D., and Morgan, J.E. (2011). A novel method for the induction of experimental glaucoma using magnetic microspheres. *Invest Ophthalmol Vis Sci* 52(3)**,** 1671-1675. doi: 10.1167/iovs.09-3921.

Sanes, J.R., and Masland, R.H. (2015). The types of retinal ganglion cells: current status and implications for neuronal classification. *Annu Rev Neurosci* 38(1)**,** 221-246. doi: 10.1146/annurev-neuro-071714-034120.

Sappington, R.M., Carlson, B.J., Crish, S.D., and Calkins, D.J. (2010). The microbead occlusion model: a paradigm for induced ocular hypertension in rats and mice. *Invest Ophthalmol Vis Sci* 51(1)**,** 207-216. doi: 10.1167/iovs.09-3947.

Sathyamangalam, R.V., Paul, P.G., George, R., Baskaran, M., Hemamalini, A., Madan, R.V., et al. (2009). Determinants of glaucoma awareness and knowledge in urban Chennai. *Indian J Ophthalmol* 57(5)**,** 355-360. doi: 10.4103/0301-4738.55073.

Saxena, S., and Caroni, P. (2011). Selective neuronal vulnerability in neurodegenerative diseases: from stressor thresholds to degeneration. *Neuron* 71(1)**,** 35-48. doi: 10.1016/j.neuron.2011.06.031.

Schluter, A., Rossberger, S., Dannehl, D., Janssen, J.M., Vorwald, S., Hanne, J., et al. (2019). Dynamic Regulation of Synaptopodin and the Axon Initial Segment in Retinal Ganglion Cells During Postnatal Development. *Front Cell Neurosci* 13**,** 318. doi: 10.3389/fncel.2019.00318.

Schmidt, T.M., Alam, N.M., Chen, S., Kofuji, P., Li, W., Prusky, G.T., et al. (2014). A role for melanopsin in alpha retinal ganglion cells and contrast detection. *Neuron* 82(4)**,** 781-788. doi: 10.1016/j.neuron.2014.03.022.

Schmidt, T.M., Chen, S.K., and Hattar, S. (2011a). Intrinsically photosensitive retinal ganglion cells: many subtypes, diverse functions. *Trends Neurosci* 34(11)**,** 572-580. doi: 10.1016/j.tins.2011.07.001.

Schmidt, T.M., Do, M.T., Dacey, D., Lucas, R., Hattar, S., and Matynia, A. (2011b). Melanopsin-positive intrinsically photosensitive retinal ganglion cells: from form to function. *J Neurosci* 31(45)**,** 16094-16101. doi: 10.1523/JNEUROSCI.4132-11.2011.

Schwab, I.R. (2018). The evolution of eyes: major steps. The Keeler lecture 2017: centenary of Keeler Ltd. *Eye (Lond)* 32(2)**,** 302-313. doi: 10.1038/eye.2017.226.

Scuderi, G., Contestabile, M.T., Scuderi, L., Librando, A., Fenicia, V., and Rahimi, S. (2019). Pigment dispersion syndrome and pigmentary glaucoma: a review and update. *Int Ophthalmol* 39(7)**,** 1651-1662. doi: 10.1007/s10792-018-0938-7.

Segal, M. (2018). Calcium stores regulate excitability in cultured rat hippocampal neurons. *J Neurophysiol* 120(5)**,** 2694-2705. doi: 10.1152/jn.00447.2018.

Shekhar, K., and Sanes, J.R. (2021). Generating and Using Transcriptomically Based Retinal Cell Atlases. *Annu Rev Vis Sci* 7(1)**,** 43-72. doi: 10.1146/annurev-vision-032621-075200.

Shrivastava, A.N., Redeker, V., Fritz, N., Pieri, L., Almeida, L.G., Spolidoro, M., et al. (2015). α-synuclein assemblies sequester neuronal α3-Na+/K+-ATP ase and impair Na+ gradient. *The EMBO journal* 34(19)**,** 2408-2423.

Siskova, Z., Justus, D., Kaneko, H., Friedrichs, D., Henneberg, N., Beutel, T., et al. (2014). Dendritic structural degeneration is functionally linked to cellular hyperexcitability in a mouse model of Alzheimer's disease. *Neuron* 84(5)**,** 1023-1033. doi: 10.1016/j.neuron.2014.10.024.

Skarie, J.M., and Link, B.A. (2008). The primary open-angle glaucoma gene WDR36 functions in ribosomal RNA processing and interacts with the p53 stress-response pathway. *Hum Mol Genet* 17(16)**,** 2474-2485. doi: 10.1093/hmg/ddn147.
Skou, J.C. (1957). The influence of some cations on an adenosine triphosphatase from peripheral nerves. *Biochim Biophys Acta* 23(2)**,** 394-401. doi: 10.1016/0006-3002(57)90343-8.
Sladek, A.L., and Nawy, S. (2020). Ocular Hypertension Drives Remodeling of AMPA Receptors in Select Populations of Retinal Ganglion Cells. *Front Synaptic Neurosci* 12**,** 30. doi: 10.3389/fnsyn.2020.00030.
Slaughter, M.M., and Miller, R.F. (1983). An excitatory amino acid antagonist blocks cone input to sign-conserving second-order retinal neurons. *Science* 219(4589)**,** 1230-1232. doi: 10.1126/science.6131536.
Sluch, V.M., Chamling, X., Liu, M.M., Berlinicke, C.A., Cheng, J., Mitchell, K.L., et al. (2017). Enhanced Stem Cell Differentiation and Immunopurification of Genome Engineered Human Retinal Ganglion Cells. *Stem cells translational medicine* 6(11)**,** 1972-1986. doi: 10.1002/sctm.17-0059.
Sluch, V.M., Davis, C.H., Ranganathan, V., Kerr, J.M., Krick, K., Martin, R., et al. (2015). Differentiation of human ESCs to retinal ganglion cells using a CRISPR engineered reporter cell line. *Sci Rep* 5(1)**,** 16595. doi: 10.1038/srep16595.
Sobrado-Calvo, P., Vidal-Sanz, M., and Villegas-Perez, M.P. (2007). Rat retinal microglial cells under normal conditions, after optic nerve section, and after optic nerve section and intravitreal injection of trophic factors or macrophage inhibitory factor. *J Comp Neurol* 501(6)**,** 866-878. doi: 10.1002/cne.21279.
Sofroniew, M.V. (2015). Astrocyte barriers to neurotoxic inflammation. *Nat Rev Neurosci* 16(5)**,** 249-263. doi: 10.1038/nrn3898.
Sohl, G., Maxeiner, S., and Willecke, K. (2005). Expression and functions of neuronal gap junctions. *Nat Rev Neurosci* 6(3)**,** 191-200. doi: 10.1038/nrn1627.
Sohn, P.D., Huang, C.T., Yan, R., Fan, L., Tracy, T.E., Camargo, C.M., et al. (2019). Pathogenic Tau Impairs Axon Initial Segment Plasticity and Excitability Homeostasis. *Neuron* 104(3)**,** 458-470 e455. doi: 10.1016/j.neuron.2019.08.008.
Sompol, P., Furman, J.L., Pleiss, M.M., Kraner, S.D., Artiushin, I.A., Batten, S.R., et al. (2017). Calcineurin/NFAT Signaling in Activated Astrocytes Drives Network Hyperexcitability in Abeta-Bearing Mice. *J Neurosci* 37(25)**,** 6132-6148. doi: 10.1523/JNEUROSCI.0877-17.2017.
Spruston, N. (2008). Pyramidal neurons: dendritic structure and synaptic integration. *Nat Rev Neurosci* 9(3)**,** 206-221. doi: 10.1038/nrn2286.
Stein, J.D., Khawaja, A.P., and Weizer, J.S. (2021). Glaucoma in Adults-Screening, Diagnosis, and Management: A Review. *JAMA* 325(2)**,** 164-174. doi: 10.1001/jama.2020.21899.
Stirling, D.P., and Stys, P.K. (2010). Mechanisms of axonal injury: internodal nanocomplexes and calcium deregulation. *Trends Mol Med* 16(4)**,** 160-170. doi: 10.1016/j.molmed.2010.02.002.
Stone, E.M., Fingert, J.H., Alward, W.L., Nguyen, T.D., Polansky, J.R., Sunden, S.L., et al. (1997). Identification of a gene that causes primary open angle glaucoma. *Science* 275(5300)**,** 668-670. doi: 10.1126/science.275.5300.668.
Stoner, A., Harris, A., Oddone, F., Belamkar, A., Verticchio Vercellin, A.C., Shin, J., et al. (2022). Topical carbonic anhydrase inhibitors and glaucoma in 2021: where do we stand? *Br J Ophthalmol* 106(10)**,** 1332-1337. doi: 10.1136/bjophthalmol-2021-319530.
Subramaniam, M., Althof, D., Gispert, S., Schwenk, J., Auburger, G., Kulik, A., et al. (2014). Mutant alpha-synuclein enhances firing frequencies in dopamine substantia nigra neurons by oxidative impairment of A-type potassium channels. *J Neurosci* 34(41)**,** 13586-13599. doi: 10.1523/JNEUROSCI.5069-13.2014.
Suminaite, D., Lyons, D.A., and Livesey, M.R. (2019). Myelinated axon physiology and regulation of neural circuit function. *Glia* 67(11)**,** 2050-2062. doi: 10.1002/glia.23665.

Sun, D., Qu, J., and Jakobs, T.C. (2013). Reversible reactivity by optic nerve astrocytes. *Glia* 61(8)**,** 1218-1235. doi: 10.1002/glia.22507.
Sun, X., Wu, Y., Gu, M., Liu, Z., Ma, Y., Li, J., et al. (2014a). Selective filtering defect at the axon initial segment in Alzheimer's disease mouse models. *Proc Natl Acad Sci U S A* 111(39)**,** 14271-14276. doi: 10.1073/pnas.1411837111.
Sun, X., Wu, Y., Gu, M., and Zhang, Y. (2014b). miR-342-5p decreases ankyrin G levels in Alzheimer's disease transgenic mouse models. *Cell Rep* 6(2)**,** 264-270. doi: 10.1016/j.celrep.2013.12.028.
Supplie, L.M., Duking, T., Campbell, G., Diaz, F., Moraes, C.T., Gotz, M., et al. (2017). Respiration-Deficient Astrocytes Survive As Glycolytic Cells In Vivo. *J Neurosci* 37(16)**,** 4231-4242. doi: 10.1523/JNEUROSCI.0756-16.2017.
Suzuki, A., Stern, S.A., Bozdagi, O., Huntley, G.W., Walker, R.H., Magistretti, P.J., et al. (2011). Astrocyte-neuron lactate transport is required for long-term memory formation. *Cell* 144(5)**,** 810-823. doi: 10.1016/j.cell.2011.02.018.
Taylor, A.M., Blurton-Jones, M., Rhee, S.W., Cribbs, D.H., Cotman, C.W., and Jeon, N.L. (2005). A microfluidic culture platform for CNS axonal injury, regeneration and transport. *Nat Methods* 2(8)**,** 599-605. doi: 10.1038/nmeth777.
Taylor, A.M., and Jeon, N.L. (2010). Micro-scale and microfluidic devices for neurobiology. *Curr Opin Neurobiol* 20(5)**,** 640-647. doi: 10.1016/j.conb.2010.07.011.
Taylor, A.M., and Jeon, N.L. (2011). Microfluidic and compartmentalized platforms for neurobiological research. *Crit Rev Biomed Eng* 39(3)**,** 185-200. doi: 10.1615/critrevbiomedeng.v39.i3.20.
Teliska, L.H., Dalla Costa, I., Sert, O., Twiss, J.L., and Rasband, M.N. (2022). Axon initial segments are required for efficient motor neuron axon regeneration and functional recovery of synapses. *J Neurosci*. doi: 10.1523/jneurosci.1261-22.2022.
Teotia, P., Van Hook, M.J., Fischer, D., and Ahmad, I. (2019). Human retinal ganglion cell axon regeneration by recapitulating developmental mechanisms: effects of recruitment of the mTOR pathway. *Development (Cambridge, England)* 146(13)**,** dev178012. doi: 10.1242/dev.178012.
Tham, Y.C., Li, X., Wong, T.Y., Quigley, H.A., Aung, T., and Cheng, C.Y. (2014). Global prevalence of glaucoma and projections of glaucoma burden through 2040: a systematic review and meta-analysis. *Ophthalmology* 121(11)**,** 2081-2090. doi: 10.1016/j.ophtha.2014.05.013.
Theparambil, S.M., Hosford, P.S., Ruminot, I., Kopach, O., Reynolds, J.R., Sandoval, P.Y., et al. (2020). Astrocytes regulate brain extracellular pH via a neuronal activity-dependent bicarbonate shuttle. *Nat Commun* 11(1)**,** 5073. doi: 10.1038/s41467-020-18756-3.
Thome, C., Kelly, T., Yanez, A., Schultz, C., Engelhardt, M., Cambridge, S.B., et al. (2014). Axon-carrying dendrites convey privileged synaptic input in hippocampal neurons. *Neuron* 83(6)**,** 1418-1430. doi: 10.1016/j.neuron.2014.08.013.
Toft-Kehler, A.K., Skytt, D.M., and Kolko, M. (2018). A Perspective on the Muller Cell-Neuron Metabolic Partnership in the Inner Retina. *Mol Neurobiol* 55(6)**,** 5353-5361. doi: 10.1007/s12035-017-0760-7.
Tonkin, R.S., Bowles, C., Perera, C.J., Keating, B.A., Makker, P.G.S., Duffy, S.S., et al. (2018). Attenuation of mechanical pain hypersensitivity by treatment with Peptide5, a connexin-43 mimetic peptide, involves inhibition of NLRP3 inflammasome in nerve-injured mice. *Exp Neurol* 300**,** 1-12. doi: 10.1016/j.expneurol.2017.10.016.
Toris, C.B., Gabelt, B.T., and Kaufman, P.L. (2008). Update on the mechanism of action of topical prostaglandins for intraocular pressure reduction. *Surv Ophthalmol* 53 Suppl1(SUPPL1)**,** S107-120. doi: 10.1016/j.survophthal.2008.08.010.
Toris, C.B., Gleason, M.L., Camras, C.B., and Yablonski, M.E. (1995). Effects of brimonidine on aqueous humor dynamics in human eyes. *Arch Ophthalmol* 113(12)**,** 1514-1517. doi: 10.1001/archopht.1995.01100120044006.
Tout, S., Chan-Ling, T., Hollander, H., and Stone, J. (1993). The role of Muller cells in the formation of the blood-retinal barrier. *Neuroscience* 55(1)**,** 291-301. doi: 10.1016/0306-4522(93)90473-s.

Tran, N.M., Shekhar, K., Whitney, I.E., Jacobi, A., Benhar, I., Hong, G., et al. (2019). Single-Cell Profiles of Retinal Ganglion Cells Differing in Resilience to Injury Reveal Neuroprotective Genes. *Neuron* 104(6)**,** 1039-1055.e1012. doi: 10.1016/j.neuron.2019.11.006.

Trenholm, S., Johnson, K., Li, X., Smith, R.G., and Awatramani, G.B. (2011). Parallel mechanisms encode direction in the retina. *Neuron* 71(4)**,** 683-694. doi: 10.1016/j.neuron.2011.06.020.

Twig, G., Levy, H., and Perlman, I. (2003). Color opponency in horizontal cells of the vertebrate retina. *Prog Retin Eye Res* 22(1)**,** 31-68. doi: 10.1016/s1350-9462(02)00045-9.

Tworig, J.M., and Feller, M.B. (2021). Muller Glia in Retinal Development: From Specification to Circuit Integration. *Front Neural Circuits* 15**,** 815923. doi: 10.3389/fncir.2021.815923.

Twyford, P., Cai, C., and Fried, S. (2014). Differential responses to high-frequency electrical stimulation in ON and OFF retinal ganglion cells. *J Neural Eng* 11(2)**,** 025001. doi: 10.1088/1741-2560/11/2/025001.

Ueda, J., Sawaguchi, S., Hanyu, T., Yaoeda, K., Fukuchi, T., Abe, H., et al. (1998). Experimental glaucoma model in the rat induced by laser trabecular photocoagulation after an intracameral injection of India ink. *Jpn J Ophthalmol* 42(5)**,** 337-344. doi: 10.1016/s0021-5155(98)00026-4.

Uzzell, V.J., and Chichilnisky, E.J. (2004). Precision of spike trains in primate retinal ganglion cells. *J Neurophysiol* 92(2)**,** 780-789. doi: 10.1152/jn.01171.2003.

Van Hook, M.J., Monaco, C., Bierlein, E.R., and Smith, J.C. (2020). Neuronal and Synaptic Plasticity in the Visual Thalamus in Mouse Models of Glaucoma. *Front Cell Neurosci* 14**,** 626056. doi: 10.3389/fncel.2020.626056.

Van Hook, M.J., Nawy, S., and Thoreson, W.B. (2019). Voltage- and calcium-gated ion channels of neurons in the vertebrate retina. *Prog Retin Eye Res* 72**,** 100760. doi: 10.1016/j.preteyeres.2019.05.001.

Van Hook, M.J., and Thoreson, W.B. (2014). "Whole-Cell Patch-Clamp Recording," in *Current Laboratory Methods in Neuroscience Research*, eds. H. Xiong & H.E. Gendelman. (New York, NY: Springer New York), 353-367.

Van Wart, A., Boiko, T., Trimmer, J.S., and Matthews, G. (2005). Novel clustering of sodium channel Nav1. 1 with ankyrin-G and neurofascin at discrete sites in the inner plexiform layer of the retina. *Molecular and Cellular Neuroscience* 28(4)**,** 661-673.

Van Wart, A., and Matthews, G. (2006). Impaired firing and cell-specific compensation in neurons lacking nav1.6 sodium channels. *J Neurosci* 26(27)**,** 7172-7180. doi: 10.1523/jneurosci.1101-06.2006.

van Zundert, B., Peuscher, M.H., Hynynen, M., Chen, A., Neve, R.L., Brown, R.H., Jr., et al. (2008). Neonatal neuronal circuitry shows hyperexcitable disturbance in a mouse model of the adult-onset neurodegenerative disease amyotrophic lateral sclerosis. *J Neurosci* 28(43)**,** 10864-10874. doi: 10.1523/JNEUROSCI.1340-08.2008.

VanderWall, K.B., Vij, R., Ohlemacher, S.K., Sridhar, A., Fligor, C.M., Feder, E.M., et al. (2019). Astrocytes Regulate the Development and Maturation of Retinal Ganglion Cells Derived from Human Pluripotent Stem Cells. *Stem cell reports* 12(2)**,** 201-212. doi: 10.1016/j.stemcr.2018.12.010.

Vecino, E., Rodriguez, F.D., Ruzafa, N., Pereiro, X., and Sharma, S.C. (2016). Glia-neuron interactions in the mammalian retina. *Prog Retin Eye Res* 51**,** 1-40. doi: 10.1016/j.preteyeres.2015.06.003.

Virtanen, P., Gommers, R., Oliphant, T.E., Haberland, M., Reddy, T., Cournapeau, D., et al. (2020). SciPy 1.0: fundamental algorithms for scientific computing in Python. *Nat Methods* 17(3)**,** 261-272. doi: 10.1038/s41592-019-0686-2.

Vucic, S., Nicholson, G.A., and Kiernan, M.C. (2008). Cortical hyperexcitability may precede the onset of familial amyotrophic lateral sclerosis. *Brain* 131(Pt 6)**,** 1540-1550. doi: 10.1093/brain/awn071.

Wahle, P., Sobierajski, E., Gasterstadt, I., Lehmann, N., Weber, S., Lubke, J.H.R., et al. (2022). Neocortical pyramidal neurons with axons emerging from dendrites are frequent in non-primates, but rare in monkey and human. *Elife* 11**,** e76101. doi: 10.7554/eLife.76101.

Wallraff, A., Kohling, R., Heinemann, U., Theis, M., Willecke, K., and Steinhauser, C. (2006). The impact of astrocytic gap junctional coupling on potassium buffering in the hippocampus. *J Neurosci* 26(20)**,** 5438-5447. doi: 10.1523/JNEUROSCI.0037-06.2006.

Wang, F., Smith, N.A., Xu, Q., Fujita, T., Baba, A., Matsuda, T., et al. (2012). Astrocytes modulate neural network activity by Ca(2)+-dependent uptake of extracellular K+. *Sci Signal* 5(218)**,** ra26. doi: 10.1126/scisignal.2002334.

Wang, G.Y., Robinson, D.W., and Chalupa, L.M. (1998). Calcium-activated potassium conductances in retinal ganglion cells of the ferret. *J Neurophysiol* 79(1)**,** 151-158. doi: 10.1152/jn.1998.79.1.151.

Wang, J., Wang, F., Mai, D., and Qu, S. (2020). Molecular Mechanisms of Glutamate Toxicity in Parkinson's Disease. *Front Neurosci* 14**,** 585584. doi: 10.3389/fnins.2020.585584.

Wang, L., Cioffi, G.A., Cull, G., Dong, J., and Fortune, B. (2002). Immunohistologic evidence for retinal glial cell changes in human glaucoma. *Invest Ophthalmol Vis Sci* 43(4)**,** 1088-1094.

Wang, L., Dong, J., Cull, G., Fortune, B., and Cioffi, G.A. (2003). Varicosities of intraretinal ganglion cell axons in human and nonhuman primates. *Invest Ophthalmol Vis Sci* 44(1)**,** 2-9.

Ward, N.J., Ho, K.W., Lambert, W.S., Weitlauf, C., and Calkins, D.J. (2014). Absence of transient receptor potential vanilloid-1 accelerates stress-induced axonopathy in the optic projection. *J Neurosci* 34(9)**,** 3161-3170. doi: 10.1523/JNEUROSCI.4089-13.2014.

Wareham, L.K., and Calkins, D.J. (2020). The Neurovascular Unit in Glaucomatous Neurodegeneration. *Front Cell Dev Biol* 8**,** 452. doi: 10.3389/fcell.2020.00452.

Wareham, L.K., Risner, M.L., and Calkins, D.J. (2020). Protect, Repair, and Regenerate: Towards Restoring Vision in Glaucoma. *Curr Ophthalmol Rep* 8(4)**,** 301-310. doi: 10.1007/s40135-020-00259-5.

Wei, W. (2018). Neural Mechanisms of Motion Processing in the Mammalian Retina. *Annu Rev Vis Sci* 4(1)**,** 165-192. doi: 10.1146/annurev-vision-091517-034048.

Weinreb, R.N., Aung, T., and Medeiros, F.A. (2014). The pathophysiology and treatment of glaucoma: a review. *JAMA* 311(18)**,** 1901-1911. doi: 10.1001/jama.2014.3192.

Weinreb, R.N., and Khaw, P.T. (2004). Primary open-angle glaucoma. *Lancet* 363(9422)**,** 1711-1720. doi: 10.1016/S0140-6736(04)16257-0.

Welsbie, D.S., Mitchell, K.L., Jaskula-Ranga, V., Sluch, V.M., Yang, Z., Kim, J., et al. (2017). Enhanced Functional Genomic Screening Identifies Novel Mediators of Dual Leucine Zipper Kinase-Dependent Injury Signaling in Neurons. *Neuron* 94(6)**,** 1142-1154 e1146. doi: 10.1016/j.neuron.2017.06.008.

Werginz, P., Raghuram, V., and Fried, S.I. (2020). Tailoring of the axon initial segment shapes the conversion of synaptic inputs into spiking output in OFF-alpha T retinal ganglion cells. *Sci Adv* 6(37). doi: 10.1126/sciadv.abb6642.

Wetzel, R.K., Arystarkhova, E., and Sweadner, K.J. (1999). Cellular and subcellular specification of Na,K-ATPase alpha and beta isoforms in the postnatal development of mouse retina. *J Neurosci* 19(22)**,** 9878-9889. doi: 10.1523/JNEUROSCI.19-22-09878.1999.

Wienbar, S., and Schwartz, G.W. (2022). Differences in spike generation instead of synaptic inputs determine the feature selectivity of two retinal cell types. *Neuron*. doi: 10.1016/j.neuron.2022.04.012.

Williams, P.A., Tribble, J.R., Pepper, K.W., Cross, S.D., Morgan, B.P., Morgan, J.E., et al. (2016). Inhibition of the classical pathway of the complement cascade prevents early dendritic and synaptic degeneration in glaucoma. *Mol Neurodegener* 11(1)**,** 26. doi: 10.1186/s13024-016-0091-6.

Witte, H., Neukirchen, D., and Bradke, F. (2008). Microtubule stabilization specifies initial neuronal polarization. *J Cell Biol* 180(3)**,** 619-632. doi: 10.1083/jcb.200707042.

Wollner, D.A., and Catterall, W.A. (1986). Localization of sodium channels in axon hillocks and initial segments of retinal ganglion cells. *Proc Natl Acad Sci U S A* 83(21)**,** 8424-8428. doi: 10.1073/pnas.83.21.8424.

Wong, M.O., Lee, J.W., Choy, B.N., Chan, J.C., and Lai, J.S. (2015). Systematic review and meta-analysis on the efficacy of selective laser trabeculoplasty in open-angle glaucoma. *Surv Ophthalmol* 60(1)**,** 36-50. doi: 10.1016/j.survophthal.2014.06.006.

Woodward, D.F., and Gil, D.W. (2004). The inflow and outflow of anti-glaucoma drugs. *Trends Pharmacol Sci* 25(5)**,** 238-241. doi: 10.1016/j.tips.2004.03.002.

Yamada, K., and Iwatsubo, T. (2018). Extracellular alpha-synuclein levels are regulated by neuronal activity. *Mol Neurodegener* 13(1)**,** 9. doi: 10.1186/s13024-018-0241-0.

Yamada, R., and Kuba, H. (2016a). Structural and Functional Plasticity at the Axon Initial Segment. *Frontiers in Cellular Neuroscience* 10. doi: ARTN 250
10.3389/fncel.2016.00250.

Yamada, R., and Kuba, H. (2016b). Structural and Functional Plasticity at the Axon Initial Segment. *Front Cell Neurosci* 10**,** 250. doi: 10.3389/fncel.2016.00250.

Yang, C.Y., Tsai, D., Guo, T., Dokos, S., Suaning, G.J., Morley, J.W., et al. (2018). Differential electrical responses in retinal ganglion cell subtypes: effects of synaptic blockade and stimulating electrode location. *J Neural Eng* 15(4)**,** 046020. doi: 10.1088/1741-2552/aac315.

Yang, J., Weimer, R.M., Kallop, D., Olsen, O., Wu, Z., Renier, N., et al. (2013). Regulation of axon degeneration after injury and in development by the endogenous calpain inhibitor calpastatin. *Neuron* 80(5)**,** 1175-1189. doi: 10.1016/j.neuron.2013.08.034.

Yonehara, K., Shintani, T., Suzuki, R., Sakuta, H., Takeuchi, Y., Nakamura-Yonehara, K., et al. (2008). Expression of SPIG1 reveals development of a retinal ganglion cell subtype projecting to the medial terminal nucleus in the mouse. *PLoS One* 3(2)**,** e1533. doi: 10.1371/journal.pone.0001533.

You, M., Rong, R., Zeng, Z., Xia, X., and Ji, D. (2021). Transneuronal Degeneration in the Brain During Glaucoma. *Front Aging Neurosci* 13**,** 643685. doi: 10.3389/fnagi.2021.643685.

Zahs, K.R., Kofuji, P., Meier, C., and Dermietzel, R. (2003). Connexin immunoreactivity in glial cells of the rat retina. *J Comp Neurol* 455(4)**,** 531-546. doi: 10.1002/cne.10524.

Zeron, M.M., Hansson, O., Chen, N., Wellington, C.L., Leavitt, B.R., Brundin, P., et al. (2002). Increased sensitivity to N-methyl-D-aspartate receptor-mediated excitotoxicity in a mouse model of Huntington's disease. *Neuron* 33(6)**,** 849-860. doi: 10.1016/s0896-6273(02)00615-3.

Zhang, J., Li, L., Huang, H., Fang, F., Webber, H.C., Zhuang, P., et al. (2019). Silicone oil-induced ocular hypertension and glaucomatous neurodegeneration in mouse. *Elife* 8. doi: 10.7554/eLife.45881.

Zhang, N., Wang, J., Chen, B., Li, Y., and Jiang, B. (2020). Prevalence of Primary Angle Closure Glaucoma in the Last 20 Years: A Meta-Analysis and Systematic Review. *Front Med (Lausanne)* 7**,** 624179. doi: 10.3389/fmed.2020.624179.

Zhao, C., Fang, J., Li, C., and Zhang, M. (2017). Connexin43 and AMPK Have Essential Role in Resistance to Oxidative Stress Induced Necrosis. *Biomed Res Int* 2017**,** 3962173. doi: 10.1155/2017/3962173.

Zhao, H.B., Zhu, Y., and Liu, L.M. (2021). Excess extracellular K(+) causes inner hair cell ribbon synapse degeneration. *Commun Biol* 4(1)**,** 24. doi: 10.1038/s42003-020-01532-w.

Zhao, R., Grunke, S.D., Wood, C.A., Perez, G.A., Comstock, M., Li, M.H., et al. (2022). Activity disruption causes degeneration of entorhinal neurons in a mouse model of Alzheimer's circuit dysfunction. *Elife* 11**,** e83813. doi: 10.7554/eLife.83813.

Zhong, Y.S., Wang, J., Liu, W.M., and Zhu, Y.H. (2013). Potassium ion channels in retinal ganglion cells (review). *Mol Med Rep* 8(2)**,** 311-319. doi: 10.3892/mmr.2013.1508.

Zhou, D., Lambert, S., Malen, P.L., Carpenter, S., Boland, L.M., and Bennett, V. (1998). AnkyrinG is required for clustering of voltage-gated Na channels at axon initial segments and for normal action potential firing. *J Cell Biol* 143(5)**,** 1295-1304. doi: 10.1083/jcb.143.5.1295.

Zimmerman, T.J. (1993). Topical ophthalmic beta blockers: a comparative review. *J Ocul Pharmacol* 9(4)**,** 373-384. doi: 10.1089/jop.1993.9.373.